SYNTHESIS, ELECTROCHEMISTRY AND DENSITY FUNCTIONAL THEORY CALCULATIONS ON CHROME AND COBALT CARBENE AND BETADIKETONATO COMPLEXES.

R. LIU

SYNTHESIS, ELECTROCHEMISTRY AND DENSITY FUNCTIONAL THEORY CALCULATIONS ON CHROME AND COBALT CARBENE AND BETADIKETONATO COMPLEXES.

A thesis submitted to meet the requirements for the degree of

Magister Scientiae

in the

Department of Chemistry

Faculty of Natural and Agricultural Sciences

at the

University of the Free State

by

Renyuan Liu

Supervisor

Prof. J. Conradie

Acknowledgements

I would like to thank all my friends, family and colleague for their support through the period of my studies. Special appreciations must be made to the following people:

Table of Contents

Chapter 3

Results and discussion   49

Chapter 4

Experimental 121

Chapter 5

Concluding remarks and future perspectives 131

Appendix 135

Abstract 151

Opsomming 152

List of Abbreviations

β-diketones

Hacac	2,4-pentanedione (acetylacetone)
Hba	1-phenyl-1,3-butanedione (benzoylacetone)
Hdbm	1,3-diphenyl-1,3-propanedione (dibenzoylmethane)
Htfba	4,4,4-trifluoro-1-(phenyl)-1,3-butanedione (trifluorobenzoylacetone)
Htfth	4,4,4-trifluoro-1-(2-thenoyl)-1,3-butanedione (trifluorothenoylacetone)
Htffu	4,4,4-trifluoro-1-(2-furoyl)-1,3-butanedione (trifluorofuroylacetone)
Htfaa	1,1,1-trifluoro-2,4-pentanedione (trifluoroacetylacetone)
Hhfaa	1,1,1,5,5,5-hexafluoro-2,4-pentanedione (hexafluoroacetylacetone)

*The removal of H in the above abbreviations represents the anion (enolate) of the β-diketone.

Solvents

THF	tetrahydrofuran
CH_3CN	acetonitrile
DCM	dichloromethane
EtOH	ethanol

Functional Groups

Th	2-thienyl
Fu	2-furyl
dppe	1,2-bis(diphenylphosphino)ethane

Cyclic Voltammetry

CV	cyclic voltammetry
$E^{0'}$	formal reduction potential
E_{pa}	anodic peak potential
E_{pc}	cathodic peak potential

ΔE_p	separation of anodic and cathodic peak potentials
i_{pa}	anodic peak current
i_{pc}	cathodic peak current
TBAPF$_6$	tetrabutylammonium hexafluorophosphate [NBu4][PF6]
TEABF$_4$	tetraethylammonium tetrafluoroborate
SCE	saturated calomel electrode

List of Complexes

Tris(β-diketones)chromium(III) complexes

Cr(acac)$_3$ {1}   tris(2,4-pentadionato)chromium(III)

Cr(ba)$_3$ {2}   tris(1-phenyl-1,3-butanedionato)chromium(III)

Cr(dbm)$_3$ {3}   tris(1,3-diphenyl-1,3-propanedionato)chromium(III)

Cr(tfba)$_3$ {4}   tris(4,4,4-trifluoro-1-phenyl-1,3-butanedionato)chromium(III)

Cr(tfth)$_3$ {5}   tris(4,4,4-trifluoro-1-(2-thienyl)-1,3-butanedionato)chromium(III)

Cr(tffu)$_3$ {6}   tris(4,4,4-trifluoro-1-(2-furyl)-1,3-butanedionato)chromium(III)

Cr(tfaa)$_3$ {7}   tris(1,1,1-trifluoro-2,4-pentadionato)chromium(III)

Cr(hfaa)$_3$ {8}   tris(1,1,1,5,5,5-hexafluoro-2,4-pentadionato)chromium(III)

Tris(β-diketones)cobalt(III) complexes

Co(acac)$_3$ {9}   tris(2,4-pentadionato)cobalt(III)

Co(ba)$_3$ {10}   tris(1-phenyl-1,3-butanedionato)cobalt(III)

Co(dbm)$_3$ {11}   tris(1,3-diphenyl-1,3-propanedionato)cobalt(III)

Co(tfba)$_3$ {12}   tris(4,4,4-trifluoro-1-phenyl-1,3-butanedionato)cobalt(III)

Co(tfaa)$_3$ {13}   tris(1,1,1-trifluoro-2,4-pentadionato)cobalt(III)

Chromium(0) carbene complexes

[Cr(CO)$_5$C(OEt)(2-thienyl)] **{carbene 1}**

[Cr(CO)₅C(OEt)(2-furyl)] **{carbene 2}**
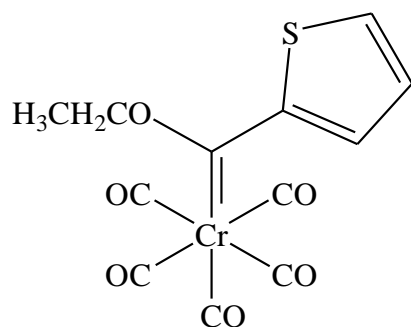
$[Cr(CO)_5C(OEt)(2\text{-furyl})]$ **{carbene 2}**
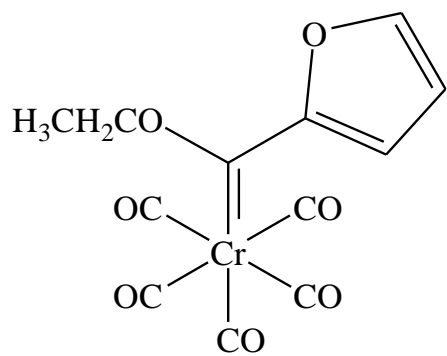
[Cr(CO)₅C(OEt)(2-(N-methylpyrrolyl))] **{carbene 3}**
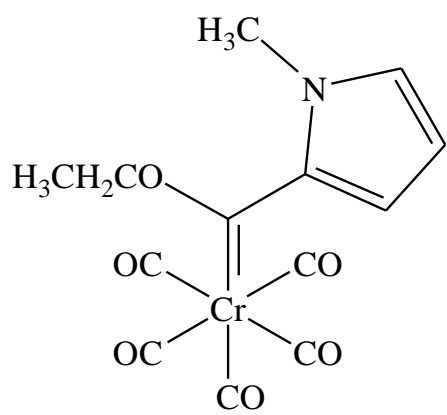
[Cr(CO)₅C(OEt)(N-methyl-2-(2'-thienyl)pyrrole)] **{carbene 4}**

VIII

[Cr(CO)₅C(OEt)2,2'-thienylfuran] **{carbene 5}**
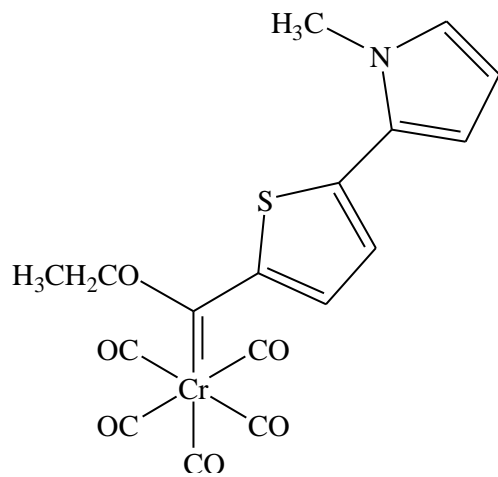
$[Cr(CO)_5C(OEt)2,2'\text{-thienylfuran}]$ **{carbene 5}**

[(CO)₃(dppe)Cr=C(OEt)Th] **{carbene 6}**
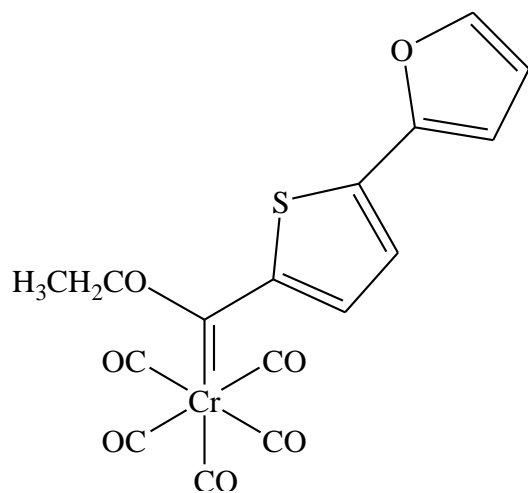
$[(CO)_3(dppe)Cr=C(OEt)Th]$ **{carbene 6}**
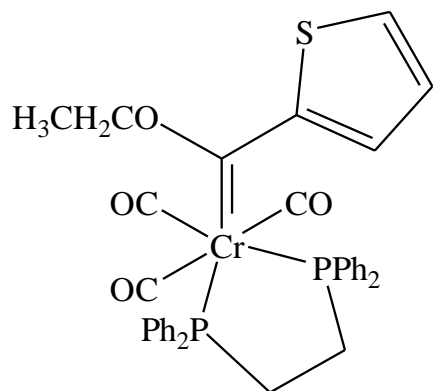
[(CO)₃(dppe)Cr=C(OEt)Fu] **{carbene 7}**

$[(CO)_3(dppe)Cr=C(OEt)Fu]$ **{carbene 7}**

IX
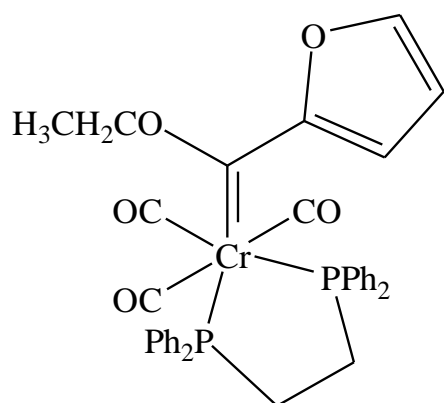
[(CO)$_3$(dppe)Cr=C(NHCy)Th] **{carbene 8}**

CyHN

OC
OC
Ph$_2$P
Cr
CO
PPh$_2$

(furan ring with O)
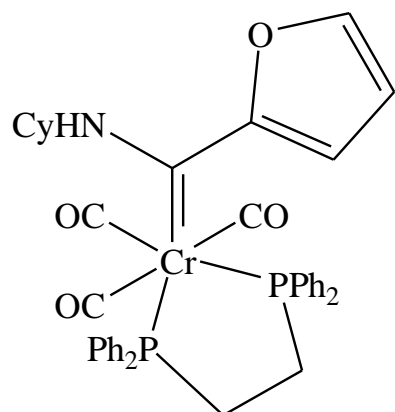
[(CO)$_3$(dppe)Cr=C(NHCy)Fu] **{carbene 9}**

CyHN

OC
OC
Ph$_2$P
Cr
CO
PPh$_2$

(thiophene ring with S)

X
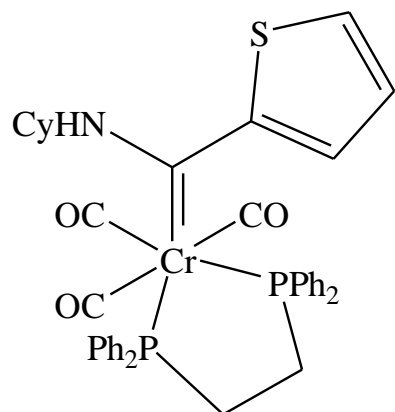
1   **Introduction**

The research in this thesis constists of three parts:

a)   Synthesis, crystal studies, electrochemistry and computational chemistry of tris(β-diketonato)chromium(III) complexes.

b)   Synthesis, crystal studies and computational chemistry of tris(β-diketonato)cobalt(III) complexes.

c)   Electrochemistry and computational chemistry of Fischer carbene complexes with a Cr(0) metal center.

A selection of β-diketonato ligands $(R_1COCHCOR_2)^{-1}$ (with substituents R_1, $R_2 = CH_3$, CH_3; CH_3, C_6H_5; C_6H_5, C_6H_5; CF_3, C_6H_5; C_4H_3S, CF_3; C_4H_3O, CF_3; CH_3, CF_3; and CF_3, CF_3) was used in parts a) and b). The Fischer carbene studies in part c) involved alkoxy and amino carbene complexes of the type $[(CO)_5Cr=C(OEt)R]$, with R = 2-thienyl, 2-furyl, 2-(N-methylpyrrolyl), N-methyl-2-((2'-thienyl)pyrrole) and 2,2'-thienylfural, as well as complexes of the type $[(CO)_3(dppe)Cr=C(X)R]$, with R = 2-thienyl or 2-furyl, and X = OEt or NHCy, and where dppe = 1,2-bis(diphenylphosphino)ethane.

1.1 Tris(β-diketonato)chromium(III) complexes

Chromium is the lightest and most abundant of the group VI transition metals. Supported chromium oxides are known to be important catalysts for the production of high-density polyethylene (HDPE) and linear low-density polyethylene.[1] Cr-based catalysts are used both as homogeneous and heterogeneous catalysts.

An example involving Cr-based homogeneous catalysis is ethylene polymerization, during the formation of 1-hexene (see **Scheme 1.1**). This mechanism starts with the coordination of two ethylene molecules to chromium, and subsequent formation of chromacyclopentane, followed by insertion of the third ethylene molecule and the β-Hydrogen transfer to ethylene. Reductive

---

[1] Fu, S. L.; Rosynek, M. P.; Linsford, J. H.; *Langmuir*, **1991**, *7*, 1179-1187

1

elimination of the product returns the original Cr-catalyst. The liberation of 1-hexene is known to be faster than further ethylene insertion, therefore further polymerization focuses on further growth of the metallocycle.[2]
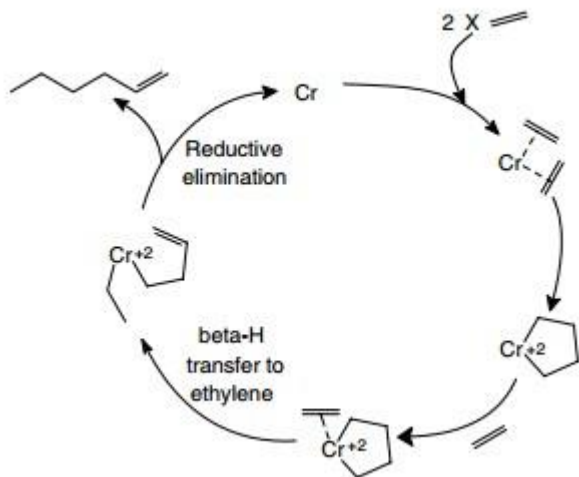
Scheme 1.1: Trimerization of ethylene to 1-hexene. (Reprinted (adapted) with permission from Dixon, J. T.; Green, M. J.; Hess, F. M.; Morgan, D. H.; *Journal of Organometallic Chemistry*, **2004**, *689*, 3641-3668. Copyright (2004) ScienceDirect).

As the most well-known member of the tris(β-diketonato)chromium(III) complexes, tris(acetylacetonato)chromium(III), Cr(acac)$_3$, is most studied as catalyst. As heterogeneous catalyst, two types of complexes are present on the surface of the support, Al-MCM-41: one has two acac ligands, and the other has three acac ligands, with H-bonding to the framework (see **Scheme 1.2**).[3] Ethylene polymerization was carried out over calcined Cr-Al-MCM-41,[4] rather than Cr-Si-MCM-41 (as in **Scheme 1.2**), for higher catalytic activity. (MCM-41, namely Mobil Composition of Matter No. 41, is one of the most favoured members in the family of mesoporous materials, called Mobil Composition of Matter (MCM).[5] MCM-41 possesses an array of hexagonal pores with very large suface area, therefore MCM-41 became an excellent support for chromium complexes.) Increasing calcination temperature also increases the catalytic activity. Cr-loading is also important to catalytic activity. Increasing Cr-loading up to

[2] Dixon, J. T.; Green, M. J.; Hess, F. M.; Morgan, D. H.; *J. Organomet, Chem,*, **2004**, *689*, 3641-3668

[3] Rao, R. R.; Weckhuysen, B. M.; Schoonheydt, R. A.; *Chem. Commun.*, **1999**, 445-446

[4] Kresge, C. T.; Leonowicz, W. J.; Roth, W. J.; Vartuli, J. C.; Beck, J. S.; Nature, 1992, 359, 710-712

[5] Kresge, C. T.; Leonowicz, W. J.; Roth, W. J.; Vartuli, J. C.; Beck, J. S.; Nature, 1992, 359, 710-712

1 wt % Cr, gives increasing activity for the catalyst. Further Cr-loading leads to the formation of Cr_2O_3 and blocking of the reacting channels.
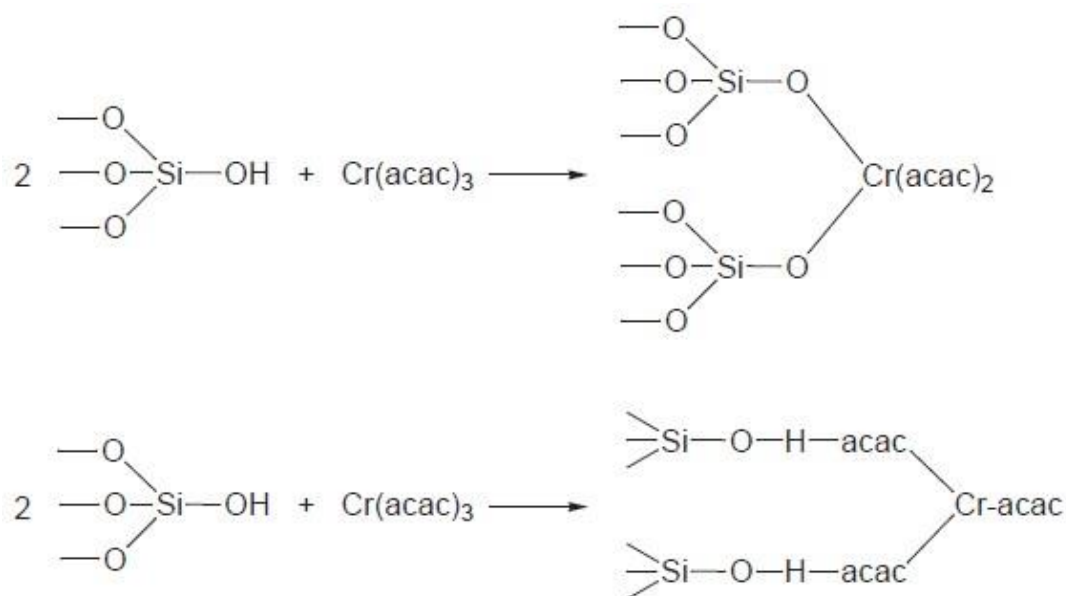
Scheme 1.2: Two types of $Cr(acac)_n$ (n = 2 or 3) complexes grafted onto the Si-MCM-41 support before calcination. (Reprinted (adapted) with permission from Rao, R. R.; Weckhuysen, B. M.; Schoonheydt, R. A.; *Chem. Comm.*, **1999**, 445-446. Copyright (1999) Royal Chemical Society).

1.2 Tris(β-diketonato)cobalt(III) complexes

Metal β-diketonato complexes are invaluable precursors for the chemical vapour deposition (CVD) of metal and non-metal thin films. The chemical vapour deposition (CVD) technique produces high-purity, high-performance solid materials, which are often used in producing semiconducting thin films. Volatile by-products need to be removed by gas flow, therefore highly volatile precusors are preferred by the CVD processes. Fahlman and Barron investigated the volatility of a series of metal β-diketonato complexes.[6] It was found that the volatility of M(β-diketonato)$_3$ complexes linearly increases with the molecular weight. Partially and fully fluorinated β-diketonato ligands also enhance the precursors' volatility. Both Co^{III}(β-diketonato)$_3$[6] and Co^{II}(β-diketonato)$_3$[7] complexes were found to be widely used in CVD processes, to produce cobalt oxide thin films. Cobalt oxide films (CoO, Co_2O_3 and Co_3O_4) are popularly produced due

---

[6] Fahlman, B. D.; Barron, A. R.; *Adv. Mater. Opt. Electron.,* **2000**, *10*, 223-232

[7] Pasko, S.; Hubert-Pfalzgraf, L. G.; Abrutis, A.; Vaissermann, J.; *Polyhedron*, **2004**, *23*, 735-741

to their wide applications, *e.g.* in catalysis, in various types of sensors, in electrochromic-, electrical- and other opto-electronic devices.[8] An interesting application of Co CVD-precursors, is the usage as electroluminescent device thin films.[9] Electroluminescent (EL) devices rely on the emission of light through the applied electric field, to a doped phosphor material. In the double-insulating-layer structure, insulating films are deposited on either side of the phosphor layer, and current is applied to the electrodes outside the insulating layers. In the capacitance structure thus created, the maximum current is limited to the level of capacitive charging and discharging displacement current, and emission of light is generated over the phosphor layer, induced by the high electric field.

1.3 Fischer carbene complexes with Cr(0) metal center

Fischer carbene complexes (FCCs) are "powerful tools" in synthetic chemistry. A considerable number of applications have been revealed, e.g. olefin metathesis,[10] cyclopropanation,[11] metathesis of dehydro amino acids,[12] and multi-component reactions (MCRs),[13] *etc*.

Scheme 1.3Error! Reference source not found. shows three typical reactions of FCCs involing alkyne insertion: Silyl-substituted acetylenes react thermally with chromium FCCs, leading to highly stable silyl vinylketenes. The silyl group electronically stabilize ketenes and the bulky silyl group, and impedes the final ring closure by the steric congestion (see **Scheme 1.3** top). When aryl-substituted alkynes are employed, the chromium moiety generally remains linked to the aryl group; its photolytic removal quantitatively affords (E)-silyl vinyl ketene, which slowly converts to an equilibrium mixture of (E)-silyl vinyl ketene and cyclobutenone (see **Scheme 1.3** middle). An almost 1-to-1 mixture of silyl-ketene and cyclobutenone has been obtained from the reaction of cyclopropyl FCC and triisopropylsilylethynyl (TIPS)-substituted phenyl acetylene; however, cyclobutenones have been isolated as sole reaction products, when TIPS-substituted furan-2-yl or cyclopropyl acetylenes were employed (see **Scheme 1.3** bottom).

---

[8] Narayan, R. V.; Kanniah, V.; Dhathathreyan, A.; *J. Chem. Sci.*, **2006**, *118*, 179–184.

[9] Tiitta, M.; Niinistö, L.; *Chem. Vap. Deposilion*, **1997**. *3*, 167-182

[10] McCinnis, J.; Katz, T. J.; l Hurwitz, S.; *J. Am. Chem. Soc.*, **1976**, *98*, 605-606

[11] Casey, C. P.; Burkhardt, T. J.; *Journal of the American Chemical Society*, **1974**, *96*, 7808-7809

[12] Dialer, H.; Polborn,K.; Beck, W.; *Journal of Organometallic Chemistry*, **1999**, *589*, 21-28

[13] Fernández-Rodriguez, M. A.; Garcia-Garcia, P.; Aguilar, E.; *Chem. Commun.,* **2010***, 46,* 7670-7687
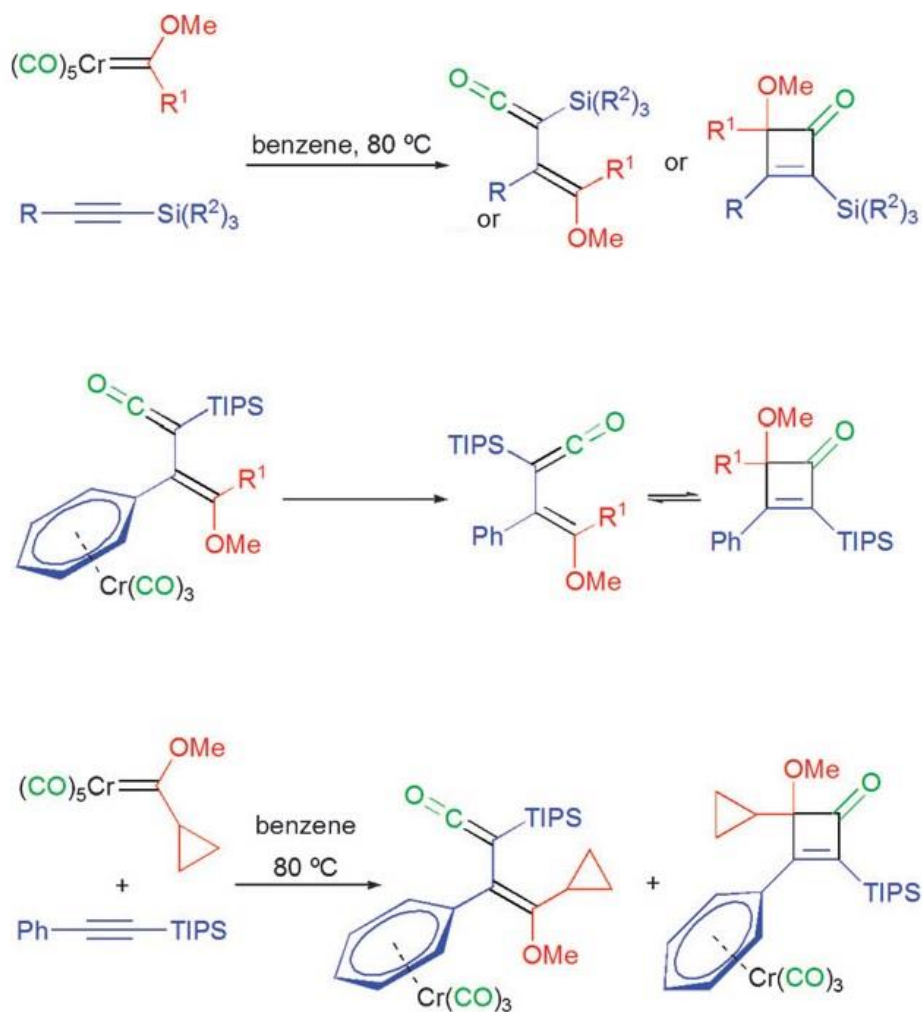
Scheme 1.3: Reactions between Cr(0) Fischer carbene complexes and Silyl acetylenes. (Reprinted (adapted) with permission from Fernández-Rodriquez, M. A.; Garcia-Garcia, P.; Aguilar, E.; *Chem. Commun.,* **2010***, 46,* 7670-7687. Copyright (2010) Royal Chemical Society).

1.4 Aims of this study

The following goals were set for the $Cr(\beta\text{-diketonato})_3$ study:

(i)   The synthesis of novel and existing $Cr(\beta\text{-diketonato})_3$ complexes.

(ii)   The characterization of newly synthesized $Cr(\beta\text{-diketonato})_3$ complexes, via mass spectroscopy, X-ray crystallography and melting points.

(iii)   The investigation of the electrochemical behaviour of the $Cr(\beta\text{-diketonato})_3$ complexes, using cyclic voltammetry, linear sweep voltammetry and square wave voltammetry.

(iv)   The identification of the three-dimensional geometry and spin state of the $Cr(\beta\text{-diketonato})_3$ complexes, by use of DFT-computational methods.

(v)   Establishing relationships between the experimental results (the reduction potential (E_{pc}) of the Cr^{III}/Cr^{II} redox processes), the DFT-calculated properties (electron affinity (EA), highest occupied molecular orbital (HOMO) energy, and lowest unoccupied molecular orbital (LUMO) energy) and the electronic parameters (acid dissociation constant (pK_a) of the uncoordinated β-diketonato ligands, the total group electronegativities $\{\Sigma(\chi_R + \chi_{R'})\}$ and total Hammett sigma constants ($\Sigma\sigma$)).

The following goals were set for the $Co(\beta\text{-diketonato})_3$ study:

(i)   The synthesis of novel and existing $Co(\beta\text{-diketonato})_3$ complexes.

(ii)   The characterization of newly synthesized $Co(\beta\text{-diketonato})_3$ complexes, via mass spectroscopy, X-ray crystallography and melting points.

(iii)   The identification of the three-dimensional geometry and spin state of the $Co(\beta\text{-diketonato})_3$ complexes, by use of DFT-computational methods.

The following goals were set for the $Cr(0)$ carbene study:

(i)   Understanding all possible isomers of the Cr(0) carbene complexes, namely *cis/trans* isomerism, *fac/mer* isomerism, and *E/Z* conformations.

(ii)   The investigation of the electrochemical behaviour of the Cr(0) carbene complexes, using cyclic voltammetry, linear sweep voltammetry and square wave voltammetry.

(iii)   Understanding the three-dimensional geometry and spin state of the Cr(0) carbene complexes, by use of DFT-computational methods.

(iv)   Establishing relationships between the experimental results (the oxidation potential (E_{pa}) of the Cr^0/Cr^I redox process, as well as the reduction potential (E_{pc}) of the carbene-ligand) and DFT-calculated properties (the highest occupied molecular orbital (HOMO) energy and lowest unoccupied molecular orbital (LUMO) energy).

2 Literature survey and fundamental aspects.

Three main techniques (Electrochemistry, Computational Chemistry and X-ray Crystallogrphy) are introduced first, followed by the background of tris(β-diketonato)chromium(III) complexes, tris(β-diketonato)cobalt(III) complexes and chromium(0)-carbene complexes.

2.1 Electrochemistry

2.1.1 Cyclic Voltammetry (CV)

Cyclic voltammetry is a very powerful and perhaps the most commonly used electroanalytical technique to study electroactive species. The theory of cyclic voltammetry is well discussed and understood since the 1980's.[1,2,3,4] A modern voltammetric system contains three electrodes: a working electrode, a reference electrode and an auxiliary electrode (see **Figure 2.1**). The surface of the working electrode (*e.g.* glassy carbon or platinum) is where the redox process takes place. The potential applied between the working electrode and the reference electrode (*e.g.* silver/silver chloride) is controlled and measured by the potentiostat. The reference electrode has a stable and well-known potential, such as silver/silver chloride (Ag/AgCl) or a saturated calomel electrode (SCE). The electrical current corresponding to the applied potential is provided by the auxiliary electrode (*e.g.* platinum or gold), and this current is carried via the supporting electrolyte in the analyte solution.

---

[1] Evans, D. H.; O'Connell, K. M.; Petersen, P. A.; Kelly, M. J.; *J. Chem. Educ.*, **1983**, *60*, 290-293

[2] Mabbott, G. A.; *J. Chem. Educ.*, **1983**, *60*, 697-702

[3] Kissinger, P. T.; Heineman, W. R.; *J. Chem. Educ.*, **1983**, *60*, 702-706

[4] Van Benschoten, J. J.; Lewis, J. Y.; Heineman, W. R.; *J. Chem. Educ.*, **1983**, *60*, 772-776
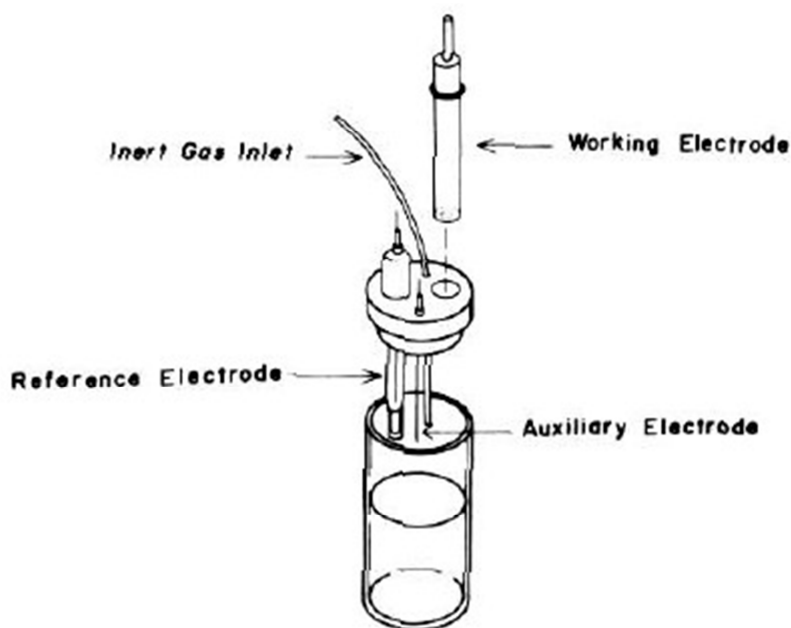
Figure 2.1: Illustration of a three-electrode cell for voltammetry.[3] (Reprinted (adapted) with permission from Kissinger, P. T.; Heineman, W. R.; *J. Chem. Educ.*, **1983**, *60*, 702-706. Copyright (1983) American Chemical Society).

During the cyclic voltammetric measurements, the potential range of the stationary working electrode changes over time; this process is called the excitation signal (see **Figure 2.2**). Cycle 1 (solid line) in **Figure 2.2** represents the first cycle of the excitation signal, which starts the forward scan at 0.8 V and ends at – 0.2 V. Then the process is reversed and the potential returns to 0.8 V. The first reduction or oxidation process of the analyte is detected from the forward scan, and the resulting intermediate/product, due to the first redox process, is then detected from the reverse scan. The scan rate of the forward scan and the reverse scan is represented by the slope of the graph (50 mV/s in **Figure 2.2**). Cycle 2 starts immediately after cycle 1 has completed. A modern potentiostat can achieve single or multiple cycles at different scan rates.
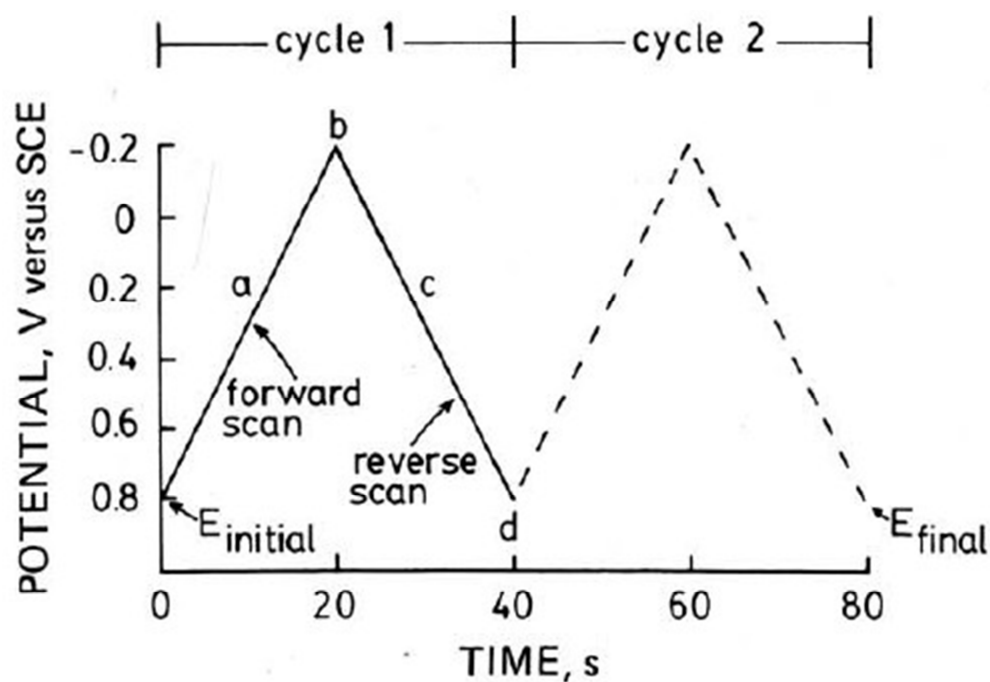
Figure 2.2: Typical excitation signal for cyclic voltammetry – a triangular potential waveform, with turning points at 0.8 V and – 0.2 V *versus* SCE[3]. (Reprinted (adapted) with permission from Kissinger, P. T.; Heineman, W. R.; *J. Chem. Educ.*, **1983**, *60*, 702-706. Copyright (1983) American Chemical Society).

Figure 2.3 is the cyclic voltammogram obtained for 6.0 mM $K_3Fe(CN)_6$, using 1.0 M KNO_3 in water as the supporting electrolyte and platinum as working electrode, measured against a saturated calomel electrode. **Figure 2.3** shows the response to the excitation signal in **Figure 2.2**. There are four important parameters (as marked in **Figure 2.3**) for understanding the electrochemical behaviour of the analyte. These parameters will be explained in **Section2.1.1.1**.
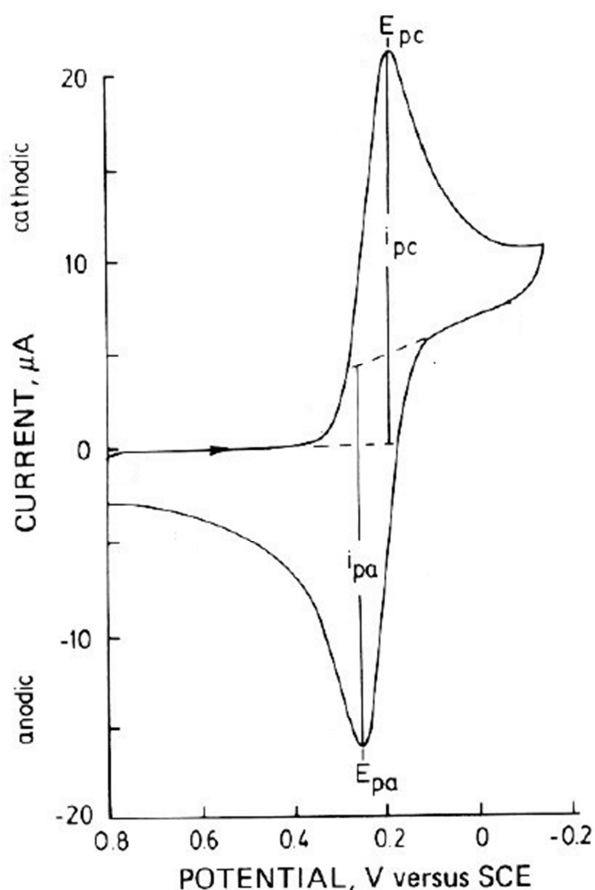
Figure 2.3: Cyclic voltammograms of 6 mM $K_3Fe(CN)_6$ in 1 M KNO_3, at scan rate of 50 mV/s[3]. (Reprinted (adapted) with permission from Kissinger, P. T.; Heineman, W. R.; *J. Chem. Educ.*, **1983**, *60*, 702-706. Copyright (1983) American Chemical Society).

2.1.1.1 Parameters

The processes that occur during an electrochemical experiment occur at the surface of the electrode. The experimental potential E (in volt) of the cell at experimental conditions at any time during the experiment is determined by the Nernst equation ($E = E^0 - \frac{RT}{nF} ln \frac{a_{Red}}{a_{Ox}}$) that relates the activity a of the reduced and oxidized form of the analyte at a specific temperature T. E° is the standard potential (in V) and is dependent on the identity of the reaction, R is the gas constant (J/molK), n is the number of electrons transferred and F is Faraday's constant (C/(mol e). The potential is thus related to both concentration and potential energy of the reactants and products, and is therefore is primarily a thermodynamic measurement.

Four important basic parameters from the cyclic voltammograms are used to understand the electrochemical behaviour of the analyte, *i.e.* the anodic peak potential (E_{pa}), the cathodic peak potential (E_{pc}), the anodic peak current (i_{pa}) and the cathodic peak current (i_{pc}). Peak currents can be obtained by reading the difference between the peak and the extension of the base line, but obtaining peak currents can be difficult for a complicated system. The peak potentials are often measured against an internal standard, such as Ferrocene (FcH/FcH^+).[5] Other parameters are derived from these basic parameters.

The ratio of anodic and cathodic peak currents should be identical ($i_{pa}/i_{pc} = 1$), for a chemically reversible redox process. The chemical reversibility can also be described as thermodynamic reversibility which refers to the ability of the products to return to reactants.

In a stationary solution of analyte, the scan rate is the only variable.

In a system where diffusion is the only mode of mass transport (diffusion-controlled) and the kinetics of electron transfer are fast (reversible), the peak current is directly proportional to the square root of the scan rate. This correlation is described by the Randle-Sevcik equation (see **Equation 2.1**):[3]

Equation 2.1: $i_p = 268600 \, n^{\frac{3}{2}} \, AD^{\frac{1}{2}} \, Cv^{\frac{1}{2}}$

where i_p = current at maximum in ampere; n = number of electrons transferred in the redox process; A = electrode area in cm^2; D = diffusion coefficient in cm^2/s; C = concentration in mol/cm^3; v = scan rate in V/s. The Randle-Sevcik equation relates current to scan rate and thus gives information of the instantaneous rate of the chemical reaction, and is thus partially controlled by the chemical kinetics of the system.

The formal reduction potential ($E^{0'}$) lies in the middle of E_{pa} and E_{pc}, for a reversible redox process (**Equation 2.2**):

Equation 2.2: $E^{0'} = \frac{E_{pa} + E_{pc}}{2}$

[5] Gagne, R. R.; Koval, C. A.; Lisensky, G. C.; *Inorg. Chem.*, **1980**, *19*, 2855–2857

The potential separation (ΔE_p, see **Equation 2.3**) determines the electrochemical reversibility of a redox process. Electrochemical irreversible processes are caused by slow electron exchange of the redox species with the working electrode. An electrochemically reversible redox process is fully obtained at 25 °C for a one-electron redox process, if the potential separation (ΔE_p) is 59 mV. Generally, a redox process is considered reversible if the potential separation is smaller than 90 mV. If ΔE_p is greater than 90 mV and smaller than 150 mV, the redox process is quasi-reversible. The redox process is considered irreversible when ΔE_p is greater than 150 mV:

Equation 2.3: $\Delta E_p = E_{pa} - E_{pc} \cong \dfrac{0.059}{n}$

where n = number of electrons transferred.

When the analyte adsorp onto the electrode, the analyte does need to travel to the electrode as in a diffusion controlled experiment. Thus, when the potential required for reaction is reached, the current increases and decreases much more rapidly than in a diffusion controlled experiment. The result is a sharp (narrow) peak with a high current (since all the analyte can react at once).

2.1.2 Linear Sweep Voltammetry (LSV)

Linear Sweep Voltammetry (LSV) is the simplest type of voltammetry. In LSV, the potential change applied on the working electrode is varied linearly over time. The scan rates are slow, *e.g.* 1 – 5 mV/s. This allows the fresh analyte to approach the electrode, and the reacted analyte to diffuse away from the electrode.[6,7] A typical excitation signal of linear sweep voltammetry is given in **Figure 2.4**.

[6] Bard, A. J.; Faulknerm L. R.; *Electrochemical Methods: Fundamentals and Applications*, 2nd Edition, John Wiley & Sons, **2001**, 226-239

[7] Skoog, D. A.; West, D. M.; Holler, F. J.; Crouch, S. R.; *Fundamentals of Analytical Chemistry*, 8th Edition, Thomson Brooks/Cole, **2004**, 667-673
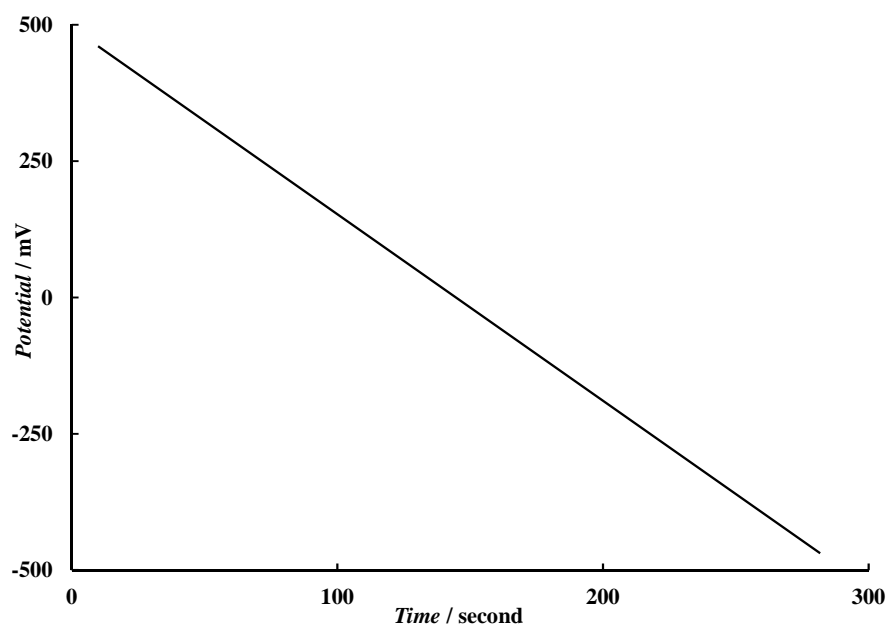
Figure 2.4: Typical excitation signal of linear sweep voltammetry.

A typical linear sweep voltammogram (voltammetric wave) is given in **Figure 2.5**. The limiting current i_l is reached when the current does not increase or decrease any further. Limiting currents are directly proportional to the analyte concentration, therefore the limiting current can be used to determine the concentration of analyte solution.[7] The half-wave potential ($E_{1/2}$) is the potential when the current is half of the limiting current, this potential can be used to identify unknown species.[7]
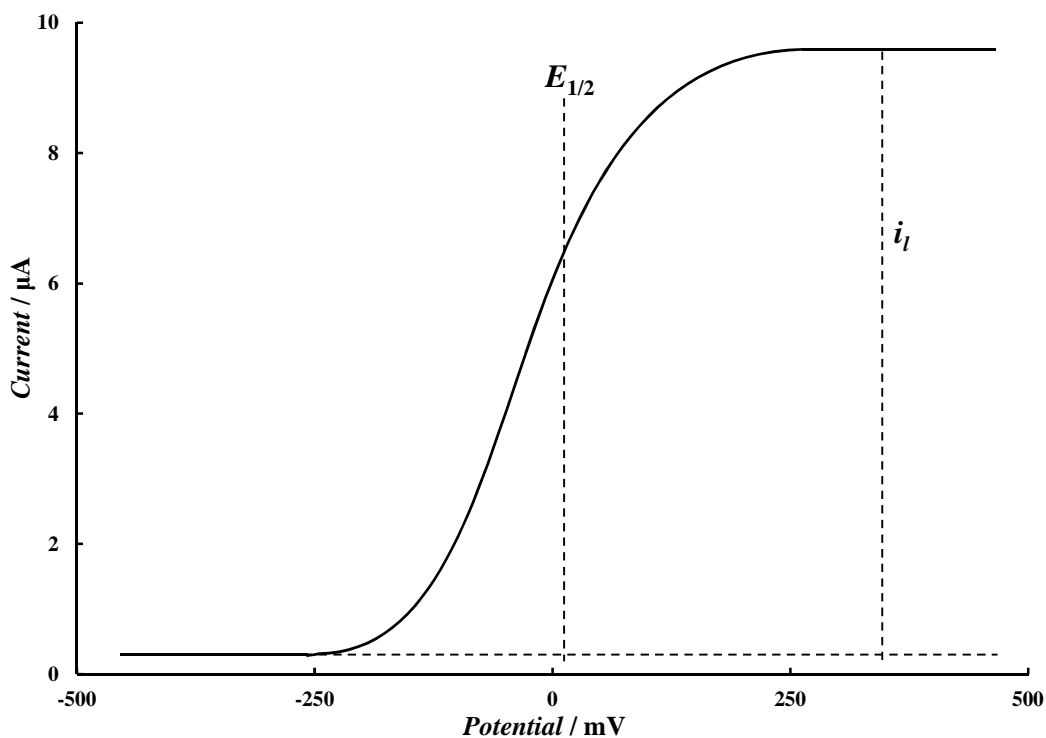
Figure 2.5: Typical linear sweep voltammogram.

2.1.3 Square Wave Voltammetry (SWV) [8,9,10]

A pulsed voltammetry technique called Square Wave Voltammetry (SWV), uses a potential waveform as shown in **Figure 2.6**, which shows the excitation signals of SWV. Each step of the staircase and the pulses have the same duration. The advantage of square wave voltammetry is that the entire scan can be performed with great speed and high sensitivity.

---

[8] O'Dea, J. J.; Osteryoung, J.; Osteryoung, R. A.; *Anal. Chem.*, **1981**, *53*, 695–701

[9] Osteryoung, J. G.; Osteryoung, R. A.; *Anal. Chem.*, **1985**, *57*, 101A–110A

[10] Osteryoung, J.; *J. Chem. Educ.*, **1983**, *60*, 296-298
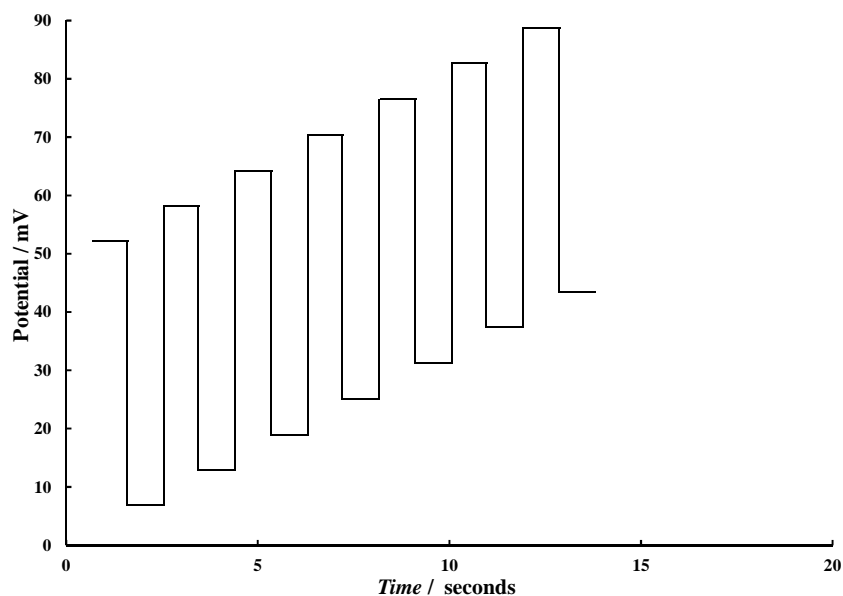
Figure 2.6: Typical excitation signals of square-wave voltammetry.

A typical square wave voltammogram for a reversible redox process, as a response to the excitation signal, is shown in **Figure 2.7**. The forward pulse (A) gives a current response i_A, and the reverse pulse (B) gives a current response i_B. The final current i_c is defined by the difference between i_A and i_B ($i_C = \Delta i = i_A - i_B$). The SWV voltammogram is obtained by plotting the current difference. This difference is directly proportional to the concentration of the analyte.[9]
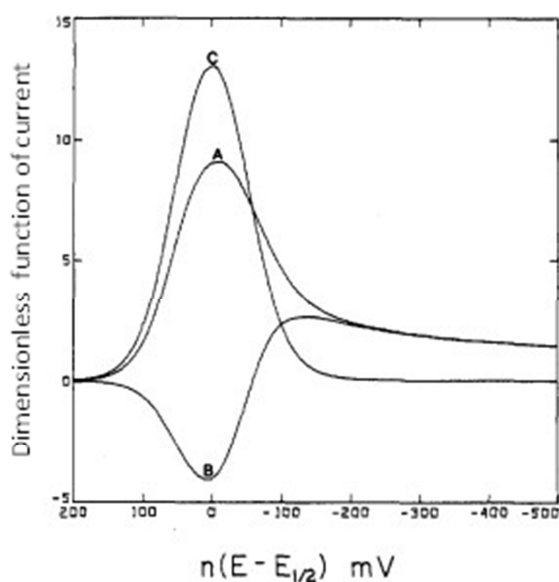
Figure 2.7: Typical square wave voltammogram for a reversible redox process.[9] (Reprinted (adapted) with permission from Osteryoung, J. G.; Osteryoung, R. A.; *Anal. Chem.*, **1985**, *57*, 101A–110A. Copyright (1985) American Chemical Society).

2.2 Computational Chemistry

2.2.1 Introduction[11,12,13,14]

Computational chemistry is a branch of chemistry, using computer simulations to solve chemical problems. It is based on the theoretical chemistry and utilizes powerful computer programmes to calculate physical and chemical properties of compounds, such as absolute/relative energies, molecular geometry and vibrational frequencies, *etc*. and to simulate chemical reactions. The advantage of computational chemistry is that it can simulate chemical reactions which are either dangerous, difficult, too expensive or even impossible to execute in a laboratory.

Five basic computational methods are described as follows:

(a)   *Molecular Mechanics* (MM) considers a molecule as balls (atoms) connected by springs (bonds). If the equilibrium spring lengths, the angle between the springs and the energy needed to bend or stretch the spring are known, geometry optimization may be achieved by finding the lowest energy.

(b)   *Ab initio* calculations solve the Schrödinger equation for a molecule to give the molecule's energy. *Ab initio* gives very accurate output, but it is time consuming and needs large computational facilities. Therefore this method is generally only used for small systems.

[11] Lewars, E.; *Computational Chemistry, Introduction to the Theory and Applications of Molecular and Quantum Mechanics*, Kluver Academic Publishers, Boston, **2003**, p1-7

[12] Hehre, W. J.; *A Guide to Molecular Mechanics and quantum chemical calculations*, Wavefunction Inc. Irvine, **2003**, p1-5

[13] Young, D. C.; *Computatioanl Chemistry, A Practical Guide for Applying Technique to Real-World Problems*, Wiley and Sons, New York, **2001**, p1-4

[14] Jensen, F.; *Introduction to Computational Chemistry*, 2nd edition, John Wiley & Sons, England, **2007**, p1-20

(c)   *Semi-empirical* (SE) calculations also are based on the Schrödinger equation, however, more approximations were added and very complicated integrals were left out. Experimental values were added as parameters to improve the accuracy.

(d)   *Density functional theory* (DFT) is relatively new. DFT was introduced in the 1960's, but serious DFT-calculations only started in the 1980's. This method is also based on the Schrödinger equation, where the many-body electronic wavefunction is replaced by electronic density. The Amsterdam Density Functional programme (ADF) was developed on the basis of density functional theory. The ADF programme can perform calculations such as energy minimisation, determination of transition states, reaction paths, and harmonic frequencies with IR intensities, *etc.*[15].

(e)   *Molecular dynamics* apply the laws of motion to molecules. This is a powerful tool to solve motions in chemical systems by computational calculations, *e.g.* one can simulate the motion of an enzyme, when binding to a substrate.

Quantum and molecular mechanics are theories implemented in computational chemistry. Quantum mechanics describes molecules by interactions among nuclei and electrons. All quantum mechanical methods of computational chemistry are based on the Schrödinger equation. Schrödinger's equation describes nuclei and electrons as waves instead of particles. The general time-independent Schrödinger equation of a multi-nuclear, multi-electron system is shown below (see **Equation 2.4**):

Equation 2.4: $\hat{H}\Psi = E\Psi$

where $\hat{H}$ = the Hamiltonian operator; E = the energy; Ψ = the wavefunction. The Hamiltonian oprator is a combination of kinetic energy (T) and potential energy (V), (see **Equation 2.5**):

---

[15] Te Velde, G.; Bickelhaupt, F. M.; Baerends, E. J.; Fonseca Guerra, C.; van Gisbergen, S. J. A.; Snijders, J. G.; Ziegler, T.; *Journal of Computational chemistry*, **2001**, *22*, 931-967

Equation 2.5: $H = T + V = -\sum_{i=1}^{N} \frac{\hbar^2 \nabla^2}{2m_i} + \sum_{i<j}^{N} \frac{q_i q_j}{r_{ij}}$

with

$\nabla_i^2 = \frac{\partial^2}{\partial x_i^2} + \frac{\partial^2}{\partial y_i^2} + \frac{\partial^2}{\partial z_i^2}$

where ∇_i^2 = the Laplacian operator acting on particle i for both nuclei and electrons; m_i = mass of particle i; q_i = charge of the particle i; r_{ij} = distance between particles i and j.

Since the multi-electron Schrödinger equation is derived from a series of one-electron quasi-particles, approximations have been introduced to provide methods for a multi-electron system. For example, the Born-Oppenheimer approximation assumes that nuclei are static and have zero nuclear kinetic energy; the Hartree-Fock approximation assumes that every single electron has independent motion from the other electrons. Hohenberg-Kohn (HK) theory showed that the electron density uniquely determines the Hamiltonian operator and thus all the properties of the system and that the ground state density minimizes the total electronic energy of the system.

2.2.2 Exchange–Correlation Functionals[16,17]

Density Functional Theory (DFT) is based on the HK theory that the electron kinetic energy should be calculated from an auxiliary set of orbitals used for representing the electron density density. A small difference between exact and calculated kinetic energy was found. The energy difference is defined as exchange–correlation terms. In the case of electrons, the exchange describes two electrons with same spin in different orbitals, and correlation describes two paired electrons with opposite spins in a same orbital. The simplest approach is to assume the electron density to be slowly varying, such that the exchange–correlation energy can be calculated using formulas derived for a uniform electron density.

The choice of exchange-correlation functionals (density functionals) makes a difference in the accuracy and results of DFT-calculations. Four basic exchange-correlations functionals are known:

[16] Jensen, F.; *Introduction to Computational Chemistry*, 2nd edition, John Wiley & Sons, England, **2007**, p232-255

[17] Koch, W.; Holtzhausen, M. C.; *A Chemist's guide to Density Functional Theory*, Wiley-VCH, **2001**, p65-91

- *Local Density Approximation* (LDA) assumes that the spin density is a uniform electron gas, or equivalently, that the density is a slowly varying function. The functionals are only dependent on the density at a given point.

- *Generalized Gradient Approximation* (GGA) applies to density which is not uniform but varies very slowly.

- *Hybrid functionals* (hybrid GGA) include a hybride between pure density functionals for exchange and exact Hartree-Fock exchange, *i.e.* a certain amount of exact exchange is incorporated.

- *Meta-generalized gradient approximation* (*meta*-GGA) takes the second order gradient on electron density, and is dependent on the orbital kinetic energy density.

The GGA-functionals can have exchange correction, correlation correction, or both. A selection of applicable GGA-functionals are summarized in **Table 2.1**.[18]

Table 2.1: Summary of applicable GGA-functionals.

Functionals with exchange correction	
Becke:	Proposed by Becke in 1988
PW91x:	Proposed by Perdew and Wang in 1991
PBEx	Proposed by Perdew and Burke and Ernzerhof in 1996
OPTX	Proposed by Handy and Cohen in 2001
Functionals with correlation correction	
Perdew	Proposed by Perdew in 1986
LYP	Proposed by Lee and Yang and Parr in 1988
PW91c	Proposed by Perdew and Wang in 1991
PBEc	Proposed by Perdew and Burke and Ernzerhof in 1996
Functionals with both corrections	
BP86	Combination of Becke and Perdew
PW91	Combination of PW91x and PW91c
PBE	Combination of PBEx and PBEc
BLYP	Combination of Becke and LYP
OLYP	Combination of OPTX and LYPc

---

[18] Conradie, M.M.; *Rhodium and Iron Complexes and Transition States: A computational, Spectroscopic and Electrochemical Study*, **2010**, PhD thesis, University of the Free State, Bloemfontein, RSA

OPBE	Combination of OPTX and PBEc
B3LYP	Combination of Becke 3 parameter functional and LYP
B3LYP*	Modified B3LYP with 15% Hartree-Fock exchange

- Energies across different functionals cannot be directly compared.

2.2.3 Basis Sets[19,20]

A basis set is a set of functions used to describe the shape of the orbitals in an atom. Most semi-empirical methods use a predefined basis set. A basis set must be specified for *ab initio* and density functional theory calculations. Two types of basis functions are commonly used, *i.e.* Gaussian type orbitals (GTO) and Slater type orbitals (STO). STO gives an exact solution to the Schrödinger equation, and can be used for atomic and diatomic systems requiring high accuracy. GTO basis sets require more functions to describe the wave function. In contrast to the increasing number and universal usage of GTO basis sets, calculations with the Amsterdam Density Functional programmes can be done with the STO basis set instead.

One notation of a basis set is to specify the number of functions (ζ) used. The term zeta (Z, ζ) describes the exponent of STO basis functions. In programs such as the Amsterdam Density Functional theory (ADF) the notation double zeta (DZ) and triple zeta (TZ) to highlight the fact that the valence basis functions are treated as a linear combination of two or three STOs respectively to present a single atomic orbital.The DZ basis set uses two *s*-functions for hydrogen (1s and 1s′), four *s*-functions (1s, 1s′, 2s and 2s′) and two sets of *p*-functions (2p and 2p′) for the first row elements, and six *s*-functions and four sets of *p*-functions for the second row elements. The smallest basis set is single zeta (SZ), and a triple zeta basis set needs three times the number of functions than in SZ.

Polarization functions (P), known as higher angular momentum functions, describe most of the important charge polarization effects. The polarization functions represent charge densities that are not locally spherically symmetric around the atomic nucleus and as such the polarization

---

[19] Young, D. C.; *Computational Chemistry, A Practical Guide for Applying Techniques to Real-World Problems*, Wiley and Sons, New York, **2001**, p78-89

[20] Jensen, F.; *Introduction to Computational Chemistry*, 2nd edition, John Wiley & Sons, England, **2007**, p192-198

functions are important for hydrogen bonding and other agnostic-type interactions. For example, DZP stands for a double zeta basis set with polarization functions.

2.2.4 Symmetry and Point Groups[21]

Molecular symmetry describes the symmetry in molecules. The operations to obtain symmetries are called symmetry elements (see **Table 2.2**). After applying an operation according to any symmetry element, the molecule must be equivalent to the molecule before that operation.

Table 2.2: Five types of symmetry elements.

Symmetry Element	Description
Identity (E)	The corresponding symmetry element is the whole molecule; every molecule has at least this symmetry element.
Rotational axis (C_n)	Rotation by 360°/n leaves the molecule unchanged. Some molecules have more than one C_n axis, and then the one with the highest value of n is called the principal axis. Rotations are counterclockwise about the axis by convention.
Plane of symmetry (σ)	Reflection in the plane leaves the molecule unchanged. In a molecule that also has an axis of symmetry, a mirror plane that includes the axis is called a vertical mirror plane and is labelled σ_v, while a mirror plane perpendicular to the axis is called a horizontal mirror plane and is labelled σ_h. A vertical mirror plane that bisects the angle between two C_2 axes is called a dihedral mirror plane, σ_d.
Inversion center (i)	A center of symmetry exists in the molecule, and inversion through the center of symmetry (i) leaves the molecule unchanged.
Rotatory reflection axis (S_n)	This operation consists of rotation by an angle of 360°/n about the axis, followed by reflection in a plane perpendicular to the axis.

A molecule can have more than one symmetry element. Point groups are groups consisting of various symmetry elements. The Schoenflies notation is used here for describing these point groups. General molecular point groups are listed in **Table 2.3**. All point groups contain the

---

[21] Atkins, P.; de Paula, J.; *Atkins' Physical Chemistry*, 8th edition, W.H. Freeman and Company, New York, **2006**, p404-411

identity operation (E), therefore this symmetry element remains unmentioned if other symmetry elements exist in the point group.

Table 2.3: General types of point groups.

Point group	Description
C_1	Contains only the Identity (E).
C_i	Contains a center of inversion (i).
C_s	Contains a plane of symmetry (σ).
C_n	Contains an n-fold rotational axis (C_n).
C_{nv}	Contains an n-fold rotational axis (C_n) and n vertical mirror planes (σ_v).
C_{nh}	Contains an n-fold rotational axis (C_n) and n horizontal mirror planes (σ_h). C_{2h} automatically implies an inversion center (i).
D_n	Contains an n-fold axis of rotation (C_n) and n 2-fold rotations (C_2) about axes perpendicular to the principal axis.
D_{nh}	Contains an n-fold axis of rotation (C_n), n 2-fold rotations (C_2) about axes perpendicular to the principal axis and a horizontal mirror plane (σ_h).
D_{nd}	Contains an n-fold axis of rotation (C_n), n 2-fold rotations (C_2) about axes perpendicular to the principal axis and a dihedral mirror plane (σ_d).
S_n	Contains one S_n axis. Previous point groups have priority over this point group, e.g. S_1 should be C_1 and S_2 should be C_2.
The following groups are cubic groups, containing more than one principal axis. T stands for tetrahedral groups and O stands for octahedral groups:	
T_d	Contains four C_3 axes, three C_2 axes and six dihedral mirror planes (σ_d).
T	Contains four C_3 axes and three C_2 axes.
T_h	Contains four C_3 axes, three C_2 axes and an inversion center (i).
O_h	The group of the chiral octahedron.
O	Same as O_h but without planes of symmetry, achiral octahedron.

2.2.5 Ligand Field Splitting[22]

Ligand field theory provides understanding of bonding and electronic properties of complexes and compounds formed by the transition metals. In the form of a free ion, the central metal (M^{m+}) has five equivalent d-orbitals. But in a ligand field (*i.e.* when ligands are attached to the metal), the *d* orbitals split into various groups. This splitting of *d* orbitals can be seen from the energy-level diagram, which shows the grouping in different crystal fields (see **Figure 2.8**): In octahedral complexes, d_{xy}, d_{yz} and d_{zx} are degenerate orbitals (at lower energy), and this group of orbitals is called the t_{2g} group of orbitals; while the two d_{x2-y2} and d_{z2} orbitals form an equal but unfavoured group (higher energy), called the e_g orbitals. The energy difference between these orbital groups is Δ_o, in an octahedral ligand field. In contrast to octahedral complexes, tetrahedral complexes have an opposite arrangement of d-orbitals for the metal center, where the t_2 group of orbitals (d_{xy}, d_{yz} and d_{zx}) is more favoured than the *e* orbitals (d_{x2-y2} and d_{z2}). This energy difference between the orbital groups is termed Δ_t, in a tetrahedral ligand field. If the octahedral and tetrahedral complexes have the same cation, anion and cation-anion distance, Δ_t is four ninths of Δ_o. Square planar complexes undergo more complicated *d*-orbital splitting, until four energy levels are reached.
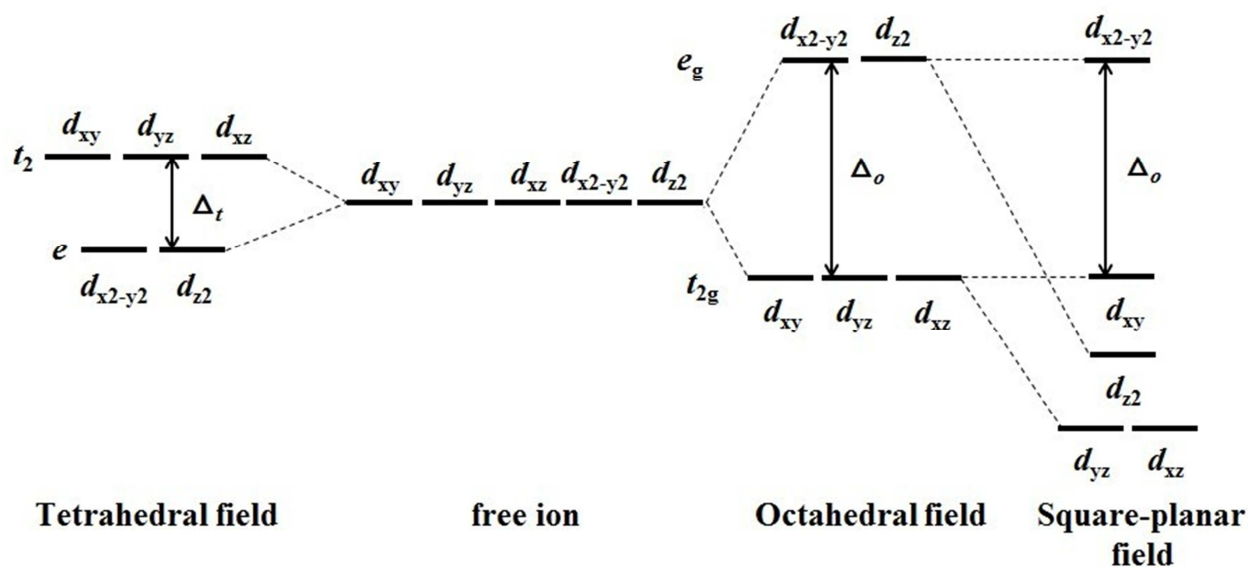
Figure 2.8: Energy-level diagram of the splitting of *d* orbitals in the metal center in octahedral, tetrahedral and square-planar complexes.

[22] Cotton, F. A.; Wilkinson, G.; Gaus, P. L.; *Basic Inorganic chemistry*, 3rd Edition, John Wiley and Sons, Canada, **1995**, p503-518

Due to the splitting of orbitals, the d-electron filling in complexes is then also different to the d-electron filling in a free metal ion. For example, in octahedral complexes, for a metal center which has 1, 2, 3, 8, 9 or 10 d electrons (d^1, d^2, d^3, d^8, d^9 and d^{10} species), the splitted d orbitals are filled in a unique way (see below **Figure 2.9**). For the remaining d^4, d^5, d^6 and d^7 species, two types of configurations are possible, namely high-spin and low-spin configurations (see **Figure 2.10**). The Pauli exclusion principle in the case of two electrons residing in the same orbital, electrons must have opposite spins or stay unpaired in different orbitals. Same as exchange-correlation energy (see **Section 2.2.2**), pairing energy describes the energy needed to pair two electrons with opposite spins. In principle to decrease electronic repulsion, when the pairing energy (P) is larger than the energy difference Δ_o in octahedral complexes, electrons tend to stay unpaired until all five d orbitals have been filled with an electron. However when the pairing energy (P) is smaller than the energy difference Δ_o, electrons tend to fill the lowest-energy orbitals.
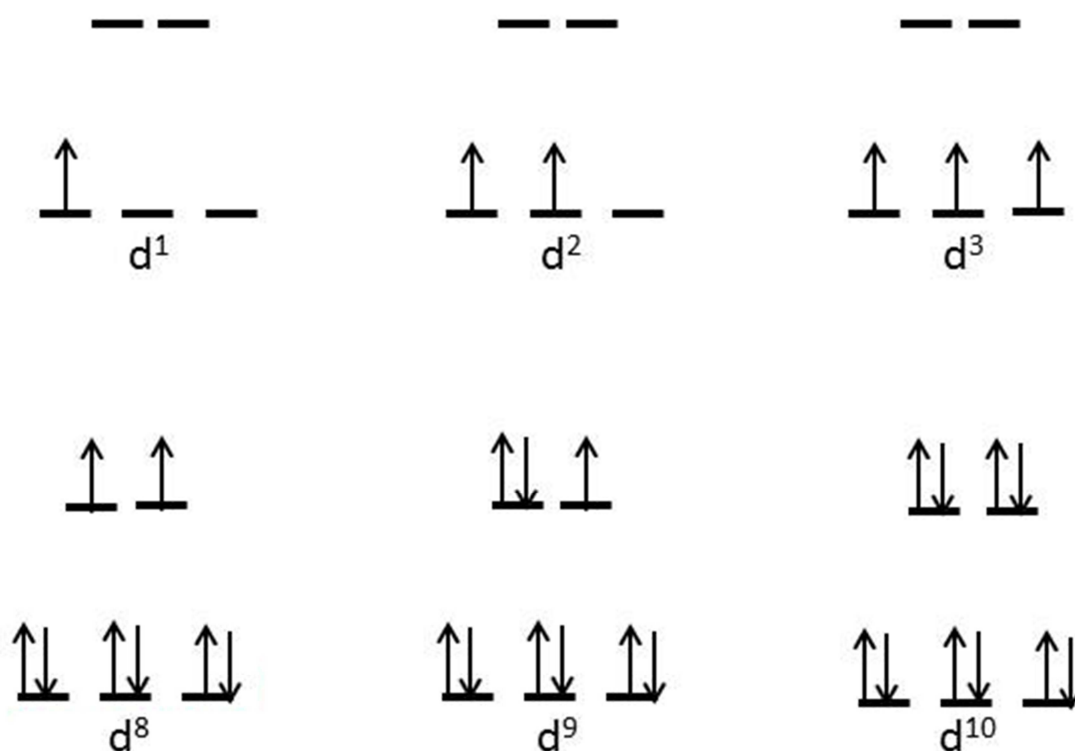
Figure 2.9: Electron configurations of d^1, d^2, d^3, d^8, d^9 and d^{10} species in octahedral fields.
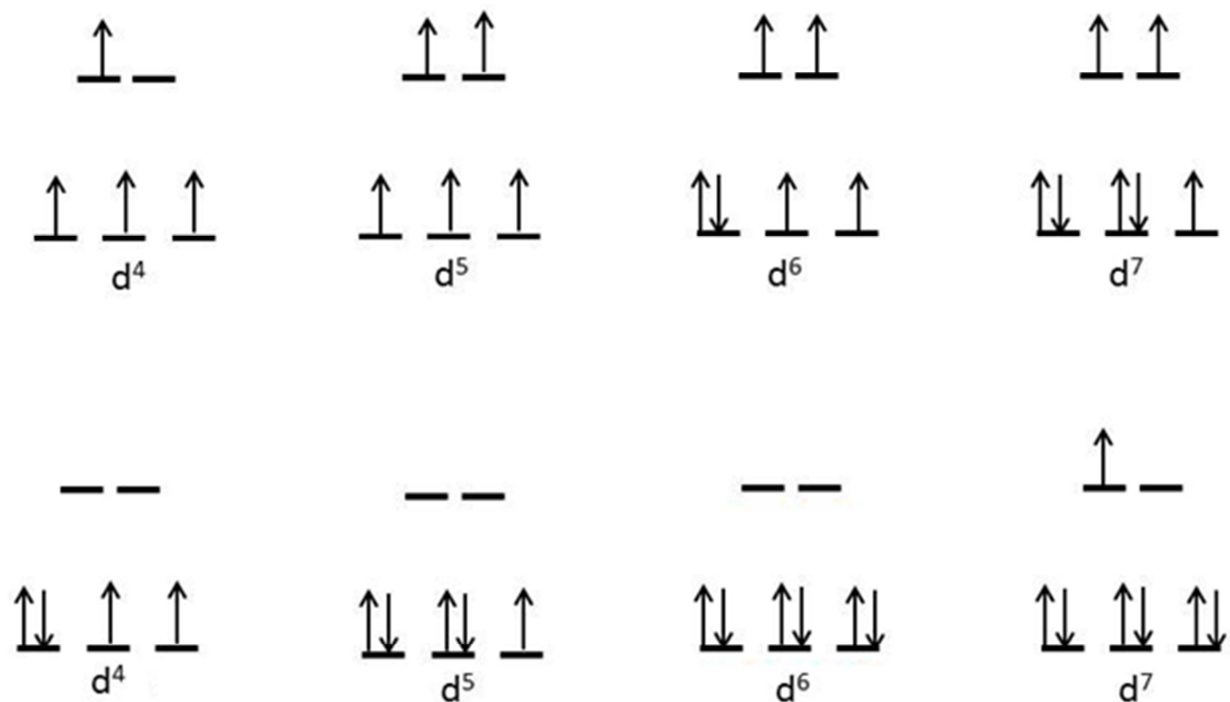
High Spin

Figure 2.10: Two possible electron configurations for d^4, d^5, d^6 and d^7 species in octahedral fields. The top row shows the high-spin d-electron configuration, while the bottom row shows the low-spin d-electron configuration.

The Cr(β-diketonato)$_3$ and Co(β-diketonato)$_3$ complexes of this study are d^3 and d^6 complexes respectively. According to the ligand field splitting for an octahedral complex, the Cr(β-diketonato)$_3$ complex will have 3 unpaired electrons (S = 3/2 or a quartet). However, the Co(β-diketonato)$_3$ complex must first be tested whether it is a high-spin (S = 4/2 or a quintet) or a low-spin (S = 0 or a singlet) complex, before the electron configuration can be specified.

2.3 X-ray Crystallography[23]

X-ray crystallography is a method used to determine the atomic and molecular structure of a crystal by measuring the angles and intensities of diffraction of incident X-ray caused by crystalline stoms.

In an X-ray diffraction measurement, a crystal is mounted on a gradually rotating goniometer while being bombarded with X-rays. According to Bragg's law for X-ray diffraction ($2d \sin\theta = n\lambda$, where θ is known as the Bragg angle, λ is the wavelength of the X-rays and d is the plane spacing,see **Figure 2.11**), a diffraction pattern of regularly spaced spots known as reflections is obtained. **Figure 2.12** gives an example of X-ray diffraction pattern of ammonium oxalate monohydrate. A three-dimentional picture of the electron density within the crystal is obtained by applying Fourier transformation on the reflections. **Figure 2.13** shows an example of a 3D electron density map of a planar molecule. Finally, these data are refined computationally with complementary chemical information to give a model of atomic arrangement called crystal structure.
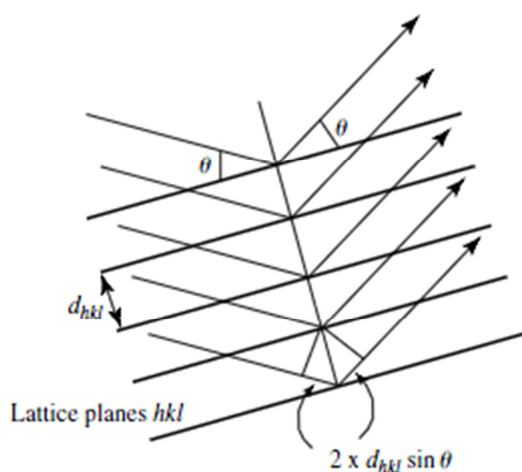
Figure 2.11: Diffraction of X-rays from crystal lattice planes illustrating Bragg's law. (Reprinted (adapted) with permission from Blake, A. J.; Clegg, W.; Cole, J. M.; Peter Main, J. S. O. E.; Parsons, S.; Watkin, D. J.; *Crystal Structure Analysis, Principles and Practice*. 2nd Edition, Oxford University Press, Copyright (2009) Oxford).

---

[23] Blake, A. J.; Clegg, W.; Cole, J. M.; Peter Main, J. S. O. E.; Parsons, S.; Watkin, D. J.; *Crystal Structure Analysis, Principles and Practice*. 2nd Edition, **2009**, 1-8
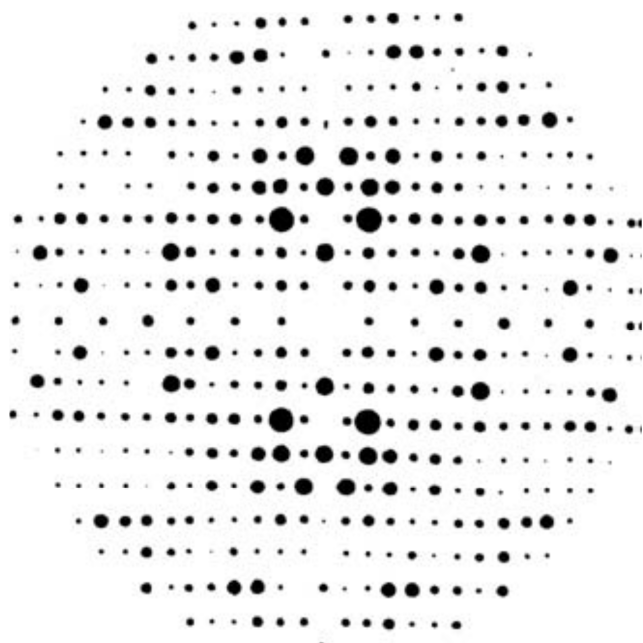
Figure 2.12: Part of the X-ray diffraction pattern of ammonium oxalate monohydrate. (Reprinted (adapted) with permission from Blake, A. J.; Clegg, W.; Cole, J. M.; Peter Main, J. S. O. E.; Parsons, S.; Watkin, D. J.; *Crystal Structure Analysis, Principles and Practice*. 2nd Edition, Oxford University Press, Copyright (2009) Oxford).
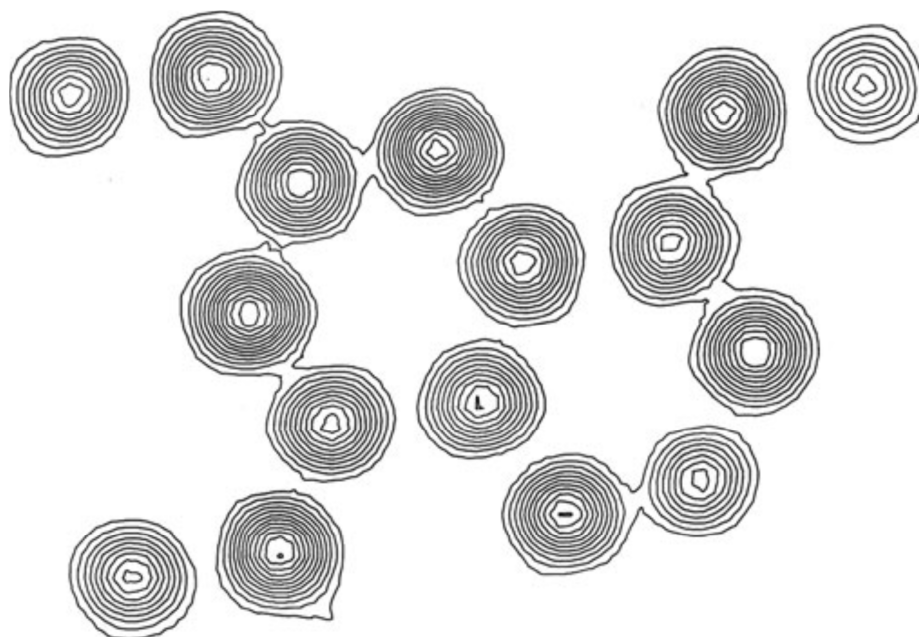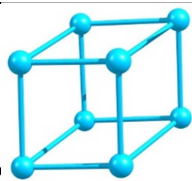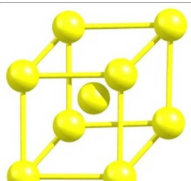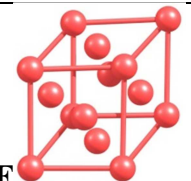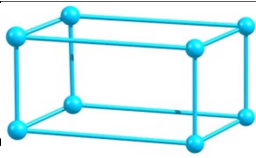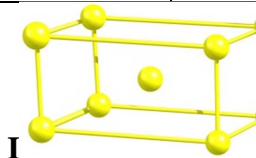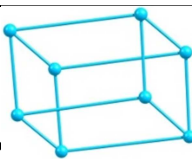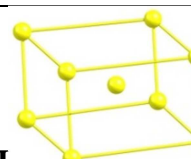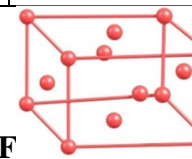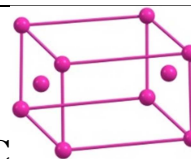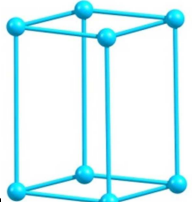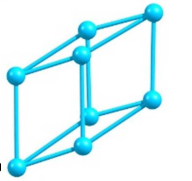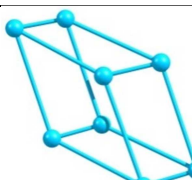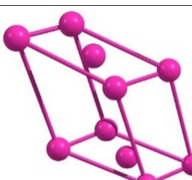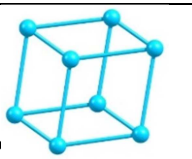
Figure 2.13: A section of the 3D electron density map of a planar molecule. (Reprinted (adapted) with permission from Blake, A. J.; Clegg, W.; Cole, J. M.; Peter Main, J. S. O. E.; Parsons, S.; Watkin, D. J.; *Crystal Structure Analysis, Principles and Practice*. 2nd Edition, Oxford University Press, Copyright (2009) Oxford).

All refined crystal structures have 7 possible crystal systems including 14 Bravais lattices. **Table 2.4** shows 7 crystal systems and 14 Bravais lattices. Restrictions are applies to the vectors along edge of the lattice unit cell (a, b and c) and interfacial angles α (between edges b and c), β (between edges a and c) and γ (between edges a and b).

Table 2.4: The seven crystal systems and fourteen Bravais lattices with restrictions.

Crystal systems	Bravais lattices
Cubic $a = b = c$ $\alpha = \beta = \gamma = 90°$	
Tetragonal $a = b \neq c$ $\alpha = \beta = \gamma = 90°$	
Orthorhombic $a \neq b \neq c$ $\alpha = \beta = \gamma = 90°$	
Hexagonal $a = b \neq c$ $\alpha = \beta = 90°$ $\gamma = 120°$	
Trigonal $a = b = c$ $\alpha = \beta = \gamma \neq 90°$	
Monoclinic $a \neq b \neq c$ $\alpha = \gamma = 90°$ $\beta \neq 120°$	
Triclinic $a \neq b \neq c$ $\alpha \neq \beta \neq \gamma \neq 90°$	

- P = Primitive; I = Body-Centered; F = Face-Centered; C = Side-Centered

One parameter worthmention is atomic displacement parameters (ADP). Ellipsoids are used in crystallography to indicate the magnitudes and directions of the thermal vibration of atoms in crystal structures. These magnitudes and directions in space are usually anisotropic, therefore atomic displacement parameters are also called anisotropic parameters

2.4 Tris(β-diketonato)chromium(III) Complexes

2.4.1 Synthesis and Characterization

The synthesis of tris(β-diketonato)chromium(III) complexes is based on the synthetic method for tris(2,4-pentadionato)chromium(III), (Cr(acac)$_3$). In 1957, Fernelius and Blanch synthesized Cr(acac)$_3$ with chromium(III) chloride-6-hydrate with urea and acetylacetone[24] (see **Scheme 2.1**). In this method, urea (excess) and acetylacetone are added to the solution of chromium(III) chloride, and the reaction mixture is heated overnight over a steam-bath. Ammonia released from the hydrolysed urea, completes the formation of the product.
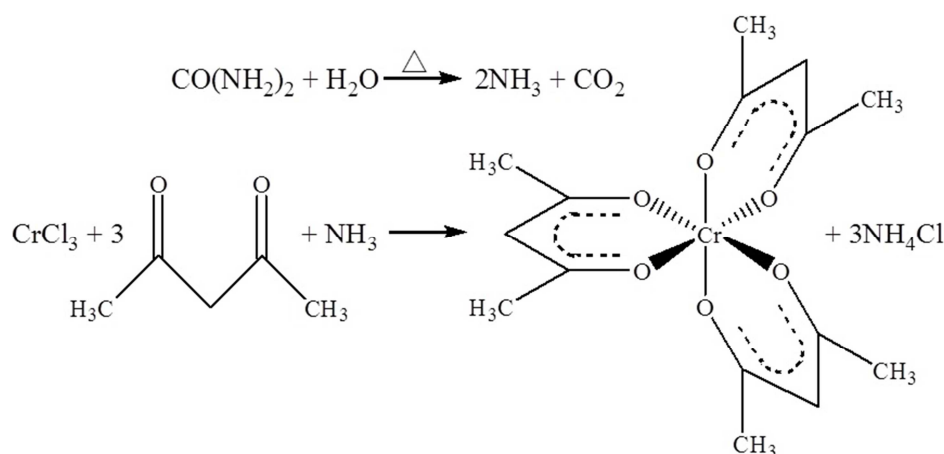
Scheme 2.1: Synthesis of Cr(acac)$_3$, as proposed by Fernelius and Blanch.

Rahman and his co-workers recently (2010) established a faster synthetic method[25] (see **Scheme 2.2**). Concentrated chromium(III) chloride solution is slowly added dropwise to an acetylacetone

---

[24] Fernelius, W.C.; Blanch, J. E.; *Inorg. Syn.*, **1957**, *5,* 130-131

[25] Rahman, A. K.; Hossain, M. B.; Halim, M. A.; Chowdhury, D. A.; Salam, M. A.; *Afr. J. Pure Appl. Chem.*, **2010**, *4,* 216-220

solution, followed by dropwise addition of concentrated sodium acetate solution, until complete precipitation has occurred.
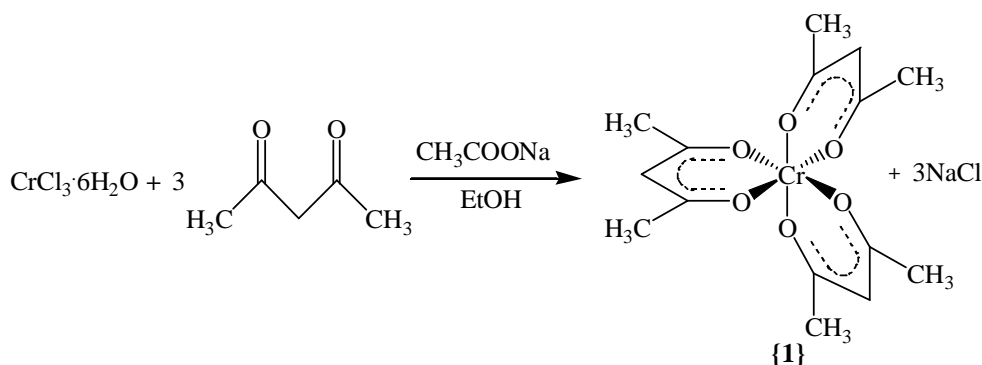
Scheme 2.2: Synthesis of Cr(acac)$_3$, by Rahman, *et al.*

When one or both methyl groups on each ligand are substituted by different functional groups, the β-diketonato ligand becomes unsymmetrical. Coordination between an unsymmetrical β-diketonato ligand and the Cr^{III} cation, leads to two possible isomers: a facial isomer (*fac*) or a meridional isomer (*mer*), (see **Scheme 2.3**). A facial isomer (*fac*) contains three identical substituents (from the three different unsymmetrical ligands), each occupying the vertices of one face of the octahedron of the complex. On the other hand, a meridional isomer (*mer*) contains a plane passing through the central metal atom, which is formed by each of three identical substituents on the three different unsymmetrical ligands.

fac-isomer   *mer*-isomer
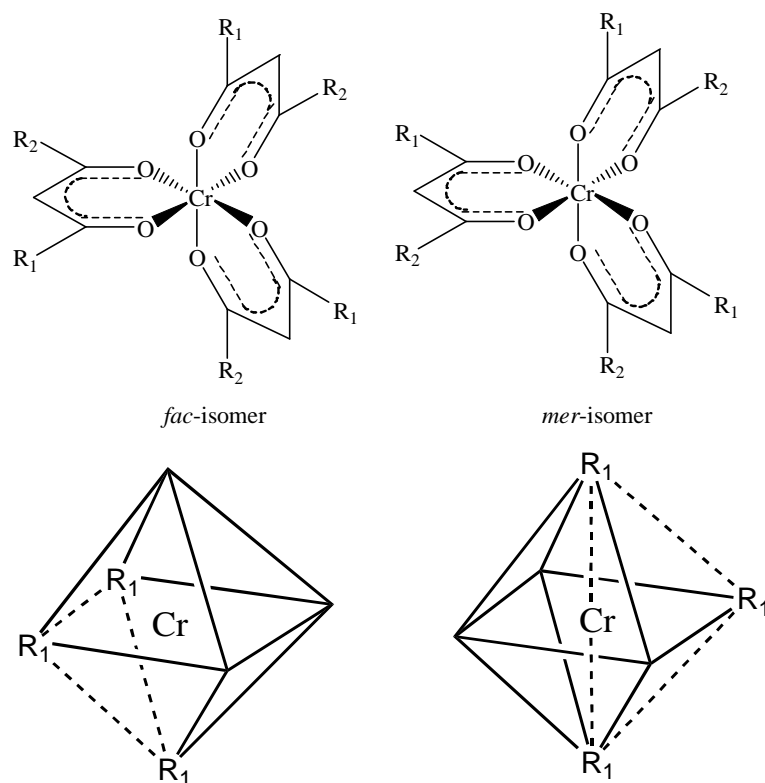
Scheme 2.3: Illustration of the *fac*-isomer and *mer*-isomer.

The synthesis of tris(1,1,1,5,5,5-hexafluoro-2,4-pentadionato)chromium(III), (Cr(hfaa)$_3$), is an exception from the general synthetic methods mentioned above. In 1993, Elisabeth Bouwman and her co-workers discovered that the ligand Hhfaa reacts with water.[26] Doubly hydrated Hhfaa becomes a tetraol (a tetradentate linkage ligand), which coordinates to a metal center. In 1965, Morris and Aikens discovered a direct method to synthesize Cr(hfaa)$_3$[27]: Finely powdered potassium dichromate and the ligand Hhfaa were refluxed in carbon tetrachloride for 3 hours. Cr(hfaa)$_3$ was obtained by filtration and evaporation of the solution to dryness. In 2007, Harada and Girolami also used a direct synthesis, which involved the bis(trimethylsilyl)amido complex (Cr[N(SiMe$_3$)$_2$]$_2$(thf)$_2$), (thf = tetrahydrofuran) and Hexafluoroacetylacetone.[28] The structural parameters of complexes Cr(acac)$_3$ and Cr(hfaa)$_3$ were reported in literature and are summarized in **Table 2.5** and **Table 2.6**. The Cr-O bonds of Cr(acac)$_3$ and the Cr-O bonds of Cr(hfaa)$_3$ are similar within experimental accuracy. The Cr(β-diketonato)$_3$ crystals were all found to be octahedral, with six similar Cr-O bonds and three nearly 90° O-Cr-O angles.

---

[26] Bouwman, E.; Caulton, K. G.; Christou, G.; Folting, K.; Gasser, C.; Hendrickson, D. N.; Huffman, J. C.; Lobkovsky, E. B.; Martin, J. D.; Michel, P.; Tsai, H.; Xue, Z.; *Inorg. Chem.*, **1993**, *32*, 3463-3470

[27] Morris, M. L.; Aikens, D. A.; *Nature*, **1965**, *207*, 631-632

[28] Harade, Y.; Girolami, G. S.; *Polyhedron*, **2007**, *26*, 1758-1762

Table 2.5: Cr – O bond length for reported structural parameters of Cr(acac)₃ and Cr(hfaa)₃.

Complex	Cr(acac)₃, R₁ = R₂ = CH₃						Average	Ref
	1.962	1.960	1.946	1.946	1.955	1.963	1.955(8)	**29**
	1.956(1)	1.957(2)	1.939(2)	1.950(1)	1.957(2)	1.963(2)	1.954(8)	**30**
	1.950(3)	1.959(3)	1.951(3)	1.962(3)	1.951(3)	1.942(4)	1.953(7)	**31**
	1.941(2)	1.955(2)	1.965(2)	1.961(2)	1.961(2)	1.957(2)	1.957(8)	
	1.965(2)	1.944(2)	1.957(2)	1.958(2)	1.969(2)	1.970(2)	1.961(10)	
Cr – O	1.957(2)	1.948(1)	1.954(2)	1.971(2)	1.966(2)	1.969(2)	1.961(9)	
Bond	1.956(2)	1.962(2)	1.961(2)	1.965(2)	1.968(2)	1.970(2)	1.964(5)	**32**
length	1.966(2)	1.946(1)	1.964(2)	1.968(2)	1.970(2)	1.970(2)	1.964(9)	
	1.956(2)	1.956(2)	1.960(2)	1.967(2)	1.967(2)	1.967(2)	1.962(5)	
	1.950(2)	1.965(2)	1.957(2)	1.975(2)	1.968(2)	1.963(2)	1.963(9)	
	1.961(5)	1.966(5)	1.947(4)	1.961(5)	1.964(4)	1.966(5)	1.961(7)	**33**
	1.966(5)	1.963(4)	1.965(3)	1.953(4)	1.963(6)	1.963(6)	1.962(5)	
						Average all	1.960(8)	
	Cr(hfaa)₃, R₁ = R₂ = CF₃						Average	Ref
	1.960(1)	1.950(1)	1.959(1)	1.956(1)	1.951(1)	1.964(1)	1.957(5)	**34**
	1.942(6)	1.956(5)	1.942(5)	1.955(6)	1.944(7)	1.956(5)	1.949(7)	
	1.924(6)	1.924(6)	1.924(8)	1.924(6)	1.924(6)	1.924(8)	1.924(0)	**28**
						Average all	1.943(15)	

Table 2.6: O - Cr – O angle for reported structural parameters of Cr(acac)₃ and Cr(hfaa)₃.

Complex	Cr(acac)₃, R₁ = R₂ = CH₃			Average	Ref
	90.7	91.0	91.7	91.1(5)	**29**
	90.5	91.1	91.7	91.1(6)	**30**
	91.3	91.3	90.4	91.0(5)	**31**
	91.3	91.5	90.6	91.1(5)	
	90.7	91.4	91.5	91.2(4)	
	90.7	91.6	91.5	91.3(5)	
O - Cr – O	90.9	91.1	91.3	91.1(2)	**32**
Angle	90.4	91.5	91.5	91.1(6)	
	91.1	90.9	91.2	91.1(2)	
	91.2	91.1	91.2	91.1(1)	
	90.9	91.1	91.2	91.1(1)	**33**
	91.0	89.9	90.5	90.5(5)	
			Average all	91.1(4)	
	Cr(hfaa)₃, R₁ = R₂ = CF₃			Average	Ref
	89.7	88.5	89.9	89.4(7)	**34**
	89.7	89.7	89.7	89.7(0)	**28**
	89.4	89.4	89.4	89.4(0)	
			Average all	90.6(2)	

2.4.2 Electrochemical Studies

2.4.2.1 Tris(acetylacetonato)chromium(III), Cr(acac)$_3$

In 1984, Anderson *et al.* reported a two-step reduction process (quasi-reversible $Cr^{III} \rightarrow Cr^{II}$ and $Cr^{II} \rightarrow Cr^{I}$) and a two-step oxidation process ($Cr^{III} \rightarrow Cr^{IV}$ and $Cr^{IV} \rightarrow Cr^{V}$) for chromium(III) acetylacetonate.[29] In 2010, Liu *et al.* reported fine cyclic voltammograms of Cr(acac)$_3$,[30] (see **Figure 2.14**).

Anderson *et al.* proposed a dissociation mechanism for the reduction process. On grounds of the observance of $Cr^{II}(acac)_2$ by spectroelectrochemial studies, he proposed that the reduction processes caused the dissociation of ligands (**Equation 2.6**):

Equation 2.6: $Cr^{III}(acac)_3 + e^- \leftrightarrow [Cr^{II}(acac)_3]^- \leftrightarrow Cr^{II}(acac)_2 + acac^-$
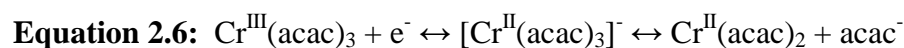
Liu focussed on the oxidation of $Cr^{III}(acac)_3$. On grounds of electrochemical studies with additional acetylacetone in support solution, he proposed that the oxidation processes caused the ligand dissociation (**Equation 2.7**):

Equation 2.7: $Cr^{III}(acac)_3 \leftrightarrow [Cr^{IV}(acac)_3]^+ + e^- \leftrightarrow [Cr^{IV}(acac)_2]^{2+} + acac^-$
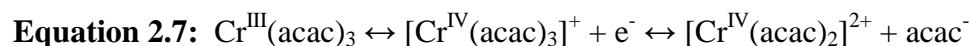
[29] Anderson, C. W.; Lung, K. R.; *Inorg. Chim Acta*, **1984**, *85*, 33-36

[30] Liu, Q.; Shinkle, A. A.; Li, Y.; Monroe, C. W.; Thompson, L. T.; Sleightholme, A. E. S.; *Electrochem.Commun.*, **2010**, *12*, 1634-1637
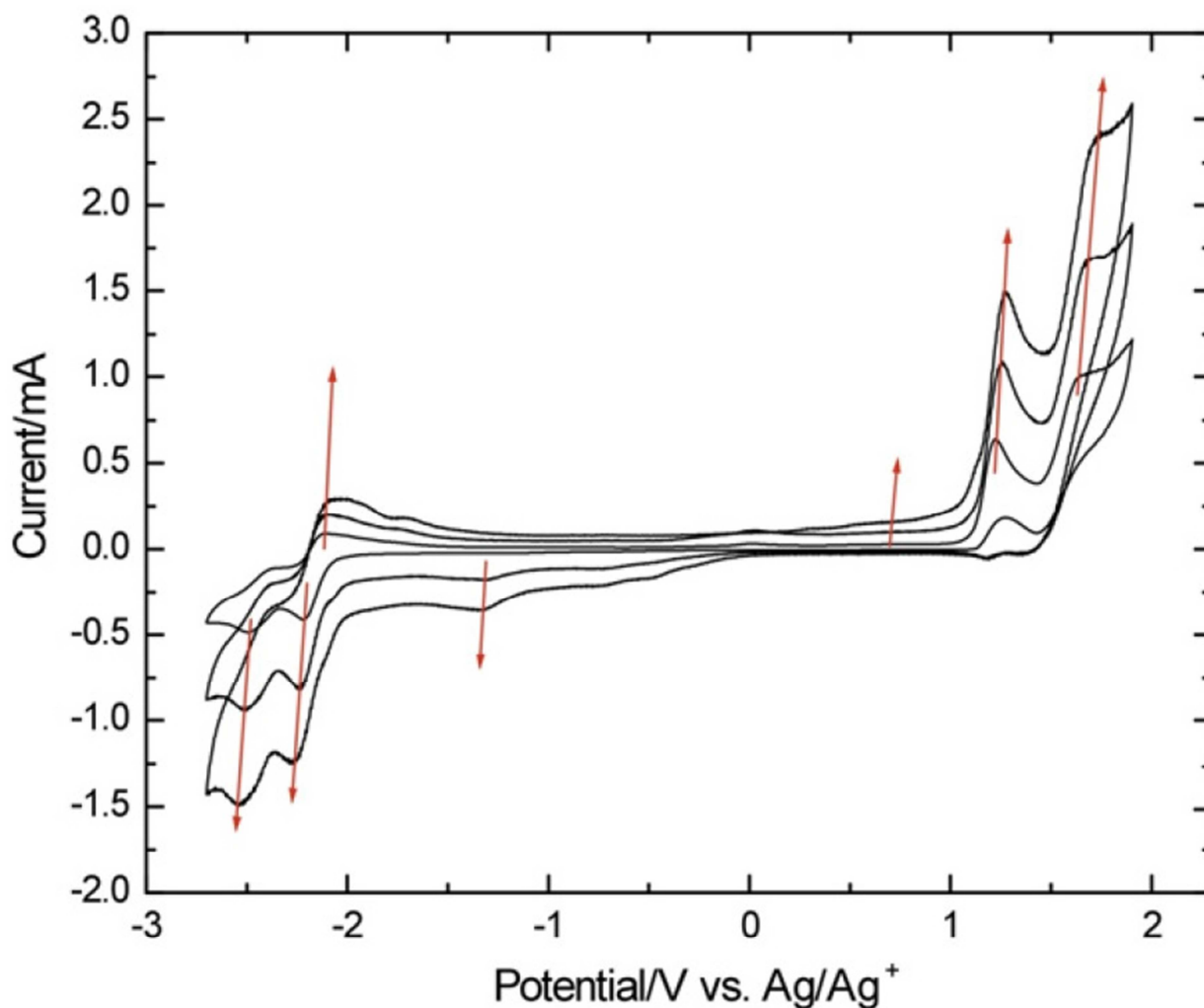
Figure 2.14: The cyclic voltammograms of Cr(acac)$_3$, as reported by Liu *et al.*[30] Measured at a glassy carbon electrode, in 0.05 M Cr(acac)$_3$ and 0.5 M TEABF$_4$, in CH$_3$CN, at scan rates of 50, 200 and 500 mV·s^{-1}. Arrows show direction of increasing scan rate; at room temperature. (Reprinted (adapted) with permission from Liu, Q.; Shinkle, A. A.; Li, Y.; Monroe, C. W.; Thompson, L. T.; Sleightholeme, A. E. S.; *Electrochemistry Communication*, **2010**, *12*, 1634-1637. Copyright (2010) Elsevier).

The quasi-reversible Cr^{III} ↔ Cr^{II} reduction process becomes more chemically reversible when an excess free ligand (Hacac) is present. Urbanczyk reported a chemically reversible Cr^{III} ↔ Cr^{II} process, with 40-fold excess of free ligand present.[31] The free ligand inhibits the ligand dissociation (formation of free ligand), therefore the electrochemical process is driven to the left of **Equation 2.6**.

---

[31] Urbanczyk, A.; Debek, E.; Kalinowski, M. K.; *Journal of Electroanalytical Chemistry*, **1995**, *389*, 141-148

2.4.2.2 Tris(β-diketonato)chromium(III) Complexes[32]

In 1988, Tsiamis *et al.* reported electrochemical research on a series of Cr(β-diketonato)$_3$ complexes (see **Table 2.7** and **Figure 2.15**). His studies focused on the quasi-reversible Cr^{III} ↔ Cr^{II} redox process. Tsiamis observed that electron-donating substituents (R$_1$, R$_2$) on the β-diketonato ligands hinder reduction (more negative potential), while electron-withdrawing substituents (R$_1$, R$_2$) on the β-diketonato ligands enhance reduction (more positive potential).

Table 2.7: Reduction potentials, cyclic voltammetric cathodic and anodic peak values of first reduction, and Hammett Σσ$_\chi$ constants for tris(β-diketonato)chromium(III) chelates for the Cr^{III} ↔ Cr^{II} redox process, as reported by Tsiamis *et al.* [32] Measured at a hanging Hg electrode, in 0.1 M tetraethylammonium perchlorate (TEAP) as supporting electrolyte, against saturated calomel electrode (SCE) in acetone or acetonitrile.

Complex	$E_{1/2}$ (V)[a]	P_c (V)[b]	P_a (V)[b]	$(P_c+P_a)/2$ (V)	P_c-P_a (V)	Σσ$_x$[c]
Cr(bda)$_3$, [1]	–1.68	—	—	—	—	-0.17
Cr(acac)$_3$, [2]	–1.94	—	—	—	—	–0.34
Cr(Cl–acac)$_3$, [3]	–1.57	–1.62	0.00	–0.81	–1.62	0.03
Cr(Br–acac)$_3$, [4]	–1.58	–1.63	–0.30	–0.97	–1.33	0.05
Cr(NO$_2$–acac)$_3$, [5]	–1.15	–1.15	0.35	–0.40	–1.50	0.37
Cr(SCN–acac)$_3$. [6]	–1.21	–1.17	–1.20	–0.90	–0.54	0.28
Cr(CN–acac)$_3$, [7]	–1.21	–1.26	–1.20	–1.23	–0.06	0.34
Cr(tfaa)$_3$, [8]	–1.06	—	—	—	—	0.38
Cr(bzac)$_3$, [9]	–1.69	–1.71	–1.65	–1.68	–0.06	–0.16
Cr(Br–bzac)$_3$, [10]	–1.28	–1.24	–0.12	–0.68	–1.12	0.23
Cr(NO$_2$–bzac)$_3$, [11]	–1.00	–1.09	0.45	–0.32	–1.54	0.55
Cr(SCN–bzac)$_3$, [12]	–1.02	–1.06	–0.51	–0.78	–0.54	0.46
Cr(bztfac)$_3$, [13]	–0.89	–0.90	–0.84	–0.87	–0.06	0.56
Cr(dbm)$_3$, [14]	–1.63	–1.65	–1.59	–1.62	–0.06	0.02
Cr(Br–dbm)$_3$, [15]	–1.18	—	—	—	—	0.41
Cr(NO$_2$–dbm)$_3$, [16]	–0.81	—	—	—	—	0.73
Cr(SCN–dbm)$_3$, [17]	–0.70	—	—	—	—	0.64
Cr(dpm)$_3$, [18]	–2.15	—	—	—	—	–0.40
Cr(Cl–dbm)$_3$, [19]	–1.61	—	—	—	—	–0.03
Cr(NO$_2$–dbm)$_3$, [20]	–1.21	—	—	—	—	0.31

[32] Tsiamis, C.; Hadjikostas, C. C.; Karageorgiou, S.; Manoussakis, G.; *Inorganica Chimica Acta*, **1988**, *143*, 17-23

Cr(hfaa)$_3$, [21]	–0.20	—	—	—	—	1.10
Cr(hfod)$_3$, [22]	–1.13	—	—	—	—	0.41

a. $E_{1/2}$ is the first reduction potential, obtained from polarograms.

b. P_c and P_a are the cathodic and anodic peak values, obtained from cyclic voltammetry, respectively.

c. $\Sigma\sigma_\chi$ is the sum of the Hammett σ constants of the complexes (see Section 2.4.2.3).

2.4.2.3 Hammett constants, electronegativity and pK_a

In 1937, Louis P. Hammett discovered that a substituent in the *meta-* or *para-* position of benzene has a linear effect on the relationship between the rate of base-catalysed hydrolysis of a group of ethyl esters to form a series of carboxylic acids, and the equilibrium position of the ionisation in water of the corresponding group of acids. The concept of Hammett-substituent constants (σ) has been developed from this fact.[33] The Hammett constants σ_R are empirical constants that relates the log of rate or equilibrium constants for reactions of the substituted (k_R, R = substituent) and the unsubstituted (k_H, no substituent) benzoic acid derivatives to the reaction rate ρ: log (k_R/k_H) = (σ_R)ρ. σ_R depends solely on the nature and position of the substituent R.[34] The β-diketonato ligands form a six-membered ring with the metal center, with the substituents R$_1$ and R$_2$ in the *meta*-position to the metal center (see **Scheme 2.3**). The *meta*-Hammett constant can thus be used in relationships involving metal-β-diketonato complexes.[35] The core-electron binding energy (measured using X-ray photoelectron spectroscopy on free and supported metal clusters) is linearly correlated to the Hammett substituent constants.[36,37] In this study, the core-electron binding energy is affected by the substituents R$_1$ and R$_2$ on the three β-diketonato ligands. Tsiamis *et al.*[32] observed a linear correlation between the reduction potentials ($E_{1/2}$ in mV, measured in acetone or acetonitrile *versus* SCE) and the sum of the Hammett constants, Σσ (see **Figure 2.15**). The linear correlation obtained is given in **Equation 2.8**:

Equation 2.8: $E_{1/2}$ (V) = – 1.62 + 1.14 Σσ

[33] Hammett, L. P.; *J. Am. Chem. Soc.*, **1937**, *59*, 96-103

[34] McDaniel, D. H.; Brown, H.C.; *J. Org. Chem.*, **1958**, *420*, 420-427

[35] Lintvedt, R.L.; Russell, H.D.; Holtzclaw, H.F.; *Inorg. Chem.*, **1966**, *5*, 1603-1607

[36] Lindberg, B.; Svensson, S.; Malmquist, P. A.; Basilier, E.; Gelius, U.; Siegbahn, K.; *Chem. Phys. Lett.*, **1976**, *40*, 175-179

[37] Wertheim, G. K.; *Z. Phys. B - Condensed Matter*, **1987**, *66*, 53-63

This equation is valid when acetone or acetonitrile is used as the solvent in the electro-chemical measurements.
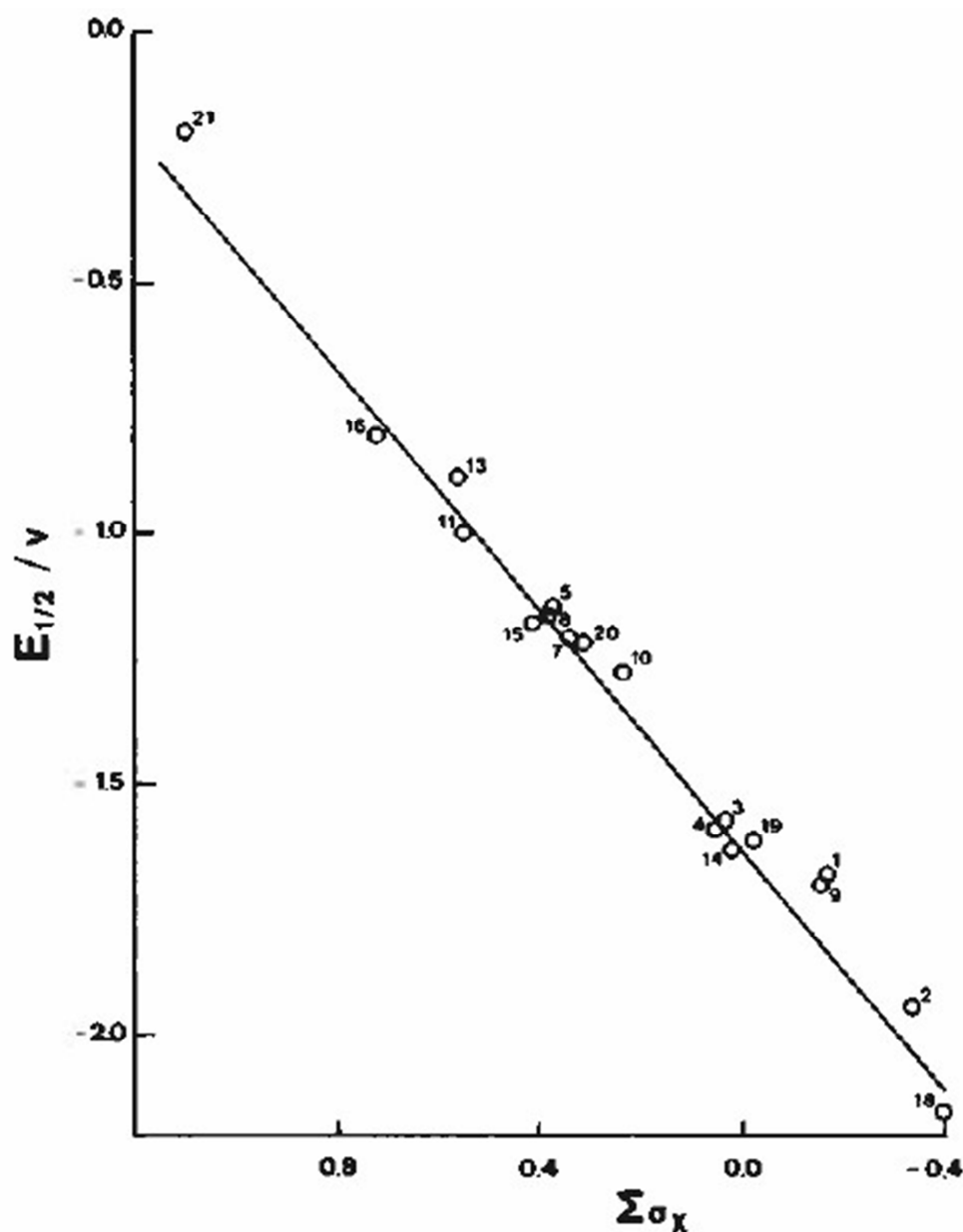
Figure 2.15: Correlation of $E_{1/2}$ with the sum of the Hammett σ constants of the Cr(β-diketonato)$_3$ series, reported by Tsiamis *et al.*[32] (Reprinted (adapted) with permission from Tsiamis, C.; Hadjikostas, C. C.; Karageorgiou, S.; Manoussakis, G.; *Inorganica Chimica Acta*, **1988**, *143*, 17-23, Copyright (1988) Elsevier). Data is given in **Table 2.7**.

Gordy scale group electronegativities values of a group R, χ_R, are empirical numbers that express the combined tendency of not only one atom, but a group of atoms, to attract electrons (including those in a covalent bond) as a function of the number of valence electrons, n, and the

covalent radius, r (in Å).[38] It is empirically adjusted to be aligned with Pauling atomic electronegativities. The group electronegativity χ_R of the substituents ($\chi_R = \chi_{R1} + \chi_{R2}$) on a β-diketonato ligand, determines the tendency of the ligand to attract electrons towards itself. For a chemically reversible single-electron transfer redox process, the formal reduction potential $E^{0'}$ of ferrocene, in a series of ferrocene-containing β-diketonato-ligands, is found to be directly proportional to the group electronegativity, χ_R.[39]

The equilibrium of the dissociation process ($R_1COCH_2COR_2 \rightarrow [R_1COCHCOR_2^- + H^+$), is described by the acid dissociation constant (K_a) of a β-diketone (see **Scheme 2.4**). In a metal chelate, a high pK_a value leads to a low energy change (electron transition energy), where an electron migrates from one energy level to another.[40] The acid dissociation constant of most β-diketones are known from literature, e.g. Hfaa, Htfaa, Htfba, Hba, Hacac measured in water, Hdbm measured in water as well as in various organic solvents and ferrocenyl-containing β-diketones in water containing 10% acetonitrile, $I = 0.1$ mol dm^{-3} (NaClO$_4$).[41]

$$K_a = \frac{[R_1COCHCOR_2^-][H^+]}{[R_1COCH_2COR_2]}$$

$$\mathrm{p}Ka = -\log_{10} K_a$$

$$R_1COCH_2COR_2 \rightarrow [R_1COCHCOR_2]^- + H^+$$
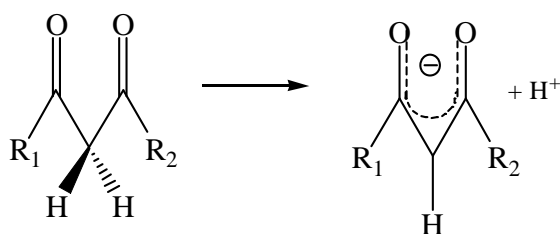
Scheme 2.4: The acid dissociation process of a β-diketonato ligand.

[38] (a) Wells, P. R. In *Progress in Physical Organic Chemistry*, John Wiley & Sons, Inc.: New York, 1968; Vol. 6, pp. 111-145. (b) Kagarise, R. E. *J. Am. Chem. Soc.* **1955**, *77*, 1377.

[39] Conradie, J.; Cameron, T. S.; Aquino, M. A. S.; Lamprecht, G. J.; Swarts, J. C.; *Inorg. Chim. Acta*, **2005**, *358*, 2530-2542

[40] Polyakov, O. V.; Badalyan, A. M.; Kaletinal, I. V.; Belyi, V. I.; *Chemistry for Sustainable Development*, **2000**, *8*, 261-265

[41] W.C. du Plessis, T.G. Vosloo, J.C. Swarts, J. Chem. Soc. Dalton Trans. **1998**, 2507. (b) J. Starý, The Solvent Extraction of Metal Chelates, MacMillan Company, New York, 1964, Appendix. (c) M. Ellinger, H. Duschner, K. Starke, J. Inorg. Nucl. Chem. **1978,** 40, 1063.

2.5 Tris(β-diketonato)cobalt(III) Complexes

2.5.1 Synthesis and Characterization

Typical synthesis of tris(β-diketonato)cobalt(III) complexes involves oxidation of a Cobalt(II) salt. In 1957, Bryant and Fernelius have prepared cobalt(III) acetylacetonato, (Co(acac)$_3$), by oxidizing Co(II) salt in the presence of excess ligand.[42] 10% hydrogen peroxide (large excess) was added dropwise to the suspension of Co(II) carbonate and acetylacetone (10-fold excess), (see **Scheme 2.5** *(a)*). In 1960, Bauer and Drinkard prepared a new intermediate for general synthesis of Cobalt(III) complexes. [43] The intermediate sodium triscarbonatocobaltate(III) trihydrate, Na$_3$[Co(CO$_3$)$_3$·3H$_2$O], was synthesized by initial addition of Co(NO$_3$)$_2$·6H$_2$O and 30% hydrogen peroxide to a sodium bicarbonate solution. Co(acac)$_3$ was then synthesized from this intermediate and acetylacetone, with 70% HNO$_3$ under reflux. (See **Scheme 2.5** *(b)*). Several crystal structures of Co(β-diketonato)$_3$ were reported. This structural parameters is summarized in **Table 2.8**. The Co(β-diketonato)$_3$ crystals, like the Cr(β-diketonato)$_3$ crystals, were all found to be octahedral, with six similar Co-O bonds and three nearly 90° O-Co-O angles. The average Co-O distances in Co(β-diketonato)$_3$ complexes are ca 0.07 Å smaller than the Cr-O distances in Cr(β-diketonato)$_3$, (**Table 2.5**).

(a) $2CoCO_3 + 6C_5H_8O_2 + H_2O_2 \rightarrow 2[Co(C_5H_7O_2)_3] + 4H_2O + 2CO_2$

(b) $2Co(NO_3)_2 \cdot 6H_2O + 6NaHCO_3 + H_2O_2 \rightarrow 2Na_3[Co(CO_3)_3 \cdot 3H_2O] + 4HNO_3 + 8H_2O$

$\quad Na_3[Co(CO_3)_3 \cdot 3H_2O] + 3C_5H_8O_2 \rightarrow [Co(C_5H_7O_2)_3] + NaHCO_3 + 3H_2O$
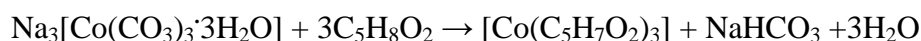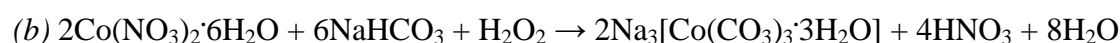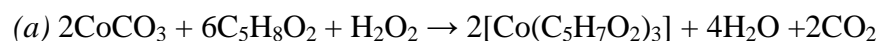
Scheme 2.5: Synthesis of Co(acac)$_3$, by *(a)* Bryant's method, and *(b)* Bauer's method.

---

[42] Bryant, B. E.; Fernelius, W.C.; *Inorg. Syn.,* **1957**, *5*, 188-189

[43] Bauer, H. F.; Drinkard, W. C.; *J. Am. Chem. Soc.*, **1960**, *82*, 5031–5032

Table 2.8: Co – O bond length for reported structural parameters of Co(β-diketonato)$_3$ complexes.

Complex	Co(acac)3						Average	Ref
	1.879(1)	1.894(2)	1.919(1)	1.883(1)	1.926(1)	1.883(1)	1.897(20)	**44**
	1.885(6)	1.883(7)	1.886(9)	1.891(6)	1.889(9)	1.878(7)	1.885(5)	**45**
	1.887(2)	1.889(2)	1.880(2)	1.875(2)	1.884(2)	1.883(2)	1.883(5)	
	1.888(2)	1.889(2)	1.881(2)	1.875(2)	1.884(2)	1.883(2)	1.883(5)	
Cr-O	1.889(1)	1.890(2)	1.881(2)	1.876(2)	1.885(2)	1.885(1)	1.884(5)	**46**
Bond	1.890(1)	1.891(1)	1.880(2)	1.877(1)	1.886(2)	1.883(1)	1.885(6)	
length	1.890(1)	1.891(1)	1.883(1)	1.877(1)	1.886(1)	1.886(1)	1.886(5)	
						Average all	1.886(10)	
	Co(tfaa)3						Average	Ref
	1.877(2)^a	1.876(2)^b	1.906(2)^a	1.870(2)^b	1.870(1)^a	1.879(2)^b	1.884(19)^a	
							1.875(5)^b	
	1.931(2)^a	1.940(2)^b	1.868(2)^a	1.914(2)^b	1.895(2)^a	1.871(2)^b	1.898(32)^a	**47**
							1.908(35)^b	
						Average all	1.891(25)	
	Co(dbm)3						Average	Ref
	1.876(3)	1.897(4)	1.869(4)	1.883(4)	1.884(4)	1.888(3)	1.883(10)	**48**
	1.891(3)	1.884(2)	1.873(3)	1.878(3)	1.875(3)	1.897(3)	1.883(9)	**49**
						Average all	1.883(9)	

a bond nearest to CH$_3$ group

b bond nearest to CF$_3$ group

[44] Hon, P. K.; Pfluger, C. E.; *J. Coord. Chem.*, **1973**, *1*, 67-76

[45] Kruger, G. J.; Reynhardt, E. C.; *Acta Crystallogr., Sect.B: Struct. Crystallogr. Cryst. Chem.*, **1974**, *30*, 822-824

[46] von Chrzanowski, L. S.; Lutz, M.; Spek, A. L.; *Acta Crystallogr., Sect.C: Cryst. Struct. Commun.*, **2007**, *63*, m283-m288

[47] Vogelson, C. T.; Edwards, C. L.; Kobylivker, A. N.; Chacko, S. B.; Moran, C. E.; Dalton, K.; Stewart, S. M.; Werner, B. C.; Bott, S. G.; *J. Chem. Cryst.*, **1998**, *28*, 815-824

[48] Kaitner, B.; Mestrovic, E.; *Z. Kristallogr.*, **1994**, 209, 818-821

[49] Kaitner, B.; Mestrovic, E.; *Z. Kristallogr.*, **1995**, 210, 952-955

Table 2.9: O – Cr – O angle for reported structural parameters of Co(β-diketonato)₃ complexes

Complex	Co(acac)3			Average	Ref
O - Cr – O Angle	97.4	97.5	97.1	97.3(2)	**44**
	96.3	96.6	96.7	96.5(2)	**45**
	96.7	96.3	96.8	96.6(2)	**46**
	96.7	96.4	96.9	96.6(2)	
	96.7	96.4	96.8	96.6(2)	
	96.8	96.4	96.9	96.7(2)	
	96.8	96.6	96.8	96.7(1)	
	Average all			96.7(3)	
	Co(tfaa)3			**Average**	**Ref**
	95.5	96.5	94.3	95.4(1.1)	**47**
	95.4	97.0	97.9	96.8(1.2)	
	Average all			96.1(1.3)	
	Co(dbm)3			**Average**	**Ref**
	95.8	94.9	96.1	95.6(7)	**48**
	95.0	96.2	95.3	95.5(6)	**49**
	Average all			95.5(6)	

43

2.6 Chromium(0)-Carbene Complexes

2.6.1 Introduction[50,51,52,53,54,55,56]

Metal carbene complexes are known to have a formal metal-carbon double bond, *i.e.* M=CR$_2$. Almost all transition metals have been reported to have been used in carbene complexes, however, the Fischer carbene complexes are the point of interest in this study. Fischer carbenes are named after German chemist Ernst O. Fischer. These complexes have a metal center with low oxidation state, *e.g.* Fischer carbene complexes with metals from group VI: Fe(0), Mo(0), Cr(0) and W(0). At the metal center, Fischer carbene complexes have π-acceptor ligands (such as CO) and the complexes are electrophilic at the carbene carbon atom. This electrophilic carbene carbon has π-donor substituents, such as alkoxy and alkylated amino groups (see substituent X in **Figure 2.16**). Preparation of Fischer carbene complexes normally involves the carbene ligand substituting one carbonyl group from a metal hexacarbonyl complex. Subsequently, different non-carbene ligands can be added to Fischer carbenes, by further substitution of carbonyl groups.

50 Fischer, E. O.; *Advances in Organometallic Chemistry*, **1976**, *14*, 1-32

51 Hoskovcova, I.; Rohacova, J.; Dvorak, D.; Tobrman, T.; Zalis, S.; Zverinova, R.; Ludvik, J.; *Electrochimica Acta*, **2010**, *55*, 8341-8351

52 Landman, M.; Liu, R.; Fraser, R.; van Rooyen, P.; Conradie, J.; *Journal of Organometallic Chemistry*, **2014**, *752*, 171-182

53 Hoskovcova, I.; Rohacova, J.; Meca, L.; Tobrman, T.; Dvorak, D.; Ludvik, J.; *Electrochimica Acta*, **2005**, *50*, 4911-4955

54 Baldoli, C.; Cerea, P.; Falciola, L.; Giannini, C.; Licandro, E.; Maiorana, S.; Mussini, P.; Perdicchia, D.; *Journal of Organometallic Chemistry*, **2005**, *690*, 5777-5787

55 Metalkova, R.; Tobrman, T.; Kvapilova, H.; Hoskovcova, I.; Ludvik, J.; *Electrochimica Acta*, **2012**, *82*, 470-477

56 Schobert, R.; Kempe, R.; Schmalz, T.; Gmeiner, A.; *Journal of Organometallic Chemistry*, **2006**, *691*, 859-868

(a)   *(b)*
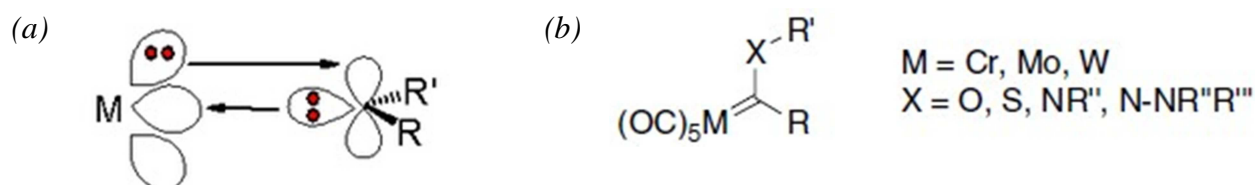
Figure 2.16: Illustration of Fischer carbene complexes: *(a)* bonding information, *(b)* general structure of a typical Fischer carbene complex, as proposed by Baldoli *et al.*[54] (Reprinted (adapted) with permission from Baldoli, C.; Cerea, P.; Falciola, L.; Giannini, C.; Licandro, E.; Maiorana, S.; Mussini, P.; Perdicchia, D.; *Journal of Organometallic Chemistry*, **2005**, *690*, 5777-5787. Copyright (2005) Elsevier).

2.6.2 Electrochemical Studies[50,51,52,53,54,55,56,57,58,]

Most electrochemical studies on Fischer carbene complexes were focused on the metal center and the carbene carbon. The redox processes of Fischer carbene complexes, involve oxidation of the metal center and reduction of the carbene carbon. Computational calculations comfirmed these results. The structures of these series (I, II, V and VI) of Fischer carbenes are shown in **Figure 2.17**. **Figure 2.18** shows a typical cyclic voltammogram of a Fischer carbene complex, as shown in the figure obtained by Hoskovcava *et al.* in 2005[53]. They observed a two-electron irreversible reduction process with electrode adsorption (see Section 2.1.1), and a one-electron reversible oxidation process. Both oxidation and reduction have linear dependence on the Hammett constant σ (see Section 2.1.1.1). **Figure 2.19** shows this linear dependence for different series of Fischer carbene complexes.[53,57]

---

[57] Hoskovcova, I.; Zverinova, R.; Rohacova, J.; Dvorak, D.; Tobrman, T.; Zalis, S.; Ludvik, J.; *Electrochimica Acta*, **2011**, *56*, 6853-6859

[58] Casey, C. P.; Albin, L. D.; Saeman, M. C.; Evans, D. H.; *Journal of Organometallic Chemistry*, **1978**, *155*, C37-C40
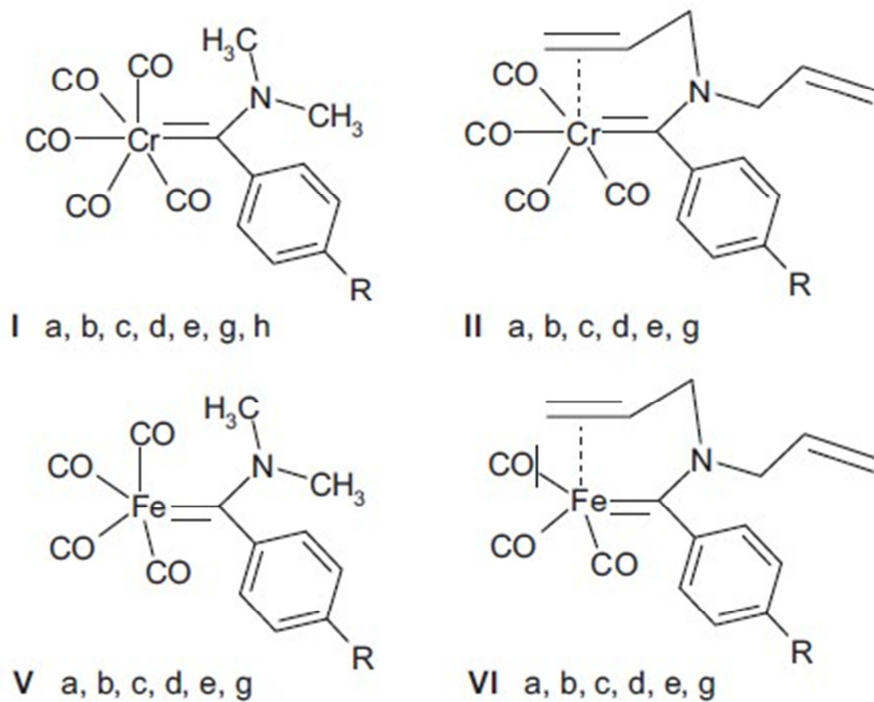
Figure 2.17: Structures of four series (I, II, V and VI) of Fischer carbene complexes, studied by Hoskovcova and her coworkers,[53,57] where R = -OCH$_3$ (a); -CH$_3$ (b); -H (c); -Cl (d); -CF$_3$ (e); -COOCH$_3$ (g); -COOH (h). (Reprinted (adapted) with permission from Hoskovcova, I.; Zverinova, R.; Rohacova, J.; Dvorak, D.; Tobrman, T.; Zalis, S.; Ludvik, J.; *Electrochimica Acta*, **2011**, *56*, 6853-6859. Copyright (2011) Elsevier).
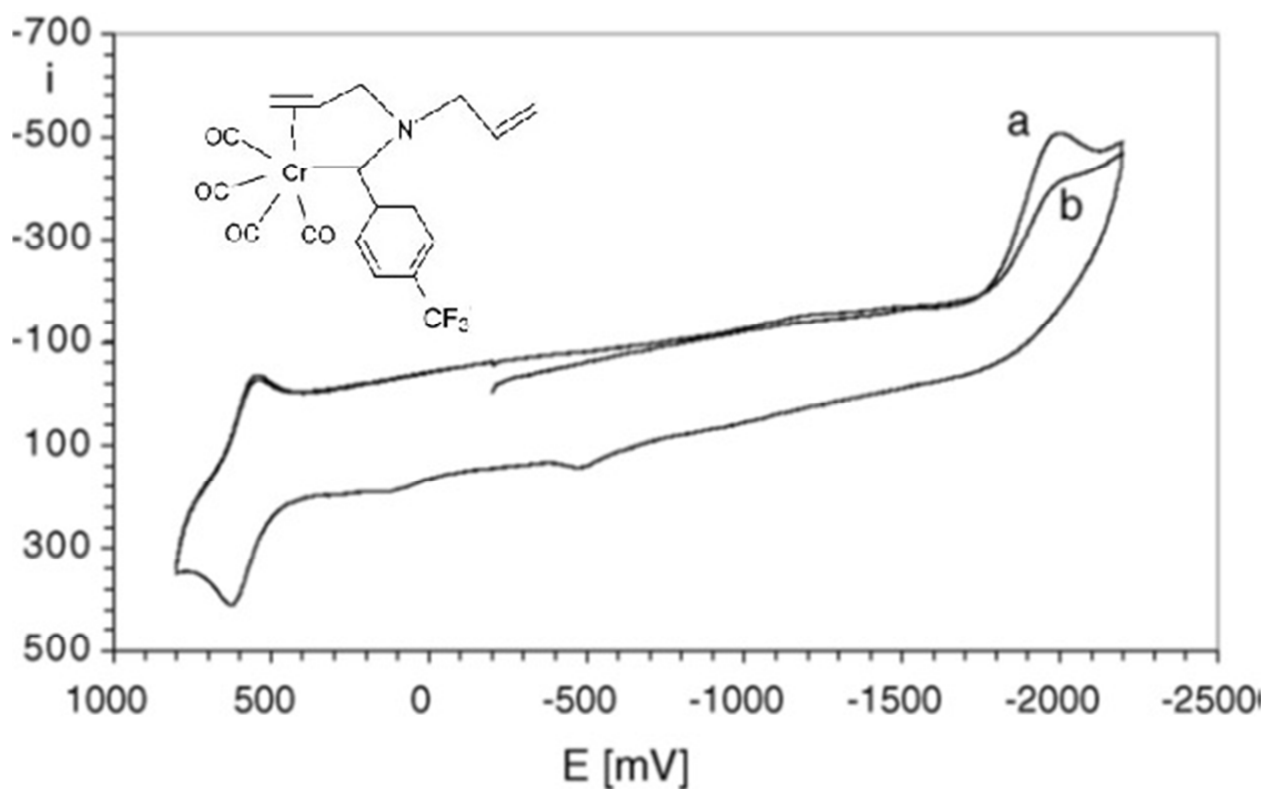
Figure 2.18: Cyclic voltammograms of Fischer carbene complex II.e, from **Figure 2.17**[53] (as shown in this Figure), in solvent DMF on Pt as working electrode, at scan rate 400mV/s *vs.* Ag/AgCl: *(a)* First scan, *(b)* Second scan[53] (Reprinted (adapted) with permission from Hoskovcova, I.; Rohacova, J.; Meca, L.; Tobrman, T.; Dvorak, D.; Ludvik, J.; *Electrochimica Acta*, **2005**, *50*, 4911-4955. Copyright (2005) Elsevier).

(a)

(b)

(c)

(d)
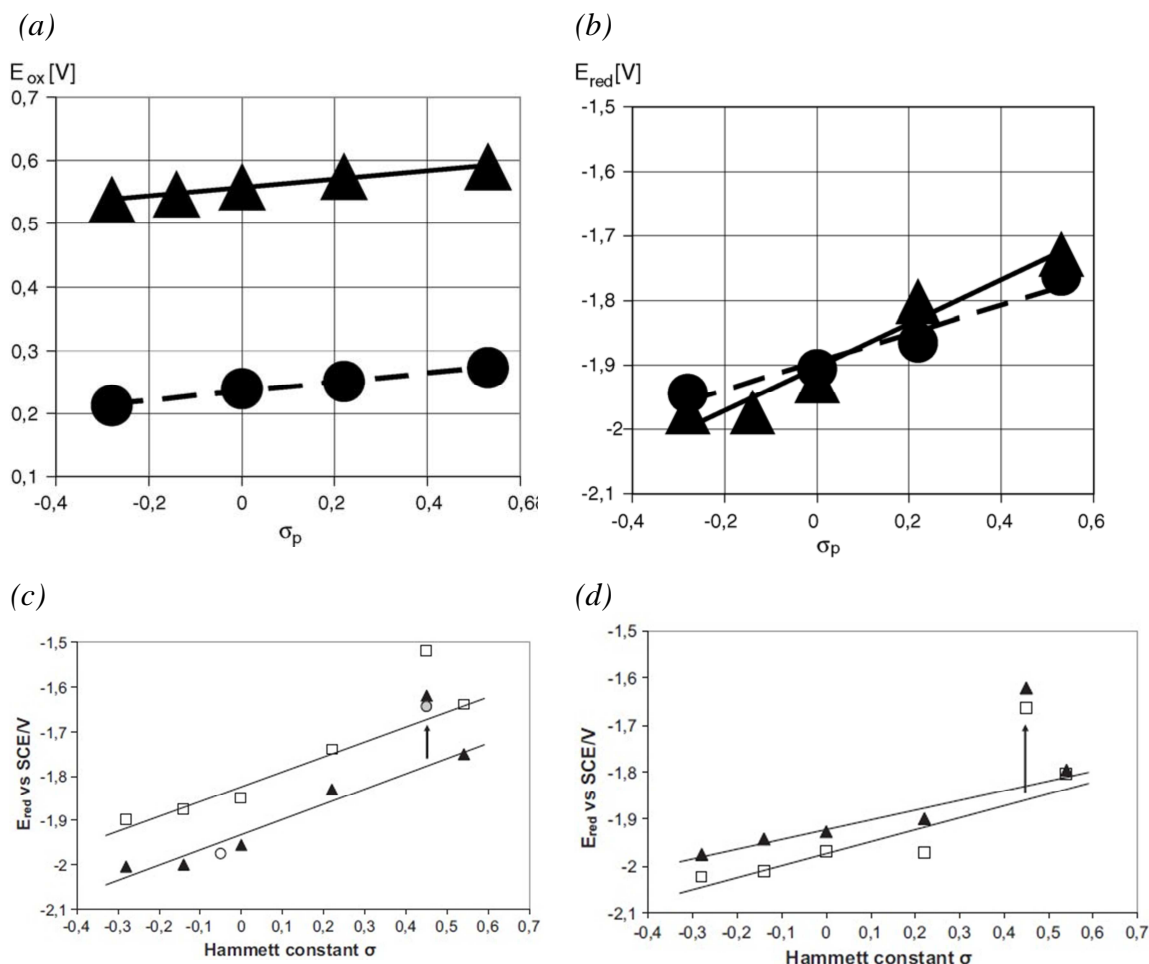
Figure 2.19: Linear dependence of the reduction of Fischer carbene complexes on the Hammett constant: *(a)* and *(b)* were reported by Hoskovcova *et al.* in 2005 and represent the carbene series I. a-e (▲) and carbene series II. a, c-e (●), from **Figure 2.17**.[53] (Reprinted (adapted) with permission from Hoskovcova, I.; Rohacova, J.; Meca, L.; Tobrman, T.; Dvorak, D.; Ludvik, J.; *Electrochimica Acta*, **2005**, *50*, 4911-4955. Copyright (2005) Elsevier);

(c) and *(d)* were reported by Hoskovcova *et al.* in 2011 and represent the carbene series I (▲) and carbene series V (□); where (○) and (◉) represent the dissociated form and non-dissociated form respectively, of carbene I. h.[57] (Reprinted (adapted) with permission from Hoskovcova, I.; Zverinova, R.; Rohacova, J.; Dvorak, D.; Tobrman, T.; Zalis, S.; Ludvik, J.; *Electrochimica Acta*, **2011**, *56*, 6853-6859. Copyright (2011) Elsevier).

3   Results and Discussion

Three classes of transition-metal complexes are investigated in this study:

i)   tris(β-diketonato)chromium(III) complexes (synthesis, crystallography, electrochemistry and computational chemistry)

ii)   tris(β-diketonato)cobalt(III) complexes (synthesis and crystallography)

iii)   chromium(0) carbene complexes (electrochemistry and computational chemistry)

3.1   Tris(β-diketonato)chromium(III) Complexes

3.1.1 Synthesis

Tris(β-diketonato)chromium(III) complexes {1} - {7} were synthesized using the method reported by Rahman *et al.*[1] (see **Scheme 3.1**). Complexes {1} and {2} were reported by Rahman, complexes {2} and {3} were reported by Collman *et al.*[2], complexes {1} – {4}, {7} and {8} were reported by Tsiamis[3] utilizing Collman's method, while complexes {5} and {6} are reported here for the first time. During synthesis, chromium(III) chloride (2.05 mmole) was dissolved in a minimum amount of water. The dark green chromium(III) chloride solution was added dropwise to 40 mL of an ethanol : water solution (1:1) containing β-diketone (6.0 mmole). All β-diketonato-ligands that were used are completely soluble in ethanol/water. The chromium(III) chloride solution was added in slight excess to drive the reaction to completion, since the excess is removed by water during the purification process. The reaction mixture was stirred for 2 hours. Saturated sodium acetate solution was added dropwise until complete precipitation. Basic sodium acetate deprotonated the methine group of the β-diketone, which completed the coordination with the Cr^{III} cation. The product was the only precipitate, and was

---

[1] Rahman, A. K.; Hossain, M. B.; Halim, M. A.; Chowdhury, D. A.; Salam, M. A.; *African Journal of Pure and Applied Chemistry*, **2010**, *4,* 216-220

[2] Collman, J. P.; Moss, R. A.; Maltz, H.; Heindel, C. C.; *J. Am.Chem. Soc.*, **1961**, *83*, 531-534

[3] Tsiamis, C.; Hadjikostas, C. C.; Karageorgiou, S.; Manoussakis, G.; *Inorganica Chimica Acta*, **1988**, *143*, 17-23

purified by washing with excess water. The product was filtered and dried on the funnel and then in a desiccator, at room temperature.
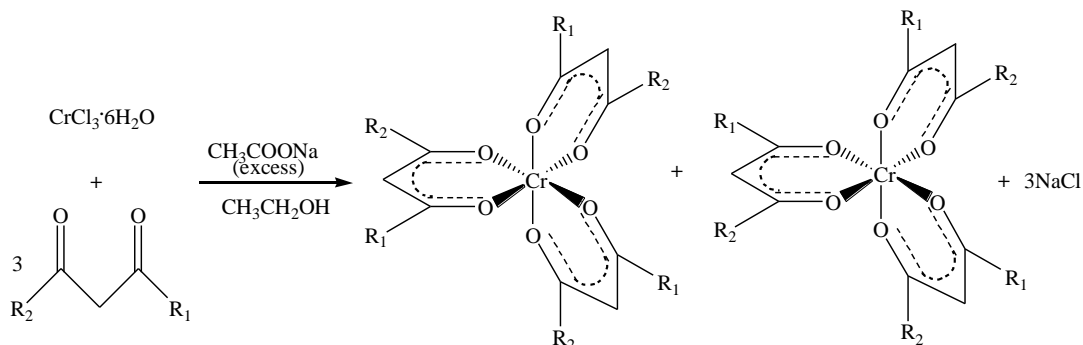
Scheme 3.1: General synthetic method for tris(β-diketonato)chromium(III) complexes, where R_1, R_2 = CH_3, CH_3 {1}; CH_3, C_6H_5 {2}; C_6H_5, C_6H_5 {3}; CF_3, C_6H_5 {4}; C_4H_3S, CF_3 {5}; C_4H_3O, CF_3 {6}; CH_3, CF_3 {7}; CF_3, CF_3 {8}.

It was found that Rahman's method could not be applied to synthesize $Cr(hfaa)_3$ (complex {8}; see **Table 3.1**). In 1993, Elisabeth Bouwman *et al.* showed[4] that water reacts with Hhfaa to produce a tetraol (doubly-hydrated form of Hhfaa), *i.e.* 1,1,1,5,5,5-hexafluoropentane-2,2,4,4-tetraol.[4] The two CF_3 groups in the ligand cause both carbonyl groups to be electrophilic, which then accommodate the oxygen's electrons from water. Therefore, both ketone structures are destroyed (**Scheme 3.2**). The deprotonated tetraol then complexes to the metal centre as a tetradentate bridging ligand, therefore not producing the desired product $Cr(hfaa)_3$ via this method. The alternative synthetic method for complex {8} reported by Harada and Girolami[5] as described in **Section 2.1.1**, used the starting material $Cr[N(SiMe_3)_2]_2(thf)_2$ (thf = tetrahydrofuran). Collman's method[2] on the other hand used urea as starting material.
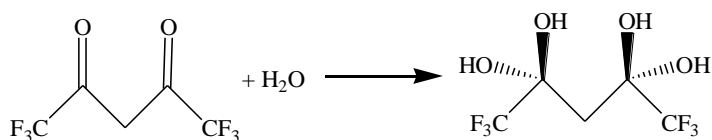
Scheme 3.2: The reaction between water and hexafluoroacetylacetone.

[4] Bouwman, E.; Caulton, K. G.; Christou, G.; Folting, K.; Gasser, C.; Hendrickson, D. N.; Huffman, J. C.; Lobkovsky, E. B.; Martin, J. D.; Michel, P.; Tsai, H.; Xue, Z.; *Inorg. Chem.*, **1993**, *32*, 3463-3470

[5] Harada, Y.; Girolami, G. S.; *Polyhedron*, **2007**, *26*, 1758-1762

The following procedure was designed to avoid the above-mentioned problem (**Scheme 3.3**). Thionyl chloride (SOCl$_2$, in excess) was added to CrCl$_3$·6H$_2$O (dark green, 3 mmole) under slight gentle heating, and the gaseous side product SO$_2$ and excess SOCl$_2$ were trapped by a concentrated sodium acetate solution. A light green product was obtained, namely CrCl$_3$•3H$_2$O. This product was then dissolved in dry THF (tetrahydrofuran). A dark purple solution was obtained, while the dry THF removed the rest of the crystal water. Volatile hexafluoroacetylacetonato (Hhfaa, 2 mL) was injected into this solution by a syringe. The reaction mixture was stirred overnight (±15 hours). The precipitate was filtered, washed with excess water, and then dried on the funnel and in a desiccator at room temperature. Sodium acetate was not required, since the electron-withdrawing CF$_3$ group causes the Hhfaa ligand to easily coordinate to the metal centre, in this case the Cr^{III} cation. Low yield was obtained for Cr(hfaa)$_3$ since the small amount of crystal water in THF destroyed some of the ligand Hhfaa.

$$CrCl_3 \cdot 6H_2O + 3SOCl_2 \rightarrow CrCl_3 \cdot 3H_2O + 3SO_2 + 6HCl$$
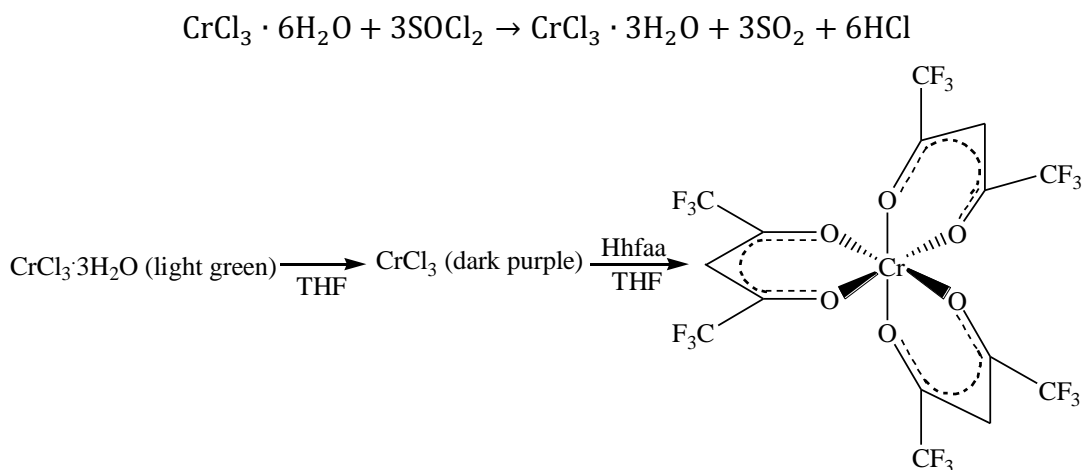
Scheme 3.3: Synthetic method of Cr(hfaa)$_3$, complex {8}.

Table 3.1 gives a summary of the yields obtained during the synthesis of complexes {1} − {8}. The general trend observed is that the non-CF$_3$-containing complexes produced higher yields and Cr(hfaa)$_3$ the lowest.

Since the Cr(β-diketonato)$_3$ complexes are paramagnetic, it was not possible to characterize them by NMR[6]. Characterization methods used include MS, elemental analysis and the crystal structures (see chapter 4 for experimental details).

---

[6] Bertini, I.; Luchinat, C.; Parigi, G.; *Progress in Nuclear Magnetic Resonance Spectroscopy*, **2002**, *40*, 249-273

Table 3.1: Summary of the yields of all the tris(β-diketonato)chromium(III) complexes that were synthesized.

Complex	Name	Yield (%)
Cr(acac)$_3$ {1}	tris(2,4-pentadionato)chromium(III)	83.0
Cr(ba)$_3$ {2}	tris(1-phenyl-1,3-butanedionato)chromium(III)	67.1
Cr(dbm)$_3$ {3}	tris(1,3-diphenyl-1,3-propanedionato)chromium(III)	90.4
Cr(tfba)$_3$ {4}	tris(4,4,4-trifluoro-1-phenyl-1,3-butanedionato)chromium(III)	53.6
Cr(tfth)$_3$ {5}	tris(4,4,4-trifluoro-1-(2-thienyl)-1,3-butanedionato)chromium(III)	28.3
Cr(tffu)$_3$ {6}	tris(4,4,4-trifluoro-1-(2-furyl)-1,3-butanedionato)chromium(III)	71.8
Cr(tfaa)$_3$ {7}	tris(1,1,1-trifluoro-2,4-pentadionato)chromium(III)	42.1
Cr(hfaa)$_3$ {8}	tris(1,1,1,5,5,5-hexafluoro-2,4-pentadionato)chromium(III)	15.9

3.1.2 Crystal Structures

Crystal structures of complexes Cr(acac)$_3$ {1} [7] and Cr(hfaa)$_3$ {8} [8] have been published previously. The structure of Cr(dbm)$_3$ {3} is presented and discussed here, as representative example of the structures of the Cr(β-diketonato)$_3$ type of complexes with chromium. The molecular structure of {3} with the atom-numbering scheme, is shown in **Figure 3.1**. Selected bond lengths and angles for the same complex are given in **Table 3.2**, and their averages compared to the corresponding geometrical parameters of complexes {1} and {8} in **Table 3.3**. The cif file with the complete crystallographic data is given in **Appendix D**.

---

[7] Cambridge Structural Database (CSD), Version 5.34, May 2013 update, CSD reference codes: ACACCR, ACACCR02, ACACCR05, ACACCR07, ACACCR08, ACACCT

[8] Cambridge Structural Database (CSD), Version 5.34, May 2013 update, CSD reference codes: IGAGEC, IGAGEC01
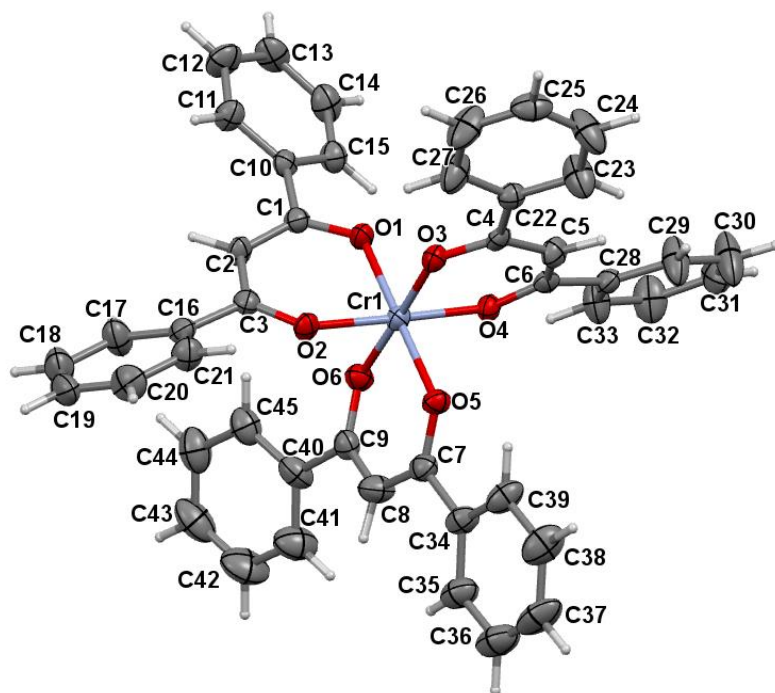
Figure 3.1 A perspective drawing of the molecular structure of Cr(dbm)$_3$ {3}, showing the atom numbering scheme. Atomic dispacement parameters (ADPs) are shown at the 50 % probability level.

Table 3.3 compares the averages of the selected bond lengths, bond angles and dihedral angles of Cr(dbm)$_3$ {3}, with the same parameters of complexes Cr(acac)$_3$ {1}[7], and Cr(hfaa)$_3$ {8}[8], using the average values of these published crystal structures. These are three of the chromium complexes in this study, containing symmetrically substituted ligands (meaning that the R$_1$ and R$_2$ groups on the ligands are both the same).

Firstly considering the bond lengths, it can be seen that complex {3}, Cr(dbm)$_3$, has six similar Cr – O bond lengths which differ less than 0.02 Å from average Cr - O bond length. Similar results were also observed for complexes {1} and {8}, namely six near identical Cr – O bonds within each complex. The average Cr – O bond length for complex {3} was found to be 1.953(11) Å, compared to the average bond lengths of 1.960(8) Å and 1.944(15) Å, for complexes {1} and {8} respectively. This similarity of bond lengths within experimental accuracy, in all three complexes, indicates that the variation of substituents (in this case the increasingly electron-withdrawing Ph or CF$_3$ groups) on symmetrically substituted β-diketonato ligands, has no significant influence on the Cr – O bond length.

Secondly, considering the bond angles O – Cr – O, which describe the angle formed by two Cr – O bonds within a β-diketonato ligand: the average O – Cr – O bond angles found for complexes {1}, {3}, and {8} were essentially the same size, namely $\pm$ 90 ° (differing only within 1.1 °). Therefore, the variation of substituents (with added electronegative effect) on symmetrically substituted β-diketonato ligands, only has negligible influence on O – Cr – O bond angles.

Lastly considering the dihedral angles, which are the angles formed between any two planes within the molecule: each of these planes containing four oxygen atoms at the four vertices (corner points), with one chromium atom in the middle. As tabulated in **Table 3.2** for Cr(dbm)$_3$ {3}, the angle between the two planes O1-O2-Cr-O4-O5 and O2-O3-Cr-O4-O6 is 88.5 °; the angle between the two planes O1-O2-Cr-O4-O5 and O1-O3-Cr-O5-O6 is 89.3 °; and the angle between the two planes O2-O3-Cr-O4-O6 and O1-O3-Cr-O5-O6 is 89.4 °. These three dihedral angles give an average of 89.1 ° for complex {3}, which is the average dihedral angle tabulated in **Table 3.3**, together with the averages for complexes {1} and {8}. These average dihedral angles for all three complexes are basically the same, within experimental accuracy, and close to 90 °, which is the angle for perfect octahedral geometry. Once again, the symmetrical addition of increasingly electronegative substituents onto the ligand, does not effectively change the size of the dihedral angles.

Table 3.2: Selected geometrical parameters for Cr(dbm)$_3$ {3}.

Cr – O Bond length (Å)	O – Cr – O Bond angle (°)	Dihedral angle (°)
1.945(2)	89.6(9)	88.5(3)
1.971(2)	90.4(9)	89.3(3)
1.954(2)	90.6(9)	89.4(3)
1.959(2)		
1.949(2)		
1.939(2)		
1.953 (11) average	**90.2 (5) average**	**89.1 (5) average**

Table 3.3: Selected averages of geometrical parameters for Cr(dbm)$_3$ {3} (this study), and Cr(acac)$_3$ {1}[7] and Cr(hfaa)$_3$ {8}[8].

Average values for:	Cr(dbm)$_3$ {3}	Cr(acac)$_3$ {1} [7]	Cr(hfaa)$_3$ {8} [8]
Cr – O Bond length (Å)	1.953(11)	1.960(8)	1.943(15)
O – Cr – O Bond angle (°)	90.2(5)	91.1(4)	90.6(3)
Dihedral angle (°)	89.1(5)	87.8(2)	89.5(4)

All three complexes have similar geometrical parameters: From the results in **Table 3.3**, all three complexes {1}, {3} and {8} show octahedral geometry, since the average dihedral angle within each complex is close to 90°. It may be seen from **Table 3.6** that Cr(dbm)$_3$ {3} from this study has a monoclinic crystal system. Similarly, most reported structures for Cr(acac)$_3$ {1} and Cr(hfaa)$_3$ {8}, fall into the same lattice point group (namely the monoclinic crystal system); the only exception being one crystal structure of Cr(hfaa)$_3$ {8}, reported by Harada and Girolami[5], which has a trigonal crystal system. Further, the P 2_1/c space group was found for Cr(dbm)$_3$ {3} in this study, as seen in **Table 3.6**. This once again corresponds with the published structures for chromium complexes: seven reported crystal structures for Cr(acac)$_3$ {1} have a P2_1/c space group, and one has a P2_1 space group (CSD code:ACACCT). The structures published for Cr(hfaa)$_3$ {8} fall into the space groups of P2_1/n (CSD code: IGAGEC) and P3c1 (CSD code: IGAGEC01). Therefore, these complexes with symmetrically substituted β-diketonato ligands tend to crystallize into the same isomorphous series, as can be seen from their similar geometries, lattice point groups and space groups.

Figure 3.1 shows that the phenyl rings on the ligands of Cr(dbm)$_3$ {3} do not all align with the backbones of their β-diketonato ligands. **Table 3.4** gives a summary of angles formed between the phenyl rings and the backbones of the β-diketonato ligands which the phenyl rings are attached to, in Cr(dbm)$_3$ {3}. These angles vary from 12° to 32°, due to the π-π stacking between the intermolecular phenyl rings.

Table 3.4: Angles between phenyl rings and the plane of β-diketonato ligands in Cr(dbm)$_3$ {3}.

Ligands	Angle formed by phenyl ring 1	Angle formed by phenyl ring 2
1	12.82 °	25.66 °
2	12.44 °	13.71 °
3	30.02 °	31.68 °
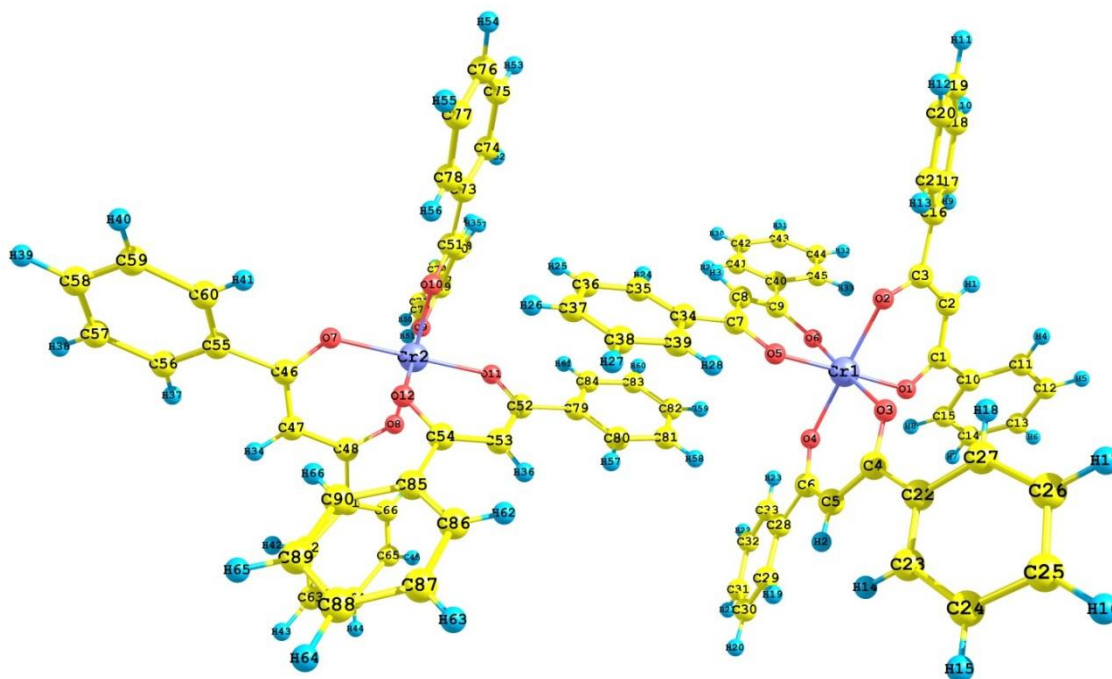
Figure 3.2: π-π stacking in Cr(dbm)$_3$ crystals.

Figure 3.2 illustrates the π-π stacking between molecules in the packing of the Cr(dbm)$_3$ crystals, the phenyl rings of the two molecules (one formed by C34-C35-C36-C37-C38-C39, another formed by C79-C80-C81-C82-C83-C84) do not overlap. Instead, two stacked rings are slipped away from each other, which is called parallel displaced π-π stacking. See Table 3.5 for the relatively large C − C distances between the C-s of the phenyl rings in parallel molecules (compared to the inter-planar distance of d$_1$ = 3.305 Å), due to this parallel displaced π-π stacking. This way of stacking is one of the most common and most stable (lowest energy) π-π stacking motifs.[9,10]

Figure 3.3 gives the typical parameters of π-π stacking in Cr(dbm)$_3$. The distance (d$_1$) between two planes formed by two phenyl rings in different molecules (*e.g.* C34-C35-C36-C37-C38-C39 and C79-C80-C81-C82-C83-C84) is 3.305 Å, while the centroid displacement (d$_2$) is 1.474 Å, the distance (d$_3$) between centroids of two phenyl rings is 3.619 Å, and the displacement angle (θ) of centroids is 24.0 °. Janiak[10] stated that the interplanar distance has a common range of 3.3 − 3.8 Å. In this study, the parameter between two planes in different molecules (d$_1$ = 3.305 Å) also falls in this region.

---

[9] Sinnokrot, M. O.; Valleev, E. F.; Sherrill, C. D.; *J. Am. Chem. Soc.,* **2002**, *124*, 10887-10893

[10] Janiak. C.; *J. Chem. Soc., Dalton Trans.,* **2000**, 3885-3896

Table 3.5: The C – C distance between two phenyl rings, of π-π stacking in Cr(dbm)$_3$ crystals.

C – C distance of π-π stacking (Å)	
C34 – C82	3.562
C35 – C83	3.563
C36 – C84	3.570
C37 – C79	3.562
C38 – C80	3.563
C39 – C81	3.570
Average distance:	**3.565 (0)**
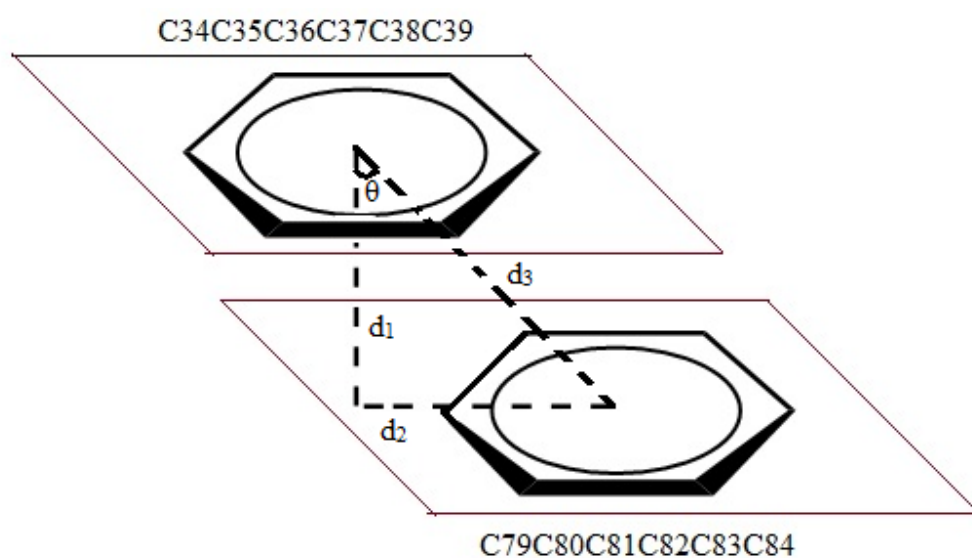
Figure 3.3: The parameters of π-π stacking in Cr(dbm)$_3$ crystals, {3}.

Table 3.6: Crystal data and structure refinement of $Cr(dbm)_3$, {3}.

Empirical formula	$C_{45}H_{33}CrO_6$
Formula weight	721.71
Temperature	150(2) K
Wavelength	0.71073 Å
Crystal system	Monoclinic
Space group	$P\,2_1/c$
Unit cell dimensions	a = 16.9785(6) Å, α = 90°
	b = 9.7442(3) Å, β = 92.772(2) °
	c = 21.2271(7) Å, γ = 90°
Volume	3507.7(2) $Å^3$
Z	4
Density (calculated)	1.367 Mg/m^3
Absorption coefficient	0.378 mm^{-1}
F(000)	1500
Crystal size	0.168 x 0.110 x 0.103 mm^3
Theta range for data collection	2.300 to 26.373 °.
Index ranges	-21<=h<=21, -12<=k<=11, -26<=l<=26
Reflections collected	32119
Independent reflections	7168 [R(int) = 0.0708]
Completeness to theta = 25.242 °	99.90 %
Refinement method	Full-matrix least-squares on F2
Data / restraints / parameters	7168 / 0 / 469
Goodness-of-fit on F^2	1.068
Final R indices [I>2sigma(I)]	R1 = 0.0658, wR2 = 0.1356
R indices (all data)	R1 = 0.1114, wR2 = 0.1534
Extinction coefficient	n/a
Largest diff. peak and hole	0.448 and -0.640 $e.Å^{-3}$

3.1.3 Electrochemical Studies

The electrochemical behaviour of the tris(β-diketonato)chromium(III) complexes (where Cr(β-diketonato)$_3$ = Cr(acac)$_3$ {1}, Cr(ba)$_3$ {2}, Cr(dbm)$_3$ {3}, Cr(tfba)$_3$ {4}, Cr(tfth)$_3$ {5}, Cr(tffu)$_3$ {6}, Cr(tfaa)$_3$ {7}, Cr(hfaa)$_3$ {8}, see **Table 3.1**) is described in this section. Both the Cr-metal and the respective β-diketonato ligands are electrochemically active. Studies done by Liu[11] reported that the Cr^{III}(acac)$_3$ {1} complex undergoes four redox processes: Cr^{I} ← Cr^{II} ← Cr^{III} → Cr^{IV} → Cr^{V}. The electrochemical behaviour of complexes {1} – {4}, {7} and {8} has been reported previously by Tsiamis *et al.*,[3] whereas complexes {5} and {6} are reported here for the first time. The reduction potential of a metal-coordinated β-diketonato ligand generally occurs at a more negative position than for the free ligand, and was not observed for complexes {1} – {8} in the potential window of the solvent (CH$_3$CN) that was used.[12,13] The different substituents on the β-diketonato ligands have different influences on electron densities at the metal centre, therefore the redox potentials of the various complexes differ. The method used for electrochemical measurements is described in Chapter 4 (see Section 4.2.1). The complete cyclic voltammograms of all Cr^{III}(β-diketonato)$_3$ complexes are given in **Appendix A**.

Figure 3.4 shows the cyclic voltammograms of Cr(acac)$_3$, complex {1}. The expected[11] four redox processes were observed: peak A and B in **Figure 3.4** represent two irreversible oxidation prosesses presenting the Cr$^{III/IV}$ and Cr$^{IV/V}$ oxidation respectivily. The reduction peak B has an oxidation peak near to it representing the Cr$^{III/II}$ redox couple. The reduction peak A present the irreversible Cr$^{II/I}$ reduction process. Only the Cr^{III} ↔ Cr^{II} redox process (peak B in **Figure 3.4**) indicated *quasi*-reversibility. **Table 3.7** to **Table 3.10** give summaries of the data of the four redox processes of Cr(acac)$_3$.

[11] Liu, Q.; Shinkle, A. A.; Li, Y.; Monroe, C. W.; *Electrochemistry Communications*, **2010**, *12*, 1634-1637

[12] Kuhn, A.; Conradie, J.; *Electrochimica Acta,* **2010**, *56*, 257-264

[13] Ferreira, H.; Conradie, M. M.; Conradie, J.; *Electrochimica Acta*, **2013**, *113*, 519-526

Cr(acac)$_3$ (25 mM) in TEABF$_4$/CH$_3$CN (0.5 M)
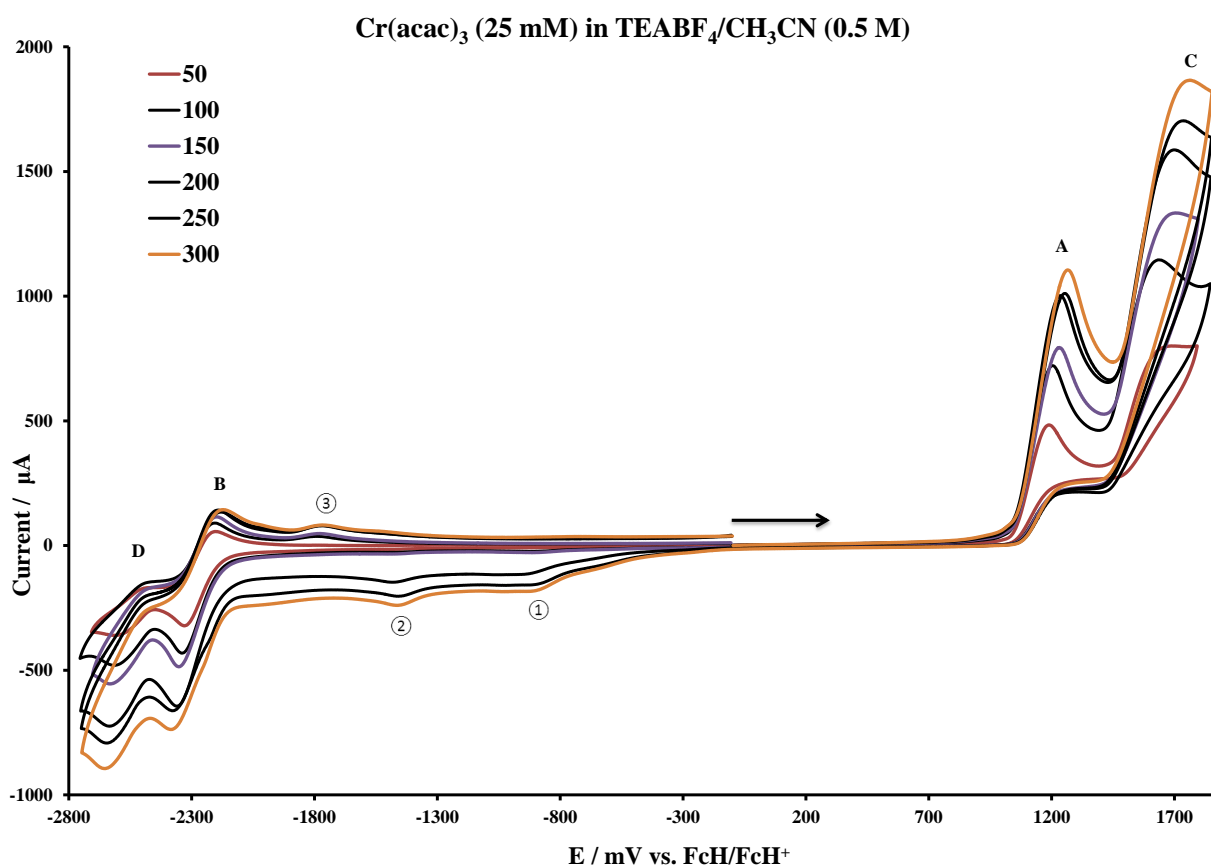
Figure 3.4: Cyclic voltammograms of 25 mM Cr(acac)$_3$ {1}, *vs.* FcH/FcH$^+$. (Solvent = CH$_3$CN, supporting electrolyte TEABF$_4$, scan rate = 50 (smallest peak current), 100, 150, 200, 250 and 300 (largest peak current) mV•s^{-1}, with glassy carbon as working electrolyte at 20 °C, scan direction as indicated by the arrow).

Table 3.7: Electrochemical data of [Cr(acac)$_3$] for the Cr^{III}→Cr^{IV} redox process (peak A in **Figure 3.4**).*

Scan Rate	E_{pa} (mV)	E_{pc} (mV)	ΔE_p (mV)	$E^{0'}$ (mV)	i_{pa} (µA)	i_{pc} (µA)	i_{pa}/i_{pc}
50 mV•s^{-1}	1182	—	—	—	426	—	—
100 mV•s^{-1}	1201	—	—	—	636	—	—
150 mV•s^{-1}	1236	—	—	—	661	—	—
200 mV•s^{-1}	1236	—	—	—	802	—	—
250 mV•s^{-1}	1263	—	—	—	819	—	—
300 mV•s^{-1}	1273	—	—	—	918	—	—

*the data are obtained in 0.1 mol dm^{-3} TEABF$_4$/CH$_3$CN, on a glassy carbon working electrolyte, at 20 °C. Potentials are reported *vs.* FcH/FcH$^+$

Table 3.8: Electrochemical data of [Cr(acac)$_3$] for the Cr^{IV}→Cr^V redox process (Peak C in **Figure 3.4**).*

Scan Rate	E$_{pa}$ (mV)	E$_{pc}$ (mV)	ΔE$_p$ (mV)	E$^{0'}$ (mV)	i_{pa} (μA)	i_{pc} (μA)	i_{pa}/i_{pc}
50 mV•s^{-1}	1668	––	––	––	508	––	––
100 mV•s^{-1}	1640	––	––	––	737	––	––
150 mV•s^{-1}	1700	––	––	––	891	––	––
200 mV•s^{-1}	1700	––	––	––	991	––	––
250 mV•s^{-1}	1725	––	––	––	1069	––	––
300 mV•s^{-1}	1763	––	––	––	1190	––	––

*the data are obtained in 0.1 mol dm^{-3} TEABF$_4$/CH$_3$CN, on a glassy carbon working electrolyte, at 20 ℃. Potentials are reported *vs.* FcH/FcH$^+$

Table 3.9: Electrochemical data of [Cr(acac)$_3$] for the Cr^{III}↔Cr^{II} redox couple (peak B in **Figure 3.4**).*

Scan Rate	E$_{pa}$ (mV)	E$_{pc}$ (mV)	ΔE$_p$ (mV)	E$^{0'}$ (mV)	i_{pa} (μA)	i_{pc} (μA)	i_{pa}/i_{pc}
50 mV•s^{-1}	-2209	-2322	113	-2265	125	207	0.60
100 mV•s^{-1}	-2206	-2332	126	-2269	212	352	0.60
150 mV•s^{-1}	-2200	-2343	143	-2272	251	424	0.59
200 mV•s^{-1}	-2187	-2354	167	-2271	293	491	0.60
250 mV•s^{-1}	-2183	-2378	195	-2280	259	422	0.61
300 mV•s^{-1}	-2164	-2382	218	-2273	276	452	0.61

*the data are obtained in 0.1 mol dm^{-3} TEABF$_4$/CH$_3$CN, on a glassy carbon working electrolyte, at 20 ℃. Potentials are reported *vs.* FcH/FcH$^+$

The Cr$^{III/II}$ redox process (Peak B in **Figure 3.4**) has a ΔE$_p$ larger than 110 mV and i_{pa}/i_{pc} ratios of 0.6. This process is thus chemically irreversible (i_{pa}/i_{pc} ≠ 1) and electrochemically *quasi* reversible (ΔE$_p$ > 90mV).[14]

---

[14] Kissinger, P. T.; Heineman, W. R.; *J. Chem. Educ.*, **1983**, *60*, 702-706

Two unexpected peaks (Peak 1 and 2 in **Figure 3.4** and **Figure 3.5**) were observed in the reduction cycle (*ca.* -850 mV and *ca.* -1400 mV). One unexpected peak (Peak 3 in **Figure 3.4** and **Figure 3.5**) was observed in the oxidation cycle (*ca.* -1800 mV). Consequently, a series of cyclic voltammograms was performed to investigate the cause of these unexpected peaks, as illustrated in **Figure 3.5**:

Table 3.10: Electrochemical data of [Cr(acac)$_3$] for the Cr^{II}→Cr^{I} redox process (peak D in **Figure 3.4**).*

Scan Rate	E$_{pa}$ (mV)	E$_{pc}$ (mV)	ΔE$_p$ (mV)	E$^{0'}$ (mV)	i_{pa} (μA)	i_{pc} (μA)	i_{pa}/i_{pc}
50 mV•s^{-1}	––	-2609	––	––	––	129	––
100 mV•s^{-1}	––	-2611	––	––	––	181	––
150 mV•s^{-1}	––	-2627	––	––	––	201	––
200 mV•s^{-1}	––	-2632	––	––	––	233	––
250 mV•s^{-1}	––	-2645	––	––	––	241	––
300 mV•s^{-1}	––	-2651	––	––	––	241	––

*the data are obtained in 0.1 mol dm^{-3} TEABF$_4$/CH$_3$CN, on a glassy carbon working electrolyte, at 20 ℃. Potentials are reported *vs.* FcH/FcH$^+$

Cr(acac)₃ (25 mM) in TEABF₄/CH₃CN (0.5 M)
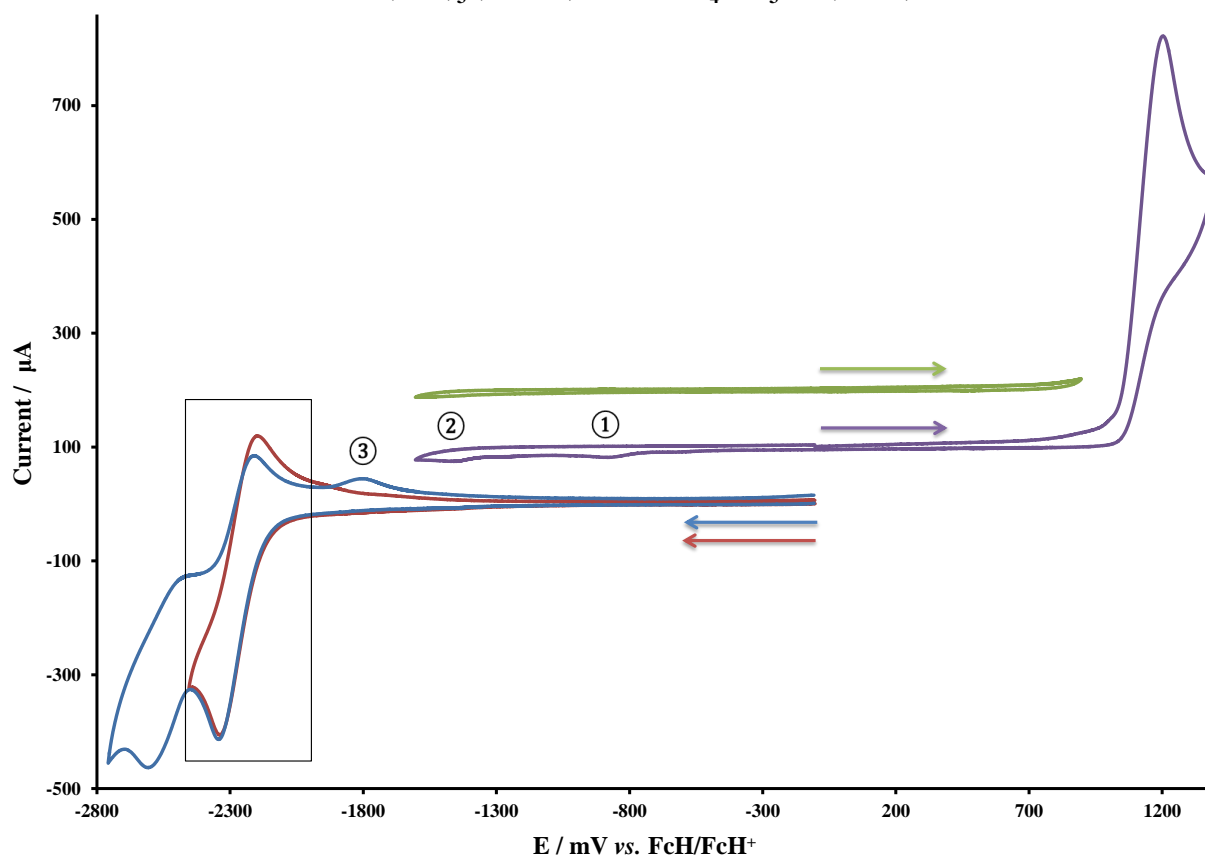
Figure 3.5: Comparative cyclic voltammograms of Cr(acac)$_3$ {1}, at scan rates of 100 mV•s^{-1} and scan directions as indicated. (Solvent = CH$_3$CN, supporting electrolyte TEABF$_4$, with glassy carbon as working electrolyte at 20 ℃, scan direction as indicated by the arrow).

In **Figure 3.5**, the same peaks 1 and 2 were observed at scan rates of 100 mV and higher, the current of these peaks increasing at higher scan rates. A scan excluding the first oxidation (green segment) showed no redox process. Peaks 1 and 2 were however observed on the scan including the first oxidation, Cr^{III}→Cr^{IV} (purple segment). It is therefore clear that the first oxidation caused the appearance of these two peaks. Peaks 1 and 2 thus most probably indicate the reduction of decomposition products resulting from the irreversible Cr$^{III/IV}$ oxidation process:

Qinghua Liu *et al.*[11] proposed that the small peaks 1 and 2 in **Figure 3.5** result from the fact that the oxidized species [Cr^{IV}(acac)$_3$]$^+$ gives up one acac ligand to form [Cr^{IV}(acac)$_2$]$^{2+}$, as shown in **Equation 3.1**:

Equation 3.1: $Cr^{III}(acac)_3 \leftrightarrows [Cr^{IV}(acac)_3]^+ + e^- \rightarrow [Cr^{IV}(acac)_2]^{2+} + acac^-$
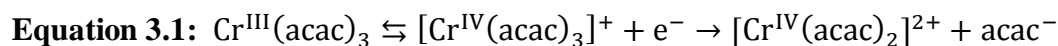
RESULTS AND DISCUSSION

The cyclic voltammograms of most of the other $Cr^{III}(\beta\text{-diketonato})_3$ complexes also showed small peaks (similar to peaks 1 and 2) related to the reduction of decomposition products resulting from the respective oxidation processes.

A scan including only the first reduction peak (red segment in **Figure 3.5**) showed a smooth segment after the $Cr^{II} \rightarrow Cr^{III}$ oxidation. Peak 3 was observed only after the 2nd reduction $Cr^{II} \rightarrow Cr^{I}$ (blue segment) at 100 mV scan rate and higher, which intensified with higher scan rates. Peak 3 is thus a result of the second reduction, $Cr^{II} \rightarrow Cr^{I}$.

Anderson *et al.* [15] proposed that peak 3 in **Figure 3.5** is due to the dissociation of acetylacetonate, as shown in **Equation 3.2** and **Equation 3.3**, where the reduced species $[Cr(acac)_3]^{2-}$ loses two acac$^-$ ligands to form Cr(acac).

Equation 3.2: $Cr^{III}(acac)_3 + e^- \leftrightarrows [Cr^{II}(acac)_3]^- \rightarrow Cr^{II}(acac)_2 + acac^-$

Equation 3.3: $[Cr^{II}(acac)_3]^- + e^- \leftrightarrows [Cr^{I}(acac)_3]^{2-} \rightarrow Cr^{I}(acac) + 2acac^-$
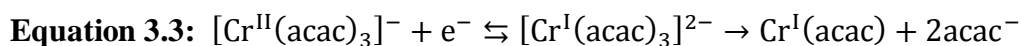
The approximation of **Equation 3.2** was not observed, since $Cr^{III} \leftrightarrow Cr^{II}$ is a reversible redox process, and the singly reduced species $[Cr^{II}(acac)_3]^-$ is stable to be furtherly reduced.

---

[15] Anderson, C. W.; Lung, K. R.; Nile, T. A.; *Inorganica Chemica Acta,* **1984**, *85*, 33-36

Cr(ba)$_3$ (25 mM) in TEAPF$_6$/CH$_3$CN (0.5 M)
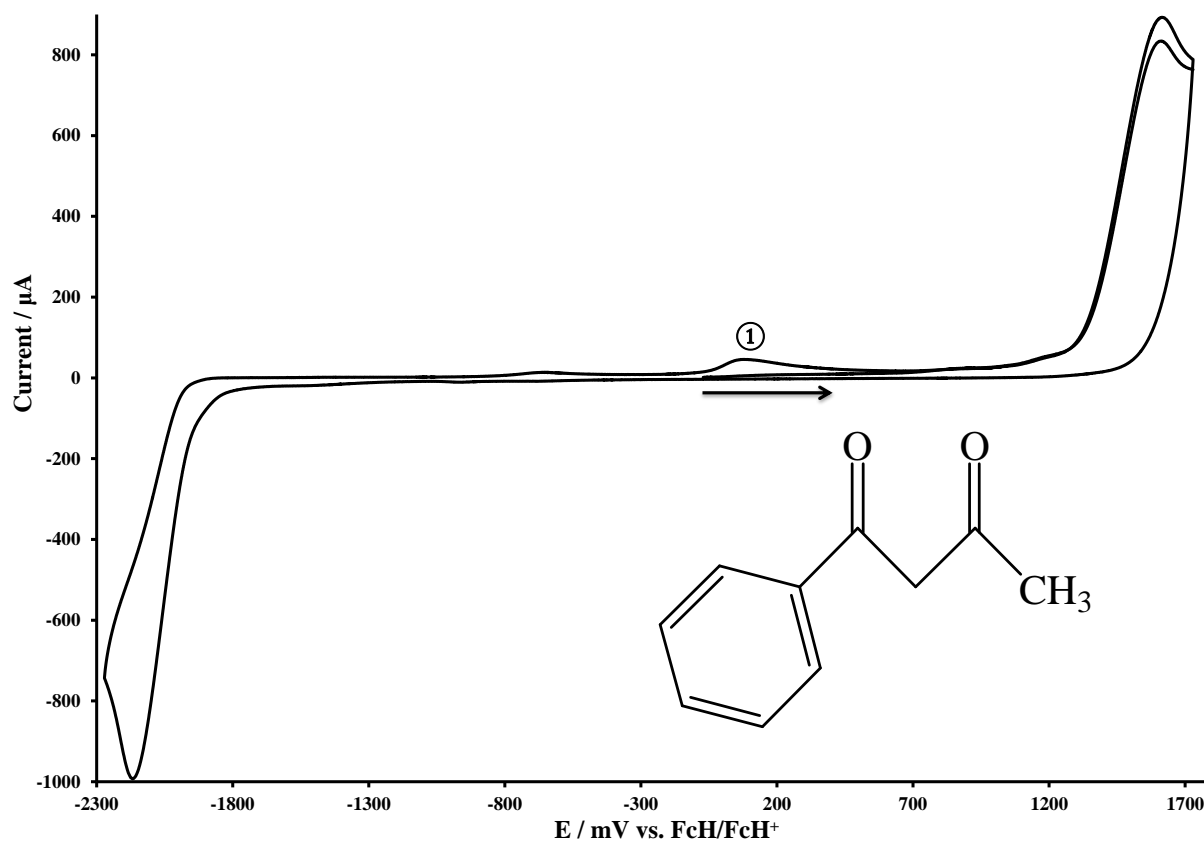
Figure 3.6: Comparative cyclic voltammograms of Cr(ba)$_3$ {2}, at scan rates of 100 mV•s^{-1} and scan directions as indicated. (Solvent = CH$_3$CN, supporting electrolyte TEABF$_4$, with glassy carbon as working electrolyte at 20 °C, scan direction as indicated by the arrow).

In evaluating the cyclic voltammograms in **Figure 3.6** of Cr(ba)$_3$, complex {2}, an unexpected peak was once again observed: Peak 1 (*ca.* 180 mV) in **Figure 3.6** appeared on the 3rd segment, at all scan rates higher than 100 mV•s^{-1}. It is observed after the first reduction, Cr^{III}→Cr^{II}, probably due to decomposition products of the reduced species (similar to peak 3 of complex {1}, in **Figure 3.5**). The second reduction Cr^{II}→Cr^{I} for Cr(ba)$_3$ was not observed at all in the working window of the solvent (CH$_3$CN).

Cr(ba)$_3$ (25 mM) in TEABF$_4$/CH$_3$CN (0.5 M)
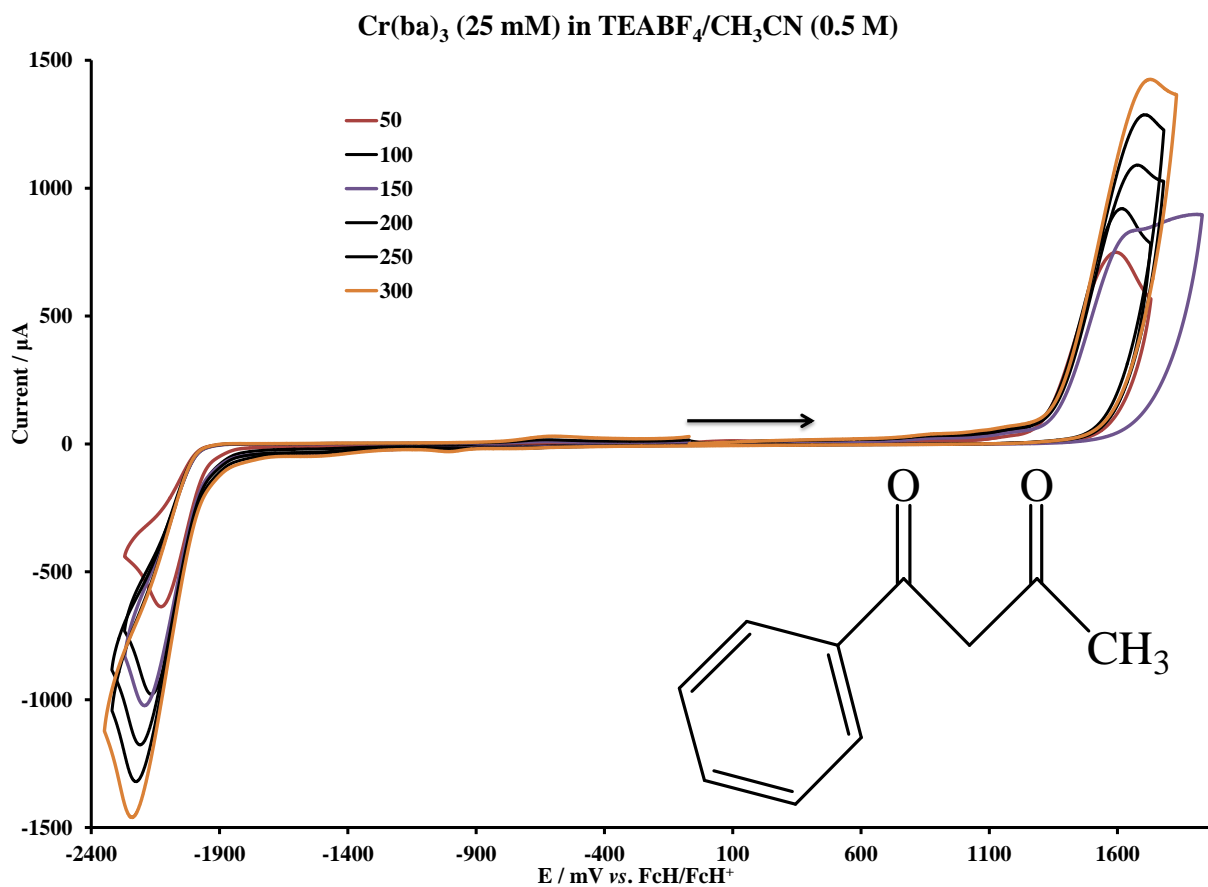
Figure 3.7: Cyclic voltammograms of 25 mM Cr(ba)$_3$ {2}, *vs.* FcH/FcH$^+$. (Solvent = CH$_3$CN, supporting electrolyte TEABF$_4$, scan rate = 50 (smallest peak current), 100, 150, 200, 250 and 300 (largest peak current) mV•s^{-1}, with glassy carbon as working electrolyte at 20 ℃, scan direction as indicated by the arrow).

Figure 3.7 shows the cyclic voltammograms of complex Cr(ba)$_3$ {2}, at different scan rates. Oxidation process Cr$^{III/IV}$ causes electrode adsorption and decomposition, and leads to relatively large peaks, compared to the reduction peak Cr$^{III/II}$. Only one reduction peak was observed in the active window of the solvent (CH$_3$CN), the Cr$^{II/III}$ oxidation peak was not observed through any of the scan rates.
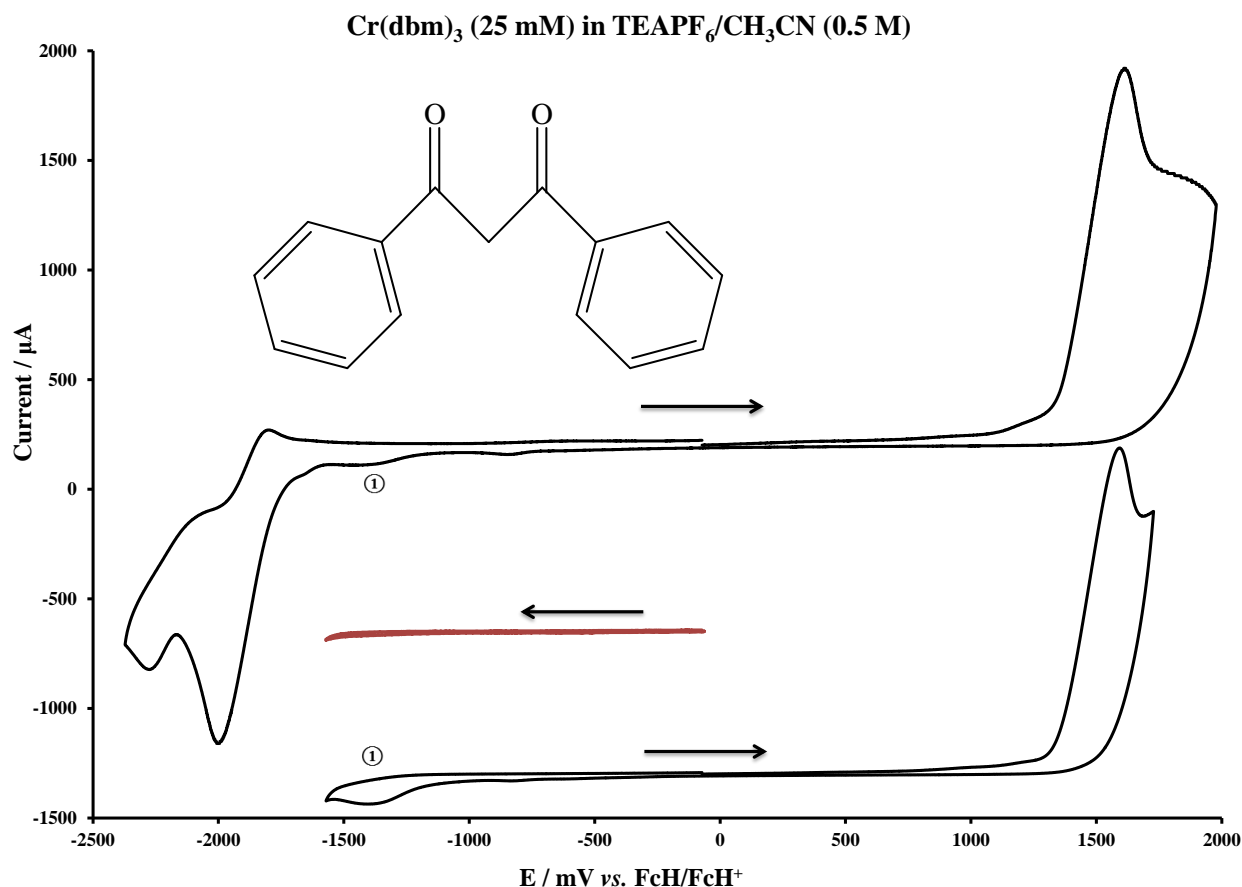
Figure 3.8: Comparative cyclic voltammograms of Cr(dbm)$_3$ {3}, at scan rates of 250 mV•s^{-1}. (Solvent = CH$_3$CN, supporting electrolyte TEABF$_4$, with glassy carbon as working electrolyte at 20 °C, scan direction as indicated by the arrow).

The above cyclic voltammogram of Cr(dbm)$_3$, complex {3}, showed similar decomposition of the oxidized species (peak 1 in **Figure 3.8**, *ca.* -1400 mV) as described in **Equation 3.1**, as shown in **Figure 3.8**. Peak 1 is related to the first oxidation Cr^{III}→Cr^{IV}, and can only be seen at scan rates of 250 mV and higher. Similarly, the red segment (where no redox process took place) showed that peak 1 is not due to any impurities.

Cr(dbm)$_3$ (25 mM) in TEABF$_4$/CH$_3$CN (0.5 M)
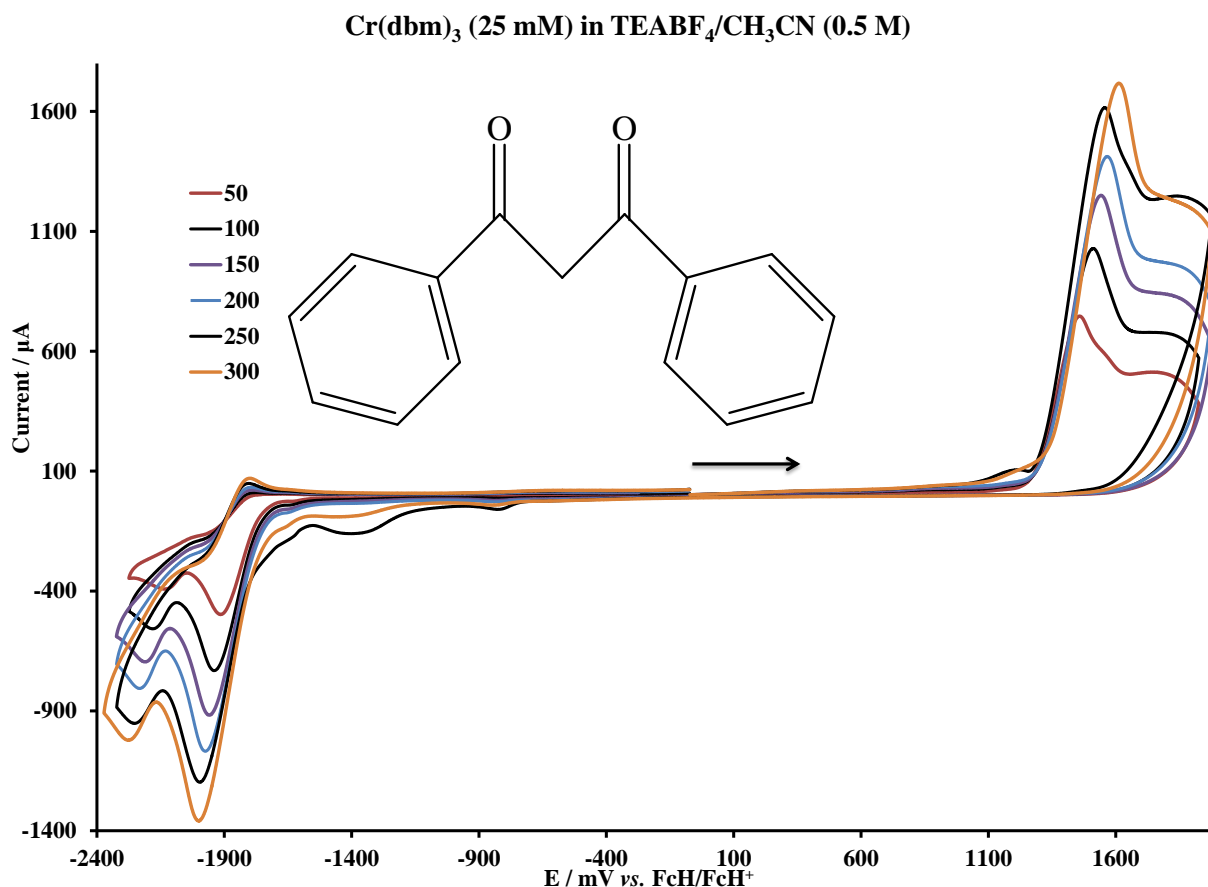
Figure 3.9: Cyclic voltammograms of 25 mM Cr(dbm)$_3$ {3}, *vs.* FcH/FcH$^+$. (Solvent = CH$_3$CN, supporting electrolyte TEABF$_4$, scan rate = 50 (smallest peak current), 100, 150, 200, 250 and 300 (largest peak current) mV•s^{-1}, with glassy carbon as working electrolyte at 20 °C, scan direction as indicated by the arrow).

Figure 3.9 shows the cyclic voltammograms of Cr(dbm)$_3$ {3}, at different scan rates. The oxidation process of Cr$^{II/III}$ was only observed when the scan rate was 150 mV/s and higher. Two oxidation peaks are observed, a sharp Cr$^{III/IV}$ oxidation process and another broad peak that resembles the Cr$^{IV/V}$ oxidation of Cr(acac)$_3$, **Figure 3.4**. These two oxidation peaks overlap, are large and broad, indicating electrode adsorption and decomposition. The small peak (ca. -1400 mV) due to decomposition products of the oxidation Cr^{III}→Cr^{IV} of Cr(dbm)$_3$, was discussed above and is illustrated in **Figure 3.8**.

Cr(tffu)$_3$ (25 mM) in TEAPF$_6$/CH$_3$CN(0.5 M)
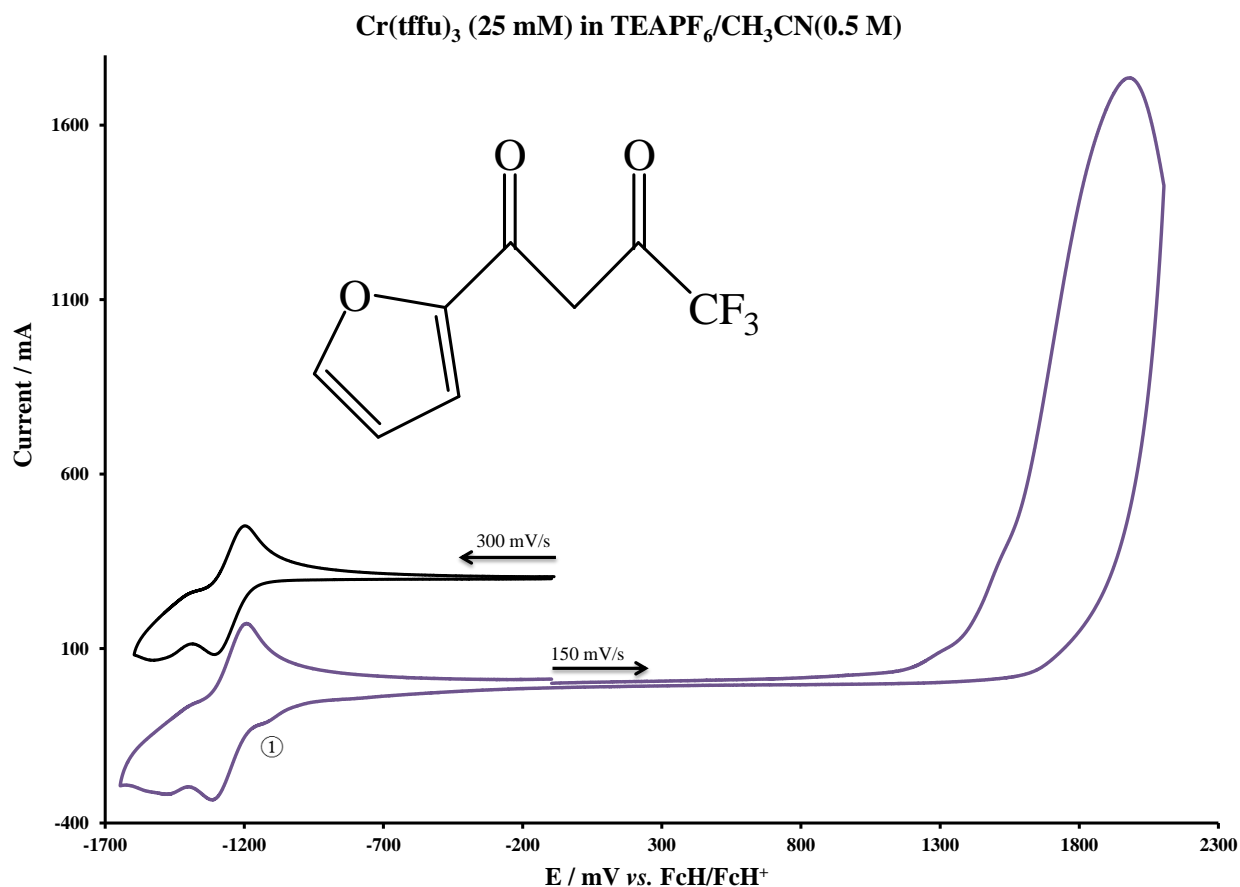
Figure 3.10: Comparative cyclic voltammograms of Cr(tffu)$_3$ {6}, with scan rates and scan directions as indicated. (Solvent = CH$_3$CN, supporting electrolyte TEABF$_4$, scan rate = 50 (smallest peak current), 100, 150, 200, 250 and 300 (largest peak current) mV•s^{-1}, with glassy carbon as working electrolyte at 20 ℃, scan direction as indicated by the arrow).

As shown in **Figure 3.10**, only one oxidation peak (Cr^{III} → Cr^{IV}) was observed for complex {6}, Cr(tffu)$_3$. A small peak (peak 1 in **Figure 3.10**) appeared before the Cr$^{III/II}$ reduction. This small peak was observed when the scan rate was 150 mV•s^{-1} and higher, and was only seen after the oxidation peak Cr^{III} → Cr^{IV} (purple segment). In contrast to this, a scan started from the reduction processes has a smooth baseline before the first reduction (black segment). This observation also agrees with Liu's proposal: that the oxidized species [Cr^{IV}(ba)$_3$]$^+$ gives up one acac ligand to form [Cr^{IV}(ba)$_3$]$^{2+}$.[12] The irreversible oxidation peak (Cr^{III} → Cr^{IV}) leads to electrode adsorption and is therefore relatively large compared to the reduction peak (Cr^{III} → Cr^{II}), which also includes those of the decomposition products of the complex.

Tris(β-diketonato)chromium(III) (25 mM) in TBAPF$_6$/CH$_3$CN
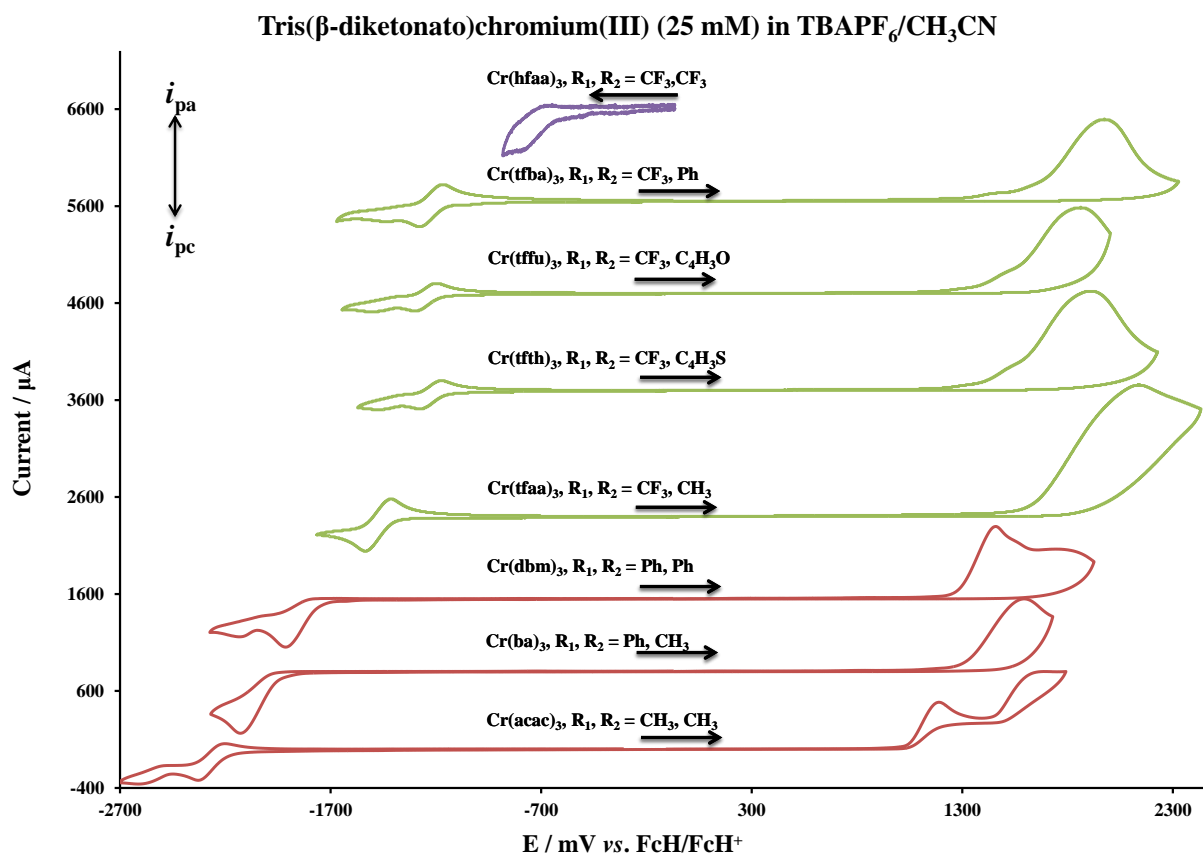
Figure 3.11: Cyclic voltammograms of 25 mM Cr(β-diketonato)$_3$, *vs.* FcH/FcH$^+$ (supporting electrolyte: TBAPF$_6$, scan rate = 100 mV•s^{-1}). (Solvent = CH$_3$CN, supporting electrolyte TEABF$_4$, scan rate = 100 mV•s^{-1}, with glassy carbon as working electrolyte at 20 °C, scan direction as indicated by the arrow).

Figure 3.11 gives the cyclic voltammograms of all the complexes {1} – {8}, at scan rates of 100 mV/s. Only for Cr(acac)$_3$, complex {1}, was it possible to clearly distinguish the two oxidation processes, *i.e.* Cr^{III} → Cr^{IV} → Cr^{V}. The oxidation of complexes {2} – {8} all lead to electrode adsorption and decompositions, resulting in broad oxidation peaks. The Cr$^{III/II}$ redox process is generally electrochemically *quasi* reversible. However, two exceptions were observed: **1.** For Cr(dbm)$_3$, complex {3}, the Cr$^{II/III}$ oxidation process was observed only at scan rates of 150 mV/s and higher, see **Figure 3.9**; **2.** For Cr(ba)$_3$, complex {2}, the Cr$^{II/III}$ oxidation process was not observed for any of the scan rates, see **Figure 3.7**. The second reduction process Cr$^{II/I}$ is irreversible and was not observed for complexes Cr(ba)$_3$ {2}, Cr(tfaa)$_3$ {4}, and Cr(hfaa)$_3$ {8}. Therefore, the reduction process Cr^{III} → Cr^{II} proved to be the best target for the study of these Cr(β-diketonato)$_3$ complexes, since it is easily observed for all these complexes.

As shown by the three different colours in **Figure 3.11**, the reduction process of $Cr^{III} \rightarrow Cr^{II}$ can be divided into three groups: *1.* **Red group**: the $Cr(acac)_3$, complex {1}, is reduced at the most negative potential. The substitution of methyl groups (CH_3) by more electron-withdrawing phenyl groups (Ph) made the corresponding $Cr(\beta\text{-diketonato})_3$ complexes to reduce at a less negative potential, as in $Cr(ba)_3$, complex {2} (reduced at less negative potential than $Cr(acac)_3$). The reduction process was further promoted when doubly substituted phenyl rings existed in the ligand, as in $Cr(dbm)_3$, complex {3}. *2.* **Green group:** The promotion to even less negative potential values continued to develop, when a strongly electron-withdrawing trifluoro group (CF_3) substituted the methyl group. The trifluoro group still dominated the reduction potential at these less negative values, even when used in combination with a variety of other substituents, as in complexes {4}-{7} . *3.* **Purple group:** both methyl groups were substituted by the strongly electron-withdrawing trifluoro groups, and this complex {8}, ($Cr(hfaa)_3$), is therefore most easily reduced of all (at the least negative potential).

Table 3.11: Reduction potential *vs.* FcH/FcH^+ of the $Cr^{III/II}$ processes, sum of the Hammett constants, sum of the group electronegativities of the R_1 and R_2 groups in $[Cr(R_1COCHCOR_2)_3]$ (**Scheme 3.1**), and pK_a values of the free β-diketone ligand.

Complex	R_1	R_2	$\sigma_{R1} + \sigma_{R2}$ [16]	$\Sigma\sigma$	$\chi_{R1} + \chi_{R2}$ [17,18,19]	$\Sigma\chi$	pK_a [17,20,21]	E_{pc} (mV)
$Cr(acac)_3$	CH_3	CH_3	-0.14	-0.42	4.68	14.04	8.95	-2329
$Cr(ba)_3$	CH_3	C_6H_5	-0.01	-0.03	4.55	13.65	8.7	-2132
$Cr(dbm)_3$	C_6H_5	C_6H_5	0.12	0.36	4.42	13.26	9.35	-1910
$Cr(tfba)_3$	CF_3	C_6H_5	0.49	1.47	5.22	15.66	6.30	-1273
$Cr(tfth)_3$	CF_3	C_4H_3S	0.52	1.56	5.11	15.33	6.497	-1371
$Cr(tffu)_3$	CF_3	C_4H_3O	0.49	1.47	5.13	15.39	6.5	-1293
$Cr(tfaa)_3$	CH_3	CF_3	0.36	1.08	5.35	16.05	6.30	-1547
$Cr(hfaa)_3$	CF_3	CF_3	0.86	2.58	6.02	18.06	4.35	-807

[16] Hansch, C.; Leo, A.; Taft, R. W.; *Chem. Rev.,* **1991**, *91*, 165-195

[17] du Plessis, W. C.; Vosloo, T. G.; Swarts, J. C.; *J. Chem. Soc., Dalton Trans.,* **1998**, *15*, 2507-2514

[18] Kagarise, R. E.; *J. Am. Chem. Soc.,* **1955**, *77*, 1377-1379

[19] Conradie, M. M.; Muller, A. J.; Conradie, J.; *S. Afr. J. Chem.,* **2008**, *61*, 13-21

[20] Ellinger, M.; Duschner, H.; Starke, K.; *J. Inorg. Nucl. Chem.*, **1978**, *40*, 1063-1067

[21] Star ý, J.; *The Solvent Extraction of Metal Chelates, MacMillan Company,* **1964**, Appendix

Table 3.11 summarizes the reduction potentials of the Cr(β-diketonato)$_3$ series {1}-{8}, as well as the total sum of Hammett constants, total electronegativities, and pK_a values. Since three β-diketonato ligands bind to one metal centre, the total sum of Hammett constants and total electronegativities are calculated according to **Equation 3.4** and **Equation 3.5**:

Equation 3.4: Total f Hammettsum o constants, $\sum\sigma = 3 \times (\sigma_{R1} + \sigma_{R2})$

Equation 3.5: Total electronegativities, $\sum\chi = 3 \times (\chi_{R1} + \chi_{R2})$
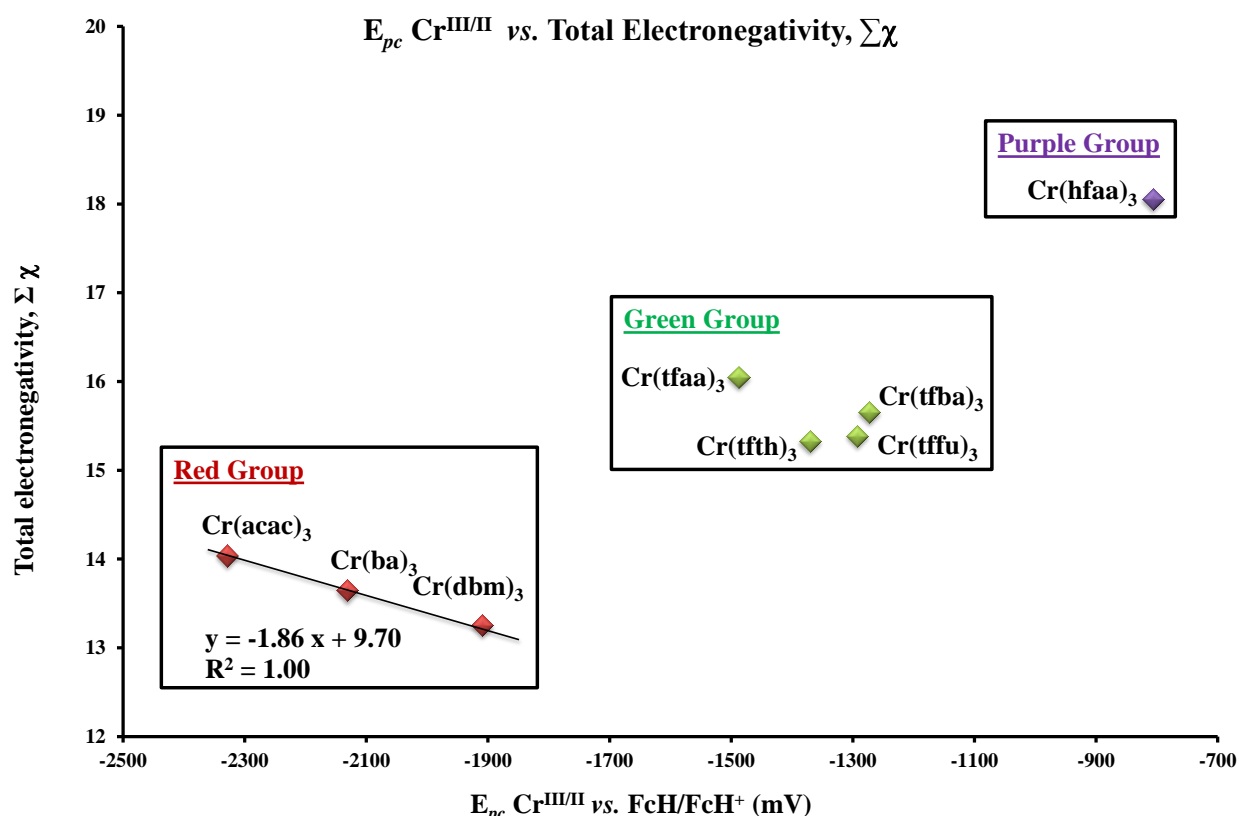
Figure 3.12: The relation of the reduction potential of the Cr^{III}(β-diketonato)$_3$ complexes, E_{pc}Cr$^{III/II}$ *vs.* total group electronegativity of the R$_1$ and R$_2$ groups in [Cr(R$_1$COCHCOR$_2$)$_3$]. (Data from **Table 3.11**).

Figure 3.12 relates the reduction potential of the Cr$^{III/II}$ redox couple with the total group electronegativity of the R$_1$ and R$_2$ groups in complexes [Cr(R$_1$COCHCOR$_2$)$_3$]. The same conclusion is drawn as from **Figure 3.11**, namely that the data can be divided into three groups. The red group indicates the most negative reduction potentials of the Cr^{III}(β-diketonato)$_3$ complexes without any CF$_3$ groups. The green group contains complexes with one CF$_3$ group on each β-diketonato ligand. This strongly electron-withdrawing CF$_3$ group dominates the value of

the reduction potential, since it causes the Cr^{III}-complex to be more easily reduced (at less negative potential) than in the red group. $Cr(hfaa)_3$, complex {8}, is the only component in the purple group, with two strongly electron-withdrawing CF_3 substituents on each ligand. Therefore $Cr(hfaa)_3$ is reduced most easily (at the least negative potential), due to the largest electronegativity of the CF_3 groups . The strong electron-withdrawing ability of both CF_3 groups makes the Cr^{III} metal centre more positive causing it therefore to more easily accept another electron on the Cr^{III}. Therefore, more electron-withdrawing substituents on the β-diketonato ligand cause the metal centre to be more positive, and the resulting complex gets reduced at a less negative potential.

A good linearity was observed within the red group ($R^2 = 1.00$), and this relation is defined by **Equation 3.6**:

Equation 3.6: $\Sigma\chi = -1.86\ E_{Cr^{III/II}} + 9.70$ where $\Sigma\chi = 3 \times (\chi_{R_1} + \chi_{R_2})$ (6)

The same trend in reduction potentials (as in the red group in **Figure 3.10**) has also been observed for other M^{III}(β-diketonato)$_3$ complexes with M = Fe[22] and Mn[23], namely:

Most negative reduction: $E_{pc}(M(acac)_3) < E_{pc}(M(ba)_3) < E_{pc}(M(dbm)_3)$

---

[22] Conradie, M.M.; *Rhodium and Iron Complexes and Transition States: A Computational, Spectroscopic and Electrochemical Study*, **2010**, PhD thesis, University of the Free State, Bloemfontein, RSA

[23] Freitag, R.; *Computational, Structural and Electrochemical properties of Metal(III) tris-betadiketonato Complexes*, **2011**, MSc thesis, University of the Free State, Bloemfontein, RSA
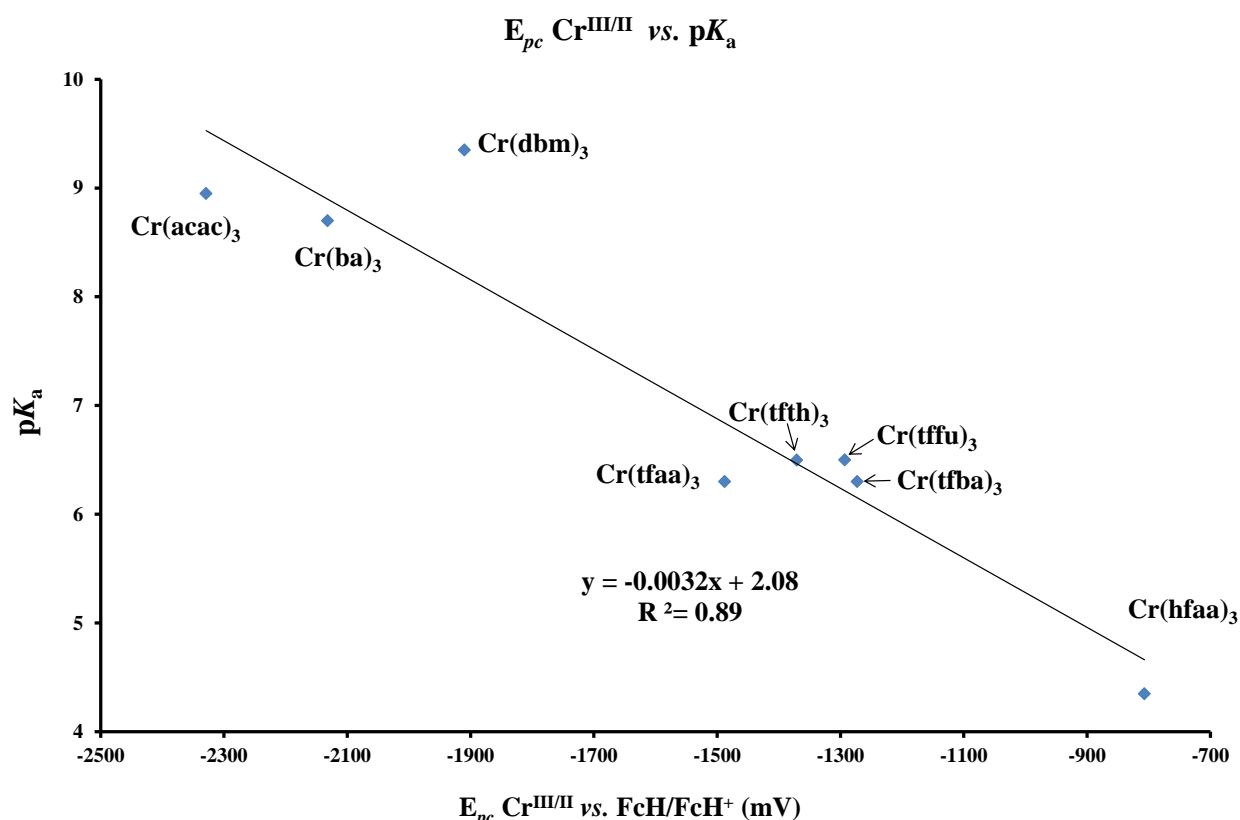
Figure 3.13: The relation of the reduction potential of the $Cr^{III}(\beta\text{-diketonato})_3$ complexes, $E_{pc}Cr^{III/II}$ *vs.* the pK_a values of the free β-diketone ligand. (Data from **Table 3.11**).

In **Figure 3.13,** the reduction potential of the metal centre, Cr^{III}, in the complexes is related to the acid dissociation constant (pK_a) of the free β-diketonato ligands for complexes {1}-{8}. The metal centre coordinated to a β-diketonato ligand with a smaller pK_a value, carries a lower electron density and is more easily reduced, since less energy is needed to remove an electron. Although the E_{pc}/pK_a data are also divided into roughly three groups, a fairly linear trend in the data over a large pK_a range is observed. From **Figure 3.13**, the relation between the reduction potential and the acid dissociation constants (pK_a) is given in **Equation 3.7** with $R^2 = 0.89$:

Equation 3.7: $pK_a = -0.0032\,E_{Cr^{III/II}} + 2.08$ \hspace{2cm} (7)
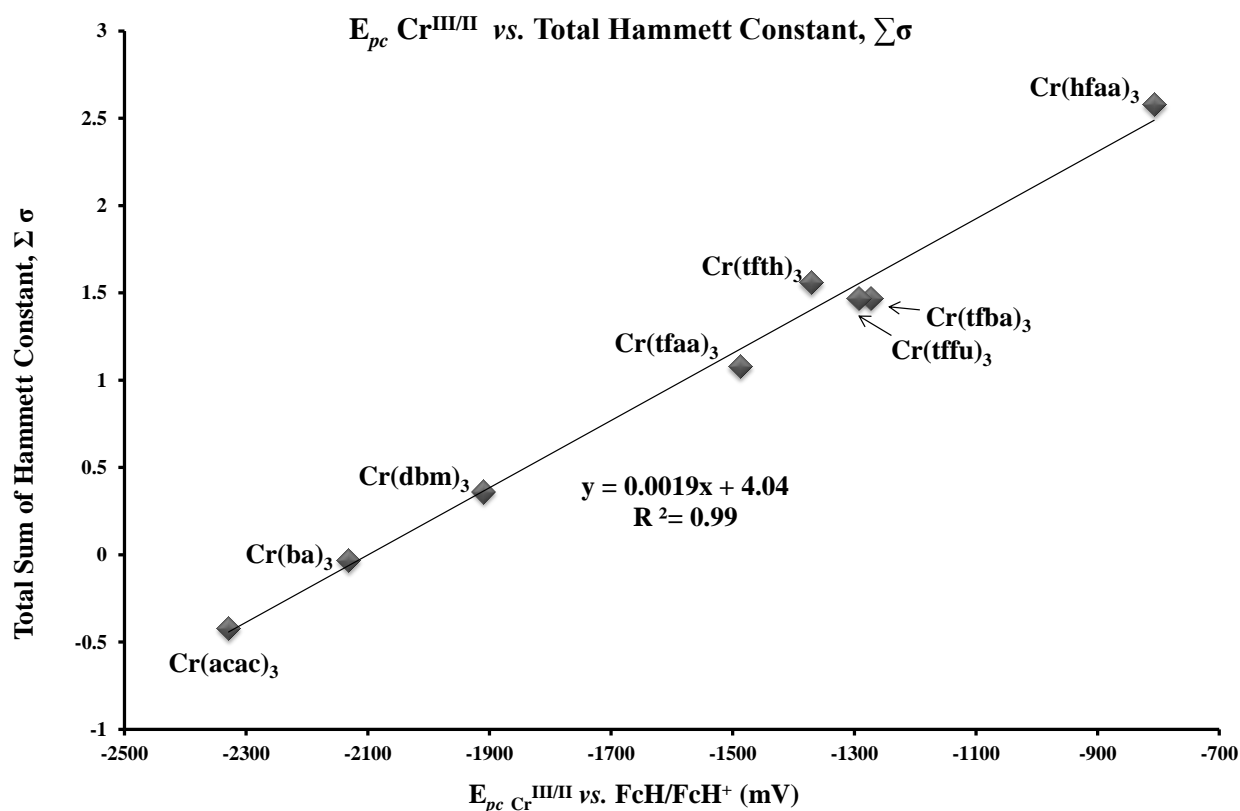
Figure 3.14: The relation of the reduction potential of the $Cr^{III}(\beta\text{-diketonato})_3$ complexes, $E_{pc}Cr^{III/II}$ *vs.* total sum of the Hammett constants of the R_1 and R_2 groups in $[Cr(R_1COCHCOR_2)_3]$. (Data from **Table 3.11**).

Figure 3.14 presents the relation between $E_{Cr^{III/II}}$ and the sum of the Hammett constants of the various substituents on the ligand. This relation is given by **Equation 3.8**, with $R^2 = 0.99$:

Equation 3.8: $\Sigma\sigma = 0.0019\, E_{Cr^{III/II}} + 4.04$ where $\Sigma\sigma = 3 \times \left(\sigma_{R_1} + \sigma_{R_2}\right)$

Hexafluoroacetylacetone (the ligand of complex {8}) has the highest total sum of Hammett constants. Reduction of $Cr^{III}(\beta\text{-diketonato})_3$ complexes involves addition of an electron to the metal centre to form (Cr^{II}). The group of substituents with increasingly positive Hammett values therefore stabilizes the added electrondensity on the metal centre via a stronger electron withdrawing effect via conjugation through the ligand. The more stable the $[Cr^{II}(\beta\text{-diketonato})_3]^-$ species becomes, the more easily the $Cr^{III}(\beta\text{-diketonato})_3$ will be reduced. A ligand with larger total Hammett constans leads to a more positive $Cr^{III/II}$ reduction potential, this linear relation was also observed by Taiamis's electrochemical studies[3] on his series of $Cr^{III}(\beta\text{-diketonato})_3$ complexes.

From the data presented above, we observe that the total sum of the Hammett constants is the best parameter by which to describe and predict the $Cr^{III/II}$ reduction process in the $Cr(\beta$ - diketonato)$_3$ complexes. The linear relations obtained above also imply good electronic communications between the metal center and different side substituents on the β-diketonato ligands.

3.1.4 Computational Results on Cr(β-diketonato)₃

3.1.4.1 Spin state and symmetry of the Cr(acac)₃ complex

Results obtained for the Cr(acac)$_3$ complex {1} will be discussed here, as representative example of the Cr(β-diketonato)$_3$ complexes. The neutral Cr^{III}(β-diketonato)$_3$ complexes are d^3 complexes. With 3 d-electrons, the spin state can either be $S = 1/2$ (one unpaired electron) or $S = 3/2$ (three unpaired electrons).

Table 3.12 gives the relative energy obtained by density functional theory (DFT) calculations, using the Amsterdam Density Functional (ADF) modelling suite, for the neutral Cr^{III}(acac)$_3$ {1} complex. Four functionals were used, namely B3LYP, OLYP, BP86 and PW91. Results from these four functionals showed that the spin state of 3/2 is more stable than the spin state of 1/2.

Table 3.12: Relative DFT-calculated energies obtained by the four different functionals, for the indicated spin states and symmetries of Cr(acac)$_3$ {1}. All unconverged calculations are given with "—".

Spin state	Sym-metry	Relative energy (eV)	Relative energy (eV)	Relative energy (eV)	Relative energy (eV)
		B3LYP	**OLYP**	**BP86**	**PW91**
1/2	C_1	1.040	1.150	0.856	0.838
	C_2	1.068	1.159	0.857	0.839
	$C_3{}^a$	1.035	1.159	—	0.839
	D_3	1.038	1.167	0.872	0.856
3/2	C_1	—	0.000	0.000	0.000
	C_2	0.000	0.000	0.000	0.000

	$C_3{}^a$	0.000	0.000	0.000	0.000
	D_3	0.000	0.000	0.000	0.000

a C_3 symmetry has complex irreducible representations which have not been implemented in ADF 2012, thus all C_3 input geometries run in C_1 symmetry.

Input geometries constructed in Chemcraft[24] in different symmetries (C_1, C_2 and C_3) all converged to D_3 symmetry as the lowest energy geometry, see **Table 3.12** (relative energy S = 3/2 is 0 for D_3) and **Table 3.13** (all Cr-O bonds and O – Cr – O angles converged to the same value). D_3 symmetry is higher than C_3, C_2 or C_1 (no symmetry). D_3 symmetry requires identical Cr – O bond lengths and O – Cr – O bond angles, with invariance upon rotation of 120°. C_2 symmetry needs a rotation of 180 ° for invariance, which is not possible for $Cr^{III}(acac)_3$. Results from **Table 3.12** and **Table 3.13** clearly show that the D_3 symmetry is preferred by the $Cr^{III}(acac)_3$ complex.

Table 3.13: DFT-calculated Cr – O bond lengths and O – Cr – O bond angles, obtained by the four different functionals for the indicated symmetries of Cr(acac)$_3$.

$Cr^{III}(acac)_3$	$d(Cr – O)$ (Å)^a				$O – Cr – O$ (°)^b			
Symmetry	B3LYP	OLYP	BP86	PW91	B3LYP	OLYP	BP86	PW91
C_1	—	2.008	1.980	1.978	—	89.7	91.5	91.5^c
C_2	1.983	2.008	1.980	1.978	91.5	89.7	91.4	91.5
$C_3{}^d$	1.983	2.008	1.980	1.978	91.5	89.7	91.4	91.5
D_3	1.983	2.008	1.980	1.978	91.5	89.7	91.4	91.5

a All Cr-O bonds converged to the same value

b All O – Cr – O angles converged to the same value

c Only functional PW91 with C_1 symmetry gave different O – Cr – O angles of 91.4 °, 91.5 ° and 91.6 ° (average: 91.5 °)

d C_3 input geometry run in C_1 symmetry in ADF.

The molecular orbitals (MOs) containing mainly Cr-d character, are displayed in **Figure 3.15**. Cr(acac)$_3$ is an octahedral complex with 3 d-electrons and a spin state of 3/2. From **Figure 3.15** we observe that, as expected from the ligand field theory for an octahedral complex, three α-orbitals (d_{xz}, d_{yz}, and d_{xy}) are occupied by unpaired electrons, while two α-orbitals (d_{z2}, d_{x2-y2}) and all the β-orbitals remain empty (LUMOs).

---

[24] http://www.chemcraftprog.com

Figure 3.15: The illustration of the calculated five *d*-orbitals of Cr(acac)$_3$, obtained by functional PW91.

α-orbitals		β-orbitals	
HOMO-2, d_{xz}		LUMO, d_{xz}	
HOMO-1, d_{yz}		LUMO+3, d_{yz}	
HOMO, d_{xy}		LUMO+2, d_{xy}	

LUMO+1, d_{z2}		LUMO+7, d_{z2}	
LUMO+4, d_{x2-y2}		LUMO+8, d_{x2-y2}	
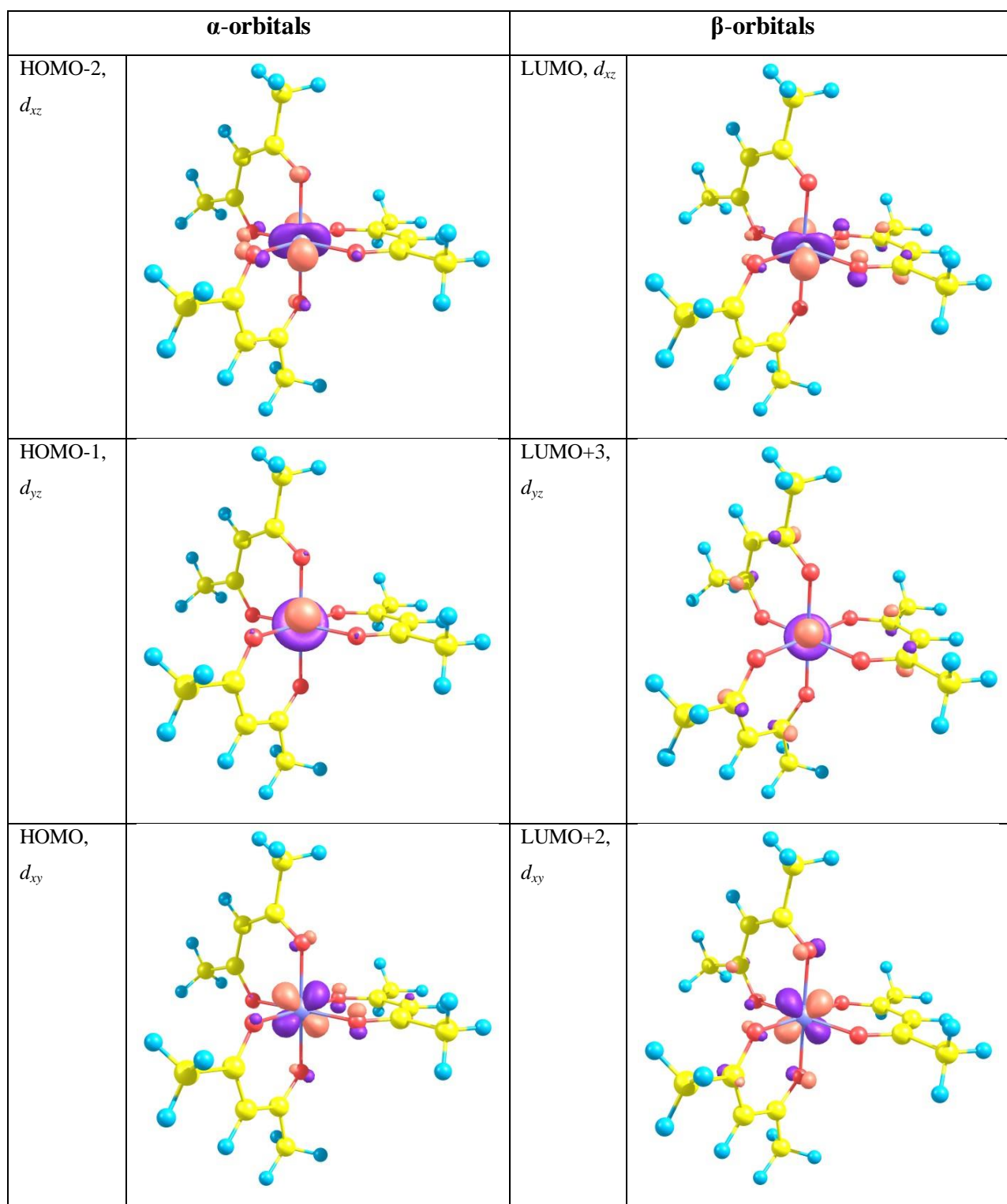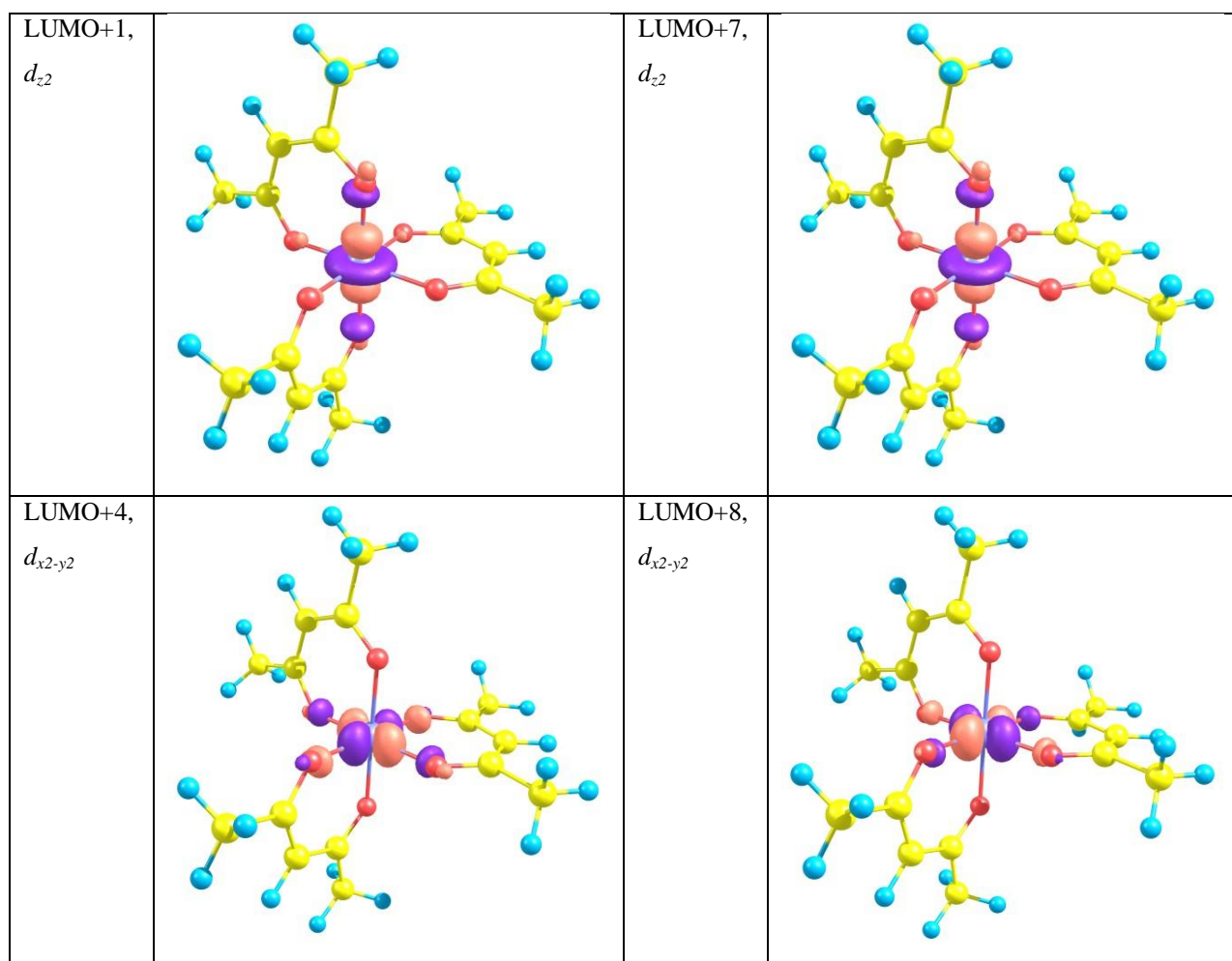
Reduction of the $Cr^{III}(acac)_3$ complex, involves the addition of an electron to the lowest unoccupied molecular orbital (LUMO) of the complex. Since the LUMO of the neutral $Cr^{III}(acac)_3$ is of Cr-d character (see **Figure 3.15**), the reduced $Cr^{II}(acac)_3^-$ (with charge q = -1) will be a d^4 complex, therefore with either 0 (S = 0), 2 (S = 2/2) or 4 (S = 4/2) unpaired electrons. The LUMO is a β-orbital, therefore a spin state of 2/2 (two unpaired electrons and 1 set of paired electons) is expected.

Table 3.14 gives the DFT results calculated for the reduced $Cr^{II}(acac)_3^-$ complex. Clearly, the spin state of 2/2 in D_3 symmetry has the lowest energy among the three possibilities. $Cr^{III}(acac)_3$ has three unpaired electrons; addition of an extra electron tends to pair one of these electrons to result in $Cr^{II}(acac)_3^-$, which has two unpaired electrons. This means that $Cr^{II}(acac)_3^-$ has a low spin on Cr, and the pairing energy (P) is lower than the splitting energy (Δ_o), between e_g and t_{2g} orbitals. (**Section 2.5.5**).

RESULTS AND DISCUSSION

Table 3.14: Relative DFT-calculated energies obtained by the different functionals, for the indicated spin states and symmetries of $Cr^{II}(acac)_3^-$ (with charge q = -1).

Spin state	Sym-metry	Relative energy (eV)	Relative energy (eV)	Relative energy (eV)	Relative energy (eV)
		B3LYP	**OLYP**	**BP86**	**PW91**
0/2	C_1	0.813	0.858	0.624	0.608
	C_2	0.810	0.861	0.624	0.607
	C_3^a	—[c]	0.861	0.624	0.607
	D_3^b	3.038	1.467	1.247	1.218
2/2	C_1	0.000	0.000	0.000	0.000
	C_2	—	0.000	0.000	0.000
	C_3^a	0.000	0.000	0.000	0.000
	D_3	—	0.000	0.000	0.000
4/2	C_1	—	0.139	0.578	0.578
	C_2	—	—	—	—
	C_3^a	—	—	—	—
	D_3^b	—	—	—	—

a C_3 input geometry run in C_1 symmetry in ADF.

b D_3 not possible for S = 0/2 or 4/2 since the E orbitals are partially occupied, no symmetry available.

c. All calculations that did not converged, are given with "—"

A second reduction of the $Cr^{III}(acac)_3$ complex can be viewed as :

(i) either the addition of an electron to the lowest unoccupied molecular orbital (LUMO) of the reduced $Cr^{II}(acac)_3^-$ complex, or

(ii) the addition of a second electron to the neutral $Cr^{III}(acac)_3$, in this case to the LUMO+1.

Since the LUMO+1 of the neutral $Cr^{III}(acac)_3$ is of Cr-d character (see **Figure 3.15**), the doubly reduced $Cr^I(acac)_3^{-2}$ (with charge q = -2) will be a d^5 complex, *i.e.* with either 1 (S = 1/2), 3 (S = 3/2) or 5 (S = 5/2) unpaired electrons.

Table 3.15 gives the DFT-results calculated for the doubly reduced $Cr^I(acac)_3^{-2}$ complex, indicating that S = 1/2 for $Cr^I(acac)_3^{-2}$. Since a low spin was obtained for $Cr^{II}(acac)_3^-$ (S = 2/2 for 4 d-electrons), it is expected that the addition of a second electron leads to another pairing of

electrons, namely S = 1/2 for $Cr^{I}(acac)_3{}^{-2}$. From the relative energy values, it follows that $Cr^{I}(acac)_3{}^{-2}$ has no symmetry since C_2 symmetry gives non-Aufbau occupation.

Table 3.15: Relative DFT-calculated energies obtained by the different functionals, for the indicated spin states and symmetries of $Cr^{I}(acac)_3{}^{-2}$ (with charge q = -2).

Spin state	Sym-Metry	Relative energy (eV)	Relative energy (eV)	Relative energy (eV)	Relative energy (eV)
		B3LYP	**OLYP**	**BP86**	**PW91**
1/2	C_1	0.000	—[d]	—[d]	—[d]
	$C_2{}^{[a]}$	0.000	—	0.000	—
	$C_3{}^{[b]}$	0.000	—	—	—
	$D_3{}^{[c]}$	0.192[c]	—	0.000	0.000
3/2	C_1	0.166	—	0.228	0.245
	$C_2{}^{[a]}$	—[d]	—	—	—
	$C_3{}^{[b]}$	—	—	—	—
	$D_3{}^{[c]}$	—	—	—	—
5/2	C_1	0.346	—	0.459	0.455
	$C_2{}^{[a]}$	—	—	—	—
	$C_3{}^{[b]}$	—	—	—	—
	$D_3{}^{[c]}$	—	—	—	—

a C_2 symmetry gives non-Aufbau occupation.

b C_3 input geometry run in C_1 symmetry in ADF.

c Symmetry not possible since the E orbitals are partially occupied and become non-degenerate.

d. All calculations that did not converged, are given with "—"

Oxidation of $Cr^{III}(acac)_3$ involves the removal of an electron from the HOMO of the complex. Since the HOMO of the neutral $Cr^{III}(acac)_3$ is of Cr-d character (see **Figure 3.15**), the oxidized $Cr^{IV}(acac)_3{}^{+}$ (with charge q = +1) will be a d^2 complex, *i.e.* with either 0 (S = 0) or 2 (S = 2/2) unpaired electrons.

Table 3.14 gives the DFT results, calculated for the oxidized $Cr^{IV}(acac)_3{}^{+}$ complex. The removal of an electron from $Cr^{III}(acac)_3$ with spin state of 3/2, will end up with two unpaired electrons,

which agrees with the results in **Table 3.14**. Therefore, it was concluded that the spin state with two unpaired electrons and D_3 symmetrywas favoured by $Cr^{IV}(acac)_3^+$ ($S = 2/2$).

Table 3.16: Relative DFT-calculated energies obtained by the different functionals, for the indicated spin states and symmetries of $Cr^{IV}(acac)_3^+$ (with charge q = +1).

Spin state	Sym-metry	Relative energy (eV)	Relative energy (eV)	Relative energy (eV)	Relative energy (eV)
		B3LYP	**OLYP**	**BP86**	**PW91**
0/2	C_1	0.350	0.705	0.495	0.504
	C_2	—[d]	0.706	0.494	0.483
	C_3[a]	—	0.706	0.494	0.482
	D_3[c]	0.924	1.202	1.633	0.992
2/2	C_1	—[d]	0.000	0.000	0.001
	C_2[b]	—	0.079[b]	0.043[b]	0.043[b]
	C_3[a]	—	0.002	0.000	0.000
	D_3[c]	0.000	0.072[b]	0.103[b]	0.108[b]

a C_3 input geometry run in C_1 symmetry in ADF.

b C_2 symmetry gives non-Aufbau occupation for S = 2/2.

c Symmetry not possible since the *E* orbitals are partially occupied and become non-degenerate.

d. All calculations that did not converged, are given with "—"

A second oxidation of $Cr^{III}(acac)_3$ involves the removal of a second electron from $Cr^{III}(acac)_3$, in this case the electron in the HOMO-1. Since the HOMO-1 of the neutral $Cr^{III}(acac)_3$ is of Cr-d character (see **Figure 3.15**), the doubly oxidized $Cr^{V}(acac)_3^{+2}$ (with charge q = +2) will be a d^1 complex, *i.e.* it must be paramagnetic with one unpaired electron (S = 1/2). **Table 3.17** gives the DFT results calculated for the doubly oxidized $Cr^{V}(acac)_3^{+2}$ complex. From the relative energy values, it follows that $Cr^{V}(acac)_3^{+2}$ has no symmetry since C_2 symmetry gives non-Aufbau occupation.

Table 3.17: Relative DFT-calculated energies, for the indicated spin states and symmetries of doubly oxidized $Cr^V(acac)_3^{+2}$ (with charge q = +2).

Spin state	Sym-metry	Relative energy[b] (eV)	Relative energy[b] (eV)	Relative energy[b] (eV)	Relative energy[b] (eV)
		B3LYP	**OLYP**	**BP86**	**PW91**
1/2	C_1	0.000	0.000	0.000	0.000
	C_2	—[c]	0.000	0.000	0.000
	C_3[a]	—	0.000	0.000	0.000
	D_3	0.000	0.000	0.000	0.000

a C_3 input geometry run in C_1 symmetry in ADF.

b. Energies within a spesific functional are compared. NOTE the energies across functional are not compared here.

c. All calculations that did not converged, are given with "—"

3.1.4.2 DFT-calculated geometry of the Cr(acac)₃ complex

In this section the DFT-calculated geometry of Cr(acac)₃, as calculated by four different functionals, will be compared to the experimental geometry of Cr(acac)₃ {1}7. The DFT results obtained in the section above, clearly show that Cr(acac)₃ has a D_3 symmetry. Due to this symmetry, all the calculated Cr-O bonds will be equal within experimental accuracy, as well as for the O – Cr – O bond angles, etc. Therefore, the calculated geometrical results will be compared to the average of the experimental values (see also **Table 3.3**). **Scheme 3.4** shows the atom numbering used for the DFT-calculated bonds and angles which are tabulated in **Table 3.18**.
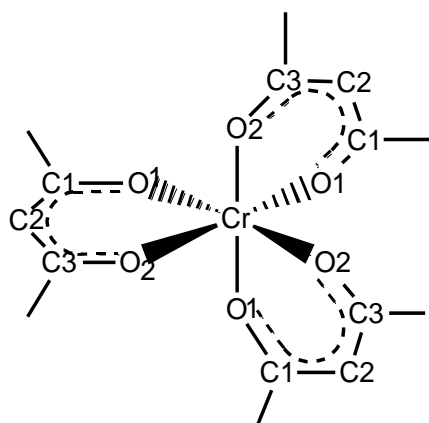
Scheme 3.4: Scheme showing atom numbering for Cr(acac)₃ {1}.

All DFT-calculated results showed longer Cr – O bonds than the average experimental bond length, but the difference is small, namely 0.052 Å (OLYP) to 0.022 Å (PW91). All calculations gave slightly longer C1 – C2 bond length than the experimental crystal data. For the O – Cr – O bond angles, OLYP gave a result smaller than the average from the experimental crystal data, and other functionals gave larger results. However, the slight difference between the calculated and experimental data is expected, since it is known that GGA density functionals tend to overestimate bonds lengths.[25] B3LYP gave the same C1 – C2 – C3 bond angle as the average of the experimental results, while other functionals gave smaller C1 – C2 – C3 angles. Generally PW91 gave geometry parameters nearest to the experimental average.

Table 3.18: DFT-calculated and experimental geometrical parameters for Cr(acac)$_3$.

	Average Experimental Values[7]	B3LYP	OLYP	BP86	PW91
Cr – O Bond length (Å)	1.960(8)	1.983	2.008	1.980	1.978
C1 - C2 Bond length (Å)	1.390(11)	1.401	1.406	1.407	1.405
O – Cr – O Bond angle ($^\circ$)	91.1(4)	91.5	89.7	91.4	91.5
C1 - C2 - C3 Bond angle ($^\circ$)	125.0(6)	125.0	124.4	124.6	124.6

3.1.4.3 Geometry of Cr(β-diketonato)$_3$ complexes

DFT-calculated results involved in this section were obtained using the PW91 functional. D_3 symmetry was used for complexes with symmetrically substituted β-diketonato ligands, *i.e.* complexes {1}, {3} and {8}. C_1 (no symmetry) was used for complexes with unsymmetrically substituted β-diketonato ligands, *i.e* complexes {2}, {4} − {7}.

Table 3.19 summarizes the DFT-calculated and experimental results of the Cr – O bond lengths and O – Cr – O bond angles for the symmetrical complexes {1}, {3} and {8}. The experimental values for complexes {1}, {3} and {8} all have the character of D_3 symmetry, namely, near-identical Cr – O bond lengths and O – Cr – O bond angles. Complexes {1}, {3} and {8} have longer calculated Cr – O distance and larger calculated O – Cr – O angles than the average published experimental values.

---

25 (a) Scheiner, A.C.; Baker, J.; Andzelm, J.W.; *J. Comput. Chem.*, **1997**, *18*, 775-795 (b) Hill, J.R.; Freeman, C.M.; Delley, B.; *J. Phys. Chem. A*, **1999**, *103*, 3772-3777. (c) Furche, F.; Perdew, J.P.; *J. Chem Phys.*, **2006**, *124*, 044103-044129.

Table 3.19: DFT-calculated Cr – O bond lengths and O – Cr – O bond angles, obtained for complexes {1}, {3} and {8} with symmetrically substituted β-diketonato ligands, using the PW91 functional and D_3 symmetry (with the average experimental geometrical parameters in brackets).

Complex	d(Cr – O) (Å)	O – Cr – O (°)
Cr(acac)$_3$ {1}[7]	1.978 (1.960(8))	91.5 (91.1(4))
Cr(dbm)$_3$ {3}^{a}	1.964 (1.953(11))	90.8 (90.2(5))
Cr(hfaa)$_3$ {8}[8]	1.975 (1.943(15))	91.1 (90.6(2))

a Experimental values from this study, see Section 3.1.2.

Table 3.20 summarizes the various Cr – O bond lengths and O – Cr – O bond angles for complexes {2}, {4} – {7}, containing unsymmetrically substituted β-diketonato ligands. Tris(β-diketonato)chromium(III) complexes with unsymmetrical ligands have two types of Cr – O bonds: the bonds near substituent R_1 and the bonds near substituent R_2.

In comparing the average of the three bond lengths in a complex near substituent R_1 with the average of the bonds near substituent R_2, we observe that values are the same within standard deviation or the difference is so small, that it can still be considered the same for all practical purposes.

The the *fac*-complexes, the calculated O – Cr – O bond angles obtained without any symmetry constraint are very similar, and all alternately calculated Cr – O bond lengths are nearly identical, implying C_3 symmetry for the *fac*-complexes, for all practical purposes. For a *mer*-complex, ligands coordinate in an "unsymmetrical" way (with one ligand pointing anti-clockwise opposite to the others), and therefore no symmetry is possible.

Table 3.20: DFT-calculated Cr – O bond lengths and O – Cr – O bond angles, obtained for complexes {2}, {4} – {7} with unsymmetrically substituted ligands, using the PW91 functional and C_1 symmetry.

Complex			d(Cr - O) (Å)	d(Cr - O) (Å) average	O - Cr - O (°)	O - Cr - O (°) average
Cr(ba)$_3$ {2}	*fac*	Bond near CH$_3$	1.969	1.969 (1)	91.2	91.2 (1)
			1.970			
			1.969		91.2	
		Bond near Ph	1.971	1.973 (2)		
			1.974		91.3	
			1.973			
	mer	Bond near CH$_3$	1.970	1.972 (2)	91.2	91.2 (0)
			1.973			
			1.973		91.2	
		Bond near Ph	1.970	1.970 (2)		
			1.972		91.2	
			1.969			
Cr(tfba)$_3$ {4}	*fac*	Bond near CF$_3$	1.970	1.969 (1)	91.1	91.1 (1)
			1.969			
			1.969		91.1	
		Bond near Ph	1.970	1.970 (0)		
			1.970		91.0	
			1.970			
Cr(tfba)$_3$ {4}	*mer*	Bond near CF$_3$	1.969	1.974 (5)	90.7	90.8 (1)
			1.974			
			1.978		90.8	
		Bond near Ph	1.968	1.971 (3)		
			1.969		90.7	
			1.974			
Cr(tfth)$_3$ {5}	*fac*	Bond near CF$_3$	1.970	1.970 (1)	91.5	91.4 (1)
			1.969			
			1.971		91.4	
		Bond near Th	1.971	1.972 (2)		
			1.970		91.3	
			1.974			
	mer	Bond near CF$_3$	1.974	1.972 (3)	91.3	91.3 (1)
			1.968			
			1.974		91.4	
		Bond near Th	1.972	1.971 (2)		
			1.968		91.3	
			1.970			

86

Cr(tffu)$_3$ {6}	*fac*	Bond near CF$_3$	1.972	1.972 (1)	91.7	91.7(1)
			1.973			
			1.971		91.5	
		Bond near Fu	1.971	1.970 (2)		
			1.972		91.7	
			1.968			
	mer	Bond near CF$_3$	1.975	1.974 (3)	91.6	91.6(1)
			1.970			
			1.976		91.7	
		Bond near Fu	1.970	1.970 (2)		
			1.966		91.5	
			1.970			
Cr(tfaa)$_3$ {7}	*fac*	Bond near CH$_3$	1.978	1.974 (0)	91.4	91.4 (0)
			1.978			
			1.978		91.4	
		Bond near CF$_3$	1.974	1.978 (0)		
			1.974		91.4	
			1.974			
	mer	Bond near CH$_3$	1.976	1.973 (2)	91.4	91.4 (1)
			1.979			
			1.977		91.3	
		Bond near CF$_3$	1.973	1.977 (1)		
			1.974		91.4	
			1.973			

3.1.4.4 Relative energies of Cr(β-diketonato)$_3$ complexes

In this section, the experimentally measured reduction potential (E$_{pc}$ Cr$^{III/II}$) is compared to the DFT-calculated energies of the chromium complexes. The reduction of complexes {1} − {8} involves the addition of an electron to the LUMO of the complex, and thus the relationship between the reduction potential (Section 3.1.3) and E_{LUMO} can be established. Electron affinity (EA) is the energy difference between the neutral complex and the single-reduced complex (see **Equation 3.9** and **Equation 3.10**):

Equation 3.9: $Cr^{III}(\beta - diketonato)_3 + e^- = Cr^{II}(\beta - diketonato)_3 + EA$
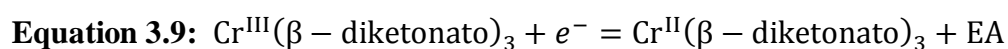
Equation 3.10: $EA = E_{Cr^{III}(\beta-diketonato)_3} - E_{Cr^{II}(\beta-diketonato)_3}$ (10)

Therefore, the relationship between the reduction potential and electron affinity, is also discussed in this section.

Table 3.21: DFT-calculated energies for complexes {1} – {8} and their reduced species, calculated by functional PW91.

Complex		$Cr^{III}(\beta)_3$ (eV)	$Cr^{II}(\beta)_3^-$ (eV)	EA (eV)	E_{LUMO} (eV)
Spin State:		3/2	2/2		
Cr(acac)$_3$ {1}		-265.838	-266.822	0.983	-2.571
Cr(ba)$_3$ {2}	*fac*	-421.955	-423.584	1.629	-2.915
	mer	-421.958	-423.586	1.628	-2.911
Cr(dbm)$_3$ {3}		-578.048	-580.042	1.994	-3.148
Cr(tfba)$_3$ {4}	*fac*	-424.740	-427.255	2.515	-3.845
	mer	-424.716	-427.231	2.515	-3.827
Cr(tfth)$_3$ {5}	*fac*	-358.946	-361.427	2.481	-3.827
	mer	-359.007	-361.465	2.458	-3.784
Cr(tffu)$_3$ {6}	*fac*	-366.4471	-368.7981	2.351	-3.716
	mer	-366.488	-368.872	2.384	-3.658
Cr(tfaa)$_3$ {7}	*fac*	-268.571	-270.743	2.172	-3.764
	mer	-268.585	-270.758	2.173	-3.765
Cr(hfaa)$_3$ {8}		-270.852	-274.192	3.340	-4.934

Table 3.21 gives a summary of the DFT-calculated energies of complexes {1} – {8} and their reduced species, calculated by functional PW91. For complexes {2}, {4} – {7} with unsymmetrically substituted ligands, the values were displayed separately for the *fac-* and *mer-* isomers. Respective ratios of these isomers were obtained by the Boltzmann distribution function, and are tabulated in **Table 3.22**.

Table 3.22: Calculated Boltzmann population of *fac*- and *mer*-isomers of $Cr^{III}(\beta\text{-diketonato})_3$ and $Cr^{II}(\beta\text{-diketonato})_3^-$.

$Cr^{III}(\beta\text{-diketonato})_3$		Boltzmann population (%)	$Cr^{II}(\beta\text{-diketonato})_3^-$		Boltzmann population (%)
$Cr^{III}(ba)_3$ {2}	*fac*	47	$Cr^{II}(ba)_3$	*fac*	49
	mer	53		*mer*	51
$Cr^{III}(tfaa)_3$ {7}	*fac*	37	$Cr^{II}(tfaa)_3$	*fac*	64
	mer	67		*mer*	36
$Cr^{III}(tfba)_3$ {4}	*fac*	72	$Cr^{II}(tfba)_3$	*fac*	72
	mer	28		*mer*	28
$Cr^{III}(tfth)_3$ {5}	*fac*	8	$Cr^{II}(tfth)_3$	*fac*	19
	mer	92		*mer*	81
$Cr^{III}(tffu)_3$ {6}	*fac*	17	$Cr^{II}(tffu)_3$	*fac*	95
	mer	83		*mer*	5

The electron affinity and final LUMO energy were obtained by the sum of *fac*- and *mer*-isomers, according to their respective ratios. These values are tabulated in **Table 3.23**, together with the reduction potential of complexes {1} − {8}.

Table 3.23: The electron affinity, LUMO energy and reduction potential of complexes {1} − {8}.

Complexes	EA (eV)	E_{LUMO} (eV)	$E_{pc}Cr^{III/II}$ (mV)
$Cr(acac)_3$ {1}	0.983	-2.571	-2329
$Cr(ba)_3$ {2}	1.629	-2.913	-2132
$Cr(dbm)_3$ {3}	1.994	-3.148	-1910
$Cr(tfba)_3$ {4}	2.515	-3.840	-1273
$Cr(tfth)_3$ {5}	2.460	-3.787	-1371
$Cr(tffu)_3$ {6}	2.388	-3.668	-1293
$Cr(tfaa)_3$ {7}	2.176	-3.764	-1547
$Cr(hfaa)_3$ {8}	3.340	-4.934	-807

By using the data from **Table 3.23**, the relationship of reduction potential against LUMO energy and electron affinity, is illustrated in **Figure 3.16** and **Figure 3.17** respectively:
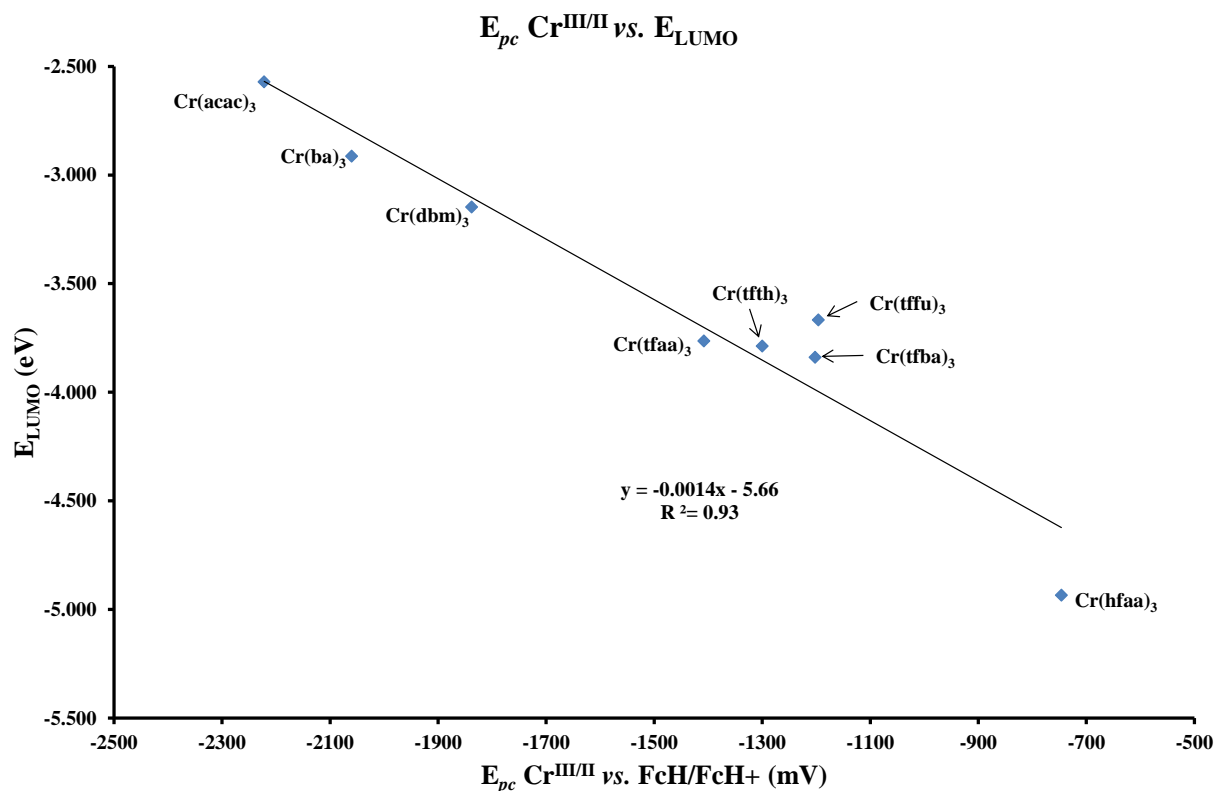
Figure 3.16: The relationship between the reduction potential of the Cr^{III}(β-diketonato)$_3$ complexes ($E_{pc}Cr^{III/II}$) *vs.* LUMO energy (E_{LUMO}), according to data from **Table 3.23**.

From **Figure 3.16**, it is clear that the LUMO energy is inversely proportional to the reduction potential of Cr^{III}(β-diketonato)$_3$ complexes. This is expected, since a lower LUMO energy (more negative value) can more easily accept the addition of an electron during reduction. The ease of acceptance of an electron naturally leads to a more positive reduction potential. The relation between reduction potential of the Cr^{III}(β-diketonato)$_3$ complexes ($E_{pc}Cr^{III/II}$) and LUMO energy (E_{LUMO}), is given by **Equation 3.11**

Equation 3.11: $E_{LUMO} = -0.0014\,E_{pc} - 5.66$
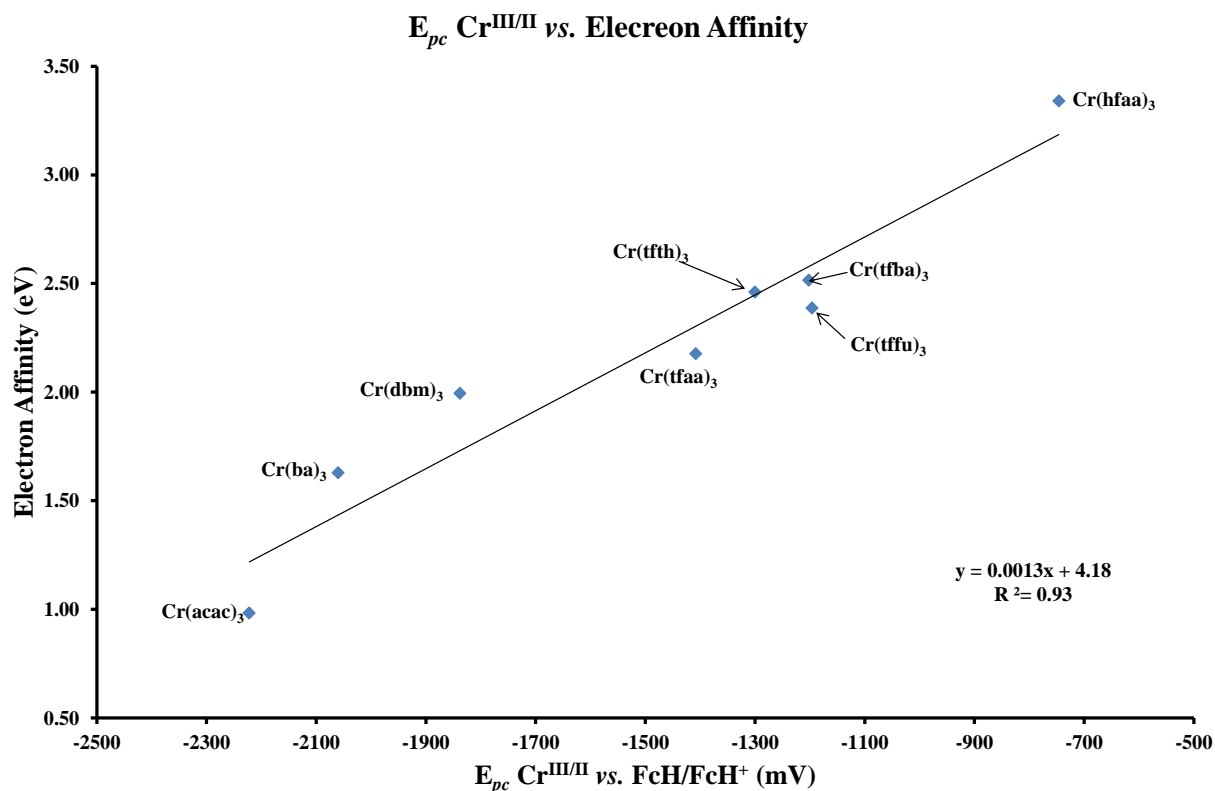
Figure 3.17: The relationship between the reduction potential of the Cr^{III}(β-diketonato)$_3$ complexes ($E_{pc}Cr^{III/II}$) *vs.* Electron Affinity (EA), according to data from **Table 3.23**.

Figure 3.17 shows the direct proportionality between electron affinity (EA) and reduction potential (E_{pc}). A higher electron affinity causes the metal center (Cr^{III}) to more easily attract an electron, therefore leading to an reduction with more positive potential. The relationship between the reduction potential of the Cr^{III}(β-diketonato)$_3$ complexes ($E_{pc}Cr^{III/II}$) and Electron Affinity (EA), is given by **Equation 3.12**

Equation 3.12: $EA = 0.0013\, E_{pc} + 4.18$

3.2 Tris(β-diketonato)cobalt(III) Complexes

3.2.1 Synthesis

All synthesized tri(β-diketonato)cobalt(III) complexes (complexes {9}-{13}) were based on the method of Bryant and Fernelius[26] (**Scheme 3.5**). Cobalt(II) carbonate (1.25 g, 0.0105 mole) and the relevant β-diketone ligand (10 mmole) were mixed with continuous stirring. An additional 10 mL of ethanol was added when the β-diketonato ligands were solids. This mixture was preheated to 95 °C. 25 % hydrogen peroxide (15 mL) was added dropwise to the suspension over 30 minutes, stirring constantly. Addition of H_2O_2 to the ligand suspension caused vigorous frothing, therefore the H_2O_2 addition was conducted very slowly. Cobalt(II) carbonate was oxidized to cobalt(III) oxide by the hydrogen peroxide. In the presence of the β-diketonato ligand in the suspension, the coordination to the freshly oxidized Co^{III} cation proceeded immediately. Stirring and heating were kept constant for another hour in order to reach complete coordination. All five desired complexes appeared to be precipitates, and were filtered and washed with excess water. Each product was filtered and dried on the funnel and then in a desiccator at room temperature.

fac-isomer   *mer*-isomer
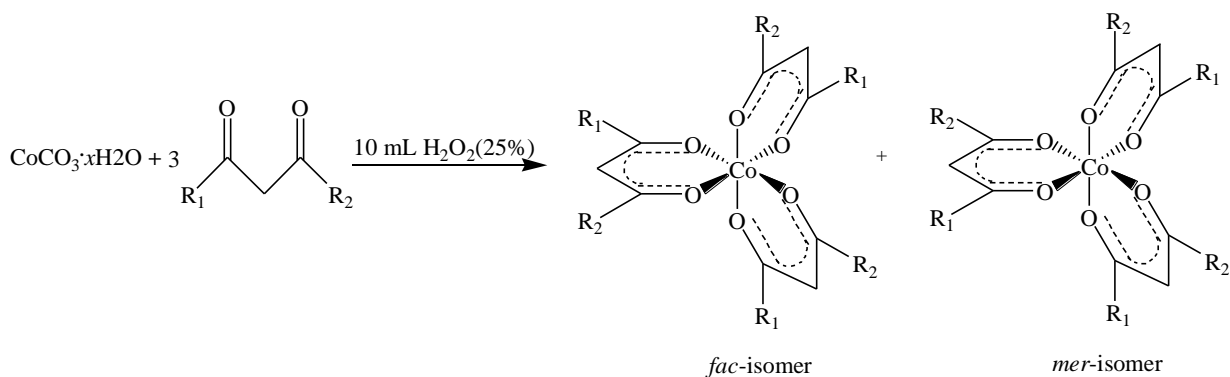
Scheme 3.5: General synthetic method for the tris(β-diketonato)cobalt(III) complexes, where R_1, R_2 = CH_3, CH_3 {9}; CH_3, C_6H_5 {10}; C_6H_5, C_6H_5 {11}; CF_3, C_6H_5 {12}; CH_3, CF_3 {13}.

---

[26] Bryant, B. E.; Fernelius, W.C.; *Inorg. Syn.,* **1957**, *5*, 188-189

Table 3.24: Summary of the yields of all the tris(β-diketonato)cobalt(III) complexes that were synthesized.

Complex	Name	Yield (%)
Co(acac)$_3$ {9}	tris(2,4-pentadionato)cobalt(III)	63.1
Co(ba)$_3$ {10}	tris(1-phenyl-1,3-butanedionato)cobalt(III)	66.3
Co(dbm)$_3$ {11}	tris(1,3-diphenyl-1,3-propanedionato)cobalt(III)	72.3
Co(tfba)$_3$ {12}	tris(4,4,4-trifluoro-1-phenyl-1,3-butanedionato)cobalt(III)	13.38
Co(tfaa)$_3$ {13}	tris(1,1,1-trifluoro-2,4-pentadionato)cobalt(III)	50.8

3.2.2 Crystal Structures

Crystal structures of complexes Co(acac)$_3$ {9}[27] and Co(dbm)$_3$ {11}[28] and Co(tfaa)$_3$ {13}[29] have been published previously. The structure of Co(ba)$_3$ {10} and Co(tfba)$_3$ {12} are presented and discussed here, as representative example of the structures of the Co(β-diketonato)$_3$ type of complexes with cobalt. The molecular structure of {10} with the atom-numbering scheme, is shown in **Figure 3.18**. The molecular structure of {12} with the atom-numbering scheme is shown in **Figure 3.19**. Selected bond lengths and angles for complexes {10} and {12} are given in **Table 3.25** and **Table 3.26**, respectively, and their averages compared to the corresponding geometrical parameters of complexes {9}, {11} and {13} in **Table 3.27**. The cif files with complete crystallographic data are given in **Appendix D**.

Two stereo isomers are possible for M(β-diketonato)$_3$ complexes with unsymmetrically substituted ligands, namely the facial isomer (*fac*) and the meridional isomer (*mer*), as illustrated above in **Scheme 3.5**. In the facial isomer, the β-diketonato ligands coordinate 'symmetrically' to the metal with the two different groups on each ligand pointing 'symmetrically' in a clockwise direction, which is not the case for the meridional isomer.

---

[27] Cambridge Structural Database (CSD), Version 5.34, May 2013 update, CSD reference codes: COACAC02, COACAC03, COACAC06, COACAC07, COACAC08, COACAC09, COACAC10

[28] Cambridge Structural Database (CSD), Version 5.34, May 2013 update, CSD reference codes: JINRIH01, JINRIH02

[29] Cambridge Structural Database (CSD), Version 5.34, May 2013 update, CSD reference codes: GUCGOA
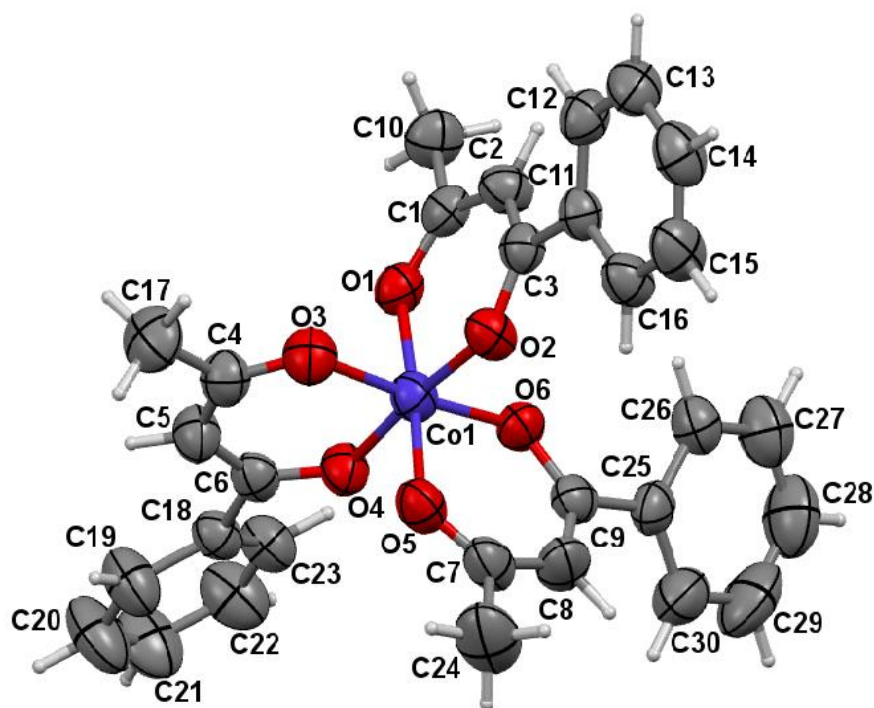
Figure 3.18: A perspective drawing of the molecular structure of the *mer* isomer of Co(ba)$_3$ {10}, showing the atom numbering scheme. Atomic dispacement parameters (ADPs) are shown at the 50 % probability level.

Table 3.27 compares the averages of the selected bond lengths, bond angles and dihedral angles of the *mer* isomer of Co(ba)$_3$ {10} and the *fac* isomer of Co(tfba)$_3$ {10}, with the same parameters of the symmetrically substituted complexes Co(acac)$_3$ {9}[27], Co(dbm)$_3$ {11}[28] and the *mer* isomer of the unsymmetrical Co(tfaa)$_3$ {13}[29].

Firstly considering the bond lengths listed in this table: complexes Co(acac)$_3$ {9} and Co(dbm)$_3$ {11} have symmetrically substituted β-diketonato ligands, with average Co – O bond lengths of 1.886(10) Å and 1.883(9) Å respectively. However, Co(ba}$_3$ {10}, Co(tfba)$_3$ {12} and Co(tfaa)$_3$ {13} have unsymmetrically substituted β-diketonato ligands. In Co(ba)$_3$ {10}, the Co – O bond (1.875(4) Å) near the trans Ph group is shorter than the Co – O bond (1.886(3) Å) near the CH$_3$ group. A similar trend was observed for Co(tfba)$_3$, the Co – O bond near CF$_3$ group (1.880(7) Å) is longer than the Co – O bond near the phenyl group (1.875(6) Å). The difference in Co – O bonds is however less obvious in the Co(tfba)$_3$ crystal. On the other hand, both types of Co – O bonds in the unsymmetrical Co(tfaa)$_3$ {13} have similar bond lengths: 1.892(29) Å for the Co – O near CF$_3$, and 1.891(25) Å for the Co – O near CH$_3$. From these results no definite trend or conclusion can be made.

Secondly, considering the bond angles O – Co – O, which describe the angle formed by two Co – O bonds within the same β-diketonato ligand: the average O – Co – O bond angles found for all four cobalt complexes are about 96 °, ranging from 95.5(6) ° (Co(dbm)$_3$ {11}) to 96.7(3) ° (Co(acac)$_3$ {9}).

Lastly considering the dihedral angles, which are the angles formed between any two planes within the molecule: Each of these planes contains four oxygen atoms at the vertices, with one cobalt atom in the middle. As tabulated in **Table 3.25** for Co(ba)$_3$ {10}, the angle formed between the two planes O1-O2-Co-O4-O5 and O2-O3-Co-O4-O6 is 87.1(3) °, the dihedral angle between planes O1-O2-Co-O4-O5 and O1-O3-Co-O5-O6 is 87.1(3) °, and the dihedral angle between planes O2-O3-Co-O4-O6 and O1-O3-Co-O5-O6 is 87.8(3) °. All four these complexes have average dihedral angles ranging from 86.2(1.9) ° (Co(tfba)$_3$ {12}) to 88.2(6) ° (Co(tfaa)$_3$ {13}). This negligible difference indicates that the changes in the R$_1$ and R$_2$ substituents on the β-diketonato ligands do not influence the dihedral angles of the tris(β-diketonato)cobalt(III) complexes.

Table 3.25: Selected geometrical parameters for *mer*-Co(ba)$_3$ {10} (this study).

	Co – O Bond length (Å)	**O – Co – O Bond angle (°)**	**Dihedral angle (°)**
Bond near Ph	1.879(2)	96.2(1)	87.1(3)
	1.875(2)		
	1.872(2)	96.3(1)	87.1(3)
Bond near CH$_3$	1.888(3)		
	1.883(2)	95.5(1)	87.8(3)
	1.887(3)		
Average	**1.875**(4) near Ph **1.886**(3) near CH$_3$	**96.0**(4)	**87.3**(4)
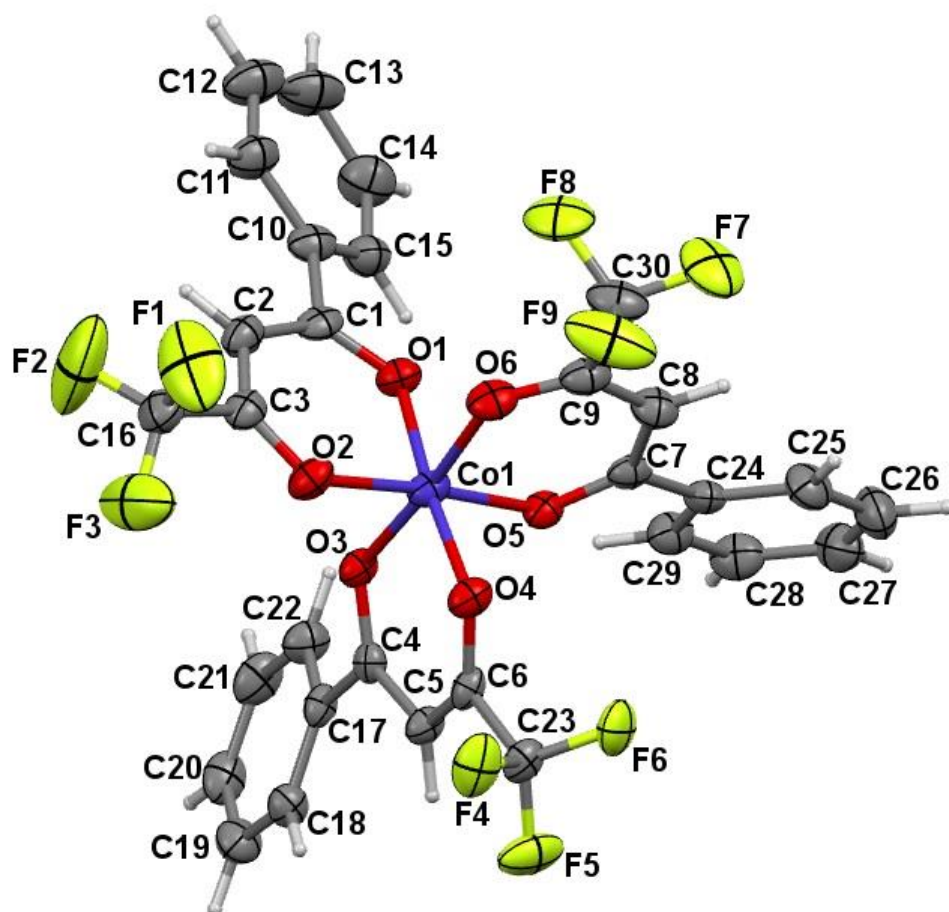
Figure 3.19: A perspective drawing of the molecular structure of the *fac* isomer of Co(tfba)₃ {12} showing the atom numbering scheme. Atomic dispacement parameters (ADPs) are shown at the 50 % probability level.

Table 3.26: Selected geometric parameters for Co(tfba)₃ {12} (this study).

	Co – O Bond length (Å)	**O – Co – O Bond angle (°)**	**Dihedral angle (°)**
Bond near CF₃	1.881(3)	95.9(1)	84.1(3)
	1.882(3)		86.7(3)
	1.875(3)	95.7(1)	87.9(3)
Bond near Ph	1.872(3)		
	1.869(3)	95.9(1)	
	1.885(3)		
Average	**1.880**(7) near CF₃ **1.875**(6) near Ph	**95.8**(1)	**86.2** (1.9)

Table 3.27: Selected average geometrical parameters for Co(ba)$_3$ {10} (this study), Co(tfba)$_3$ {12} (this study), Co(acac)$_3$ {9}, Co(dbm)$_3$ {11} and Co(tfaa)$_3$ {13}.

Average values for:	Co – O Bond length (Å)	O – Co – O Bond angle (°)	Dihedral angle (°)	Fac or Mer
Co(ba)$_3$ {10}	1.875(4) (near Ph); 1.886(3) (near CH$_3$)	96.0(4)	87.3(4)	Mer
Co(tfba)$_3$ {12}	1.880(7) (near CF$_3$) 1.875(6) (near Ph)	95.8(1)	86.2(1.9)	Fac
Co(acac)$_3$ {9}^{a}	1.886(10)	96.7(3)	87.7(2)	-
Co(dbm)$_3$ {11}^{a}	1.883(9)	95.5(6)	87.5(5)	-
Co(tfaa)$_3$ {13}^{a}	1.892(25) (near CF$_3$); 1.891(29) (near CH$_3$)	96.1(1.3)	88.2(6)	Mer

a Data form Chapter 2 **Tables 2.8** and **Table 2.9**

All five complexes have similar geometrical parameters. An interesting fact is that the meridional *mer*-isomer of Co(ba)$_3$ {10} was obtained while the facial (*fac*-) isomers were obtained for Co(tfba)$_3$. A *mer*-isomer was also reported in literature for the Co(tfaa)$_3$ crystal.[30] In a facial (*fac*-) structure, large substituents (such as phenyl rings in {10}) on the β-diketonato backbone could have a steric influence on each other, favouring a meridional isomer. Computational chemistry results on the relative energy of the *fac*- and *mer*- isomer of Co(tfaa)$_3$ showed, in agreement with the experimental structure, that the *fac*-isomer is more stable than the *mer*-isomer by 0.01 eV, see Section 3.2.3. However, computational chemistry results on the relative energy of the *fac*- and *mer*- isomers of Co(ba)$_3$ {10} and Co(tfba)$_3$ {12}, showed that while both isomers are possible for Co(ba)$_3$ {10} and Co(tfba)$_3$ {12}, in this study the minor isomer was isolated and solved by solid state crystallography in this sudy for both Co(ba)$_3$ {10} and Co(tfba)$_3$ {12}.

All five complexes are in octahedral geometry. In this study, Co(ba)$_3$ {10} crystallized in the triclinic crystal system, and *P1* space group. All of the reported Co(acac)$_3$ {9} crystals are in the monoclinic crystal system, and with space group *P2$_1$/c*[27]. Two symmetry groups were reported for Co(dbm)$_3$[28] {11}: triclinic with *P1* space group, and also monoclinic with *P2$_1$/c* space group. Co(tfaa)$_3$[29] {13} was reported to be orthorhombic with space group *Pca2$_1$*.

---

30 Vogelson, C. T.; Edwards, C. L.; Kobylivker, A. N.; Chacko, S. B.; Moran, C. E.; Dalton, K.; Werner, B. C.; Bott, S. G.; Barron, A. R.; *J. Chem. Cryst.,* **1998**, *28*, 815-824

Table 3.28: Crystal data and structure refinement of Co(ba)$_3$, {10}.

Empirical formula	C$_{30}$H$_{27}$CoO$_6$
Formula weight	542.44
Temperature	150(2) K
Wavelength	0.71073 Å
Crystal system	Triclinic
Space group	P -1
Unit cell dimensions	a = 9.7546(5) Å, α = 83.883(2) °
	b = 9.8755(6) Å, β = 84.5540(10) °
	c = 14.2557(8) Å, γ = 77.6970(10) °
Volume	1330.41(13) Å^3
Z	2
Density (calculated)	1.354 Mg/m^3
Absorption coefficient	0.687 mm^{-1}
F(000)	564
Crystal size	0.211 x 0.113 x 0.076 mm^3
Theta range for data collection	2.455 to 25.398 °
Index ranges	-11<=h<=11, -11<=k<=11, -17<=l<=17
Reflections collected	48040
Independent reflections	4881 [R(int) = 0.0611]
Completeness to theta = 25.242 °	99.90 %
Absorption correction	None
Refinement method	Full-matrix least-squares on F2
Data / restraints / parameters	4881 / 0 / 334
Goodness-of-fit on F2	1.098
Final R indices [I>2sigma(I)]	R1 = 0.0511, wR2 = 0.1225
R indices (all data)	R1 = 0.0810, wR2 = 0.1346
Extinction coefficient	n/a
Largest diff. peak and hole	0.473 and -0.225 e.Å^{-3}

Table 3.29: Crystal data and structure refinement of Co(tfba)$_3$, {12}.

Empirical formula	C$_{30}$H$_{18}$CoF$_9$O$_6$
Formula weight	704.37
Temperature	150(2) K
Wavelength	0.71073 Å
Crystal system	Monoclinic
Space group	P 21/c
Unit cell dimensions	a = 9.5067(7) Å, a= 90 °
	b = 31.906(2) Å, b= 108.122(2) °
	c = 9.9607(8) Å, g = 90 °
Volume	2871.4(4) Å^3
Z	4
Density (calculated)	1.629 Mg/m^3
Absorption coefficient	0.700 mm^{-1}
F(000)	1416
Crystal size	0.172 x 0.163 x 0.078 mm^3
Theta range for data collection	2.244 to 26.368 °.
Index ranges	-11<=h<=11, -39<=k<=39, -12<=l<=12
Reflections collected	88047
Independent reflections	5878 [R(int) = 0.0517]
Completeness to theta = 25.242 °	100.00%
Absorption correction	Semi-empirical from equivalents
Max. and min. transmission	0.7454 and 0.6577
Refinement method	Full-matrix least-squares on F2
Data / restraints / parameters	5878 / 0 / 415
Goodness-of-fit on F2	1.219
Final R indices [I>2sigma(I)]	R1 = 0.0669, wR2 = 0.1532
R indices (all data)	R1 = 0.0782, wR2 = 0.1577
Extinction coefficient	n/a
Largest diff. peak and hole	0.970 and -0.805 e.Å^{-3}

3.2.3 Computational Results on Co(β-diketonato)$_3$

3.2.3.1 Spin state and symmetry of the Co(acac)$_3$ complex

The neutral Co^{III}(β-diketonato)$_3$ complexes are d^6 complexes. With 6 d-electrons, three possible spin states were evaluated, namely S = 0/2 (no unpaired electron, low spin), S = 2/2 (two unpaired electrons, high spin) or S = 4/2 (four unpaired electrons, high spin). **Table 3.30** gives the relative energy obtained for the neutral Co^{III}(acac)$_3$ complex {9}, by using the PW91 functional. Three possible symmetries were tested, namely C_2, C_3 and D_3. The spin state of S = 0/2 (lower energy) showed preference over S = 2/2 and 4/2, for all possible symmetries. This result agrees with the findings in literature.[31]

Table 3.30: DFT-calculated relative energies obtained by the PW91 functional, for the indicated spin states and symmetries for Co^{III}(acac)$_3$ {9}.

Co^{III}(acac)$_3$	Relative Energy (eV)		
Symmetry:	S = 0/2	S = 2/2	S = 4/2
C_2	0.000	1.329	1.314
C_3	0.000	1.024	1.314
D_3	0.000	1.023	1.312

Table 3.31 lists the Co – O bond lengths and O – Co – O bond angles of Co^{III}(acac)$_3$ {9}, with S = 0/2. Calculations gave the same results for all Co – O distances and O – Co – O bond angles. Similar to the chromium complex {1}, Cr(acac)$_3$ (Section 3.1.4.1), all possible input symmetries optimized to D_3 symmetry during the calculations. Therefore, D_3 symmetry was used for all further Co^{III}(β-diketonato)$_3$ calculations.

Table 3.31: DFT-calculated Co – O bond lengths and O – Co – O bond angles obtained by the PW91 functional, for the indicated symmetries for Co(acac)$_3$ {9}.

Symmetry	d(Co – O) (Å)						O – Co – O (°)		
C_2	1.907	1.907	1.907	1.907	1.907	1.907	97.2	97.2	97.2
C_3	1.907	1.907	1.907	1.907	1.907	1.907	97.2	97.2	97.2
D_3	1.907	1.907	1.907	1.907	1.907	1.907	97.2	97.2	97.2

---

[31] Diaz-Acosta, I.; Baker, J.; Hinton, J. F.; Pulay, P.; *Spectrochimica Acta Part A*, **2003**, *59*, 363-377

3.2.3.2 Relative energies of the Co(β-diketonato)₃ complexes

Calculated energies and the respective Boltzmann population of the *fac* and *mer* isomers of the Co^{III}(β-diketonato)₃ complexes, are listed in **Table 3.32**. It follows from **Table 3.32**, that the *fac* isomer is more stable than the *mer* isomer by 0.012 eV for complex Co(ba)₃ {10}, while the *mer* isomer is more stable than the *fac* isomer by 0.034 eV for Co(tfba)₃ {12}, and the *mer* isomer is also more stable than the *fac* isomer by 0.012 eV for Co(tfaa)₃ {13}. Experimentally, crystals of *mer* isomers were found for Co(ba)₃ {10} and Co(tfaa)₃ {13}, and crystals of *fac* isomers for Co(tfba)₃ {12}. These crystals are the minor isomers of complexes {10} and {12}. It is important to note that the computational chemistry results show that both isomers are possible for complexes Co(ba)₃ {10}, Co(tfba)₃ {12}, Co(tfaa)₃ {13}, Co(tffu)₃ and Co(tfaa)₃ {13}, although only the minor isomer was experimentally solved for Co(ba)₃ {10} (*mer*-isomer) and Co(tfba)₃ {12} (*fac*-isomer) (See Section 3.2.2).

Table 3.32: PW91/TZP-calculated energies and calculated Boltzmann population (%), for Co(β-diketonato)₃ complexes.

		E (eV)	Relative E (eV)[a]	Boltzmann population (%)
Co(acac)₃ {9}		-262.69	-	100
Co(ba)₃ {10}	*fac*	-418.77	0.000	62
	mer	-418.75	0.012	38
Co(dbm)₃ {11}		-574.81	-	100
Co(tfba)₃ {12}	*fac*	-421.5	0.034	21
	mer	-421.54	0.000	79
Co(tfth)₃	*fac*	-355.69	0.058	9
	mer	-355.75	0.000	91
Co(tffu)₃	*fac*	-363.23	0.000	83
	mer	-363.19	0.040	17
Co(tfaa)₃ {13}	*fac*	-265.41	0.012	39
	mer	-265.43	0.000	61
Co(hfaa)₃		-267.68	-	100

a Relative energy is the energy difference relative to the lowest energy isomer of each complex

3.3 Chromium(0) carbene complexes

The work presented in this section was done in collaboration with the research group of Dr M. Landman at the University of Pretoria. The syntheses of the Fischer alkoxy- and amino-carbene complexes of this study were done by the group of Dr M. Landman at the University of Pretoria, and selected crystal structures were solved by Prof P. van Rooyen at the University of Pretoria. The work presented in this section has been published[32,33] and only the electrochemistry and computational chemistry that was conducted at the UFS, will be discussed. **Scheme 3.6** shows the series of the complexes investigated by electrochemistry and computational chemistry. Contrary to the Tris(β-diketonato)chromium(III) complexes that is paramagnetic, Chromium(0) carbene complexes are diamagnetic and can be measured on the NMR.
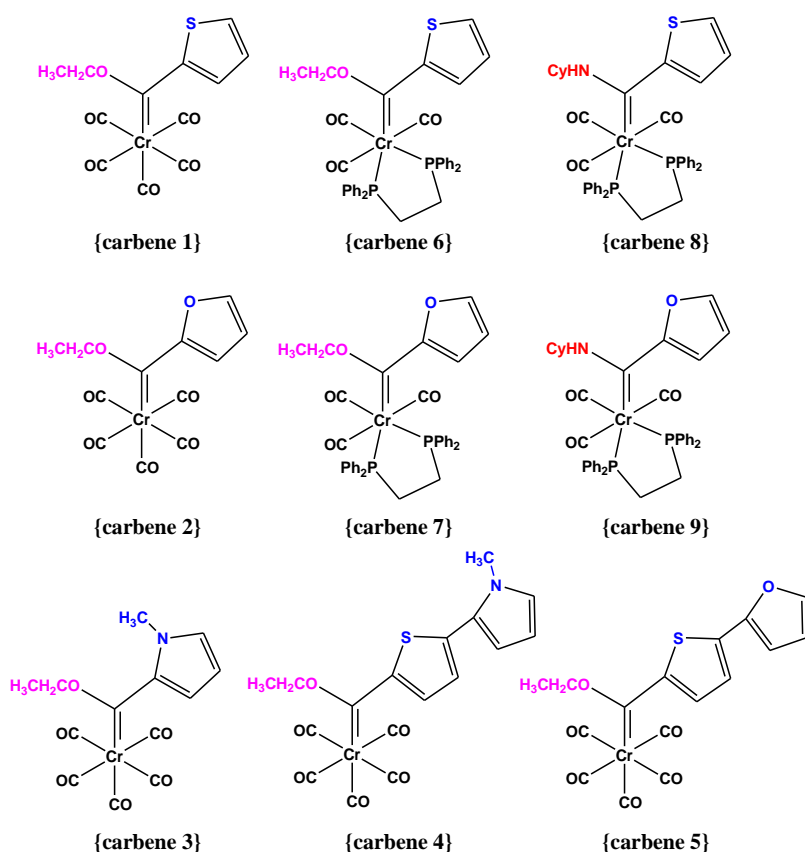
Scheme 3.6: Fischer alkoxy- and amino- Cr-carbene complexes of this study.

[32] Landman, M.; Liu, R.; van Rooyen, P. H.; Conradie, J.; "Electrochemistry of Fischer alkoxycarbene complexes of chromium: The use of DFT to predict and understand oxidation and reduction potentials", *Electrochim. Acta,* **2013**, *114*, 205-214

[33] Landman, M.; Liu, R.; Fraser, R.; van Rooyen, P. H.; Conradie, J.; "*Fac* and *Mer* Fischer DPPE-Carbene complexes of chromium: X-ray, DFT and electrochemical study", *Journal of Organometallic Chemistry*, **2014**, *752*, 171-182

3.3.1 Isomers of Cr(0) carbene complexes

Three types of notations can be applied to isomers in the range of the Cr-carbene complexes of this study, namely *cis/trans*, *fac/mer* and *E/Z* notations. *Cis* and *trans* isomers are displayed in **Scheme 3.7**, and can also be called *syn* and *anti*, respectively. A *cis* isomer is obtained when the substituents with high priorities (X, Y) lie on the same side of the bond, while a *trans* isomer has the opposite arrangement, where the high priority X and Y substituents lie on different sides of the bond. This notation can be applied to all carbene complexes in this study.
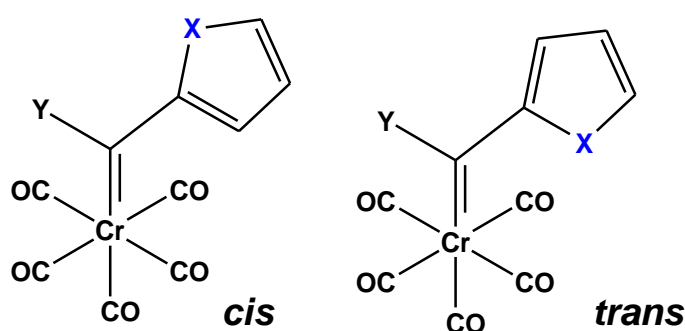
Scheme 3.7: *Cis* and *trans* isomers of alkoxy-carbene complexes.

The *fac* and *mer* isomers of Cr-carbene complexes (see **Scheme 3.8**) are similar to the *fac* and *mer* isomers of M(β-diketonato)$_3$ complexes. This notation applies to **{carbene 6}** to **{carbene 9}**, where all four these complexes have a bidentate DPPE (1,2-bis(diphenylphosphino)ethane) ligand coordinated to the metal center, as well as three carbonyl ligands. A *fac* isomer is obtained when the aryl ring (thienyl (Th) or furyl (Fu)) and the DPPE ligand occupy a face of the octahedron, while a *mer* isomer is obtained when the substituent containing the aryl ring and DPPE occupy a plane passing through the metal center.
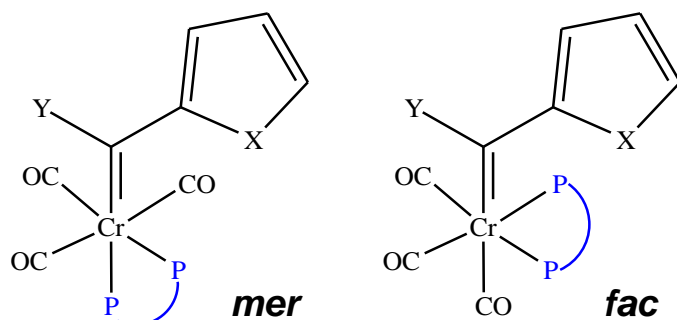
Scheme 3.8: *Mer* and *fac* isomers of DPPE-containing carbene complexes.

E/Z is an extended notation of the *cis/trans* notation, and is displayed in **Scheme 3.9**. The prefix *Z* is added when two substituents lie on the same side of a bond, *e.g.* the cyclohexyl group (Cy) and the metal center on the same side of a bond in conformer 1 (see **Scheme 3.9**). The prefix *E* is added when two substituents lie on opposite sides of the bond, *e.g.* X is opposite to the metal center in conformer 1 (see **Scheme 3.9**). This notation applies to **{carbene 8}** and **{carbene 9}**.
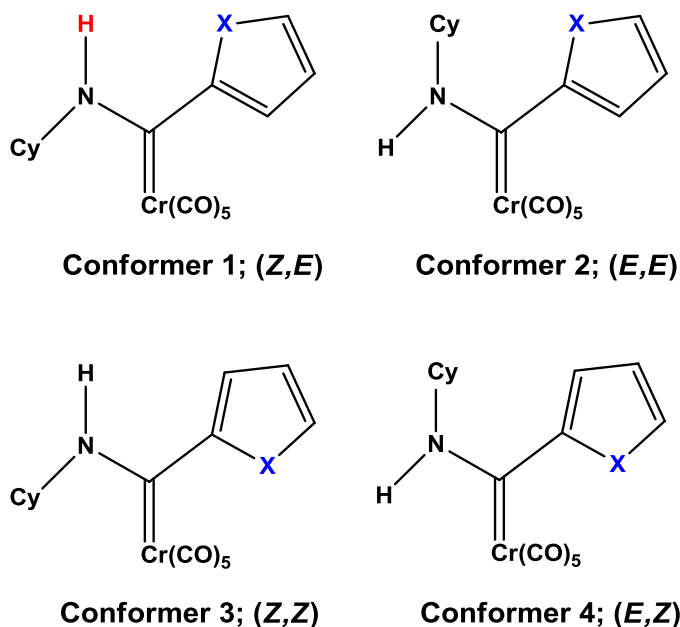
Scheme 3.9: *E/Z*-isomers of amino-carbene complexes.

3.3.2 Computational results of the Cr(0) carbene complexes

3.3.2.1 Geometries

For each of the Cr-carbene complexes shown in **Scheme 3.6**, different isomers are possible: for example two different isomers, the *syn* and the *anti*, are possible for **{carbene 1}**, **{carbene 2}** and **{carbene 3}** (see **Scheme 3.7**). For **{carbene 4}** and **{carbene 5}**, four isomers each are possible: *syn-syn; syn-anti; anti-anti* or *anti-syn*. However for **{carbene 6}** and **{carbene 7}** two different *fac* isomers (each with either a *syn* or an *anti* configuration), as well as two different *mer* isomers (each with either a *syn* or an *anti* configuration) are possible (see **Scheme 3.8**), resulting in 8 possible isomers each (4 *fac* and 4 *mer*). On the other hand, in the case of **{carbene 8}** and **{carbene 9}**, the NHCy group can also adopt two different orientations (**Scheme 3.9**), leading to 16 possible isomers each (8 *fac* and 8 *mer*), since each of the four *fac*-isomers has four conformers: namely (Z,Z), (Z,E) and (E,Z), (E,E). All these possible isomers of **{carbene 1}** to

{carbene 9} were optimized (see **Table 3.33**) and only the lowest energy isomer(s) were considered in the following discussion.

Table 3.33: B3LYP-calculated energies and calculated Boltzmann populations (%) for possible isomers of **{carbene 1}** to **{carbene 9}**.

		Relative E (eV)[a]	**Boltzmann population (%)**
{carbene 1}	*syn*	0.00	99.33
	anti	0.13	0.67
{carbene 2}	*syn*	0.08	3.54
	anti	0.00	96.46
{carbene 3}	*syn*	0.00	99.99
	anti	0.25	0.01
{carbene 4}	*syn-syn*	0.01	37.73
	syn-anti	0.00	61.62
	anti-syn	0.15	0.22
	anti-anti	0.13	0.44
{carbene 5}	*syn-syn*	0.000	50.73
	syn-anti	0.001	48.79
	anti-syn	0.136	0.25
	anti-anti	0.139	0.23
{carbene 6} *fac*	*fac1-anti*	0.39	0.10
	fac1-syn	0.24	
	fac2-anti	0.37	
	fac2-syn	0.17	
{carbene 6} *mer*	*mer1-anti*	0.16	99.90
	mer1-syn	0.00	
	mer2-anti	0.14	
	mer2-syn	0.00	
{carbene 7} *fac*	*fac1-anti*	0.11	1.40
	fac1-syn	0.37	
	fac2-anti	0.28	
	fac2-syn	0.33	
{carbene 7} *mer*	*mer1-anti*	0.00	98.60
	mer1-syn	0.15	
	mer2-anti	0.04	
	mer2-syn	0.12	
{carbene 8} *fac*[a]		0.00	50.00
{carbene 8} *mer*[a]		0.00	50.00
{carbene 9} *fac*[b]		0.10	2.00
{carbene 9} *mer*[b]		0.00	98.00

a Lowest energy isomer, Th group has rotated, therefore conformer *(E,E) = (E,Z)*

b Lowest energy isomer, Fu group has rotated, therefore conformer *(Z,E) = (Z,Z)*

3.3.2.2 Frontier orbitals

The character of the frontier orbitals gives information of the oxidation and reduction centers of a complex. **Figure 3.20** and **Figure 3.21** give a representation of selected frontier orbitals of the neutral, the reduced and the oxidized **{carbene 1}** - **{carbene 9}** complexes.

(i)   *LUMO and first reduction*

Reduction of **{carbene 1}** - **{carbene 9}** can be considered as the addition of an electron to the lowest unoccupied molecular orbital (LUMO) of the complex. All calculations on the LUMO of neutral carbene complexes, as well as on the singly occupied molecular orbital (SOMO) of singly reduced species, showed that the first reduction occurred on the carbene ligand. The Mulliken spin density plot also showed that the unpaired electron after reduction is localized on the ligand and not on the central metal (see **Figure 3.20**). The center of reduction is therefore the carbon (carbene carbon) bonded to the Cr metal.

(ii)   *HOMO and first oxidation*

Oxidation of **{carbene 1}** - **{carbene 9}** can be considered as the removal of an electron from the highest occupied molecular orbital (HOMO) of the complex. DFT-calculations showed that the HOMO of the neutral carbene complexes, as well as the singly unoccupied molecular orbital (SUMO) of singly oxidized radical cations, are centered mainly on the Cr metal. The Mulliken spin density plot also showed that the remaining unpaired electron-density after the first oxidation is localized around the Cr metal (see **Figure 3.20**). Therefore the first oxidation involves a Cr(0) to Cr(I) process. Only **{carbene 4}** and **{carbene 5}** have delocalized HOMOs, mainly contributing electron-density over the metal center as well as over the two aryl rings in the carbene ligand.
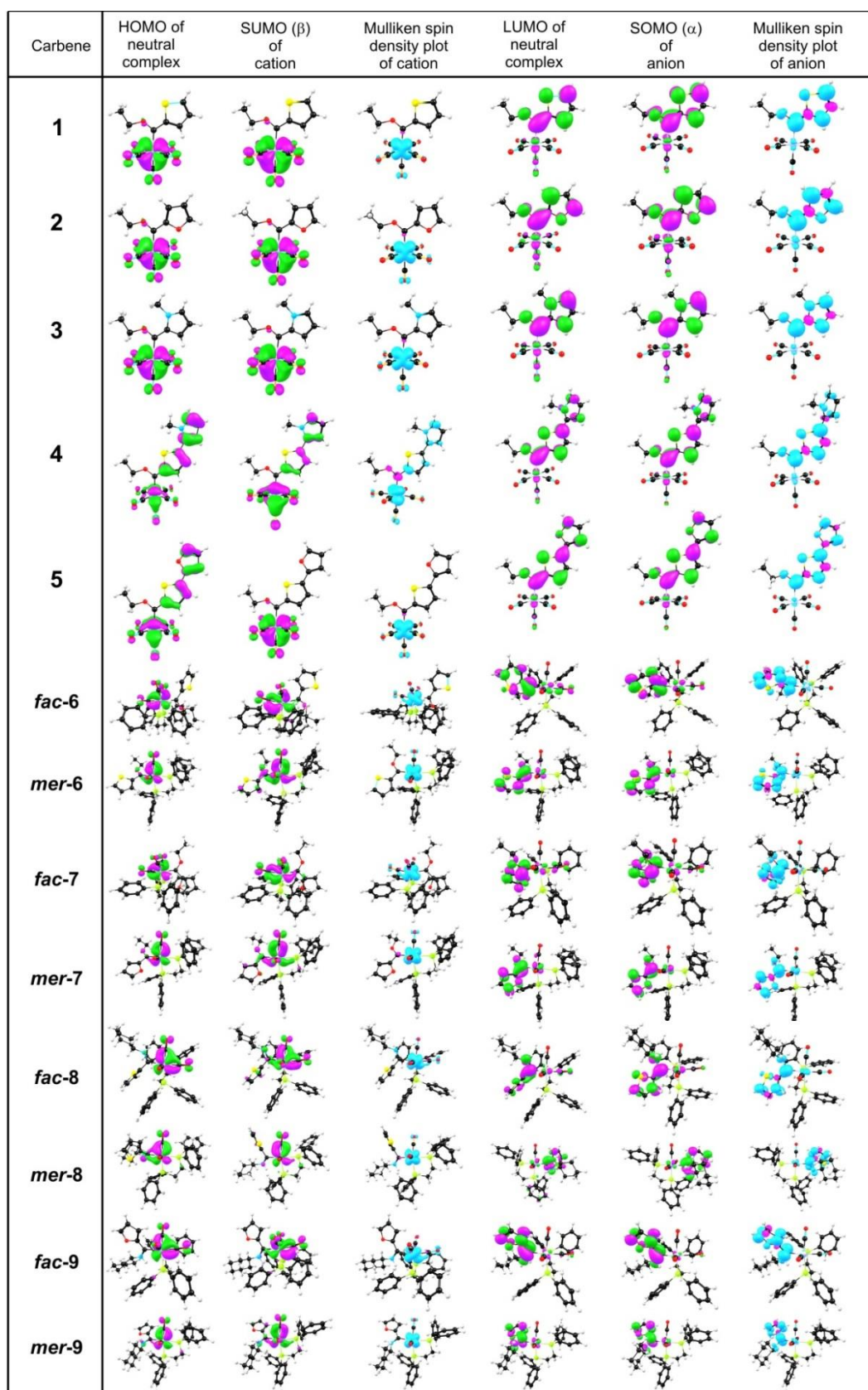
Figure 3.20: Representation of the indicated frontier MOs and Mulliken spin densities of **{carbene 1}** - **{carbene 9}**. The MO and spin density plots use a contour of 40 and 4 e/nm^3 respectively.

(iii)   *HOMO of cation and second oxidation*

The second oxidation of **{carbene 1}** - **{carbene 9}** can be considered as the removal of another electron from the HOMO of the oxidized radical cation of **{carbene 1}** to **{carbene 9}**. Since the *mer*-isomers of the singly oxidized species for **{carbene 6}** to **{carbene 9}** dominate the population, only the *mer*-isomers of the doubly oxidized species were considered for **{carbene 6}** to **{carbene 9}**.[33]   From **Figure 3.21**, the HOMO of the singly oxidized species, as well as the SUMO of the doubly oxidized species of **{carbene 1}** – **{carbene 3}** and **{carbene 6}** – **{carbene 9}**, are located mainly on the Cr metal. However these same features are found on the aryl rings of the carbene ligand for **{carbene 4}** and **{carbene 5}**. Therefore the second oxidation occurs on the Cr metal for **{carbene 1}** – **{carbene 3}** and **{carbene 6}** – **{carbene 9}**, while the second oxidation is proposed to occur on the carbene ligand for **{carbene 4}** and **{carbene 5}**.

Carbene	HOMO (β) of cation	SUMO (β) of cation²⁺	Mulliken spin density plot of cation²⁺
1			
2			
3			
4			
5			
mer-6			
mer-7			
mer-8			
mer-9			
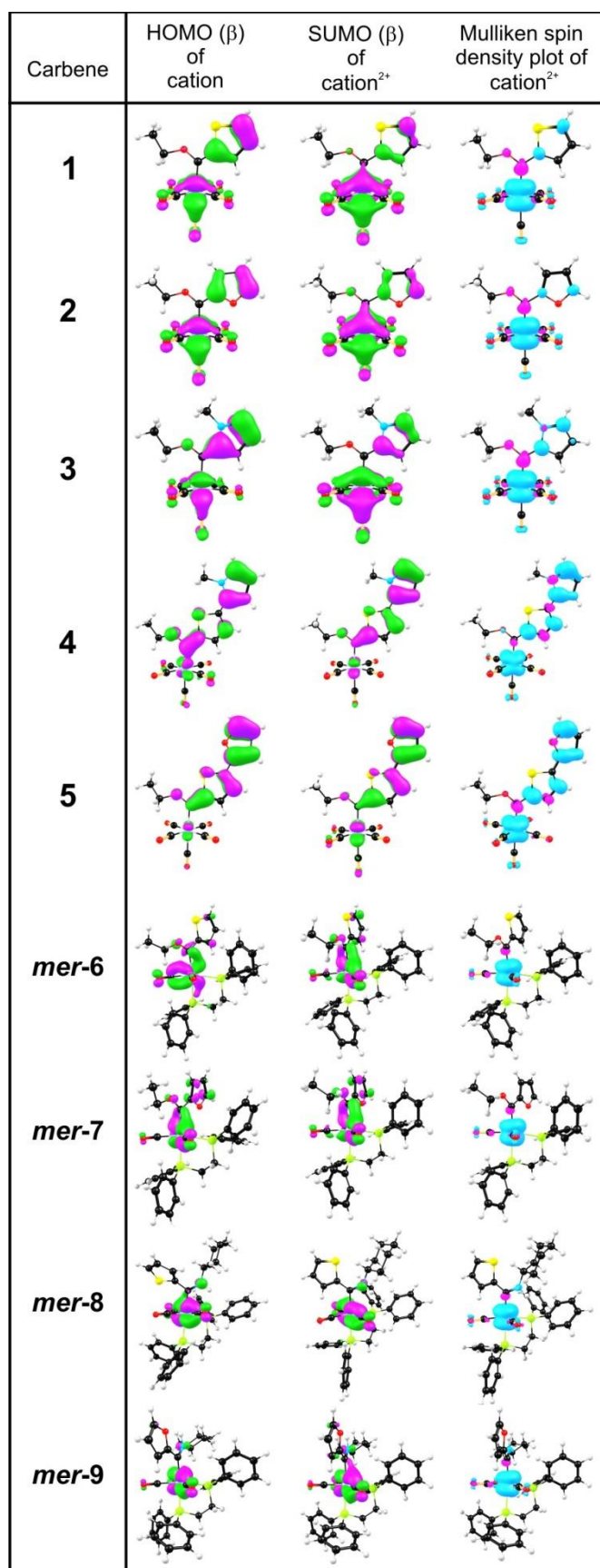
Figure 3.21: Representation of the indicated frontier MOs and spin densities of **{carbene 1}** - **{carbene 9}**, with charge q = 1 or 2. The MO and spin density plots use a contour of 40 and 4 e/nm^3 respectively.

3.3.3 Electrochemical studies of Cr(0) carbene complexes

The two redox active centers in Cr-carbene complexes are the Cr(0) metal and the carbene ligand. The cyclic voltammograms of **{carbene 1}** to **{carbene 9}** are shown in **Figure 3.22**, and the experimental detail of the cyclic voltammograms is given in **Table 3.34**. Discussions of these results will be structured in three parts, namely:

1. **{carbene 1}** to **{carbene 3}**

2. **{carbene 4}** and **{carbene 5}**

3. **{carbene 6}** to **{carbene 9}**
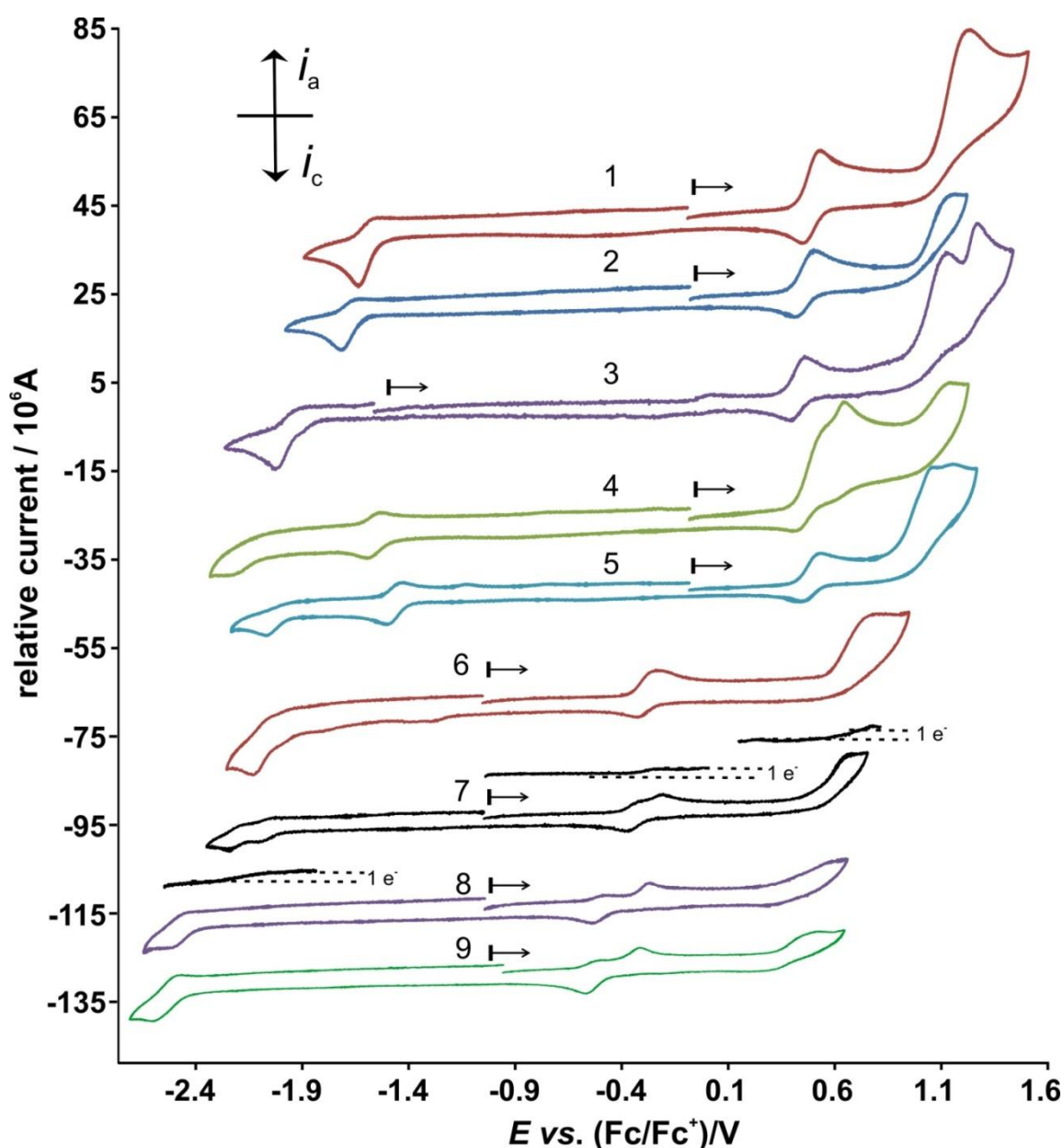
Figure 3.22: Cyclic voltammograms of 0.0005 mol dm^{-3} solutions of **{carbene 1}** - **{carbene 9}**. (Solvent = CH$_3$CN, containing 0.1 mol dm^{-3} [^{n}(Bu$_4$)N][PF$_6$] as supporting electrolyte, with glassy carbon as working electrode, scan rate = 0.100 V s^{-1}).

3.3.3.1 {carbene 1} to {carbene 3}

Different aryl rings are involved in **{carbene 1}** to **{carbene 3}**, namely the 2-(thienyl) group for **{carbene 1}**, the 2-(furyl) group for **{carbene 2}** and the 2-(N-methylpyrrolyl) group for **{carbene 3}**. In proceeding from **{carbene 1}** to **{carbene 2}** to **{carbene 3}**, both the oxidation peaks and reduction peaks shift slightly to the left, to lower potentials, of the cyclic voltammograms. Only one reduction process was observed for each of these three carbene complexes. The reduction process of all three of these carbene complexes becomes more reversible at scan rates higher than 300 mV/s (see **Figure 3.23**). These reduced species are not stable over a long time, and can only be detected at high scan rates.

Two oxidation peaks were observed for **{carbene 1}** and **{carbene 2}**, and a third oxidation peak was observed for **{carbene 3}** **(Figure 3.22)**. The first oxidation of each is both chemically and electrochemically reversible at all scan rates for **{carbene 1}** to **{carbene 3}**. From Section 3.3.2.2 (ii) and the MOs presented in **Figure 3.20**, this first oxidation process observed, is interpreted to be Cr-metal centered, *i.e.* Cr(0) to Cr(I) oxidation. The second oxidation process is chemically and electrochemically irreversible at all scan rates and is also Cr-metal centered (Section 3.3.2.2 (iii)), *i.e.* Cr(I) to Cr(II) oxidation. According to the DFT-calculations and a study of the HOMO of **{carbene 3}**$^{+2}$,[32] the third oxidation of **{carbene 3}** is interpreted to be the oxidation of the five-membered ring on the carbene ligand, *i.e.* the 2-(N-methylpyrrolyl) ring.

{carbene 1}
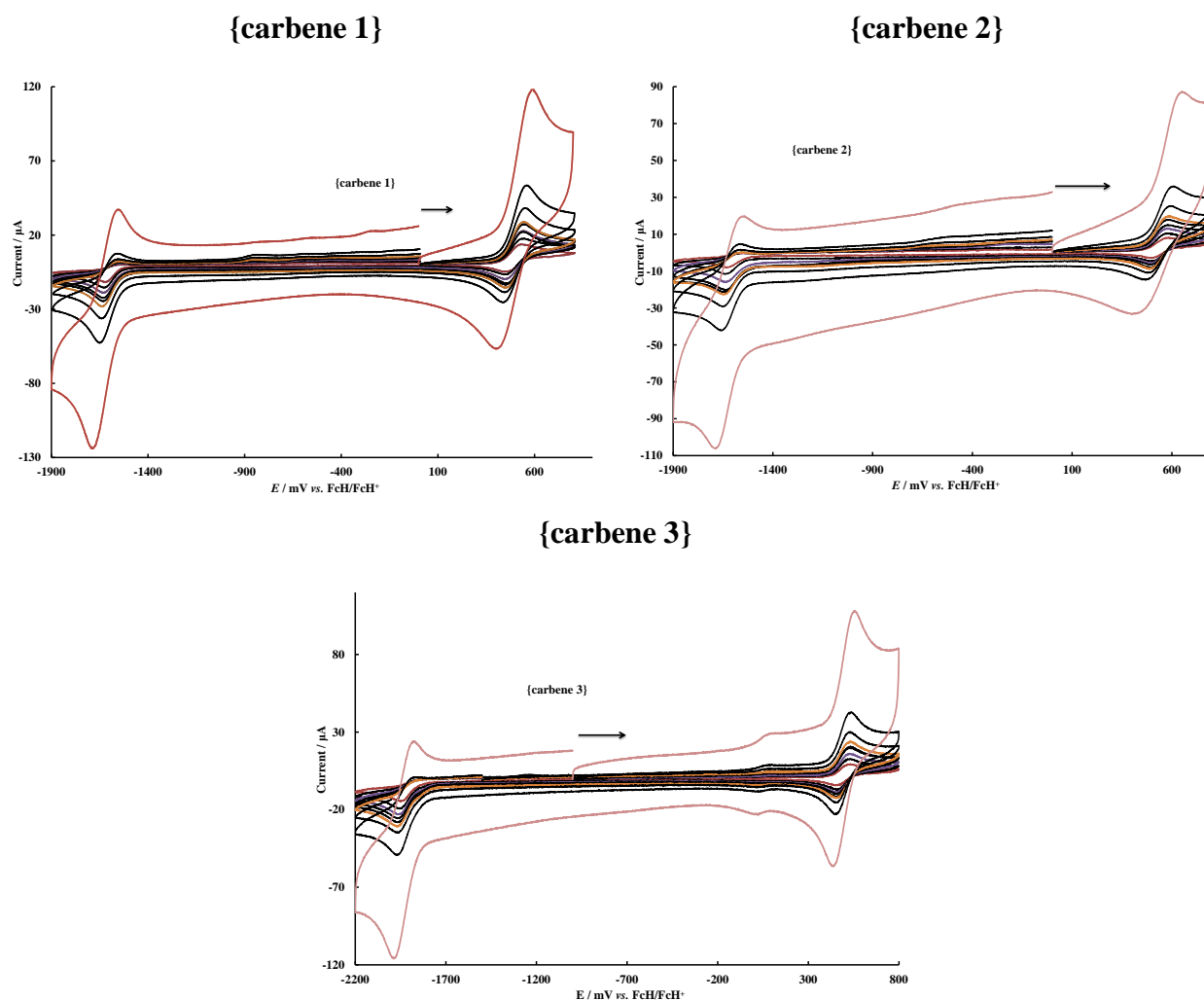
{carbene 2}

{carbene 3}

Figure 3.23: Cyclic voltammograms of 0.5 mM solutions of **{carbene 1}** (top left), **{carbene 2}** (top right) and **{carbene 3}** (bottom) *vs.* FcH/FcH$^+$. (Solvent = CH$_3$CN, supporting electrolyte TBAPF$_6$, scan rate = 50 (smallest peak current), 100, 150, 200, 250, 300, 500, 1000 and 5000 (largest peak current) mV•s^{-1}, with glassy carbon as working electrode at 20 ℃, scan direction as indicated by the arrow).

3.3.3.2 {carbene 4} and {carbene 5}

Both **{carbene 4}** and **{carbene 5}** have a second aryl ring attached to the first aryl ring, namely N-methyl-2-(2'-thienyl)pyrrole) and 2,2'-thienylfuran for **{carbene 4}** and **{carbene 5},** respectively. From **Figure 3.22** and **Table 3.34**, it is observed that the first reduction is already reversible even at low scan rate, because the unpaired electron added during the reduction process, is further stabilized through the extended aryl ring. A second irreversible reduction of **{carbene 4}** and **{carbene 5}** could be observed, due to the stabilisation of the unpaired electron density of the reduced radical through the extended aryl ring after the first reversible reduction.

Similar to **{carbene 3}**, three oxidation processes were found for **{carbene 4}** and **{carbene 5}**, but in this case the electrochemically active center is not Cr-based for the second oxidation. The first Cr-based oxidation is reversible for both **{carbene 4}** and **{carbene 5}**. For **{carbene 4}**, the first and second oxidation peaks are partially superimposed, therefore the baseline of the first oxidation peak is lifted, resulting in a relatively high peak. For **{carbene 5}**, the second and the third oxidation peaks are partially superimposed, resulting in a lifted baseline for the second oxidation peak. DFT-calculations and a visualization of the HOMO of **{carbene 4}**$^+$ and **{carbene 5}**$^+$ (**Figure 3.21**), showed that the second oxidation process observed for **{carbene 4}** and **{carbene 5}**, mainly involves the removal of an electron from the respective dimeric heteroarene five-membered rings (and not from the Cr-metal center), implying that the second oxidation of **{carbene 4}** and **{carbene 5}** leads to a $(CO)_5Cr(I)$ C(OEt)R(+)radical species.[32] The third oxidation of **{carbene 4}** and **{carbene 5}** is proposed to be Cr-metal based.

3.3.3.3 {carbene 6} to {carbene 9}

Three redox processes are observed for **{carbene 6}** – **{carbene 9}**, which are interpreted by the DFT-calculations presented in Section 3.3.2.2, as two oxidation processes of the Cr metal ($Cr^0 \rightarrow Cr^I \rightarrow Cr^{II}$) as well as one reduction process of the carbene ligand. The first oxidation process consists of two different oxidation peaks and one reduction peak. The two oxidation peaks are consistent with the oxidation of the different *mer* and *fac* isomers of **{carbene 6}** – **{carbene 9}**, each isomer being oxidized at a slightly different anodic peak potential. The second oxidation process ($Cr^I \rightarrow Cr^{II}$), observed at potentials higher than 450 mV *vs*. FcH/FcH$^+$, is irreversible. The reduction process observed at a potential lower than -2100 mV *vs*. FcH/FcH$^+$, becomes reversible at high scan rates.

Carbene complexes **{carbene 6}** – **{carbene 9}**, all four containing the bidentate ligand DPPE, undergo *fac/mer* isomerism, and this isomerism results in a different oxidation potential for the different *fac* and *mer* isomers. Since the energy of the HOMO of the *mer*-isomer is higher than the energy of the *fac*-isomer (**Table 3.34**), the *mer*-isomer will be oxidized first, at a lower, more negative potential than the *fac*-isomer. The first peak of the oxidation process, observed for each of the complexes **{carbene 6}** – **{carbene 9}**, at a potential between -600 and -250 mV *vs*. FcH/FcH$^+$, is thus interpreted as the reversible oxidation of the *mer*-isomer, whereas the second oxidation at a slightly higher potential, is interpreted as the irreversible oxidation of the *fac*-isomer.

For **{carbene 6}**, the first oxidation is reversible, with a single oxidation peak observed at low scan rate, *e.g.* see the CV of **{carbene 6}**, at 100 mV/s, in **Figure 3.22**. At higher scan rates, different oxidation peaks of the *mer* and *fac* isomers could be identified (see **Figure 3.24**). As the cycles of the CV proceeded at higher scan rates, less and less *fac* isomer was detected around the electrode, until eventually only the peak of the *mer*-isomer was detected for the first oxidation. This observation is consistent with the scan rate (500 mV/s) being much faster than the diffusion rate and that the majority of the singly oxidized species did convert to mer^+ isomer. The ease of *mer*-isomer oxidation over *fac*-isomer oxidation is also proposed by DFT-calculations. DFT calculations also showed that the mer^+ isomer dominates the population, which agrees with the electrochemical results.[33]
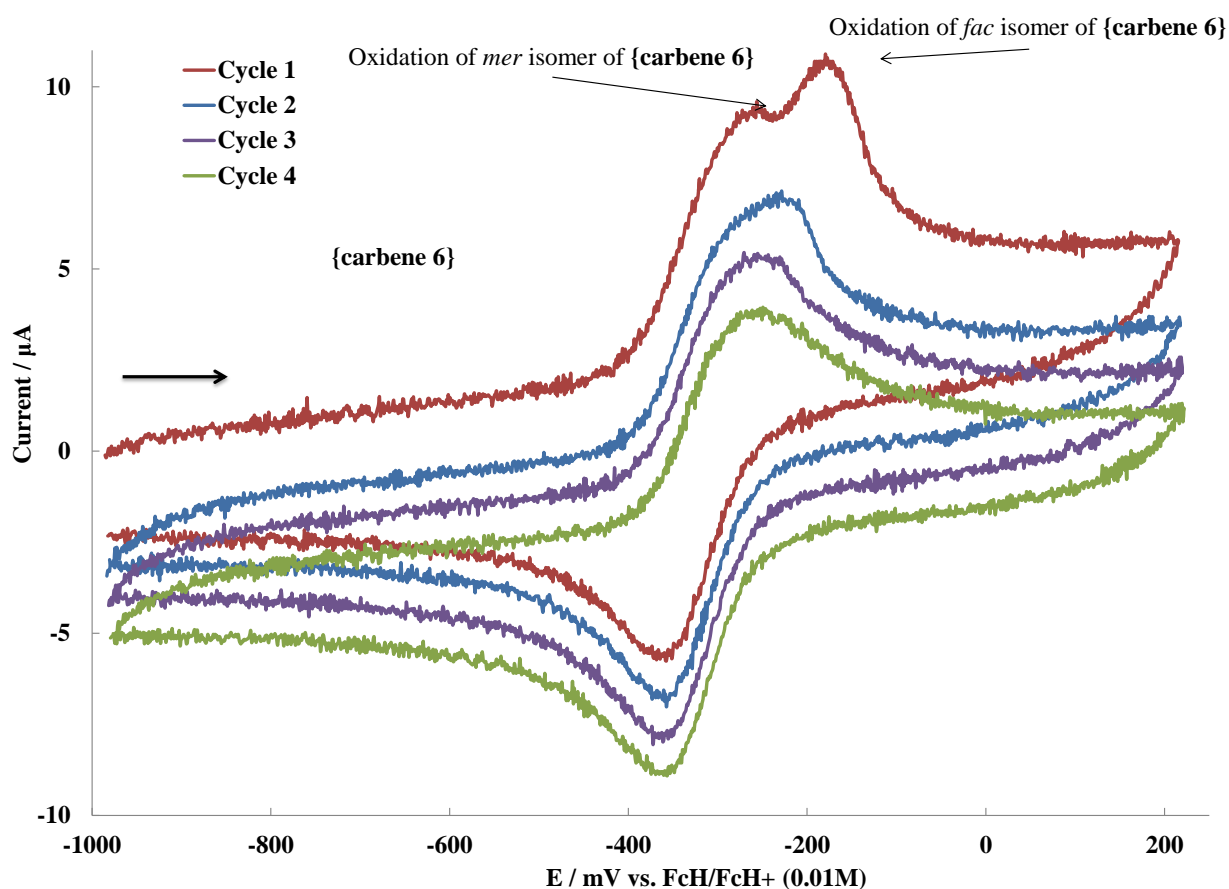
Figure 3.24: Cyclic voltammograms of a 1 mM solution of **{carbene 6}** *vs.* FcH/FcH$^+$. (Solvent = CH$_3$CN, supporting electrolyte TBAPF$_6$, scan rate = 500 mV•s^{-1}, with glassy carbon as working electrode at 20 ℃, scan direction as indicated by the arrow).

Cyclic voltammograms of the *mer*-isomer of **{carbene 9}** were performed immediately after dissolving the isomer, as shown in **Figure 3.25**. On the first cycle, only the oxidation signal of the *mer*-isomer was detected. Quick equilibrium between the *fac/mer* isomers was achieved after the first cycle, and distinct signals were observed in the cyclic voltammograms. This observation

confirms that the first reversible oxidation is due to the oxidation of the *mer*-isomer. Similarly, only the reduction of the *mer*-isomer of the singly oxidized species was detected.
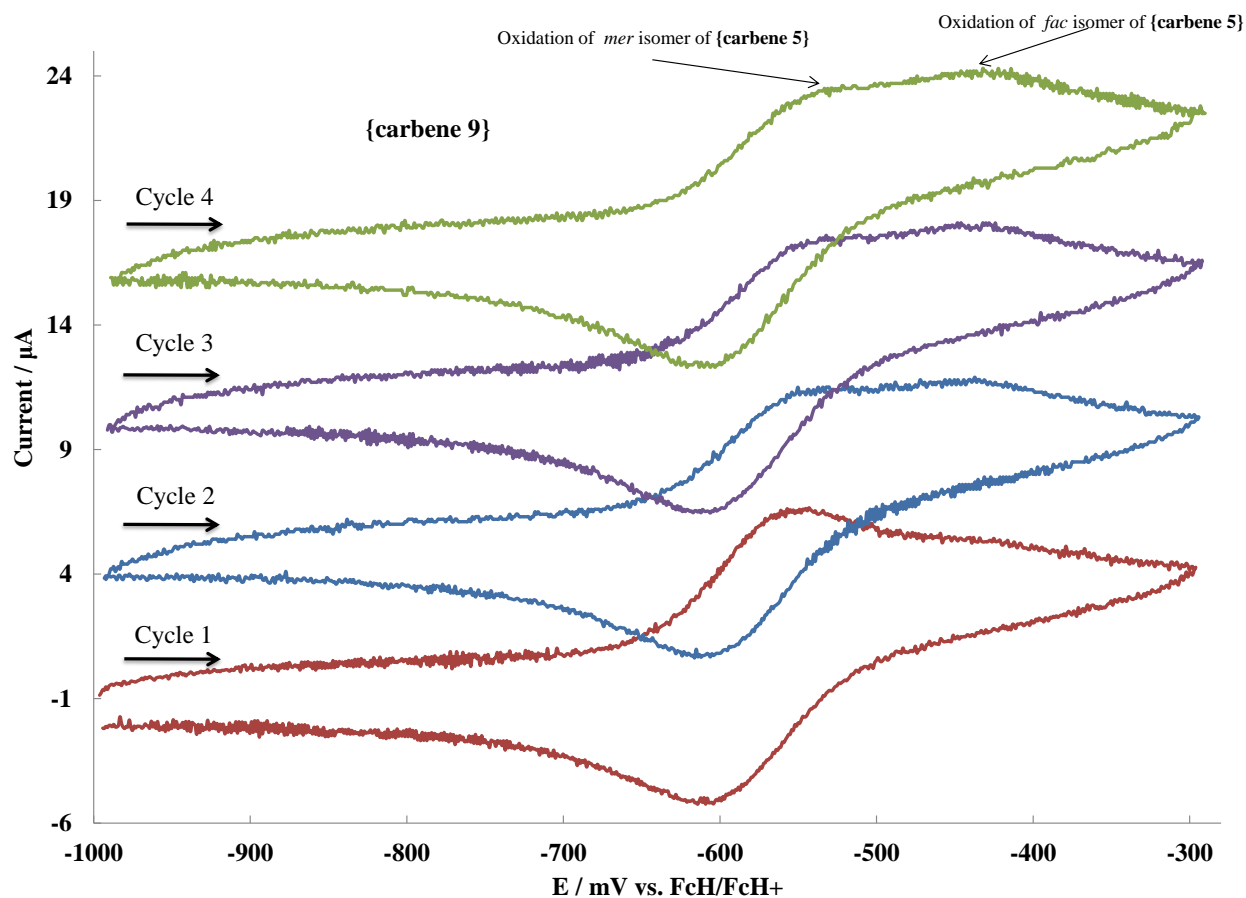
Figure 3.25: Cyclic voltammograms of a 0.5 mM solution of *mer*-{**carbene 9**} *vs.* FcH/FcH$^+$. (Solvent = CH$_3$CN, supporting electrolyte TBAPF$_6$, scan rate = 100 mV•s^{-1}, with glassy carbon as working electrode at 20 °C, scan direction as indicated by the arrow).

A series of CV's at 100 mV/s was done on *fac*-{**carbene 7**}, as shown in **Figure 3.26**. A single peak for the *fac*-isomer was detected on the first segment in Scan 1, while both *fac* and *mer* isomers were detected on the third segment in Scan 1. Both signals were found for the rest of the scans, after the equilibrium was achieved in Scan 1. This observation confirms that the second irreversible oxidation is due to the oxidation of the *fac*-isomer.
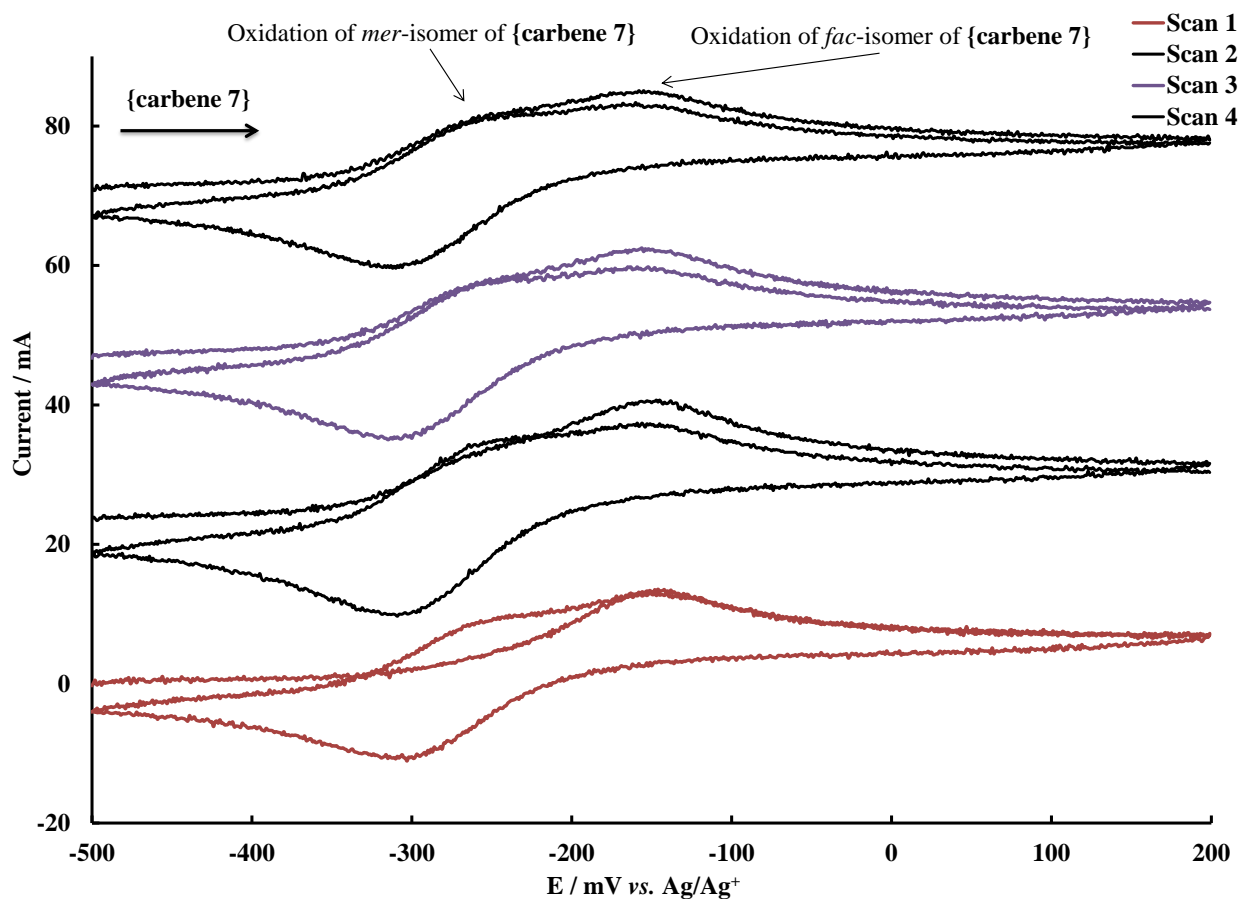
Figure 3.26: Cyclic voltammograms of a 0.5 mM solution of *fac*-{**carbene 7**} *vs.* Ag/AgCl. (Solvent = CH$_3$CN, supporting electrolyte TBAPF$_6$, scan rate = 100 mV•s^{-1}, with glassy carbon as working electrode at 20 °C, scan direction as indicated by the arrow).

Table 3.34: Cyclic voltammetry and density functional theory-calculated data for **{carbene 1}** to **{carbene 9}**. Cyclic voltammograms are obtained from 0.0005 mol dm^{-3} solutions of **{carbene 1}** to **{carbene 9}**, in solvent CH_3CN, containing 0.1 mol dm^{-3} [^{n}(Bu$_4$)N][PF$_6$] as supporting electrolyte, with glassy carbon as working electrode, at a scan rate of 0.er100 V s^{-1}, at 20 °C. Experimental potentials are in V relative to the Fc/Fc$^+$ couple.

Complex	Experimental (V *versus* FcH/FcH$^+$)										Calculated (eV)	
	1st reduction				1st oxidation				2nd oxidation	3rd oxidation	neutral complex	
	E_{pc}	E_{pa}	$E^{0'}$	ΔE	E_{pa}	E_{pc}	$E^{0'}$	ΔE	E_{pa}	E_{pa}	E_{HOMO}	E_{LUMO}
{carbene 1}	-1.625	-1.552[a]	-1.589[a]	0.073[a]	0.538	0.453	0.496	0.085	1.229	-	-6.097	-2.738
{carbene 2}	-1.719	-1.649[a]	-1.684[a]	0.070[a]	0.494	0.414	0.454	0.080	1.148	-	-5.984	-2.566
{carbene 3}	-2.019	-1.938[a]	-1.979[a]	0.081[a]	0.463	0.396	0.430	0.067	1.132	1.268	-5.854	-2.189
{carbene 4}	-1.594	-1.514	-1.554	0.080	0.558	0.420	0.489	0.138	0.648	1.134	-5.735	-2.674
{carbene 5}	-1.494	-1.435	-1.468	0.066	0.531	0.444	0.488	0.087	1.056	1.158	-5.926	-2.841
{carbene 6 *mer*}					-0.275	-0.353	0.078	-0.314	1.233		-4.816	-1.779
{carbene 6 *fac*}	-2.162				-	-	-	-	-		-4.956	-1.981
{carbene 7 *mer*}	-2.269				-0.356	-0.410	0.054	-0.383	0.625		-4.738	-1.598
{carbene 7 *fac*}	-2.124				-0.235	-	-	-	-		-4.907	-1.937
{carbene 7 *mer*}	-2.800				-0.500	-0.569	0.069	-0.534	0.758		-4.670	-1.148
{carbene 8 *fac*}	-2.545				-0.306	-	-	-	-		-4.741	-1.244
{carbene 9 *mer*}	-2.615				-0.545	-0.600	0.055	-0.573	0.456		-4.530	-1.300
{carbene 9 *fac*}					-0.368	-	-	-	-		-4.679	-1.576

a Values determined from data acquired by a 0.300 V s^{-1} scan rate (see Fig. 3.23).

3.3.4 Relationships between calculated and experimental data

As discussed in Section 3.3.2.2, the lowest unoccupied molecular orbital (LUMO) is related to the reduction, and the highest occupied molecular orbital (HOMO) is related to the oxidation process. By combining DFT-and electrochemical data, these relationships can be quantified for Cr-carbene complexes of this study.

Figure 3.27 presents a linear relationship between the HOMO energy and the first oxidation ($Cr^{0/1}$) potential, as listed in **Table 3.34**. Both **{carbene 4}** and **{carbene 5}** are the outliers, and are therefore excluded from the discussion. The reason for them being outliers is due to the delocalization of the HOMO, as discussed in 3.3.2.2. The higher HOMO energy (less negative) gives a lower (more negative) oxidation potential, *i.e.* a complex with a higher HOMO energy is oxidized more easily. This linear relation between the HOMO energy (in eV) and the peak anodic oxidation potential (in V), as shown in **Figure 3.27**, is given by **Equation 3.13**, with $R^2 = 0.99$.

Equation 3.13: $E_{pa\ Cr^{0/1}} = -0.69\ E_{HOMO} - 3.65$
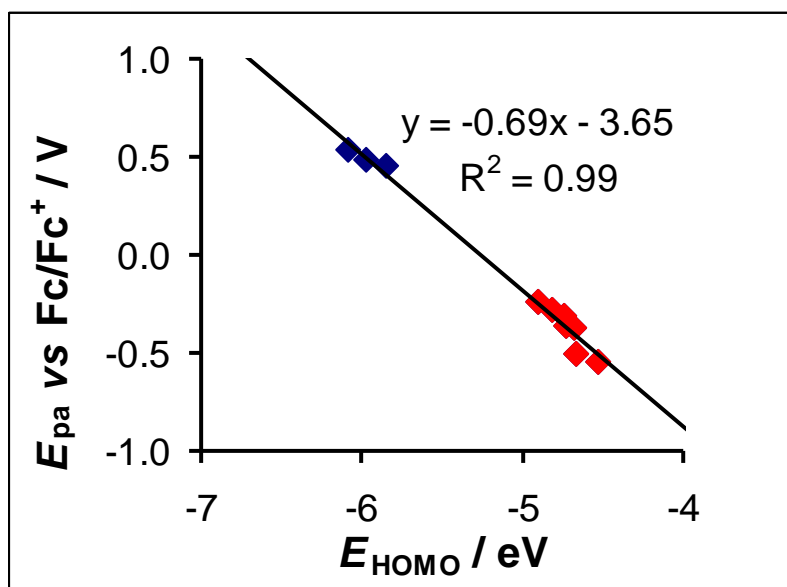
Figure 3.27: Linear relationship between the DFT-calculated E_{HOMO} values and the experimental oxidation potential E_{pa} of the first oxidation of **{carbene 1}** - **{carbene 3}** and **{carbene 6}** - **{carbene 9}**. Data is presented in **Table 3.34**. Experimental potentials are relative to the FcH/FcH$^+$ couple. Blue markers are for **{carbene 1}** - **{carbene 3}**, and red markers for **{carbene 6}** - **{carbene 9}**.

Figure 3.28 shows a linear relationship between the LUMO energy and the first reduction potential of **{carbene 1}** – **{carbene 9}**. This reduction process happens on the carbene carbon bonding to the Cr-metal; therefore the electrophilicity of the carbene ligand (especially the aryl substituents) plays a decisive role in this reduction. A complex with a higher LUMO energy (less negative) can be reduced more easily (at a more negative potential). **Equation 3.14** gives the relationship between the LUMO energy (in eV) and the first cathodic reduction potential (in V) of carbene carbon, with $R^2 = 0.98$.

Equation 3.14: $E_{\text{pa carbene carbon}} = -0.69\,E_{\text{LUMO}} - 3.49$
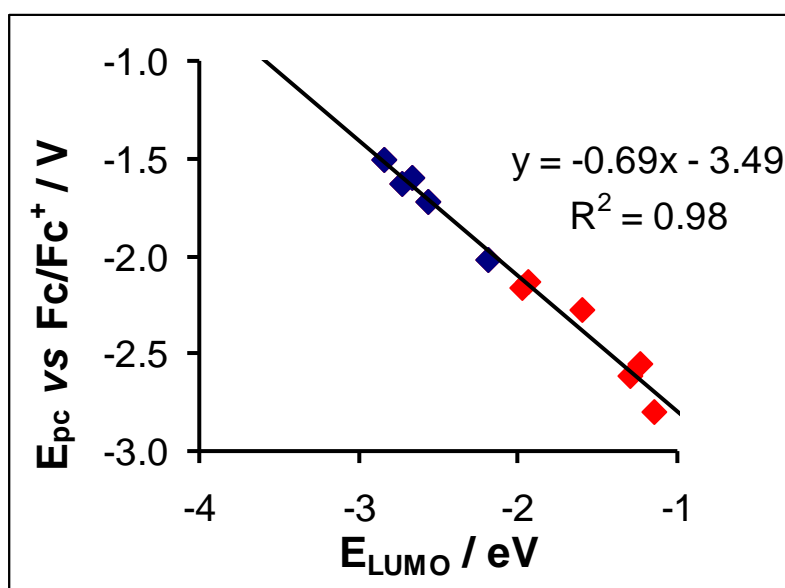
Figure 3.28: Linear relationship between the DFT-calculated E_{LUMO} values and the experimental reduction potential E_{pc} of the first reduction of **{carbene 1}** - **{carbene 9}**. Data is presented in **Table 3.34**. Experimental potentials are relative to the FcH/FcH$^+$ couple. Blue markers are for **{carbene 1}** - **{carbene 5}**, and red markers for **{carbene 6}** - **{carbene 9}**.

For Cr-carbene complexes of the type [(CO)$_5$Cr=C(OEt)R] (where R = 2-thienyl, 2-furyl, 2-(N-methylpyrrolyl), N-methyl-2-(2'-thienyl)pyrrole or 2,2'-thienylfuran) and of the type [(CO)$_3$(dppe)Cr]C(X)R] (where R = 2-thienyl or 2-furyl, and where X = OEt or NHCy), the linear relationships obtained between the calculated and experimental data, enable prediction of the reduction potential of these type of complexes by DFT-calculations, prior to synthesizing them. As a result, the reduction potential of the final complex can be fine-tuned, by substituting a variety of different substituents and ligands onto the Cr-carbene complex.

4   Experimental

4.1 Materials

Reagents were obtained from Merck and Sigma-Aldrich. Solid reagents were used without further purification. Doubly distilled H_2O was used. Organic solvents were distilled for water-free reactions.

4.2 Electrochemistry

Measurements of Cyclic voltammograms (CV's) and linear sweep voltammograms (LSV's) were performed on 0.0005 mol dm^{-3} compound solutions in dry acetonitrile. Tetra-*n*-butylammonium hexafluorophosphate, ($[N(^nBu_4)][PF_6]$), (0.1 mol dm^{-3}) was used as supporting electrolyte. The CV's were collected under a blanket of purified argon at 25 °C utilizing a Princeton Applied Research PARSTAT 2273 voltammograph running PowerSuite (Version 2.58).

4.2.1 Tris(β-diketonato)chromium(III) Complexes

Cyclic voltammetry of tris(β-diketonato)chromium(III) complexes were measured using 1 mL of 25 mM solutions with CH_3CN as solvent, and tetraethylammonium tetrafluoroborate (0.5 M, TEABF$_4$, $[NEt_4][BF_4]$) as supporting electrolyte. Argon gas was used as experimental environment for a three-electrode cell, consisting of a Pt auxiliary electrode, a glassy carbon (working surface area 0.0707 cm^2) working electrode and a Ag/Ag$^+$ (10 mM AgNO$_3$ made from supporting electrolyte solution) reference electrode. The working electrode was polished with 1 μm Diapat diamond then ¼ μm Diapat diamond paste on a Buehler polish pad, rinsed with H_2O and acetone, and dried. This was repeated before every measurement. Measurements of each complex were done at a series of scan rates: 50 mV/s, 100 mV/s, 150 mV/s, 200 mV/s, 250 mV/s, 300 mV/s, 500 mV/s, 1000mV/s and 5000 mV/s. Ferrocene was used as internal reference.

4.2.2 Chromium(0) Carbenes

Concentration of carbenes was 0.5 mM in 1 mL CH_3CN solution, tetrabutylammonium hexafluorophosphate (0.1 M $[NBu_4][PF_6]$) was used as electrolyte. A three-electrode cell, with a glassy carbon (surface area 7.07 x 10^{-6} m^2) working electrode, Pt auxiliary electrode and a Ag/Ag^+ (0.010 mol dm^{-3} $AgNO_3$ in CH_3CN) reference electrode[1] mounted on a Luggin capillary, was used.[2,3] All temperatures were kept constant to within 0.5 °C. Scan rates were 0.050 – 5.000 V s^{-1}. Successive experiments under the same experimental conditions showed that all oxidation and formal reduction potentials were reproducible within 6 mV. All cited potentials were referenced against the FcH/FcH^+ couple as suggested by IUPAC.[4] Ferrocene exhibited a formal reduction potential $E^{\circ} = 0.079$ V *vs.* Ag/Ag^+, a peak separation $\Delta E_p = E_{pa} - E_{pc} = 0.069$ V and $i_{pc}/i_{pa} = 0.98$ under our experimental conditions. E_{pa} (E_{pc}) = anodic (cathodic) peak potential and i_{pa} (i_{pc}) = anodic (cathodic) peak current. E° (FcH/FcH^+) = 0.66(5) V *vs.* SHE in $[NBu_4]/CH_3CN$ and 0.77(5) V *vs.* SHE in $[NBu_4]/DCM$.[5]

4.3 Measurements

^{1}H NMR spectra were recorded on the Bruker Advance DPX 300 [[1]H (300.130 MHz)] spectrometer at 18 °C, using deuterated chloroform ($CDCl_3$).

Infrared (IR) spectra were recorded on Bruker-Tensor 27 FTIR spectrometer.

UV/Vis spectra were recorded on the Shimadzu UV-1650PC spectrophotometer with a CPS-240A temperature control unit.

All melting points (M.p.) were determined on the Olympus BX51 microscope fitted with a Linkam-THMS600 hot stage (up to 250 °C)

---

[1] Sawyer, D.T.; Roberts (Jr), J. L.; *Experimental Electrochemistry for Chemists*, Wiley, New York, **1974**, 54

[2] Evans, D.H.; O'Connell, K.M.; Peterson, R.A.; Kelly, M.J.; *J. Chem. Educ.*, **1983**, *60*, 290-293

[3] Mabbott, G. A.; *J. Chem. Educ.*; **1983**, *60*, 697-701.

[4] Gritzner, G.; Kuta, J.; *Pure Appl. Chem.*, **1984**, *56*, 461-466

[5] Pombeiro, A. J. L.; *J. Organomet. Chem.*, **2005**, *690*, 6021-6040

4.4 Synthesis

The β-diketones used in this study were obtained from Merck and Sigma-Aldrich.

4.4.1 Tris(β-diketonato)chromium(III) complexes

Tris(β-diketonato)chromium(III) complexes {1}-{7} were synthesised according to Rahman's method[6]. The chromium chloride (2.05 mmole in minimum amount of water) solution was added drop wise to ethanol/water solution of β-diketone (6.0 mmole in 40 mL 1:1 ethanol/water). The reaction mixture was stirred for 2 hours. Concentrated solution of sodium acetate was added drop wise until complete precipitation. The precipitate was washed with excess water, and then dried in a desiccator at room temperature.

Tris(hexafluoroacetylacetonato)chromium(III) (Cr(hfaa)$_3$, {8}) was synthesised by the following method: Thionyl Chloride (excess SOCl$_2$) was added to CrCl$_3$·6H$_2$O (dark green, 3 mmole) with slight gentle heat; the gaseous side product and excess SOCl$_2$ were trapped with a concentrated sodium acetate solution. The desired product was light green CrCl$_3$.3H$_2$O, and was treated with dry THF. A dark purple solution was obtained. Into this solution, hexafluoroacetylacetonato (Hhfaa, 2 mL) was injected with a syringe. The reaction mixture was stirred overnight (±15 hours). The precipitate was filtered, washed with excess water, and then dried in a desiccator at room temperature.

All synthesized tris(β-diketonato)chromium(III) complexes are paramagnetic.

4.4.1.1 Tris(acetylacetonato)chromium(III) [Cr(acac)$_3$] {1}
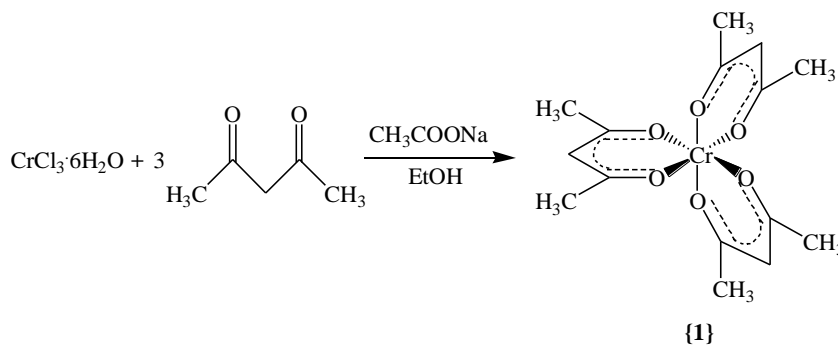
Yield 74 % Colour: Purple.

[6] Rahman, A. K.; Hossain, M. B.; Halim, M. A.; Chowdhury, D.A.; and Salam, M. A.; *African Journal of Pure and Applied Chemistry*, 2010, *4*, 216-220

4.4.1.2 Tris(1-phenyl-1,3-butanedionato)chromium(III) [Cr(ba)$_3$] {2}
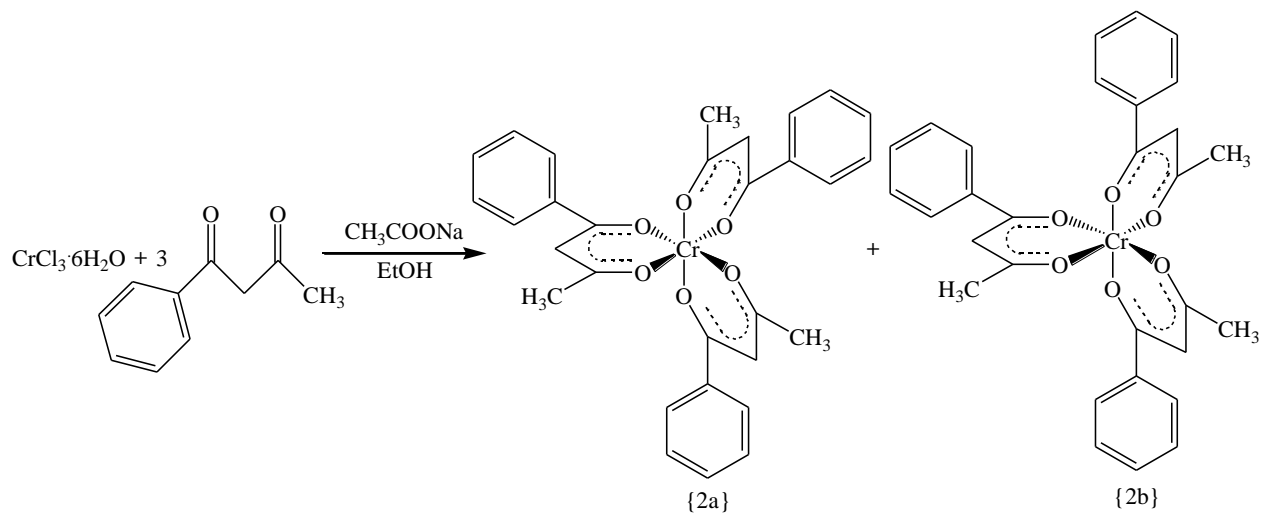
Yield 67 % Colour: Pale yellow.

4.4.1.3 Tris(1,3-diphenyl-1,3-propanedionato)chromium(III) [Cr(dbm)$_3$] {3}
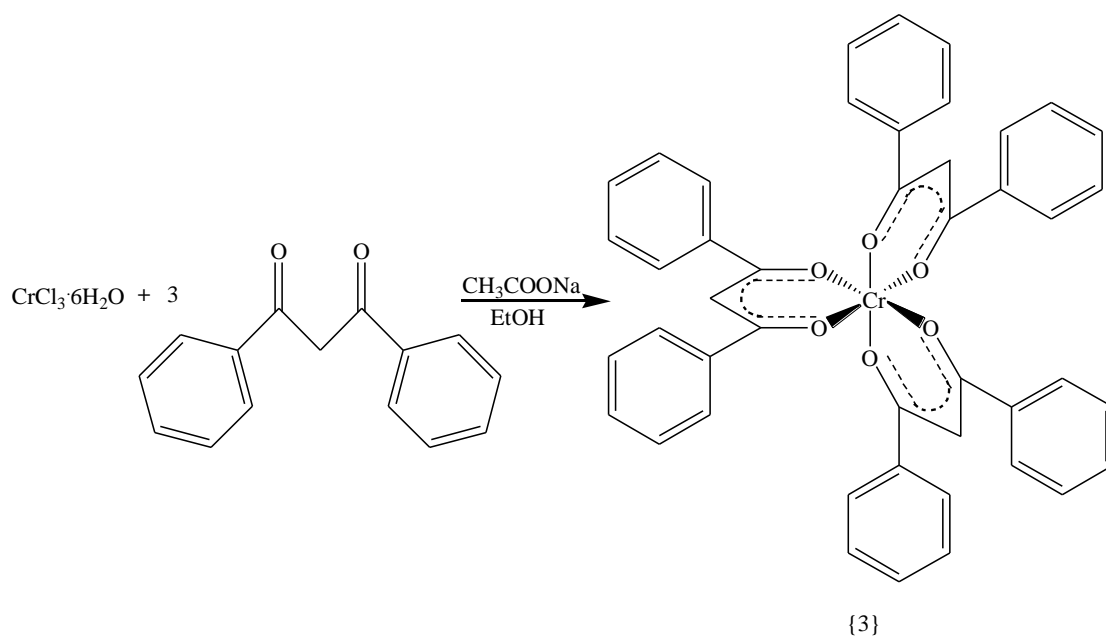
Yield 90 % Colour: Yellow. MS Calcd. m/z 721.73, Found: m/z 723.06. M.P. 75.8 ℃

4.4.1.4 Tris(4,4,4-trifluoro-1-phenyl-1,3-butanedionato)chromium(III) [Cr(tfba)₃] {4}

{4a}   {4b}

Yield 54 % Colour: Green
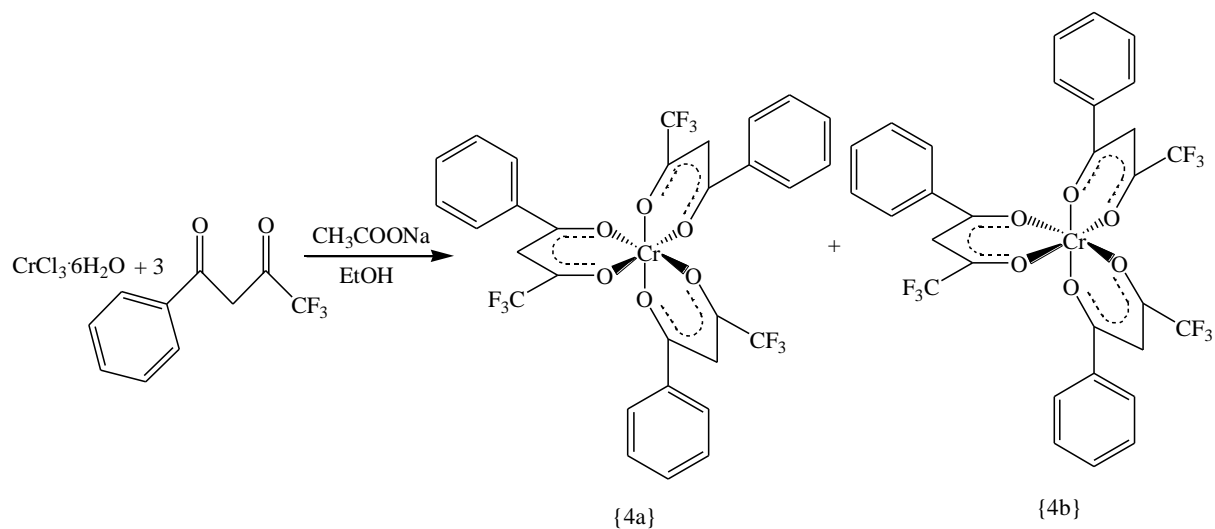
4.4.1.5 Tris(4,4,4-trifluoro-1-(2-thienyl)-1,3-butanedionato)chromium(III) [Cr(tfth)₃] {5}

{5a}   {5b}
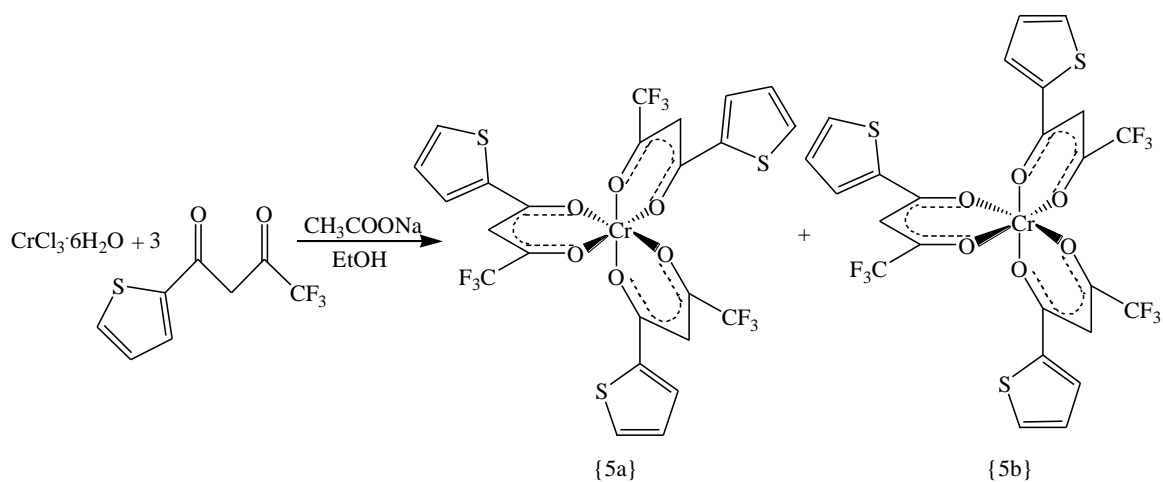
Yield 28 % Colour: Green.

4.4.1.6 Tris(4,4,4-trifluoro-1-(2-furyl)-1,3-butanedionato)chromium(III) [Cr(tffu)₃] {6}
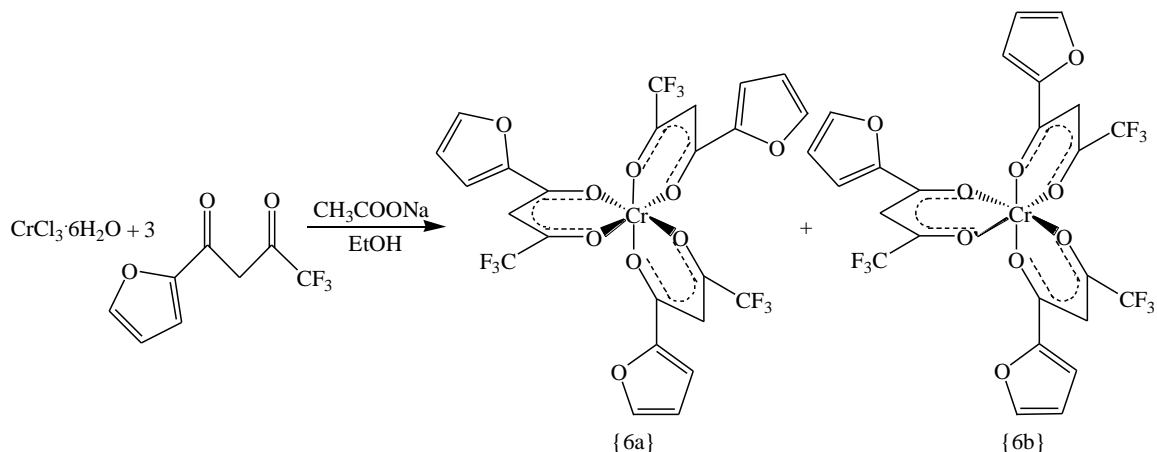
Yield 71 % Colour: Green.

4.4.1.7 Tris(1,1,1-trifluoro-2,4-pentadionato)chromium(III) [Cr(tfaa)₃] {7}
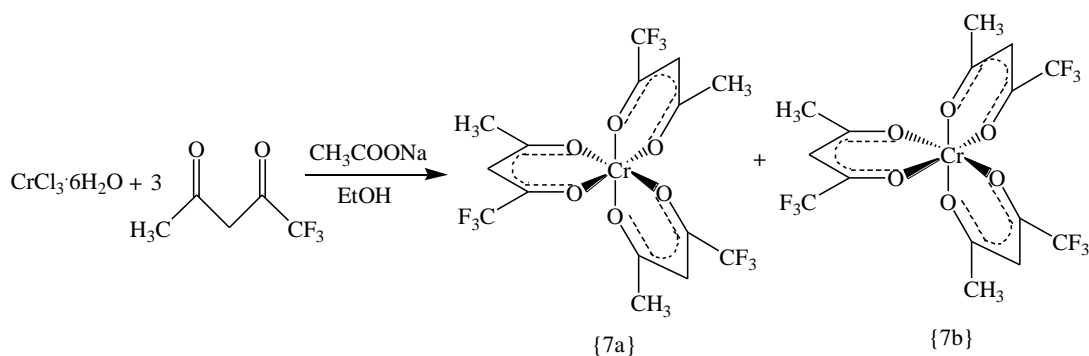
Yield 21 % Colour: Grey.

4.4.1.8 Tris(1,1,1,5,5,5-hexafluoro-2,4-pentadionato)chromium(III) [Cr(hfaa)₃] {8}

$$CrCl_3 \cdot 6H_2O \xrightarrow{SOCl_2} CrCl_3 \cdot 3H_2O(\text{light green}) + 3SO2(g) + 6HCl(g)$$

$CrCl_3 \cdot 3H_2O$ (light green) $\xrightarrow{THF}$ $CrCl_3$ (dark purple) $\xrightarrow[THF]{Hhfaa}$
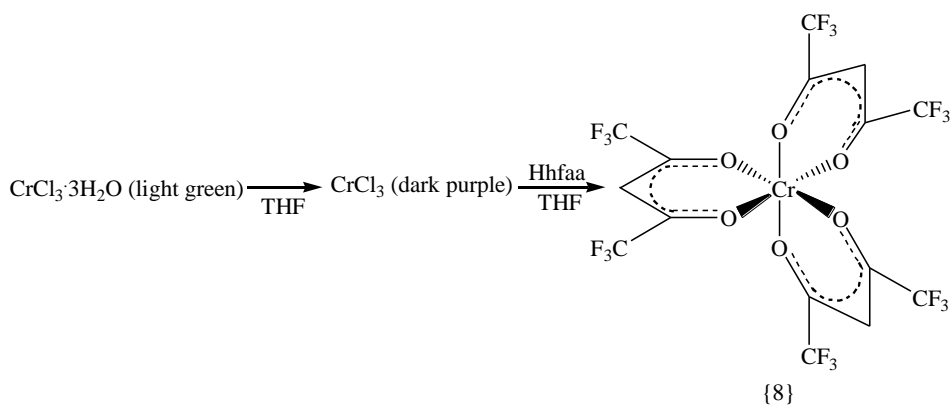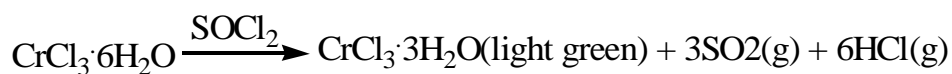
Yield 17 % Colour: Dark green.

126

4.4.2 Tris(β-diketonato)cobalt(III) Complexes

Complexes {9, 10, 11 12 and 13} were synthesised by the method of Bryant and Fernelius with minor changes[7]. A homogeneous suspension was made of cobalt(II) carbonate (1.25 g, 0.0105 mole) and 10 mL β-diketone under reflux. This mixture were preheated to 95 °C 15 mL 25 % hydrogen peroxide was added drop wise to the suspension over 30 minutes. The precipitate was filtered and washed with excess water, and then dried in a desiccator at room temperature.

4.4.2.1 Tris(acetylacetonato)cobalt(III) [Co(acac)₃] {9}
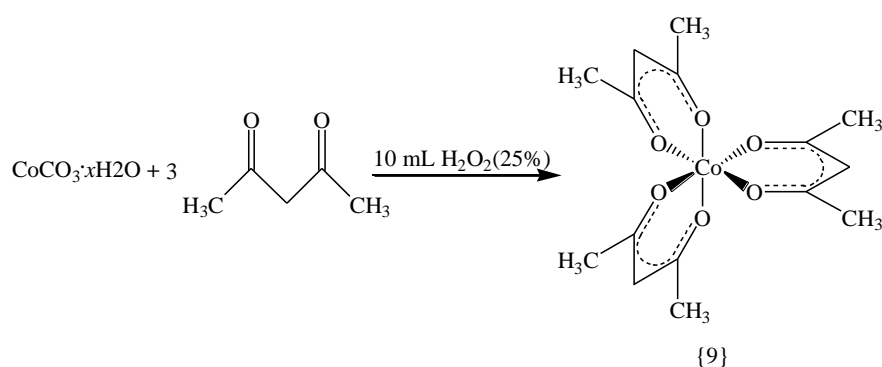
Yield 63 % Colour: Dark green. ^{1}H NMR: (300 MHz, δ/ppm, CDCl$_3$): 2.19 (s, 18H, 6 × CH$_3$) 5.53 (s, 3H, 3 × CH).

4.4.2.2 Tris(1-phenyl-1,3-butanedionato)cobalt(III) [Co(ba)₃] {10}
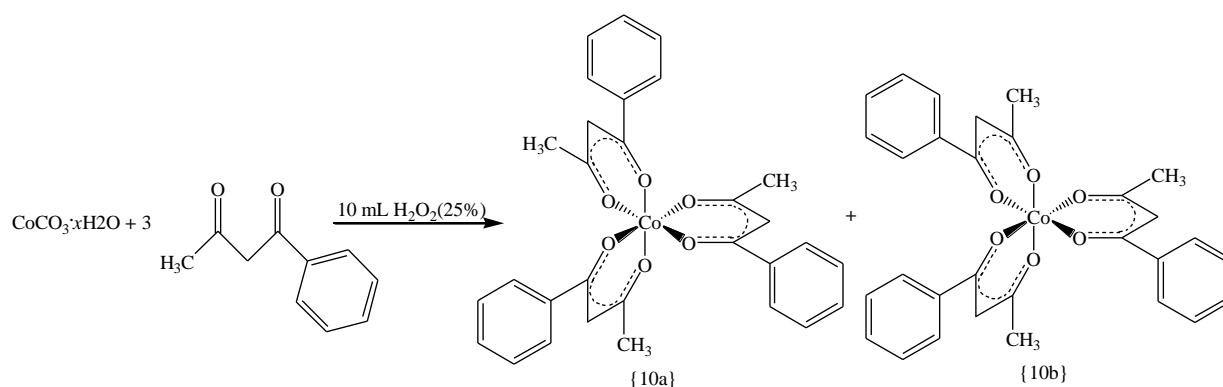
Yield 66 % Colour: Dark green. ^{1}H NMR: (300 MHz, δ/ppm, CDCl$_3$): 2.32-2.42 (q, 9H, 3 × CH$_3$), 6.23 (d, 3H, 3 × CH), 7.28-7.46 (m, 9H, 9 × PhH), 7.85 (t, 6H, 6 × PhH). MS Calcd. MS Calcd. m/z 542.46, Found: m/z 601.53. M.P. 184.3 °C

---

[7] Bryant, B. E.; Fernelius, W.C.; *Inorg. Syn.,* **1957**, *5*, 188-189

4.4.2.3 Tris(1,3-diphenyl-1,3-propanedionato)cobalt(III) [Co(dbm)₃] {11}

{11}
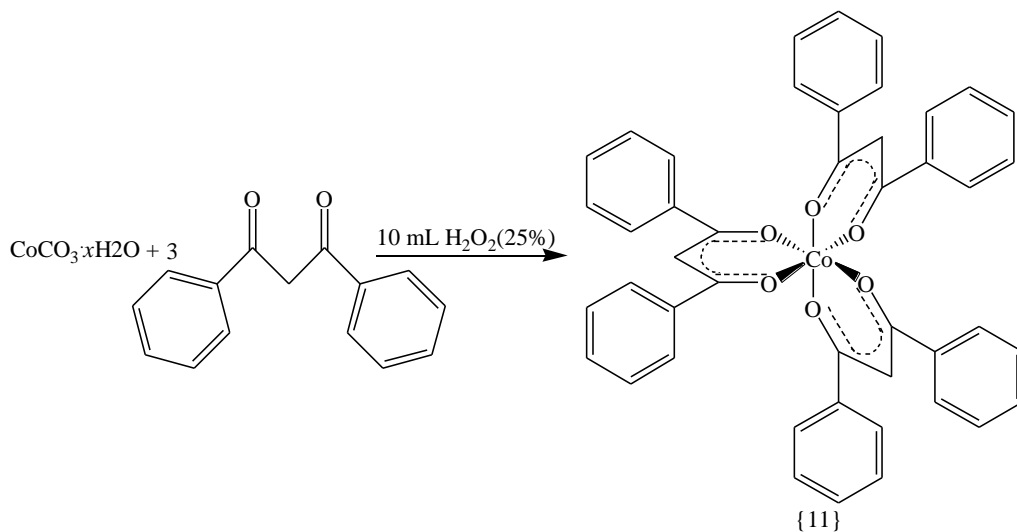
Yield 72 % Colour: Dark green.

4.4.2.4 Tris(4,4,4-trifluoro-1-phenyl-1,3-butanedionato)cobalt(III) [Co(tfba)₃] {12}

{12a}   {12b}
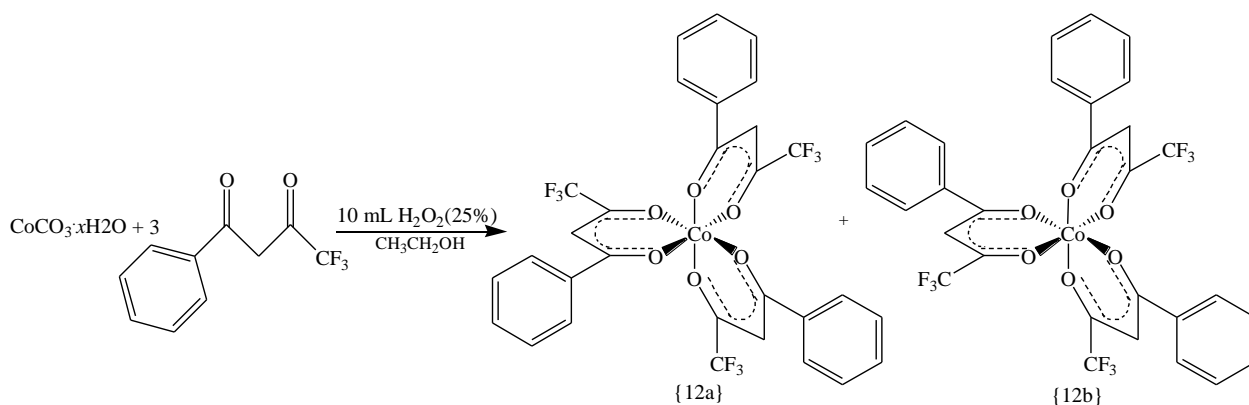
Yield 13 % Colour: Dark green. MS Calcd. m/z 905.95 Found: m/z 978.94. M.P. 107.6 ℃

4.4.2.5 Tris(1,1,1-trifluoro-2,4-pentadionato)cobalt(III) [Co(tfaa)₃] {13}

{15a}   {15b}
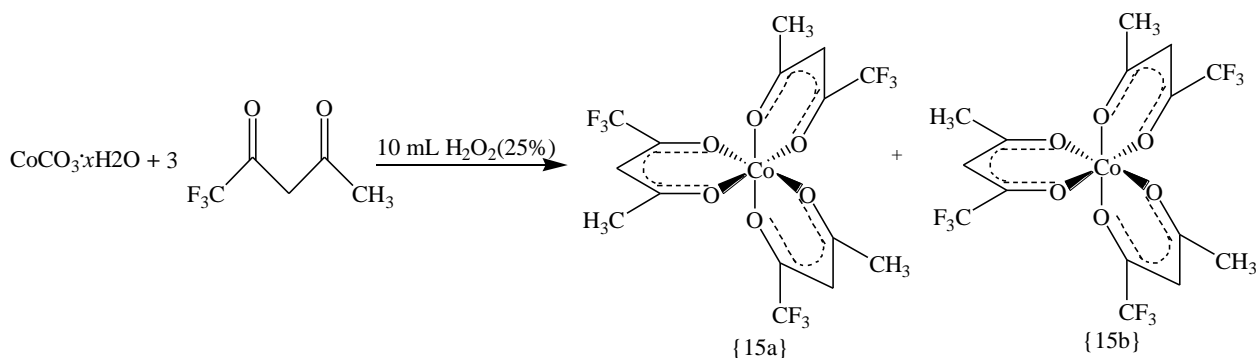
Yield 51 % Colour: Dark green.

4.5 Crystallography

Data for the crystals, obtained from solutions in diethyl ether, were collected on a Bruker D8 Venture kappa geometry diffractometer, with duo Iμs sources, a Photon 100 CMOS detector and APEX II[8] control software using Quazar multi-layer optics monochromated, Mo-$K\alpha$ radiation by means of a combination of ϕ and ω scans. Data reduction was performed using SAINT+ [8] and the intensities were corrected for absorption using SADABS.[8] The structure was solved by intrinsic phasing using SHELXTS and refined by full-matrix least squares, using SHELXTL + [9] and SHELXL-2013+.[9] In the structure refinement, all hydrogen atoms were added in calculated positions and treated as riding on the atom to which they are attached. All non-hydrogen atoms were refined with anisotropic displacement parameters, all isotropic displacement parameters for hydrogen atoms were calculated as $X \times U_{eq}$ of the atom to which they are attached, where $X = 1.5$ for the methyl hydrogens and 1.2 for all other hydrogens. The standard deviations from the experimental average value ($\overline{\omega}$) were calculated by equation $\sqrt{\frac{\Sigma(\overline{\omega}-\omega)^2}{n-1}}$, where n values were measured of ω.

4.6 Computational Calculations

4.6.1 Tris(β-diketonato)chromium and -cobalt complexes

Approximate coordinates of Cr^{III}(β-diketonato)$_3$ complexes were obtained by drawing the structure on Chemcraft Version 1.6.[10] Geometry optimizations of those coordinates were performed using Amsterdam Density Functional (ADF) 2012 system[11] with the gradient-corrected correlation functional PW91 (Perdew-Wang, 1991 exchange) the Triple-Zeta with Polarisation (TZP) basis set based on the Density Functional Theory (DFT). All minimum

---

[8] APEX2 (including SAINT and SADABS); Bruker AXS Inc., Madison, WI, 2012

[9] Sheldrick, G. M.; *Acta Cryst.*, **2008**, *A64*, 112-122

[10] http://www.chemcraftprog.com

[11] Te Velde, G.; Bickelhaupt, F. M.; Baerends, E. J.; Guerra, C. F.; Van Gisbergen, S. J. A.; Snijders, J. G.; Ziegler, T.; *J. Comput. Chem.*, **2001**, *22*, 931-967

structures were confirmed by a frequency analysis. The spin plots and orbital plots were obtained from ADF T21 and T41 file and visualized in Chemcraft.

4.6.2 Cr-carbene complexes

Density functional theory calculations on Cr-carbene complexes were carried out using the hybrid functional B3LYP[12,13] as implemented in the Gaussian 09 program package.[14] Geometries were optimized in gas phase with the triple-ζ basis set 6-311G(d,p) on all atoms except chromium, where LANL2DZ was used (corresponding to the Los Alamos Effective Core Potential plus DZ.[15] Calculations taking solvation effects into account did not alter the character of the frontier orbitals or the relationship relative to experimental values.[16] All minimum structures were confirmed by a frequency analysis. The spin plots and orbital plots were obtained from the Gaussian checkpoint files, and visualized in Chemcraft.

[12] Becke, A. D.; *Phys. Rev. A*, **1988**, *38*, 3098-3100

[13] Lee, C.; Yang, W.; Parr, R. G.; *Phys. Rev. B*, **1988**, *37*, 785-789

[14] Frisch, M. J.; Trucks, G. W.; Schlegel, H. B.; Scuseria, G. E.; Robb, M. A.; Cheeseman, J. R.; Scalmani, G.; Barone, V.; Mennucci, B.; Petersson, G. A.; Nakatsuji, H.; Caricato, M.; Li, X.; Hratchian, H. P.; Izmaylov, A. F.; Bloino, J.; Zheng, G.; Sonnenberg, J. L.; Hada, M.; Ehara, M.; Toyota, K.; Fukuda, R.; Hasegawa, J.; Ishida, M.; Nakajima, T.; Honda, Y.; Kitao, O.; Nakai, H.; Vreven, T.; Montgomery (Jr), J. A.; Peralta, J. E.; Ogliaro, F.; Bearpark, M.; Heyd, J. J.; Brothers, E.; Kudin, K. N.; Staroverov, V. N.; Keith, T.; Kobayashi, R.; Normand, J.; Raghavachari, K.; Rendell, A.; Burant, J. C.; Iyengar, S. S.; Tomasi, J.; Cossi, M.; Rega, N.; Millam, J. M.; Klene, M.; Knox, J. E.; Cross, J. B.; Bakken, V.; Adamo, C.; Jaramillo, J.; Gomperts, R.; Stratmann, R. E.; Yazyev, O.; Austin, A. J.; Cammi, R.; Pomelli, C.; Ochterski, J. W.; Martin, R. L.; Morokuma, K.; Zakrzewski, V. G.; Voth, G. A.; Salvador, P.; Dannenberg, J. J.; Dapprich, S.; Daniels, A. D.; Farkas, O.; Foresman, J. B.; Ortiz, J. V.; Cioslowski, J.; Fox, D. J.; Gaussian 09, Revision C.01, Gaussian Inc., Wallingford CT, **2010**.

[15] (a) Dunning (Jr), T. H.; Hay, P. J.; *Modern Theoretical Chemistry*, Ed. H.F. Schaefer III, *3*, Plenum, New York, **1976**

(b) Hay, P. J.; Wadt, W. R.; *J. Chem. Phys.*, 1985, 82, 270-283

(c) Hay, P. J.; Wadt, W. R.; *J. Chem. Phys.*, 1985, 82, 284-298

(d) Hay, P. J.; Wadt, W. R.; *J. Chem. Phys.*, 1985, 82, 299-310

[16] Landman, M.; Liu, R.; van Rooyen, P. H.; Conradie, J.; *Electrochim. Acta*, **2013**, 114, 205-214

5 Concluding remarks and future perspectives

5.1 Concluding Remarks

5.1.1 Tris(β-diketonato)chromium(III) complexes

A series of Cr(β-diketonato)$_3$ complexes were studied by experimental and computational methods, where β-diketonato = acac, ba, dbm, tfba, tfth, tffu, tfaa, hfaa. All eight Cr(β-diketonato)$_3$ complexes were successfully synthesized. The crystal structure of Cr(dbm)$_3$ was solved and presented in this study. The electrochemical behaviour of the Cr(β-diketonato)$_3$ complexes was studied by the use of cyclic voltammetry. A maximum of four redox processes were observed:

$$Cr^I \leftarrow Cr^{II} \leftrightarrow Cr^{III} \rightarrow Cr^{IV} \rightarrow Cr^V$$
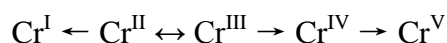
Only the Cr^{III}(β-diketonato)$_3$ $\leftrightarrow$ Cr^{II}(β-diketonato)$_3$ redox process was found to be *quasi-reversible* (except in Cr(ba)$_3$), the other redox processes were irreversible. The oxidation of Cr(hfaa)$_3$ was not observed, since it was shifted out of the working solvent window. Side groups R$_1$ and R$_2$ of the β-diketonato ligands ([R$_1$COCHCOR$_2$]$^-$) have a decisive role in the shifting of redox potentials: more electron-withdrawing side groups shift the redox processes to more positive potentials. This influence is established by the linear dependence of E_{pc} of $Cr^{III/II}$ on the total Hammett sigma meta constants [$\Sigma(\sigma_{R1} + \sigma_{R2})$] of the side groups on β-diketonato ligands, on the total group electronegativities [$\Sigma(\chi_{R1} + \chi_{R2})$], and on the acid dissociation constant (pK_a) of the uncoordinated β-diketone. The linear equations of these relationships can be expressed as follows:

pK_a = -0.0032 E_{pc} + 2.08 R^2 = 0.89

$\Sigma\chi$ = -1.86 E_{pc} + 9.70, R^2 = 1.00 (for Cr(acac)$_3$, Cr(ba)$_3$ and Cr(dbm)$_3$)

$\Sigma\sigma$ = 0.0019 E_{pc} + 4.04 R^2 = 0.99

DFT-studies showed that Cr(β-diketonato)$_3$ has a spin-state preference of 3/2, and D_3 symmetry. This observation agrees with the experimental results obtained. The reduction potentials (E_{pc}) of

the $Cr^{III/II}$ redox processes are linearly dependent on the LUMO energies (E_{LUMO}) and electron affinity (EA). The linear equations of these relationships can be expressed as follows:

E_{LUMO} = -0.0014 E_{pc} -5.66 R^2 = 0.93

EA = 0.0013 E_{pc} + 4.18 R^2 = 0.93

5.1.2 Tris(β-diketonato)cobalt(III) complexes

A series of Co(β-diketonato)$_3$ complexes were studied by experimental and computational methods, where β-diketonato = acac, ba, dbm, tfba, tfaa. All five Co(β-diketonato)$_3$ complexes were successfully synthesized. The crystal structures of Co(ba)$_3$ and Co(tfba)$_3$ were solved and presented in this study. DFT-studies showed that Co(β-diketonato)$_3$ has a spin-state preference of 0/2 (diamagnetic), and D_3 symmetry. This observation agrees with the experimental results obtained.

5.1.3 Chromium(0) carbene complexes

Electrochemical behaviour of nine chromium(0) carbene complexes was investigated by cyclic voltammetry. Generally, one reduction and two oxidation processes were observed: 1) $Cr^0 \leftrightarrow$ $Cr^I \rightarrow Cr^{II}$ oxidation processes of the metal, and 2) the reduction of the carbene ligand at the carbene carbon. The first redox process on the Cr metal center was found to be reversible, while the second oxidation process of the Cr^I species is totally irreversible. The reduction process of the carbene ligands became *quasi*-reversible at high scan rates (300 mV/s or higher). Four of the carbene complexes, with a bidentate ligand 1,2-bis(diphenylphosphino)ethane (DPPE), were found to have different oxidation potentials for the different *fac-* or *mer*-isomers. The redox behaviour of the *fac-* and *mer*-isomers was understood, via the results obtained from the computational studies. The *mer*-isomers are ionized at a lower potential than the *fac*-isomers for chromium(0) carbene complexes, and also the *mer*-isomers of the oxidized species dominate the population. The oxidation potentials (E_{pa}) of the chromium metal center are linearly dependent on the HOMO energy (E_{HOMO}), while the reduction potentials (E_{pc}) of the carbene carbon on the ligand are linearly dependent on the LUMO energy (E_{LUMO}). The linear equations of these relationships can be expressed as follows:

$E_{pa\ Cr^{0/1}} = -0.69\ E_{HOMO} - 3.65$ R^2 = 0.99

$E_{pc\ carbene\ carbon} = -0.69\ E_{LUMO} - 3.49$ R^2 = 0.98

5.2 Future perspectives

The study of the Cr(β-diketonato)$_3$ complex series can be expanded as follows:

(i) Anchoring the Cr(β-diketonato)$_3$ complexes onto a support, *e. g.* Silica wafer, MCM-41 support.

(ii) Conducting catalytic studies on the free Cr(β-diketonato)$_3$ complexes, as well as when anchored onto a support. Evaluating their catalytic activities.

The study of the Co(β-diketonato)$_3$ complex series can be expanded as follows:

(i) Completing the syntheses for the series of Co(β-diketonato)$_3$ complexes, where β-diketonato = tfth, tffu, hfaa.

(ii) Studying the electrochemical behaviour for the full series of Co(β-diketonato)$_3$ complexes.

(iii) Using electronic parameters and computational methods to investigate the electrochemical behaviour of Co(β-diketonato)$_3$ complexes.

(iv) Anchoring the Co(β-diketonato)$_3$ complexes onto a Silica wafer support.

(v) Conducting catalytic studies on the free Co(β-diketonato)$_3$ complexes, as well as when anchored onto a support. Evaluating their catalytic activities.

The study of the Cr(0) carbene complex series can be expanded as follows:

(vi) Studying the catalytic activities of the Cr(0) carbene complexes.

(vii) Conducting electrochemistry and computational chemistry studies of a series of M(0) carbene complexes, establishing the influence of the metal on the activity of the complex.

Appendix

A. Cyclic Voltammetry (CV)
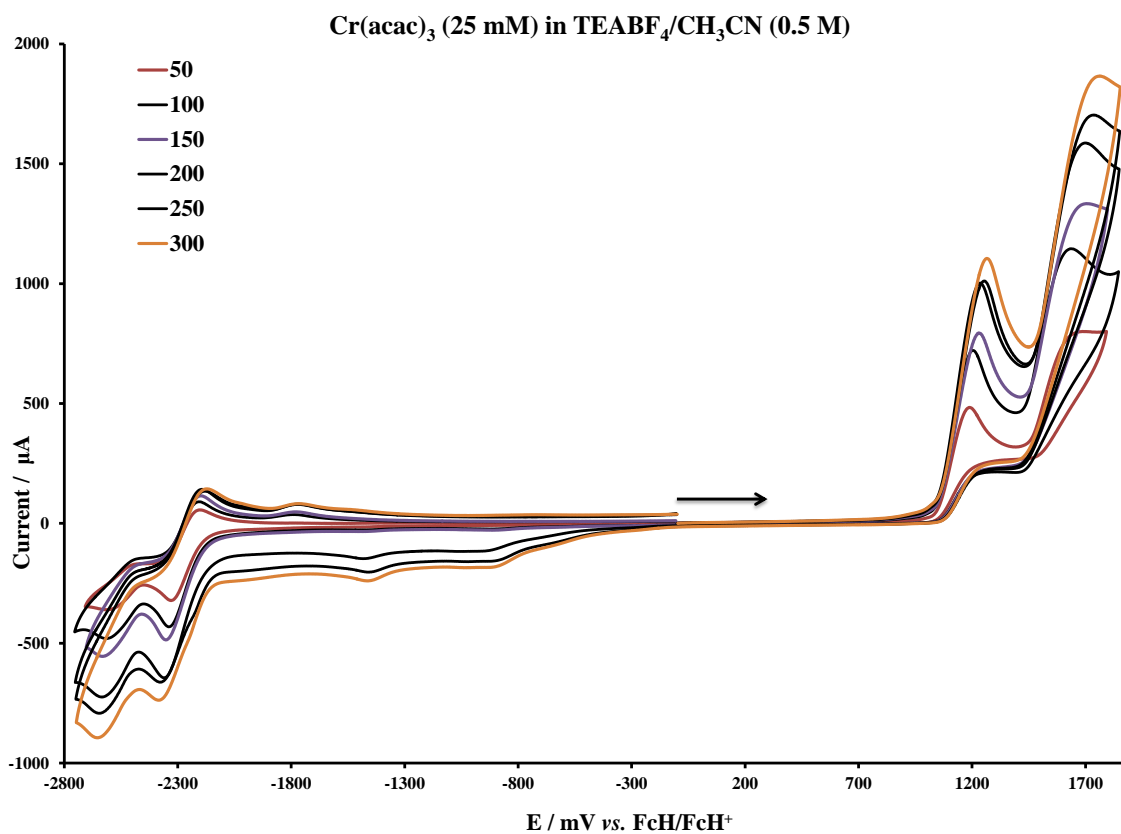
Figure A.1: Cyclic voltammograms of 25 mM Cr(acac)$_3$ {1}, *vs.* FcH/FcH[+]. (Solvent = CH$_3$CN, supporting electrolyte TEABF$_4$, scan rate = 50, 100, 150, 200, 250 and 300 mV•s[-1], with glassy carbon as working electrolyte at 20 ℃, scan direction as indicated by the arrow).

Cr(ba)$_3$ (25 mM) in TEABF$_4$/CH$_3$CN (0.5 M)
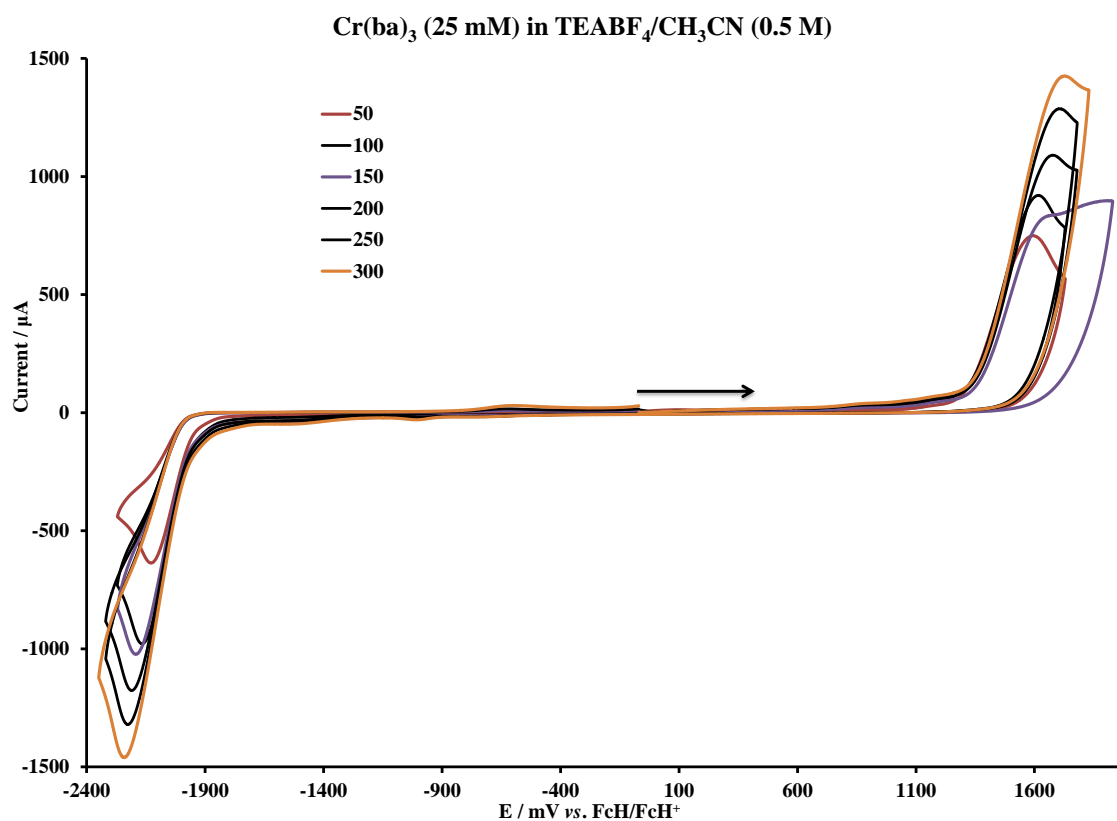
Figure A.2: Cyclic voltammograms of 25 mM Cr(ba)$_3$ {2}, *vs.* FcH/FcH$^+$. (Solvent = CH$_3$CN, supporting electrolyte TEABF$_4$, scan rate = 50, 100, 150, 200, 250 and 300 mV•s^{-1}, with glassy carbon as working electrolyte at 20 °C, scan direction as indicated by the arrow).

Cr(dbm)$_3$ (25 mM) in TEABF$_4$/CH$_3$CN (0.5 M)
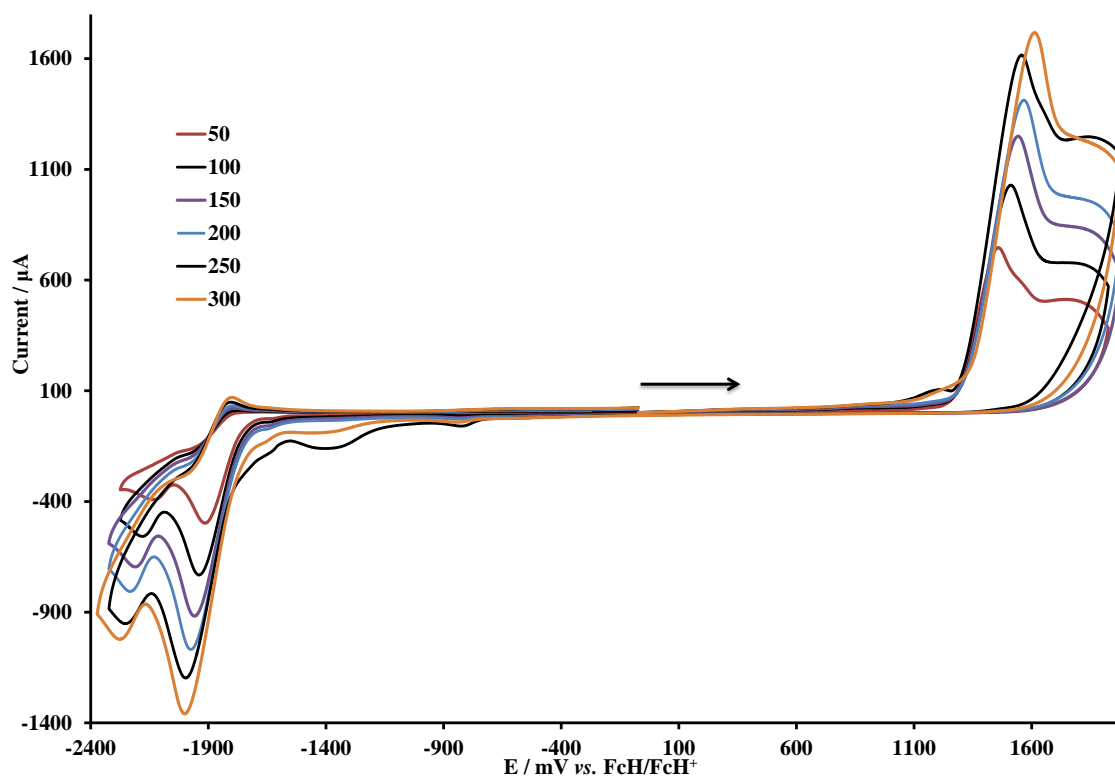
Figure A.3: Cyclic voltammograms of 25 mM Cr(dbm)$_3$ {3}, *vs.* FcH/FcH$^+$. (Solvent = CH$_3$CN, supporting electrolyte TEABF$_4$, scan rate = 50, 100, 150, 200, 250 and 300 mV•s^{-1}, with glassy carbon as working electrolyte at 20 ℃, scan direction as indicated by the arrow).

Cr(tfba)$_3$ (25 mM) in TEABF$_4$/CH$_3$CN (0.5 M)
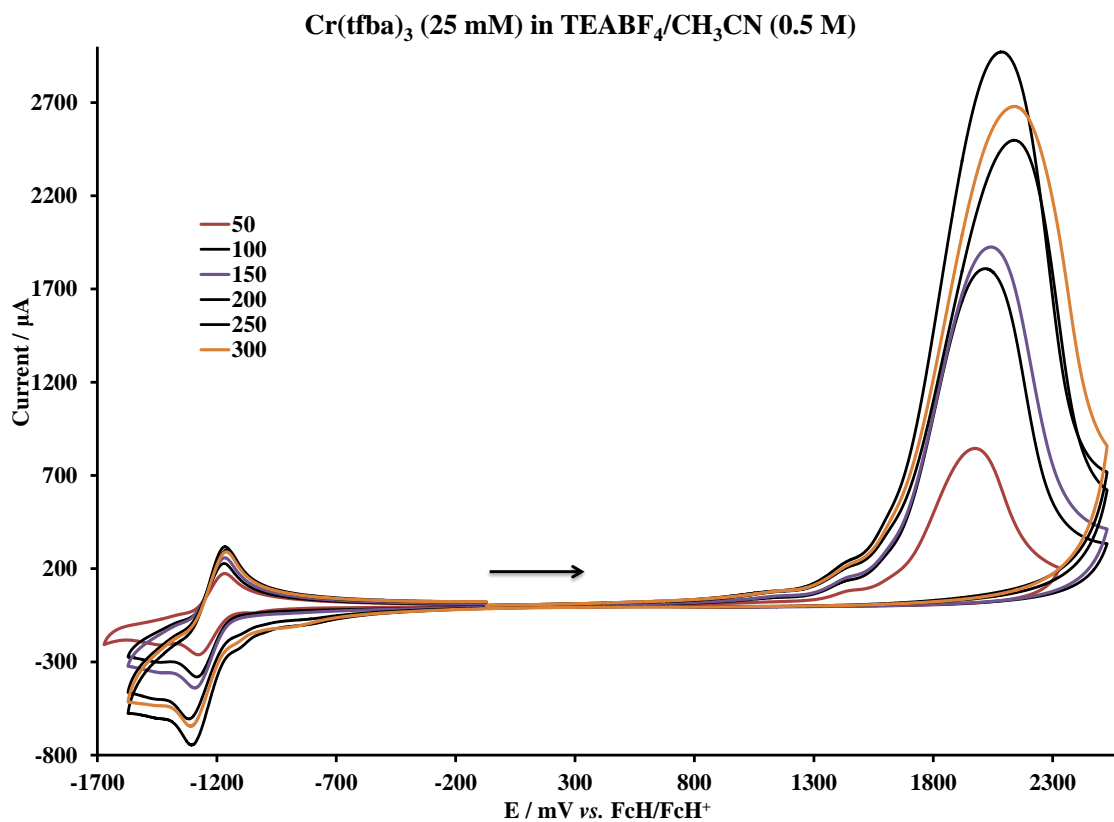
Figure A.4: Cyclic voltammograms of 25 mM Cr(tfba)$_3$ {4}, *vs.* FcH/FcH$^+$. (Solvent = CH$_3$CN, supporting electrolyte TEABF$_4$, scan rate = 50, 100, 150, 200, 250 and 300 mV•s^{-1}, with glassy carbon as working electrolyte at 20 °C, scan direction as indicated by the arrow).

Cr(tfth)$_3$ (25 mM) in TEABF$_4$/CH$_3$CN (0.5 M)
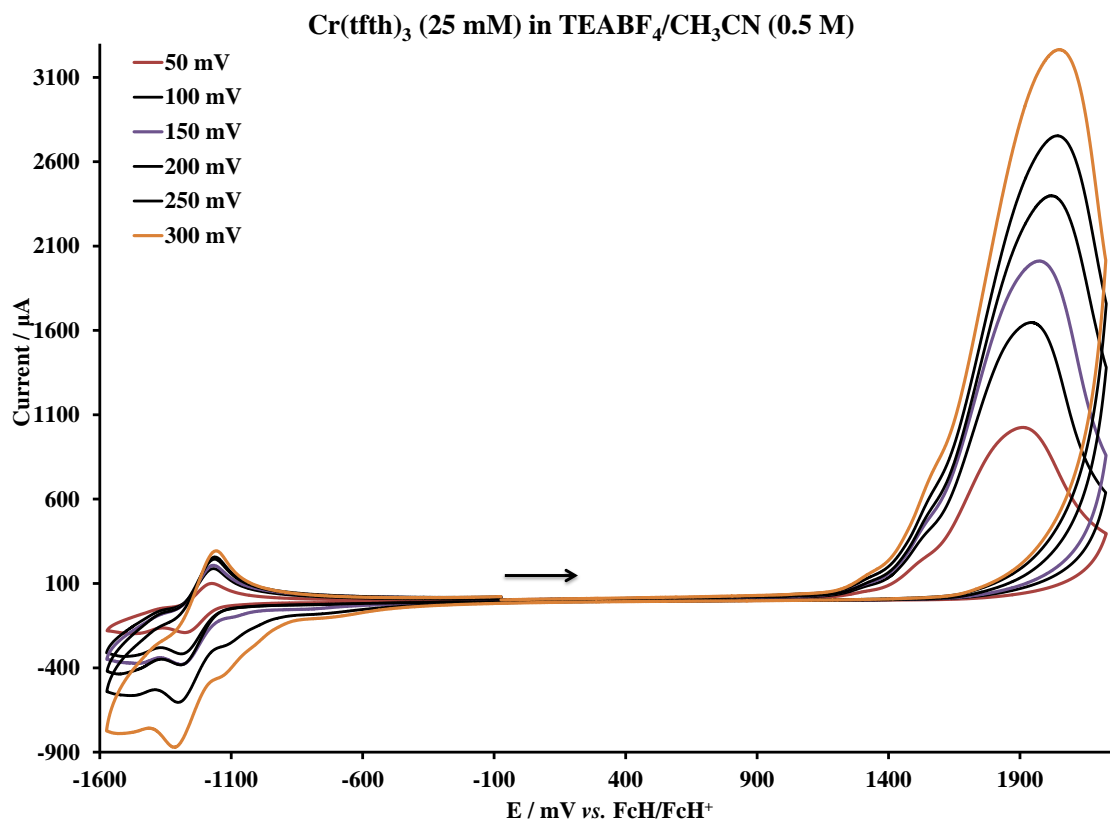
Figure A.5: Cyclic voltammograms of 25 mM Cr(tfth)$_3$ {5}, *vs.* FcH/FcH$^+$. (Solvent = CH$_3$CN, supporting electrolyte TEABF$_4$, scan rate = 50, 100, 150, 200, 250 and 300 mV•s^{-1}, with glassy carbon as working electrolyte at 20 °C, scan direction as indicated by the arrow).

Cr(tffu)$_3$ (25 mM) in TEAPF$_6$/CH$_3$CN(0.5 M)
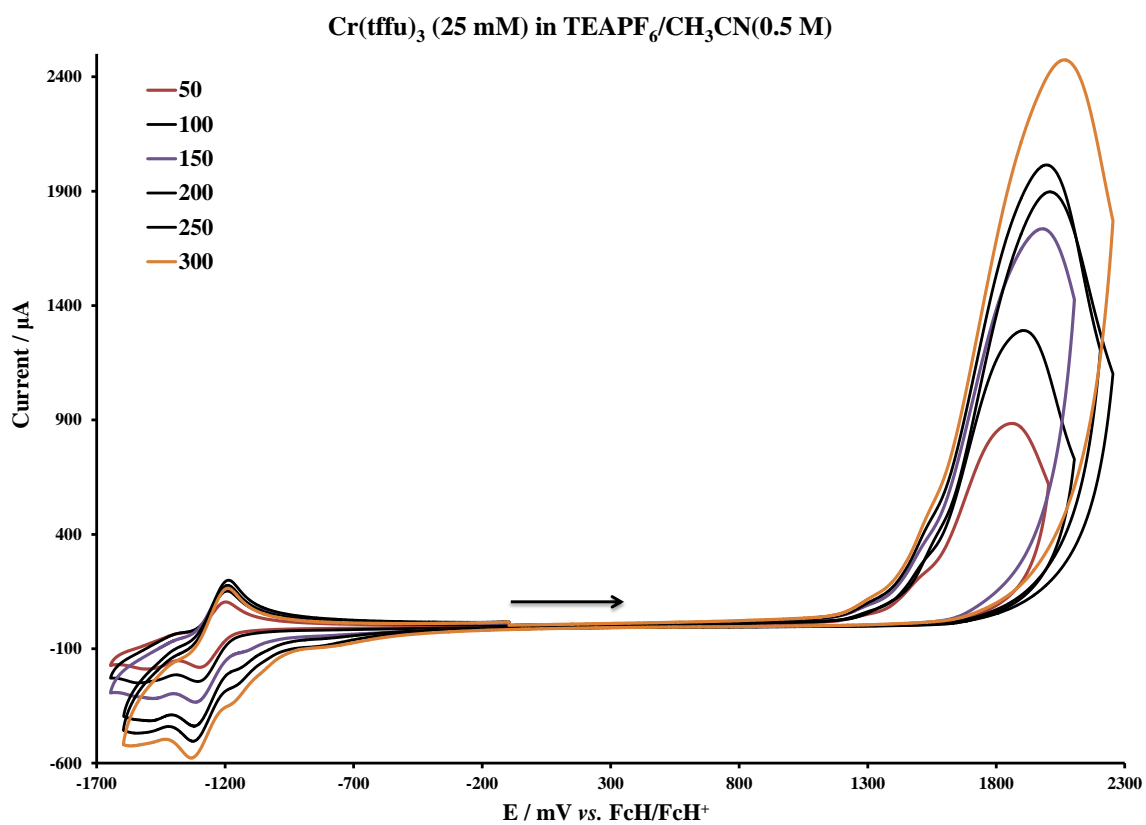
Figure A.6: Cyclic voltammograms of 25 mM Cr(tffu)$_3$ {6}, *vs.* FcH/FcH$^+$. (Solvent = CH$_3$CN, supporting electrolyte TEABF$_4$, scan rate = 50, 100, 150, 200, 250 and 300 mV•s^{-1}, with glassy carbon as working electrolyte at 20 ℃, scan direction as indicated by the arrow).

Cr(tfaa)3 (25 mM) in TEABF4/Acetonitrile (0.5 M)
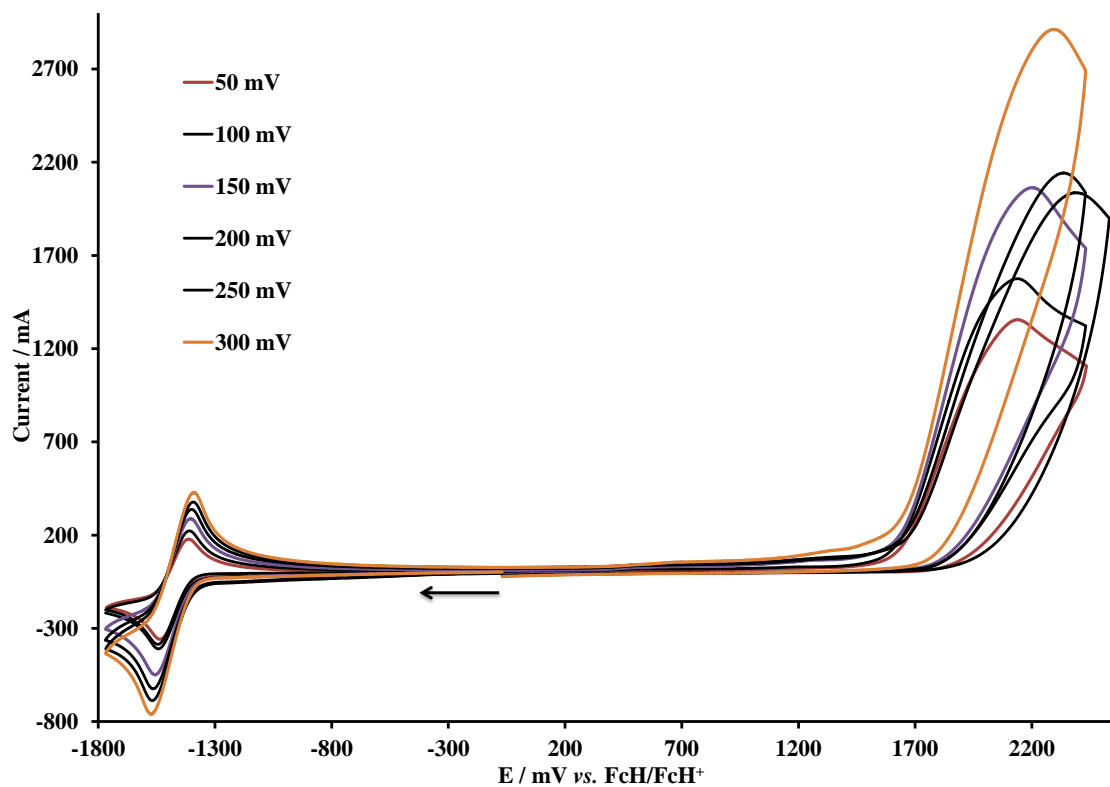
Figure A.7: Cyclic voltammograms of 25 mM Cr(tfaa)$_3$ {7}, *vs.* FcH/FcH$^+$. (Solvent = CH$_3$CN, supporting electrolyte TEABF$_4$, scan rate = 50, 100, 150, 200, 250 and 300 mV•s^{-1}, with glassy carbon as working electrolyte at 20 °C, scan direction as indicated by the arrow).
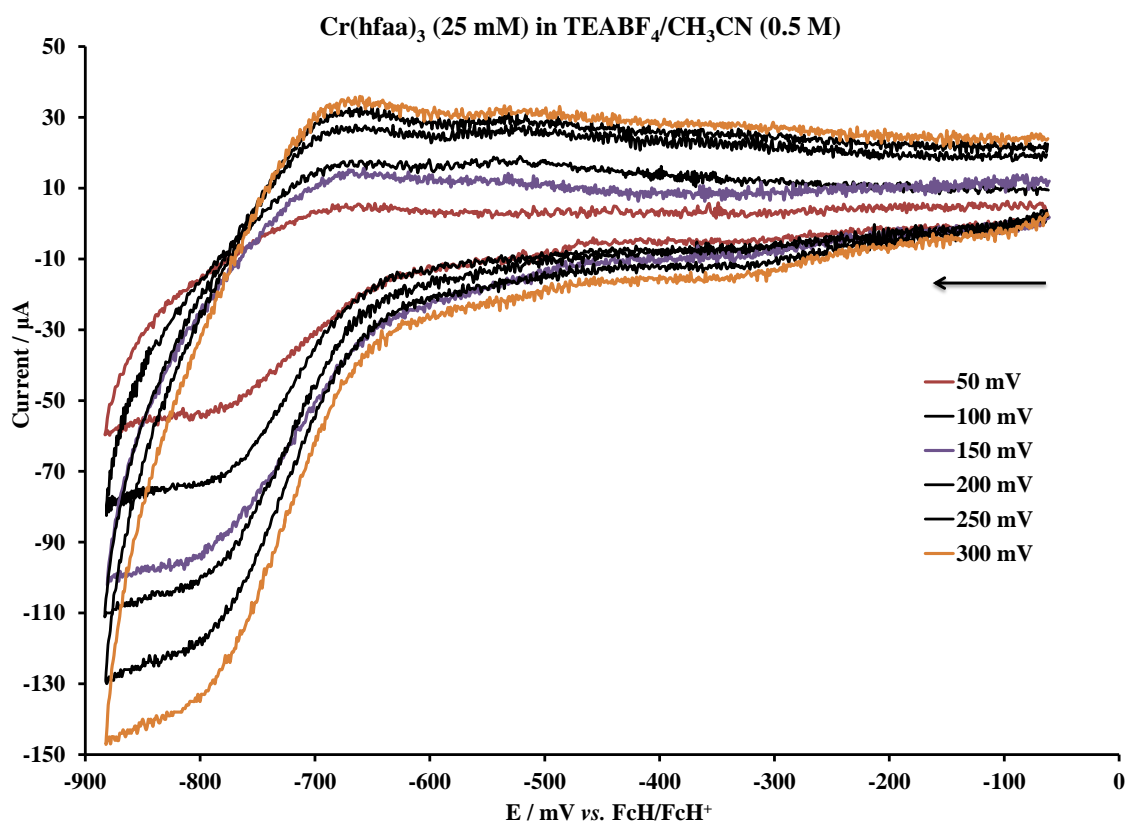
Figure A.8: Cyclic voltammograms of 25 mM Cr(hfaa)$_3$ {8}, *vs.* FcH/FcH$^+$. (Solvent = CH$_3$CN, supporting electrolyte TEABF$_4$, scan rate = 50, 100, 150, 200, 250 and 300 mV•s^{-1}, with glassy carbon as working electrolyte at 20 °C, scan direction as indicated by the arrow).

B. Mass Spectroscopy (MS)
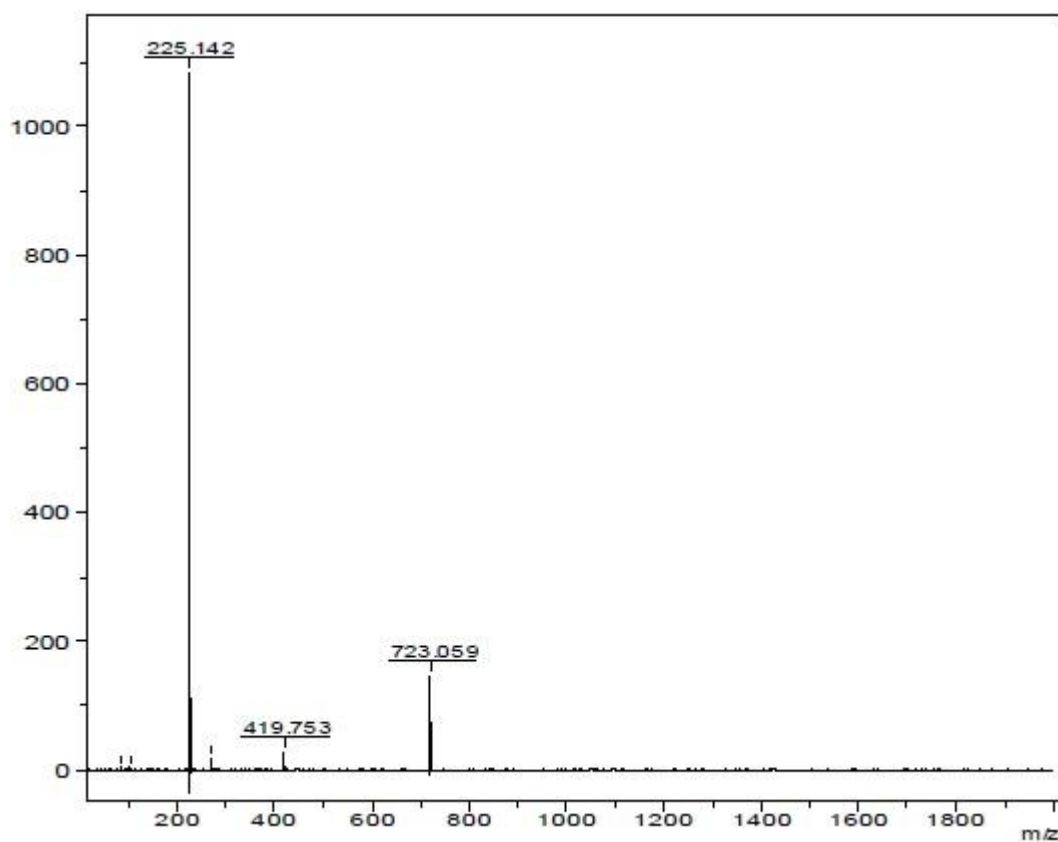
Figure B.1: Gas chromatography-mass spectrometry (GC-MS) spectrum of Cr(dbm)$_3$ {3}, MS Calculated: MS Calculated: Mr = 721.73 g/mol, Found: m/z 723.06 g/mol
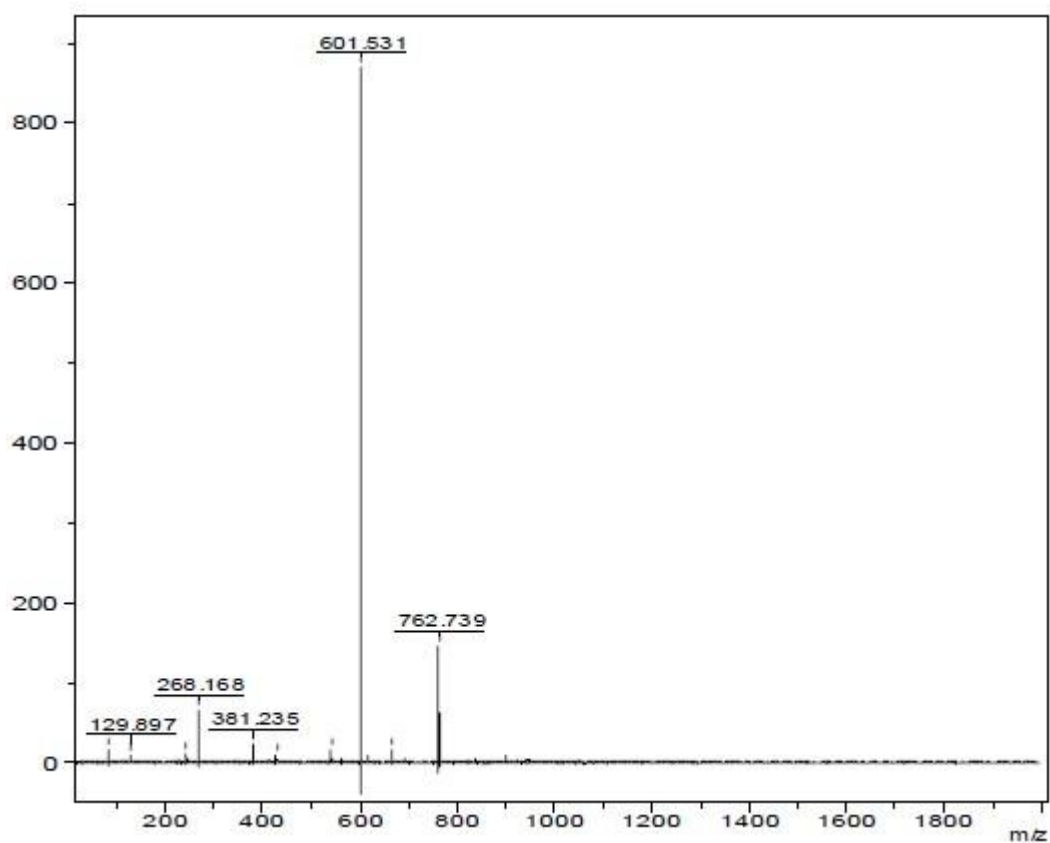
Figure B.2: Gas chromatography-mass spectrometry (GC-MS) spectrum of Co(ba)$_3$ {10}, MS
Calculated: Mr = 542.46 g/mol, Found: m/z 601.53 g/mol
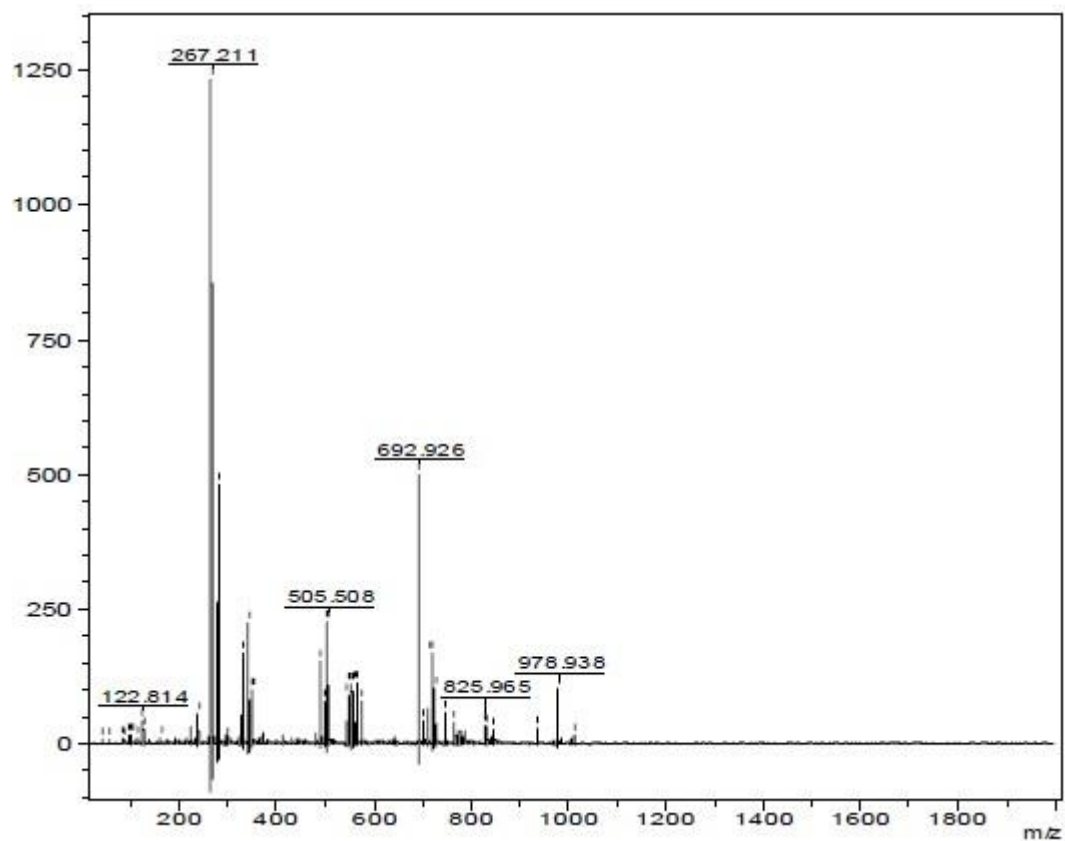
Figure B.3: Gas chromatography-mass spectrometry (GC-MS) spectrum of Co(tfba)$_3$ {12}, MS Calculated: Mr = 905.95 g/mol, Found: m/z 978.94 g/mol

C. Nuclear Magnetic Resonance (NMR)
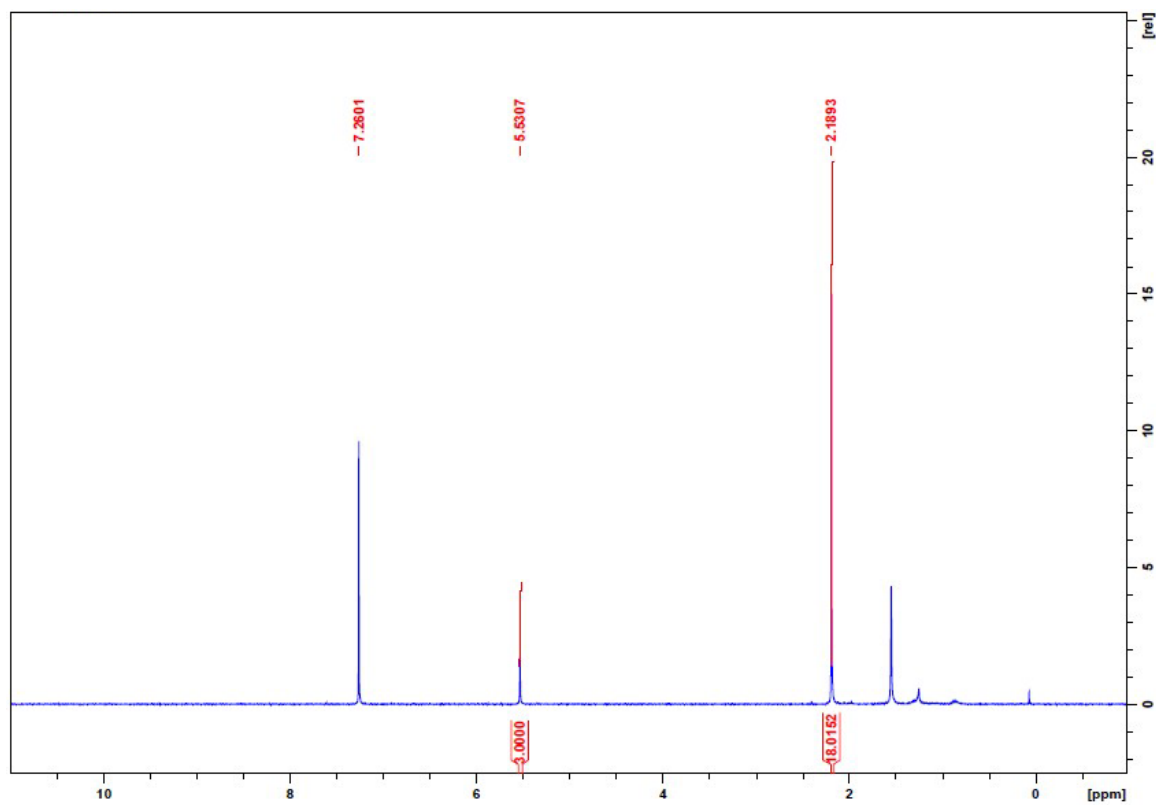
Figure C. 1: ^{1}H NMR spectrum of Co(acac)$_3$ {9}, 2.19 (s, 18H, 6 $\times$ CH$_3$) 5.53 (s, 3H, 3 $\times$ CH).
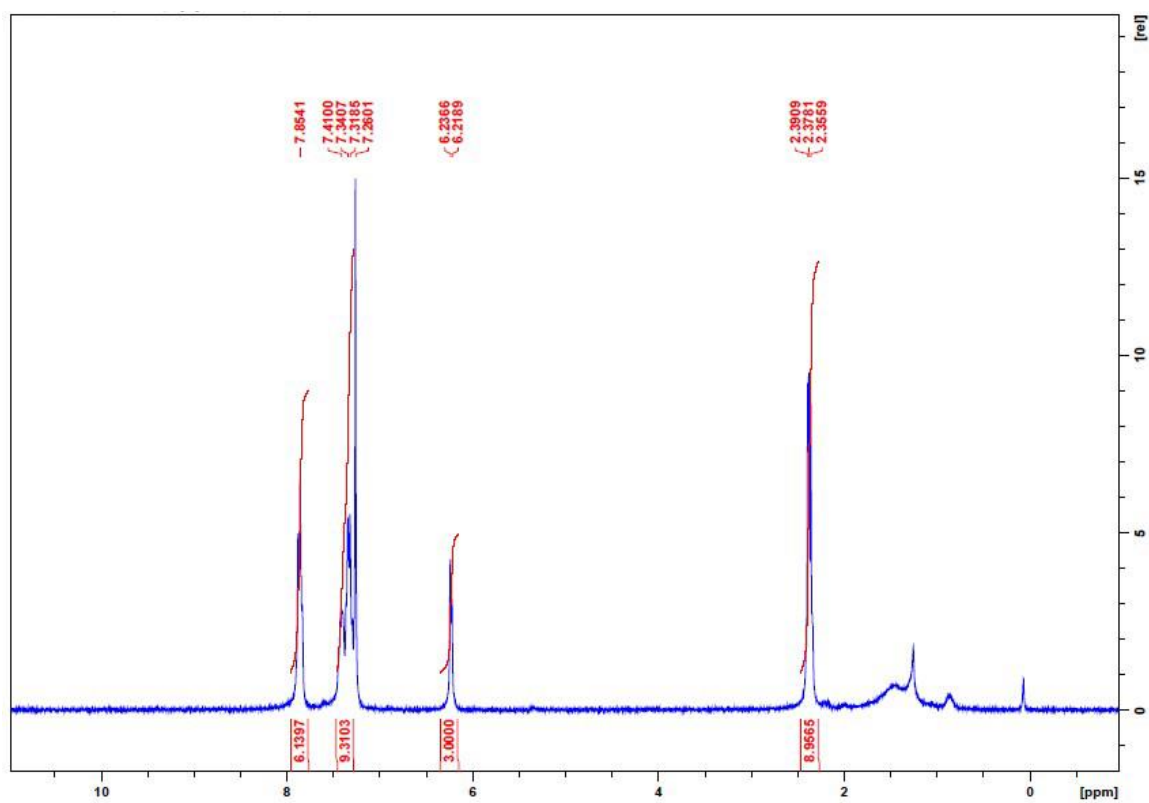
Figure C. 2: ^{1}H NMR spectrum of Co(ba)$_3$ {10}, 2.32-2.42 (3 ×s, 9H, 3 ×CH$_3$), 6.23 (2 ×s, 3H, 3 ×CH), 7.28-7.46 (m, 9H, 9 ×PhH), 7.85 (t, 6H, 6 ×PhH).
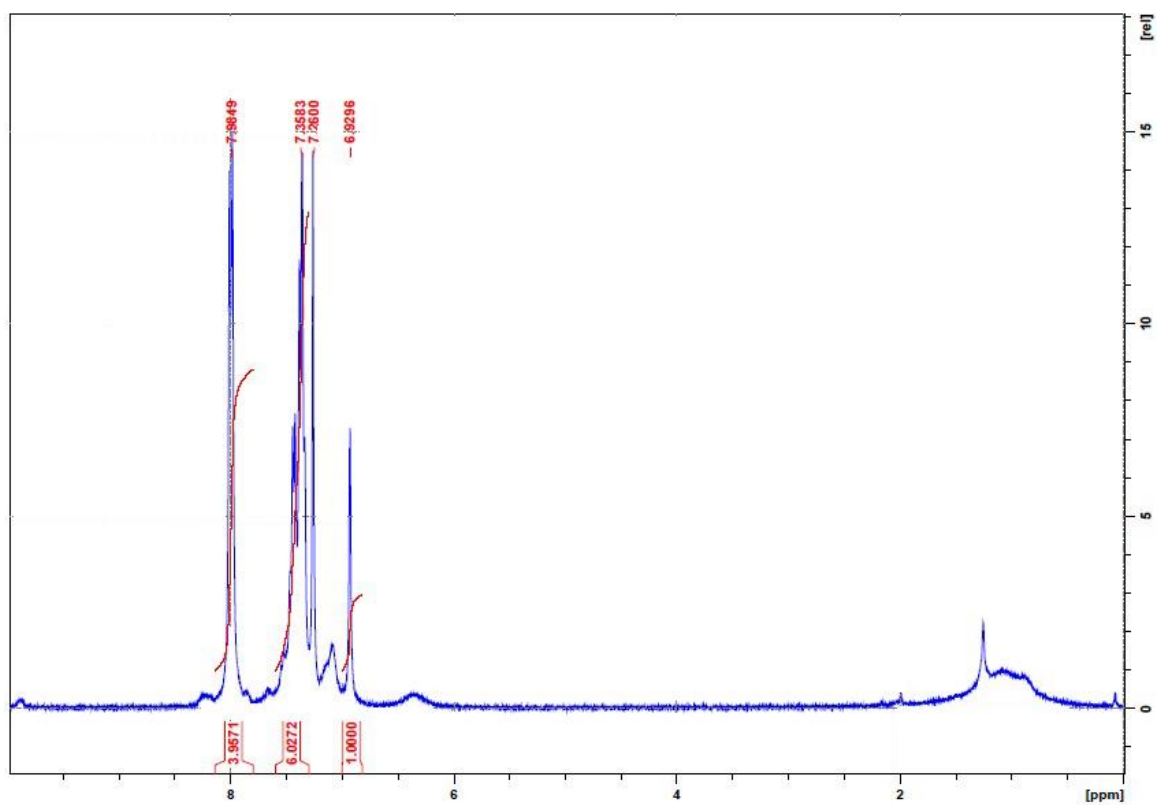
Figure C. 3: ^{1}H NMR spectrum of Co(dbm)$_3$ {11}, 6.93 (s, 3H, 3 ×CH), 7.29-7.59 (m, 18H, 18 ×PhH), 7.78-8.14 (d, 12H, 12 ×PhH).
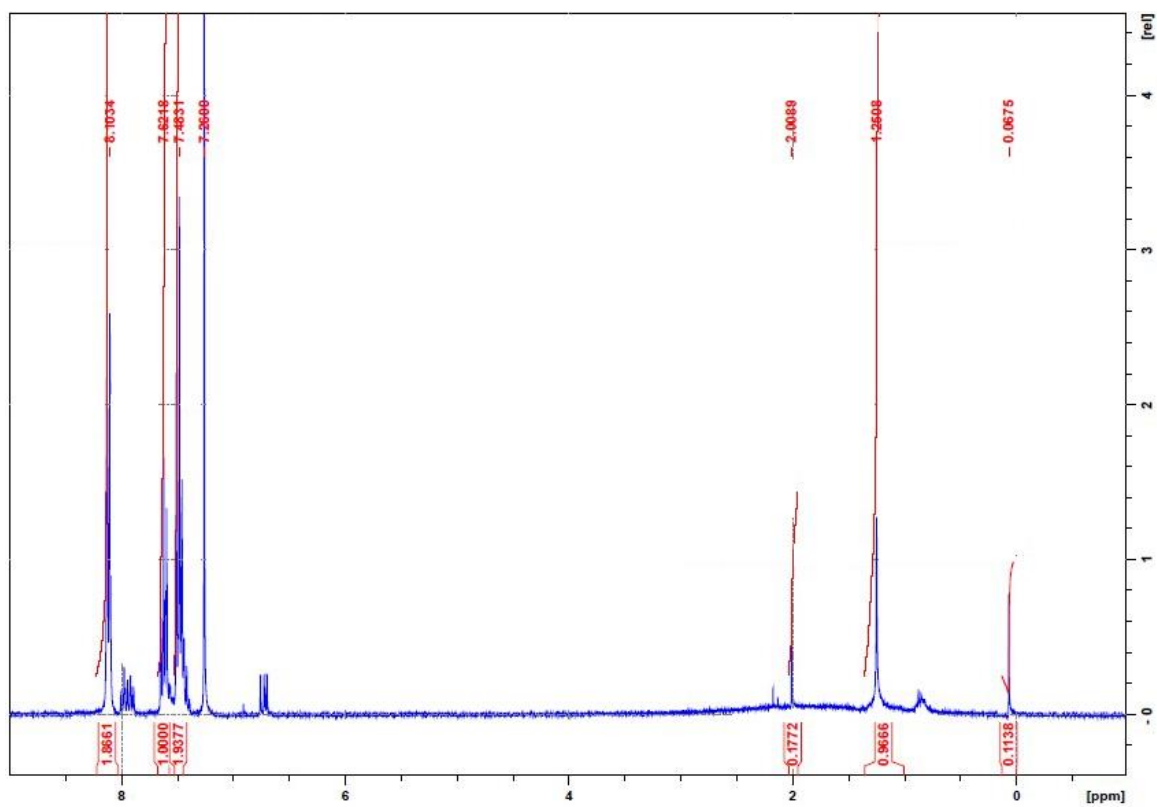
Figure C.4: ^{1}H NMR spectrum of Co(tfba)$_3$ {12}: 1.25 (s, 3H, 3 ×CH), 7.45-7.53 (m, 6H, 6 × PhH), 7.57-7.68 (m, 3H, 3 ×PhH), 8.03-8.22 (t, 6H, 6 ×PhH).
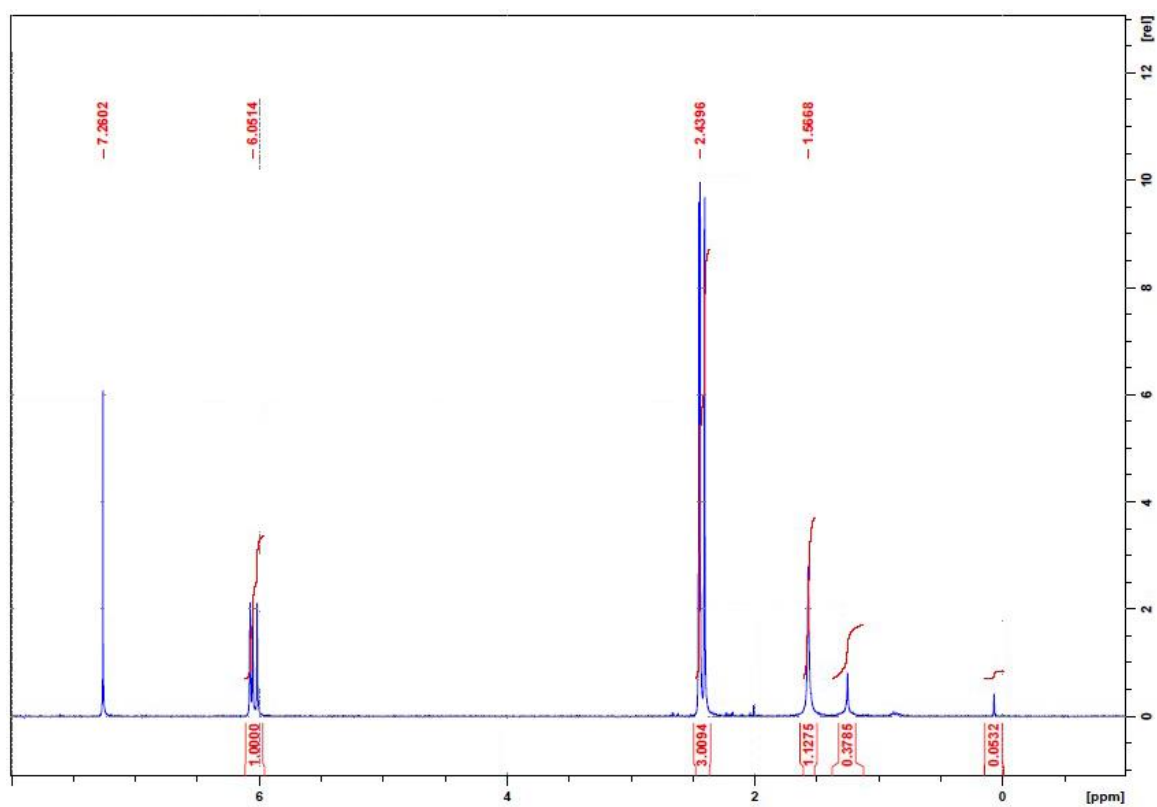
Figure C.5: ^{1}H NMR spectrum of Co(tfaa)$_3$: 2.38-2.48 (3 $\times$ s, 9H, 3 $\times$ CH$_3$), 5.98-6.10 (3 $\times$ s, 3H, 3 $\times$ CH).

Abstract

Two series of metal(β-diketonato)$_3$ complexes were synthesized: tris(β-diketonato)chromium(III) complexes (where β-diketonato = [R$_1$COCHCOR$_2$]$^-$ = acac, ba, dbm, tfba, tfth, tffu, tfaa, hfaa) and tris(β-diketonato)cobalt(III) complexes (where β-diketonato = acac, ba, dbm, tfba, tfaa). These paramagnetic complexes were characterized by mass spectroscopy, X-ray crystallography and melting point measurements. The electrochemical behaviour of tris(β-diketonato)chromium(III) complexes was investigated by cyclic voltammetry (CV), linear sweep voltammetry (LSV) and square wave voltammetry (SWV). The reduction potentials of the Cr^{III}(β-diketonato)$_3$ → Cr^{II}(β-diketonato)$_3$ process correlate linearly with the following electronic parameters: 1) the acid dissociation constant (pK_a) of the uncoordinated β-diketonato ligands, 2) the total electronegativities ($\Sigma\chi$) of the side groups (R$_1$ and R$_2$) on the β-diketonato ligands, and 3) the total Hammett sigma constant ($\Sigma\sigma$) of the side groups (R$_1$ and R$_2$) on the β-diketonato ligands. DFT-calculations were done on both series of these metal(β-diketonato)$_3$ complexes. Molecular geometry, spin state and respective population of possible isomers were calculated in this study. The understanding of crystal structures was complemented by using DFT-results. For Cr^{III}(β-diketonato)$_3$ complexes, linear dependence was found between their reduction potentials and electron affinity (EA), as well as between reduction potentials and the energies of the lowest unoccupied molecular orbitals (E_{LUMO}).

Electrochemical behaviour of chromium(0) carbene complexes was investigated by cyclic voltammetry. The difference in oxidation potential of *fac/mer* isomers was observed for the first time for chromium(0) carbene complexes and discussed in this study. DFT-calculations revealed the following linear relationships with the redox process of Cr(0) carbene complexes: 1) the linear dependence between the cathodic potential (E_{pc}) and energies of the lowest unoccupied orbitals (E_{LUMO}), and 2) the linear dependence between the anodic potential (E_{pa}) and energies of the highest occupied orbitals (E_{HOMO}).

Keywords

Chromium, Cobalt, tris(β-diketonato)metal complexes, Fischer carbene complexes, DFT, CV.

Opsomming

Twee reekse metaal(β-diketonato)₃ komplekse is in hierdie studie gesintetiseer: tris(β-diketonato)chroom(III) komplekse (met β-diketonato = $[R_1COCHCOR_2]^-$ = acac, ba, dbm, tfba, tfth, tffu, tfaa, hfaa) en tris(β-diketonato)cobalt(III) komplekse (met β-diketonato = acac, ba, dbm, tfba, tfaa). Hierdie paramagnetiese komplekse is gekarakteriseer deur massa-spektroskopie, X-straal-kristallografie en smeltpunt-bepalings. Die elektochemiese gedrag van die tris(β-diketonato)chroom(III) komplekse is ondersoek deur sikliese voltammetrie (CV), lineêre skandeer-voltammetrie (LSV) en reghoekige golf-voltammetrie (SWV). Die reduksie potensiale van die Cr^{III}(β-diketonato)₃ → Cr^{II}(β-diketonato)₃ proses korreleer lineêr met die volgende elektroniese parameters: 1) die suur dissosiasie-konstante (pK_a) van die ongekoördineerde β-diketonato ligand, 2) die som van die elektronegatiwiteite ($\Sigma\chi$) van die end-groepe (R_1 en R_2) op die β-diketonato ligand, en 3) die som van die Hammett-sigma-konstantes ($\Sigma\sigma$) van die end-groepe (R_1 en R_2) op die β-diketonato ligand. DFT-berekeninge is gedoen op beide hierdie metaal(β-diketonato)₃ series. Die molekulêre geometrie, spin-toestand en populasie van die moontlike isomere is bereken in hierdie studie. DFT-berekeninge het die begrip van die kristalstrukture gekomplementeer. Vir Cr^{III}(β-diketonato)₃ komplekse is 'n lineêre verband bepaal tussen hulle reduksie potensiale en elektron affiniteit (EA), sowel as tussen reduksie potensiale en die energieë van die laagste besette molekulêre orbitale (E_{LUMO}).

Elektrochemiese gedrag van chroom(0) karbeen komplekse is ondersoek deur sikliese voltammetrie. Die verskil in oksidasie-potensiaal van die *fac/mer* isomere, is in hierdie studie vir die eerste keer vir chroom(0) karbeen komplekse waargeneem en bespreek. DFT-berekeninge het die volgende lineêre verwantskappe met die redoks-prosesse van die Cr(0) karbeen komplekse getoon: 1) die lineêre verband tussen die katodiese potensiaal (E_{pc}) en die energieë van die laagste ongeökkupeerde molekulêre orbitale (E_{LUMO}), en 2) die lineêre verband tussen die anodiese potensiaal (E_{pa}) en die energieë van die hoogste besette molekulêre orbitale (E_{HOMO}).

Sleutelterme

Chroom, Kobalt, tris(β-diketonato)metaal komplekse, Fischerkarbeenkomplekse, DFT, CV.

Declaration.

I, Renyuan Liu, declare that the dissertation/thesis hereby handed in for the qualification Magister Scientiae in Chemistry at the University of the Free State is my own independent work and that I have not previously submitted the same work for a qualification at/in another university/faculty. I furthermore cede copyright of the thesis in favour of the University of the Free State.

Signed   Date

_____   _____

Appendix

D. Crystallography

Table D.1: Atomic coordinates (x 10^4) and equivalent isotropic displacement parameters (Å^2x 10^3) for Cr(dbm)$_3$ {3}. U(eq) is defined as one third of the trace of the orthogonalized U^{ij} tensor.

	x	y	z	U(eq)
Cr(1)	7557(1)	305(1)	8672(1)	25(1)
O(1)	8365(1)	-374(2)	8132(1)	27(1)
O(2)	7573(1)	2083(2)	8230(1)	27(1)
O(3)	8339(1)	994(2)	9300(1)	28(1)
O(4)	7560(1)	-1483(2)	9094(1)	26(1)
O(5)	6718(1)	903(2)	9203(1)	28(1)
O(6)	6785(1)	-319(2)	8032(1)	30(1)
C(1)	8536(2)	97(4)	7596(2)	26(1)
C(2)	8276(2)	1358(4)	7351(2)	28(1)
C(3)	7815(2)	2287(4)	7676(2)	28(1)
C(4)	8556(2)	434(4)	9823(2)	25(1)
C(5)	8314(2)	-871(4)	10011(2)	30(1)
C(6)	7874(2)	-1783(4)	9633(2)	25(1)
C(7)	5979(2)	987(4)	9050(2)	32(1)
C(8)	5661(2)	696(4)	8449(2)	41(1)
C(9)	6060(2)	71(4)	7975(2)	30(1)
C(10)	9061(2)	-809(4)	7235(2)	25(1)
C(11)	9606(2)	-286(4)	6832(2)	33(1)
C(12)	10119(3)	-1161(5)	6541(2)	45(1)
C(13)	10076(2)	-2561(4)	6635(2)	42(1)
C(14)	9522(3)	-3079(4)	7020(2)	41(1)
C(15)	9026(2)	-2211(4)	7325(2)	32(1)

C(16)	7579(2)	3624(4)	7379(2)	28(1)
C(17)	7459(2)	3767(4)	6729(2)	45(1)
C(18)	7208(3)	5006(5)	6470(2)	53(1)
C(19)	7085(2)	6115(5)	6854(2)	47(1)
C(20)	7205(3)	5989(4)	7495(2)	47(1)
C(21)	7450(2)	4749(4)	7756(2)	39(1)
C(22)	9136(2)	1223(4)	10227(2)	27(1)
C(23)	9376(3)	808(4)	10827(2)	51(1)
C(24)	9965(3)	1506(5)	11166(2)	59(1)
C(25)	10312(2)	2632(4)	10921(2)	42(1)
C(26)	10066(3)	3070(5)	10343(2)	56(1)
C(27)	9473(3)	2394(5)	9998(2)	49(1)
C(28)	7776(2)	-3239(4)	9843(2)	27(1)
C(29)	8019(3)	-3691(5)	10438(2)	60(1)
C(30)	7941(3)	-5061(5)	10592(2)	75(2)
C(31)	7635(2)	-5989(4)	10167(2)	47(1)
C(32)	7360(3)	-5539(4)	9585(2)	51(1)
C(33)	7428(3)	-4173(4)	9430(2)	43(1)
C(34)	5476(2)	1437(4)	9564(2)	34(1)
C(35)	4657(2)	1454(4)	9493(2)	46(1)
C(36)	4204(3)	1843(5)	9986(2)	57(1)
C(37)	4555(3)	2210(5)	10552(3)	60(1)
C(38)	5361(3)	2192(5)	10633(2)	57(1)
C(39)	5821(2)	1810(4)	10141(2)	43(1)
C(40)	5673(2)	-185(4)	7340(2)	39(1)
C(41)	4864(3)	-333(5)	7247(2)	57(1)
C(42)	4536(3)	-512(6)	6640(2)	67(2)
C(43)	5001(3)	-529(5)	6138(2)	60(1)
C(44)	5802(3)	-405(4)	6221(2)	54(1)
C(45)	6138(3)	-235(4)	6823(2)	42(1)

Table D.2: Bond lengths [Å] for Cr(dbm)$_3$ {3}

	Bond length [Å]
Cr(1)-O(6)	1.939(2)
Cr(1)-O(1)	1.945(2)
Cr(1)-O(5)	1.949(2)
Cr(1)-O(3)	1.954(2)
Cr(1)-O(4)	1.959(2)
Cr(1)-O(2)	1.971(2)
O(1)-C(1)	1.274(4)
O(2)-C(3)	1.279(4)
O(3)-C(4)	1.275(4)
O(4)-C(6)	1.274(4)
O(5)-C(7)	1.283(4)
O(6)-C(9)	1.288(4)
C(1)-C(2)	1.398(5)
C(1)-C(10)	1.492(5)
C(2)-C(3)	1.400(5)
C(3)-C(16)	1.494(5)
C(4)-C(5)	1.400(5)
C(4)-C(22)	1.489(5)
C(5)-C(6)	1.390(5)
C(6)-C(28)	1.498(5)
C(7)-C(8)	1.391(5)
C(7)-C(34)	1.483(5)
C(8)-C(9)	1.382(5)
C(9)-C(40)	1.491(5)
C(10)-C(15)	1.381(5)
C(10)-C(11)	1.387(5)
C(11)-C(12)	1.386(5)
C(12)-C(13)	1.381(6)
C(13)-C(14)	1.370(6)
C(14)-C(15)	1.377(5)
C(16)-C(21)	1.380(5)
C(16)-C(17)	1.391(5)

C(17)-C(18)	1.385(6)
C(18)-C(19)	1.376(6)
C(19)-C(20)	1.370(6)
C(20)-C(21)	1.385(5)
C(22)-C(27)	1.375(5)
C(22)-C(23)	1.378(5)
C(23)-C(24)	1.384(6)
C(24)-C(25)	1.360(6)
C(25)-C(26)	1.347(6)
C(26)-C(27)	1.383(5)
C(28)-C(33)	1.377(5)
C(28)-C(29)	1.382(5)
C(29)-C(30)	1.382(6)
C(30)-C(31)	1.362(6)
C(31)-C(32)	1.371(5)
C(32)-C(33)	1.377(5)
C(34)-C(39)	1.380(5)
C(34)-C(35)	1.392(5)
C(35)-C(36)	1.382(6)
C(36)-C(37)	1.362(7)
C(37)-C(38)	1.371(6)
C(38)-C(39)	1.386(5)
C(40)-C(45)	1.385(5)
C(40)-C(41)	1.385(6)
C(41)-C(42)	1.391(6)
C(42)-C(43)	1.356(7)
C(43)-C(44)	1.367(7)
C(44)-C(45)	1.383(5)

Table D.3: Angles [Å] for Cr(dbm)$_3$ {3}

	Angles [°]
O(6)-Cr(1)-O(1)	87.28(10)
O(6)-Cr(1)-O(5)	90.57(10)
O(1)-Cr(1)-O(5)	177.12(10)
O(6)-Cr(1)-O(3)	178.01(10)
O(1)-Cr(1)-O(3)	92.54(10)
O(5)-Cr(1)-O(3)	89.68(10)
O(6)-Cr(1)-O(4)	91.58(10)
O(1)-Cr(1)-O(4)	88.90(10)
O(5)-Cr(1)-O(4)	89.25(10)
O(3)-Cr(1)-O(4)	90.40(9)
O(6)-Cr(1)-O(2)	88.11(10)
O(1)-Cr(1)-O(2)	89.58(9)
O(5)-Cr(1)-O(2)	92.27(10)
O(3)-Cr(1)-O(2)	89.91(10)
O(4)-Cr(1)-O(2)	178.46(10)
C(1)-O(1)-Cr(1)	127.0(2)
C(3)-O(2)-Cr(1)	125.9(2)
C(4)-O(3)-Cr(1)	127.2(2)
C(6)-O(4)-Cr(1)	127.4(2)
C(7)-O(5)-Cr(1)	127.4(2)
C(9)-O(6)-Cr(1)	125.7(2)
O(1)-C(1)-C(2)	124.6(3)
O(1)-C(1)-C(10)	114.4(3)
C(2)-C(1)-C(10)	121.0(3)
C(1)-C(2)-C(3)	124.0(3)
O(2)-C(3)-C(2)	124.4(3)
O(2)-C(3)-C(16)	115.6(3)
C(2)-C(3)-C(16)	120.0(3)
O(3)-C(4)-C(5)	124.1(3)
O(3)-C(4)-C(22)	115.8(3)
C(5)-C(4)-C(22)	120.0(3)
C(6)-C(5)-C(4)	125.0(3)

142

O(4)-C(6)-C(5)	124.1(3)
O(4)-C(6)-C(28)	115.9(3)
C(5)-C(6)-C(28)	119.9(3)
O(5)-C(7)-C(8)	123.3(3)
O(5)-C(7)-C(34)	115.1(3)
C(8)-C(7)-C(34)	121.5(3)
C(9)-C(8)-C(7)	125.2(4)
O(6)-C(9)-C(8)	124.2(3)
O(6)-C(9)-C(40)	114.4(3)
C(8)-C(9)-C(40)	121.4(3)
C(15)-C(10)-C(11)	118.9(3)
C(15)-C(10)-C(1)	118.9(3)
C(11)-C(10)-C(1)	122.1(3)
C(12)-C(11)-C(10)	120.1(4)
C(13)-C(12)-C(11)	120.3(4)
C(14)-C(13)-C(12)	119.5(4)
C(13)-C(14)-C(15)	120.5(4)
C(14)-C(15)-C(10)	120.7(4)
C(21)-C(16)-C(17)	118.4(3)
C(21)-C(16)-C(3)	119.6(3)
C(17)-C(16)-C(3)	122.0(3)
C(18)-C(17)-C(16)	120.5(4)
C(19)-C(18)-C(17)	120.1(4)
C(20)-C(19)-C(18)	119.9(4)
C(19)-C(20)-C(21)	120.2(4)
C(16)-C(21)-C(20)	120.9(4)
C(27)-C(22)-C(23)	117.5(4)
C(27)-C(22)-C(4)	119.9(3)
C(23)-C(22)-C(4)	122.6(3)
C(22)-C(23)-C(24)	120.7(4)
C(25)-C(24)-C(23)	120.8(4)
C(26)-C(25)-C(24)	118.9(4)
C(25)-C(26)-C(27)	121.1(4)
C(22)-C(27)-C(26)	120.8(4)

C(33)-C(28)-C(29)	118.1(3)
C(33)-C(28)-C(6)	119.2(3)
C(29)-C(28)-C(6)	122.7(3)
C(28)-C(29)-C(30)	119.8(4)
C(31)-C(30)-C(29)	121.5(4)
C(30)-C(31)-C(32)	119.1(4)
C(31)-C(32)-C(33)	119.8(4)
C(32)-C(33)-C(28)	121.6(4)
C(39)-C(34)-C(35)	118.1(4)
C(39)-C(34)-C(7)	119.6(3)
C(35)-C(34)-C(7)	122.2(4)
C(36)-C(35)-C(34)	120.7(4)
C(37)-C(36)-C(35)	120.3(4)
C(36)-C(37)-C(38)	120.0(4)
C(37)-C(38)-C(39)	120.2(4)
C(34)-C(39)-C(38)	120.6(4)
C(45)-C(40)-C(41)	118.8(4)
C(45)-C(40)-C(9)	118.7(4)
C(41)-C(40)-C(9)	122.5(4)
C(40)-C(41)-C(42)	119.7(5)
C(43)-C(42)-C(41)	120.4(5)
C(42)-C(43)-C(44)	120.8(4)
C(43)-C(44)-C(45)	119.5(5)
C(44)-C(45)-C(40)	120.8(4)

Table D.4: Anisotropic displacement parameters $(\text{Å}^2 \text{x } 10^3)$ for Cr(dbm)$_3$ {3}. The anisotropic displacement factor exponent takes the form: $-2p^2[\, h^2 \, a^{*2} U^{11} + ... \; + 2 \, h \, k \, a^* \, b^* \, U^{12} \,]$

	U^{11}	U^{22}	U^{33}	U^{23}	U^{13}	U^{12}
Cr(1)	25(1)	29(1)	21(1)	2(1)	4(1)	2(1)
O(1)	28(1)	31(1)	22(1)	4(1)	6(1)	5(1)
O(2)	32(1)	28(1)	22(1)	-1(1)	7(1)	5(1)
O(3)	30(1)	31(1)	23(1)	3(1)	5(1)	-1(1)
O(4)	28(1)	32(1)	20(1)	2(1)	2(1)	-2(1)
O(5)	25(1)	35(1)	26(1)	-3(1)	5(1)	3(1)

O(6)	28(1)	33(1)	30(1)	-1(1)	1(1)	5(1)
C(1)	24(2)	29(2)	26(2)	0(2)	2(1)	0(2)
C(2)	35(2)	29(2)	20(2)	1(2)	7(2)	6(2)
C(3)	25(2)	31(2)	27(2)	2(2)	-1(2)	-2(2)
C(4)	22(2)	33(2)	22(2)	0(2)	9(1)	1(2)
C(5)	35(2)	37(2)	18(2)	-2(2)	2(2)	-4(2)
C(6)	22(2)	29(2)	24(2)	0(2)	7(1)	5(2)
C(7)	29(2)	29(2)	37(2)	3(2)	5(2)	-1(2)
C(8)	29(2)	52(3)	42(2)	-8(2)	-1(2)	4(2)
C(9)	35(2)	28(2)	28(2)	2(2)	0(2)	4(2)
C(10)	29(2)	30(2)	17(2)	-2(2)	0(1)	2(2)
C(11)	40(2)	26(2)	34(2)	-2(2)	10(2)	2(2)
C(12)	46(3)	53(3)	39(2)	-8(2)	19(2)	6(2)
C(13)	54(3)	39(2)	33(2)	-9(2)	6(2)	20(2)
C(14)	58(3)	36(2)	29(2)	-5(2)	0(2)	9(2)
C(15)	38(2)	32(2)	27(2)	0(2)	1(2)	0(2)
C(16)	26(2)	27(2)	32(2)	1(2)	7(2)	1(2)
C(17)	59(3)	45(3)	31(2)	3(2)	4(2)	18(2)
C(18)	64(3)	56(3)	40(2)	14(2)	5(2)	15(2)
C(19)	40(3)	43(3)	59(3)	22(2)	4(2)	8(2)
C(20)	54(3)	25(2)	62(3)	0(2)	10(2)	6(2)
C(21)	48(2)	35(2)	36(2)	-1(2)	7(2)	5(2)
C(22)	27(2)	30(2)	24(2)	-4(2)	3(1)	0(2)
C(23)	66(3)	36(2)	48(3)	7(2)	-20(2)	-14(2)
C(24)	71(3)	48(3)	56(3)	6(2)	-34(3)	-2(2)
C(25)	30(2)	52(3)	46(2)	-20(2)	-1(2)	-3(2)
C(26)	65(3)	59(3)	45(3)	-9(2)	11(2)	-34(3)
C(27)	59(3)	63(3)	25(2)	0(2)	3(2)	-21(2)
C(28)	25(2)	27(2)	30(2)	3(2)	7(2)	-2(2)
C(29)	80(4)	51(3)	44(3)	20(2)	-25(2)	-34(3)
C(30)	99(4)	64(3)	58(3)	34(3)	-37(3)	-40(3)
C(31)	47(3)	37(2)	57(3)	17(2)	-1(2)	-6(2)
C(32)	82(3)	31(2)	39(2)	-6(2)	-5(2)	-9(2)
C(33)	68(3)	31(2)	28(2)	2(2)	-5(2)	-2(2)

C(34)	33(2)	26(2)	44(2)	-4(2)	12(2)	2(2)
C(35)	38(3)	44(3)	57(3)	-3(2)	14(2)	4(2)
C(36)	43(3)	48(3)	83(4)	-3(3)	23(3)	5(2)
C(37)	56(3)	51(3)	76(4)	-15(3)	38(3)	1(2)
C(38)	63(3)	59(3)	50(3)	-21(2)	19(2)	-8(3)
C(39)	43(3)	46(3)	43(2)	-13(2)	17(2)	-7(2)
C(40)	41(2)	39(2)	37(2)	-5(2)	-9(2)	10(2)
C(41)	44(3)	76(3)	50(3)	-17(3)	-7(2)	4(2)
C(42)	50(3)	87(4)	63(3)	-18(3)	-22(3)	5(3)
C(43)	73(4)	52(3)	52(3)	-10(2)	-29(3)	10(3)
C(44)	79(4)	45(3)	38(2)	0(2)	-6(2)	0(2)
C(45)	53(3)	37(2)	35(2)	-2(2)	-7(2)	1(2)

Table D.5: Hydrogen coordinates (x 10^4) and isotropic displacement parameters ($Å^2$x 10^3) for Cr(dbm)$_3$ {3}.

	x	y	z	U(eq)
H(2)	8420	1600	6938	33
H(5)	8461	-1153	10429	36
H(8)	5127	948	8357	49
H(11)	9628	674	6756	40
H(12)	10502	-797	6275	55
H(13)	10428	-3161	6436	51
H(14)	9480	-4043	7076	49
H(15)	8657	-2580	7601	39
H(17)	7549	3008	6461	54
H(18)	7120	5090	6026	64
H(19)	6917	6966	6676	57
H(20)	7121	6755	7760	56
H(21)	7531	4671	8200	47
H(23)	9133	34	11009	61
H(24)	10130	1196	11576	71
H(25)	10721	3102	11154	51
H(26)	10304	3857	10169	67
H(27)	9295	2743	9598	59

H(29) 8239	-3062	10740	72
H(30) 8105	-5362	11003	90
H(31) 7613	-6936	10272	56
H(32) 7124	-6167	9291	61
H(33) 7230	-3869	9027	51
H(35) 4406	1196	9101	55
H(36) 3646	1854	9931	69
H(37) 4242	2478	10890	72
H(38) 5605	2442	11029	68
H(39) 6379	1804	10200	52
H(41) 4536	-312	7597	68
H(42) 3982	-623	6575	81
H(43) 4769	-629	5725	72
H(44) 6125	-435	5868	65
H(45) 6694	-151	6881	50

Table D.6: Torsion angles [º] for Cr(dbm)$_3$ {3}.

	Torsion angles [º]
Cr(1)-O(1)-C(1)-C(2)	13.0(5)
Cr(1)-O(1)-C(1)-C(10)	-167.7(2)
O(1)-C(1)-C(2)-C(3)	2.5(6)
C(10)-C(1)-C(2)-C(3)	-176.8(3)
Cr(1)-O(2)-C(3)-C(2)	-15.7(5)
Cr(1)-O(2)-C(3)-C(16)	164.7(2)
C(1)-C(2)-C(3)-O(2)	-0.8(6)
C(1)-C(2)-C(3)-C(16)	178.7(3)
Cr(1)-O(3)-C(4)-C(5)	6.4(5)
Cr(1)-O(3)-C(4)-C(22)	-177.0(2)
O(3)-C(4)-C(5)-C(6)	6.9(6)
C(22)-C(4)-C(5)-C(6)	-169.6(3)
Cr(1)-O(4)-C(6)-C(5)	-3.2(5)
Cr(1)-O(4)-C(6)-C(28)	179.4(2)
C(4)-C(5)-C(6)-O(4)	-8.5(6)
C(4)-C(5)-C(6)-C(28)	168.8(3)

Cr(1)-O(5)-C(7)-C(8)	-2.5(5)
Cr(1)-O(5)-C(7)-C(34)	178.1(2)
O(5)-C(7)-C(8)-C(9)	11.5(6)
C(34)-C(7)-C(8)-C(9)	-169.2(4)
Cr(1)-O(6)-C(9)-C(8)	-18.4(5)
Cr(1)-O(6)-C(9)-C(40)	160.6(2)
C(7)-C(8)-C(9)-O(6)	-0.3(7)
C(7)-C(8)-C(9)-C(40)	-179.2(4)
O(1)-C(1)-C(10)-C(15)	29.5(4)
C(2)-C(1)-C(10)-C(15)	-151.2(3)
O(1)-C(1)-C(10)-C(11)	-147.7(3)
C(2)-C(1)-C(10)-C(11)	31.7(5)
C(15)-C(10)-C(11)-C(12)	-1.7(5)
C(1)-C(10)-C(11)-C(12)	175.4(3)
C(10)-C(11)-C(12)-C(13)	1.9(6)
C(11)-C(12)-C(13)-C(14)	0.0(6)
C(12)-C(13)-C(14)-C(15)	-1.9(6)
C(13)-C(14)-C(15)-C(10)	2.1(6)
C(11)-C(10)-C(15)-C(14)	-0.3(5)
C(1)-C(10)-C(15)-C(14)	-177.5(3)
O(2)-C(3)-C(16)-C(21)	28.4(5)
C(2)-C(3)-C(16)-C(21)	-151.2(4)
O(2)-C(3)-C(16)-C(17)	-149.5(4)
C(2)-C(3)-C(16)-C(17)	30.9(5)
C(21)-C(16)-C(17)-C(18)	-0.7(6)
C(3)-C(16)-C(17)-C(18)	177.2(4)
C(16)-C(17)-C(18)-C(19)	0.9(7)
C(17)-C(18)-C(19)-C(20)	-0.5(7)
C(18)-C(19)-C(20)-C(21)	0.0(7)
C(17)-C(16)-C(21)-C(20)	0.2(6)
C(3)-C(16)-C(21)-C(20)	-177.8(4)
C(19)-C(20)-C(21)-C(16)	0.2(6)
O(3)-C(4)-C(22)-C(27)	-7.5(5)
C(5)-C(4)-C(22)-C(27)	169.3(4)

O(3)-C(4)-C(22)-C(23)	174.4(4)
C(5)-C(4)-C(22)-C(23)	-8.8(5)
C(27)-C(22)-C(23)-C(24)	-3.7(6)
C(4)-C(22)-C(23)-C(24)	174.4(4)
C(22)-C(23)-C(24)-C(25)	1.2(7)
C(23)-C(24)-C(25)-C(26)	0.8(7)
C(24)-C(25)-C(26)-C(27)	-0.2(7)
C(23)-C(22)-C(27)-C(26)	4.3(6)
C(4)-C(22)-C(27)-C(26)	-173.9(4)
C(25)-C(26)-C(27)-C(22)	-2.4(7)
O(4)-C(6)-C(28)-C(33)	5.9(5)
C(5)-C(6)-C(28)-C(33)	-171.6(3)
O(4)-C(6)-C(28)-C(29)	-173.9(4)
C(5)-C(6)-C(28)-C(29)	8.6(5)
C(33)-C(28)-C(29)-C(30)	2.9(7)
C(6)-C(28)-C(29)-C(30)	-177.3(4)
C(28)-C(29)-C(30)-C(31)	0.6(9)
C(29)-C(30)-C(31)-C(32)	-3.5(8)
C(30)-C(31)-C(32)-C(33)	2.8(7)
C(31)-C(32)-C(33)-C(28)	0.8(7)
C(29)-C(28)-C(33)-C(32)	-3.6(6)
C(6)-C(28)-C(33)-C(32)	176.5(4)
O(5)-C(7)-C(34)-C(39)	4.0(5)
C(8)-C(7)-C(34)-C(39)	-175.4(4)
O(5)-C(7)-C(34)-C(35)	-173.8(3)
C(8)-C(7)-C(34)-C(35)	6.9(6)
C(39)-C(34)-C(35)-C(36)	0.4(6)
C(7)-C(34)-C(35)-C(36)	178.2(4)
C(34)-C(35)-C(36)-C(37)	-0.3(7)
C(35)-C(36)-C(37)-C(38)	-0.1(7)
C(36)-C(37)-C(38)-C(39)	0.4(7)
C(35)-C(34)-C(39)-C(38)	-0.1(6)
C(7)-C(34)-C(39)-C(38)	-177.9(4)
C(37)-C(38)-C(39)-C(34)	-0.3(7)

O(6)-C(9)-C(40)-C(45)	-26.9(5)
C(8)-C(9)-C(40)-C(45)	152.1(4)
O(6)-C(9)-C(40)-C(41)	155.1(4)
C(8)-C(9)-C(40)-C(41)	-25.8(6)
C(45)-C(40)-C(41)-C(42)	-0.7(7)
C(9)-C(40)-C(41)-C(42)	177.3(4)
C(40)-C(41)-C(42)-C(43)	-0.7(8)
C(41)-C(42)-C(43)-C(44)	1.6(8)
C(42)-C(43)-C(44)-C(45)	-1.2(7)
C(43)-C(44)-C(45)-C(40)	-0.2(6)
C(41)-C(40)-C(45)-C(44)	1.1(6)
C(9)-C(40)-C(45)-C(44)	-176.9(4)

Table D.7: Atomic coordinates (x 10^4) and equivalent isotropic displacement parameters (Å^2x 10^3) for Co(ba)$_3$ {10}. U(eq) is defined as one third of the trace of the orthogonalized U^{ij} tensor.

	x	y	z	U(eq)
Co(1)	7531(1)	8713(1)	7268(1)	50(1)
O(1)	8175(2)	9641(3)	6144(2)	53(1)
O(4)	9417(2)	7869(3)	7445(2)	54(1)
O(3)	7181(3)	7317(3)	6571(2)	61(1)
O(5)	6948(3)	7681(3)	8370(2)	60(1)
O(2)	5628(2)	9571(2)	7211(2)	54(1)
O(6)	7821(2)	10204(2)	7879(2)	52(1)
C(1)	7417(4)	10663(4)	5691(2)	51(1)
C(2)	5978(4)	11132(4)	5885(3)	58(1)
C(3)	5162(4)	10548(4)	6596(2)	48(1)
C(6)	10066(4)	6729(4)	7116(2)	50(1)
C(5)	9470(4)	5944(4)	6591(3)	59(1)
C(4)	8091(4)	6244(4)	6360(3)	58(1)
C(7)	6720(4)	8139(4)	9176(3)	64(1)
C(8)	7020(5)	9379(4)	9398(3)	73(1)
C(9)	7572(4)	10312(4)	8766(3)	52(1)

C(10)	8147(4)	11386(4)	4885(3)	66(1)
C(11)	3603(3)	11045(3)	6686(3)	48(1)
C(12)	2856(4)	11589(4)	5900(3)	59(1)
C(13)	1406(4)	11964(4)	5992(3)	66(1)
C(14)	689(4)	11800(4)	6854(3)	71(1)
C(15)	1414(4)	11294(4)	7637(3)	74(1)
C(16)	2863(4)	10906(4)	7553(3)	61(1)
C(24)	6071(6)	7231(5)	9938(4)	101(2)
C(25)	7924(4)	11583(4)	9080(3)	56(1)
C(26)	7695(4)	12820(4)	8503(3)	63(1)
C(27)	8079(5)	13978(5)	8759(4)	83(1)
C(28)	8715(6)	13942(6)	9551(5)	103(2)
C(29)	8970(6)	12737(8)	10139(4)	106(2)
C(30)	8552(5)	11541(5)	9919(3)	81(1)
C(17)	7570(5)	5247(5)	5813(3)	80(1)
C(18)	11571(4)	6321(4)	7326(3)	53(1)
C(19)	12294(5)	4939(4)	7363(4)	80(1)
C(20)	13702(5)	4609(5)	7551(4)	102(2)
C(21)	14382(5)	5609(6)	7709(4)	93(2)
C(22)	13680(5)	6977(5)	7674(4)	82(1)
C(23)	12285(4)	7319(4)	7492(3)	63(1)

Table D.8: Bond lengths [Å] for Co(ba)$_3$ {10}

Co(1)-O(6)	1.872(2)
Co(1)-O(2)	1.875(2)
Co(1)-O(4)	1.879(2)
Co(1)-O(1)	1.883(2)
Co(1)-O(3)	1.887(3)
Co(1)-O(5)	1.889(3)
O(1)-C(1)	1.270(4)
O(4)-C(6)	1.280(4)
O(3)-C(4)	1.272(4)
O(5)-C(7)	1.261(5)

O(2)-C(3)	1.271(4)
O(6)-C(9)	1.277(4)
C(1)-C(2)	1.393(5)
C(1)-C(10)	1.492(5)
C(2)-C(3)	1.382(5)
C(3)-C(11)	1.493(5)
C(6)-C(5)	1.378(5)
C(6)-C(18)	1.488(5)
C(5)-C(4)	1.378(5)
C(4)-C(17)	1.512(5)
C(7)-C(8)	1.393(6)
C(7)-C(24)	1.513(6)
C(8)-C(9)	1.376(5)
C(9)-C(25)	1.493(5)
C(11)-C(16)	1.380(5)
C(11)-C(12)	1.392(5)
C(12)-C(13)	1.381(5)
C(13)-C(14)	1.366(6)
C(14)-C(15)	1.371(6)
C(15)-C(16)	1.381(5)
C(25)-C(26)	1.387(5)
C(25)-C(30)	1.387(6)
C(26)-C(27)	1.370(6)
C(27)-C(28)	1.333(7)
C(28)-C(29)	1.371(8)
C(29)-C(30)	1.403(7)
C(18)-C(23)	1.373(5)
C(18)-C(19)	1.394(5)
C(19)-C(20)	1.387(6)
C(20)-C(21)	1.349(7)
C(21)-C(22)	1.376(6)
C(22)-C(23)	1.374(5)

APPENDIX

Table D.9: Angles for Co(ba)₃ {10}

O(6)-Co(1)-O(2)	89.47(11)
O(6)-Co(1)-O(4)	87.40(10)
O(2)-Co(1)-O(4)	174.76(11)
O(6)-Co(1)-O(1)	86.30(10)
O(2)-Co(1)-O(1)	96.20(10)
O(4)-Co(1)-O(1)	87.80(10)
O(6)-Co(1)-O(3)	175.30(11)
O(2)-Co(1)-O(3)	87.89(11)
O(4)-Co(1)-O(3)	95.51(11)
O(1)-Co(1)-O(3)	90.12(11)
O(6)-Co(1)-O(5)	96.28(11)
O(2)-Co(1)-O(5)	86.06(10)
O(4)-Co(1)-O(5)	90.10(11)
O(1)-Co(1)-O(5)	176.60(11)
O(3)-Co(1)-O(5)	87.42(12)
C(1)-O(1)-Co(1)	123.6(2)
C(6)-O(4)-Co(1)	124.9(2)
C(4)-O(3)-Co(1)	124.4(2)
C(7)-O(5)-Co(1)	123.6(3)
C(3)-O(2)-Co(1)	124.2(2)
C(9)-O(6)-Co(1)	124.2(2)
O(1)-C(1)-C(2)	125.1(3)
O(1)-C(1)-C(10)	116.3(3)
C(2)-C(1)-C(10)	118.6(3)
C(3)-C(2)-C(1)	124.9(3)
O(2)-C(3)-C(2)	125.1(3)
O(2)-C(3)-C(11)	114.3(3)
C(2)-C(3)-C(11)	120.6(3)
O(4)-C(6)-C(5)	124.5(3)
O(4)-C(6)-C(18)	114.0(3)
C(5)-C(6)-C(18)	121.5(3)
C(6)-C(5)-C(4)	125.4(4)

O(3)-C(4)-C(5)	125.2(4)
O(3)-C(4)-C(17)	115.3(4)
C(5)-C(4)-C(17)	119.4(4)
O(5)-C(7)-C(8)	125.2(4)
O(5)-C(7)-C(24)	115.3(4)
C(8)-C(7)-C(24)	119.4(4)
C(9)-C(8)-C(7)	125.1(4)
O(6)-C(9)-C(8)	125.0(4)
O(6)-C(9)-C(25)	113.7(3)
C(8)-C(9)-C(25)	121.3(3)
C(16)-C(11)-C(12)	118.5(3)
C(16)-C(11)-C(3)	120.2(3)
C(12)-C(11)-C(3)	121.3(3)
C(13)-C(12)-C(11)	120.2(4)
C(14)-C(13)-C(12)	120.5(4)
C(13)-C(14)-C(15)	119.9(4)
C(14)-C(15)-C(16)	120.2(4)
C(11)-C(16)-C(15)	120.8(4)
C(26)-C(25)-C(30)	118.7(4)
C(26)-C(25)-C(9)	119.8(3)
C(30)-C(25)-C(9)	121.4(4)
C(27)-C(26)-C(25)	120.6(4)
C(28)-C(27)-C(26)	121.3(5)
C(27)-C(28)-C(29)	120.0(5)
C(28)-C(29)-C(30)	120.5(5)
C(25)-C(30)-C(29)	118.9(5)
C(23)-C(18)-C(19)	118.2(4)
C(23)-C(18)-C(6)	119.9(3)
C(19)-C(18)-C(6)	121.9(4)
C(20)-C(19)-C(18)	119.9(4)
C(21)-C(20)-C(19)	120.8(5)
C(20)-C(21)-C(22)	119.9(4)
C(23)-C(22)-C(21)	120.0(4)
C(18)-C(23)-C(22)	121.2(4)

154

Table D.10: Anisotropic displacement parameters (Å^2x 10^3) for Co(ba)$_3$ {10}. The anisotropic displacement factor exponent takes the form: $-2p^2[\,h^2\,a^{*2}U^{11} + ... + 2\,h\,k\,a^*\,b^*\,U^{12}\,]$

	U^{11}	U^{22}	U^{33}	U^{23}	U^{13}	U^{12}
Co(1)	44(1)	51(1)	54(1)	-4(1)	-1(1)	-8(1)
O(1)	42(1)	65(2)	49(1)	-8(1)	1(1)	-10(1)
O(4)	46(1)	56(2)	61(2)	-11(1)	-9(1)	-5(1)
O(3)	49(2)	66(2)	71(2)	-13(1)	-9(1)	-14(1)
O(5)	61(2)	49(2)	66(2)	3(1)	1(1)	-8(1)
O(2)	44(1)	55(2)	59(2)	5(1)	1(1)	-8(1)
O(6)	55(2)	53(2)	46(1)	-4(1)	3(1)	-9(1)
C(1)	51(2)	59(2)	46(2)	-11(2)	-1(2)	-17(2)
C(2)	50(2)	62(2)	58(2)	5(2)	-2(2)	-7(2)
C(3)	48(2)	47(2)	51(2)	-8(2)	-4(2)	-11(2)
C(6)	50(2)	46(2)	51(2)	2(2)	3(2)	-9(2)
C(5)	55(2)	54(2)	69(3)	-16(2)	-7(2)	-7(2)
C(4)	58(2)	56(2)	62(2)	-7(2)	-2(2)	-13(2)
C(7)	61(2)	54(2)	66(3)	6(2)	11(2)	1(2)
C(8)	95(3)	66(3)	50(2)	-1(2)	17(2)	-11(2)
C(9)	45(2)	53(2)	52(2)	-2(2)	-2(2)	2(2)
C(10)	58(2)	78(3)	62(2)	0(2)	9(2)	-21(2)
C(11)	42(2)	44(2)	56(2)	-7(2)	1(2)	-9(2)
C(12)	52(2)	68(3)	57(2)	-11(2)	1(2)	-11(2)
C(13)	51(2)	74(3)	70(3)	-9(2)	-9(2)	-6(2)
C(14)	46(2)	67(3)	93(3)	-7(2)	5(2)	-3(2)
C(15)	57(3)	74(3)	78(3)	3(2)	19(2)	-3(2)
C(16)	53(2)	61(2)	64(2)	4(2)	2(2)	-4(2)
C(24)	118(4)	76(3)	94(4)	17(3)	35(3)	-17(3)
C(25)	50(2)	61(2)	52(2)	-16(2)	3(2)	0(2)
C(26)	58(2)	54(2)	73(3)	-7(2)	0(2)	-7(2)
C(27)	80(3)	68(3)	103(4)	-15(3)	-2(3)	-16(2)
C(28)	102(4)	86(4)	131(5)	-45(4)	-7(4)	-24(3)
C(29)	97(4)	149(6)	82(4)	-56(4)	-11(3)	-25(4)
C(30)	87(3)	92(3)	61(3)	-18(2)	-8(2)	-5(3)
C(17)	84(3)	74(3)	92(3)	-20(2)	-21(3)	-29(2)

C(18)	47(2)	52(2)	57(2)	2(2)	-1(2)	-8(2)
C(19)	66(3)	56(3)	119(4)	-7(2)	-21(3)	-6(2)
C(20)	72(3)	68(3)	161(5)	-6(3)	-39(3)	7(3)
C(21)	49(3)	92(4)	137(5)	-8(3)	-27(3)	-4(3)
C(22)	57(3)	77(3)	116(4)	6(3)	-16(3)	-23(2)
C(23)	54(2)	55(2)	78(3)	2(2)	-7(2)	-11(2)

Table D.11: Hydrogen coordinates (x 10^4) and isotropic displacement parameters (Å^2x 10 ^{3}) for Cr(dbm)$_3$ {10}.

	x	y	z	U(eq)
H(2)	5522	11912	5499	70
H(5)	10059	5128	6369	70
H(8)	6829	9598	10037	87
H(10A)	9148	10946	4834	100
H(10B)	8043	12367	4994	100
H(10C)	7730	11320	4297	100
H(12)	3345	11704	5297	71
H(13)	903	12339	5453	79
H(14)	-310	12036	6909	85
H(15)	918	11210	8240	88
H(16)	3355	10539	8098	74
H(24A)	5926	6403	9671	151
H(24B)	5165	7756	10188	151
H(24C)	6703	6947	10451	151
H(26)	7268	12866	7926	75
H(27)	7887	14823	8364	100
H(28)	8992	14750	9708	124
H(29)	9432	12713	10700	127
H(30)	8698	10716	10337	97
H(17A)	6576	5607	5705	119
H(17B)	7677	4336	6176	119
H(17C)	8121	5154	5203	119
H(19)	11824	4225	7261	97
H(20)	14194	3668	7569	122

H(21)	15343	5369	7845	112
H(22)	14161	7684	7775	99
H(23)	11805	8264	7480	76

Table D.12: Torsion angles [°] for Cr(dbm)$_3$ {10}.

O(6)-Co(1)-O(1)-C(1)	-79.1(3)
O(2)-Co(1)-O(1)-C(1)	10.0(3)
O(4)-Co(1)-O(1)-C(1)	-166.6(3)
O(3)-Co(1)-O(1)-C(1)	97.8(3)
O(6)-Co(1)-O(4)-C(6)	-174.7(3)
O(1)-Co(1)-O(4)-C(6)	-88.3(3)
O(3)-Co(1)-O(4)-C(6)	1.6(3)
O(5)-Co(1)-O(4)-C(6)	89.0(3)
O(2)-Co(1)-O(3)-C(4)	-176.8(3)
O(4)-Co(1)-O(3)-C(4)	-0.8(3)
O(1)-Co(1)-O(3)-C(4)	87.0(3)
O(5)-Co(1)-O(3)-C(4)	-90.6(3)
O(6)-Co(1)-O(5)-C(7)	7.6(3)
O(2)-Co(1)-O(5)-C(7)	-81.4(3)
O(4)-Co(1)-O(5)-C(7)	95.0(3)
O(3)-Co(1)-O(5)-C(7)	-169.5(3)
O(6)-Co(1)-O(2)-C(3)	80.6(3)
O(1)-Co(1)-O(2)-C(3)	-5.6(3)
O(3)-Co(1)-O(2)-C(3)	-95.5(3)
O(5)-Co(1)-O(2)-C(3)	176.9(3)
O(2)-Co(1)-O(6)-C(9)	83.3(3)
O(4)-Co(1)-O(6)-C(9)	-92.5(3)
O(1)-Co(1)-O(6)-C(9)	179.5(3)
O(5)-Co(1)-O(6)-C(9)	-2.7(3)
Co(1)-O(1)-C(1)-C(2)	-8.4(5)
Co(1)-O(1)-C(1)-C(10)	172.5(2)
O(1)-C(1)-C(2)-C(3)	-0.4(6)
C(10)-C(1)-C(2)-C(3)	178.7(4)

Co(1)-O(2)-C(3)-C(2)	-0.6(5)
Co(1)-O(2)-C(3)-C(11)	179.0(2)
C(1)-C(2)-C(3)-O(2)	5.4(6)
C(1)-C(2)-C(3)-C(11)	-174.2(3)
Co(1)-O(4)-C(6)-C(5)	-0.7(5)
Co(1)-O(4)-C(6)-C(18)	177.5(2)
O(4)-C(6)-C(5)-C(4)	-1.6(6)
C(18)-C(6)-C(5)-C(4)	-179.7(4)
Co(1)-O(3)-C(4)-C(5)	-1.0(6)
Co(1)-O(3)-C(4)-C(17)	178.9(3)
C(6)-C(5)-C(4)-O(3)	2.5(7)
C(6)-C(5)-C(4)-C(17)	-177.3(4)
Co(1)-O(5)-C(7)-C(8)	-8.2(6)
Co(1)-O(5)-C(7)-C(24)	172.0(3)
O(5)-C(7)-C(8)-C(9)	2.0(7)
C(24)-C(7)-C(8)-C(9)	-178.1(4)
Co(1)-O(6)-C(9)-C(8)	-2.0(5)
Co(1)-O(6)-C(9)-C(25)	178.6(2)
C(7)-C(8)-C(9)-O(6)	3.6(7)
C(7)-C(8)-C(9)-C(25)	-177.0(4)
O(2)-C(3)-C(11)-C(16)	26.3(5)
C(2)-C(3)-C(11)-C(16)	-154.1(4)
O(2)-C(3)-C(11)-C(12)	-150.4(3)
C(2)-C(3)-C(11)-C(12)	29.2(5)
C(16)-C(11)-C(12)-C(13)	-0.7(6)
C(3)-C(11)-C(12)-C(13)	176.1(3)
C(11)-C(12)-C(13)-C(14)	-0.3(6)
C(12)-C(13)-C(14)-C(15)	1.7(7)
C(13)-C(14)-C(15)-C(16)	-2.2(7)
C(12)-C(11)-C(16)-C(15)	0.2(6)
C(3)-C(11)-C(16)-C(15)	-176.6(4)
C(14)-C(15)-C(16)-C(11)	1.2(6)
O(6)-C(9)-C(25)-C(26)	36.5(5)
C(8)-C(9)-C(25)-C(26)	-142.9(4)

O(6)-C(9)-C(25)-C(30)	-139.9(4)
C(8)-C(9)-C(25)-C(30)	40.7(5)
C(30)-C(25)-C(26)-C(27)	-0.2(6)
C(9)-C(25)-C(26)-C(27)	-176.6(4)
C(25)-C(26)-C(27)-C(28)	1.9(7)
C(26)-C(27)-C(28)-C(29)	-1.5(9)
C(27)-C(28)-C(29)-C(30)	-0.6(9)
C(26)-C(25)-C(30)-C(29)	-1.8(6)
C(9)-C(25)-C(30)-C(29)	174.6(4)
C(28)-C(29)-C(30)-C(25)	2.3(8)
O(4)-C(6)-C(18)-C(23)	-24.9(5)
C(5)-C(6)-C(18)-C(23)	153.4(4)
O(4)-C(6)-C(18)-C(19)	154.9(4)
C(5)-C(6)-C(18)-C(19)	-26.8(6)
C(23)-C(18)-C(19)-C(20)	-0.9(7)
C(6)-C(18)-C(19)-C(20)	179.3(4)
C(18)-C(19)-C(20)-C(21)	0.8(9)
C(19)-C(20)-C(21)-C(22)	-0.8(9)
C(20)-C(21)-C(22)-C(23)	1.0(8)
C(19)-C(18)-C(23)-C(22)	1.1(6)
C(6)-C(18)-C(23)-C(22)	-179.1(4)
C(21)-C(22)-C(23)-C(18)	-1.2(7)

Table D.13: Atomic coordinates (x 10^4) and equivalent isotropic displacement parameters (Å^2x 10^3) for Co(tfba)$_3$ {12}. U(eq) is defined as one third of the trace of the orthogonalized U^{ij} tensor.

	x	y	z	U(eq)
Co(1)	7096(1)	8838(1)	3945(1)	27(1)
O(1)	5916(3)	8417(1)	2819(3)	31(1)
O(2)	8523(3)	8849(1)	2993(3)	34(1)
O(3)	5924(3)	9221(1)	2644(3)	26(1)
O(4)	8208(3)	9243(1)	5189(3)	29(1)
O(5)	5665(3)	8874(1)	4871(3)	27(1)

O(6)	8245(3)	8421(1)	5131(3)	35(1)
C(1)	6137(4)	8242(1)	1764(4)	30(1)
C(2)	7368(5)	8323(1)	1314(4)	34(1)
C(3)	8443(4)	8608(1)	1956(4)	31(1)
C(10)	4982(5)	7935(1)	1006(4)	34(1)
C(11)	5265(6)	7616(1)	185(5)	43(1)
C(12)	4193(6)	7324(2)	-420(5)	54(1)
C(13)	2813(6)	7351(2)	-244(6)	58(2)
C(14)	2487(6)	7682(2)	517(6)	51(1)
C(15)	3573(5)	7973(1)	1143(5)	37(1)
C(16)	9778(5)	8649(2)	1433(5)	42(1)
F(1)	10902(4)	8429(2)	2251(5)	100(2)
F(2)	9571(5)	8510(2)	168(4)	114(2)
F(3)	10298(4)	9026(1)	1519(5)	94(1)
C(4)	5763(4)	9602(1)	2902(4)	23(1)
C(5)	6617(4)	9814(1)	4126(4)	26(1)
C(6)	7758(4)	9621(1)	5135(4)	25(1)
C(17)	4582(4)	9825(1)	1805(4)	25(1)
C(18)	4628(4)	10251(1)	1580(4)	30(1)
C(19)	3523(5)	10442(1)	506(5)	39(1)
C(20)	2354(5)	10209(2)	-320(4)	39(1)
C(21)	2279(5)	9785(2)	-88(5)	42(1)
C(22)	3386(4)	9590(1)	968(4)	34(1)
C(23)	8687(4)	9869(1)	6414(4)	30(1)
F(4)	10089(3)	9896(1)	6418(3)	48(1)
F(5)	8195(3)	10253(1)	6465(3)	54(1)
F(6)	8717(3)	9677(1)	7600(2)	44(1)
C(7)	5639(4)	8667(1)	5942(4)	27(1)
C(8)	6742(5)	8376(1)	6640(5)	35(1)
C(9)	7890(5)	8274(1)	6167(4)	34(1)
C(24)	4330(4)	8741(1)	6411(4)	28(1)
C(25)	4286(5)	8636(1)	7748(5)	42(1)
C(26)	3034(6)	8720(2)	8135(6)	49(1)
C(27)	1810(5)	8900(2)	7180(5)	45(1)

C(28)	1831(5)	9000(1)	5851(5)	41(1)
C(29)	3082(5)	8928(1)	5470(5)	34(1)
C(30)	8971(5)	7929(1)	6928(6)	46(1)
F(7)	8568(4)	7743(1)	7939(4)	68(1)
F(8)	9030(3)	7627(1)	6025(4)	63(1)
F(9)	10315(3)	8075(1)	7499(4)	81(1)

Table D.14: Bond lengths [Å] and angles [°] for Co(tfba)$_3$ {12}

	Bond lengths [Å]
Co(1)-O(5)	1.869(3)
Co(1)-O(4)	1.872(3)
Co(1)-O(3)	1.875(3)
Co(1)-O(1)	1.881(3)
Co(1)-O(2)	1.882(3)
Co(1)-O(6)	1.885(3)
O(1)-C(1)	1.265(5)
O(2)-C(3)	1.270(5)
O(3)-C(4)	1.264(4)
O(4)-C(6)	1.275(5)
O(5)-C(7)	1.261(5)
O(6)-C(9)	1.272(5)
C(1)-C(2)	1.402(6)
C(1)-C(10)	1.489(6)
C(2)-C(3)	1.369(6)
C(3)-C(16)	1.520(6)
C(10)-C(11)	1.383(6)
C(10)-C(15)	1.393(6)
C(11)-C(12)	1.375(7)
C(12)-C(13)	1.379(8)
C(13)-C(14)	1.391(8)
C(14)-C(15)	1.383(6)
C(16)-F(2)	1.292(6)
C(16)-F(3)	1.293(6)
C(16)-F(1)	1.324(6)

C(4)-C(5)	1.409(5)
C(4)-C(17)	1.482(5)
C(5)-C(6)	1.373(5)
C(6)-C(23)	1.527(5)
C(17)-C(18)	1.381(6)
C(17)-C(22)	1.400(5)
C(18)-C(19)	1.385(6)
C(19)-C(20)	1.376(6)
C(20)-C(21)	1.377(7)
C(21)-C(22)	1.382(6)
C(23)-F(5)	1.319(5)
C(23)-F(6)	1.323(5)
C(23)-F(4)	1.335(5)
C(7)-C(8)	1.412(5)
C(7)-C(24)	1.477(6)
C(8)-C(9)	1.356(6)
C(9)-C(30)	1.536(6)
C(24)-C(25)	1.387(6)
C(24)-C(29)	1.397(5)
C(25)-C(26)	1.386(7)
C(26)-C(27)	1.379(7)
C(27)-C(28)	1.368(7)
C(28)-C(29)	1.376(6)
C(30)-F(9)	1.313(6)
C(30)-F(7)	1.324(6)
C(30)-F(8)	1.329(6)

Table D.15: Angles [°] for Co(tfba)$_3$ {12}.

	Angles [°]
O(5)-Co(1)-O(4)	88.84(12)
O(5)-Co(1)-O(3)	86.21(11)
O(4)-Co(1)-O(3)	95.73(11)
O(5)-Co(1)-O(1)	86.96(12)
O(4)-Co(1)-O(1)	175.16(13)

162

O(3)-Co(1)-O(1)	86.38(11)
O(5)-Co(1)-O(2)	175.38(12)
O(4)-Co(1)-O(2)	88.46(12)
O(3)-Co(1)-O(2)	90.33(12)
O(1)-Co(1)-O(2)	95.88(12)
O(5)-Co(1)-O(6)	95.92(12)
O(4)-Co(1)-O(6)	88.52(12)
O(3)-Co(1)-O(6)	175.29(12)
O(1)-Co(1)-O(6)	89.53(12)
O(2)-Co(1)-O(6)	87.76(13)
C(1)-O(1)-Co(1)	126.1(3)
C(3)-O(2)-Co(1)	121.9(3)
C(4)-O(3)-Co(1)	124.8(2)
C(6)-O(4)-Co(1)	120.8(2)
C(7)-O(5)-Co(1)	126.5(2)
C(9)-O(6)-Co(1)	121.4(3)
O(1)-C(1)-C(2)	123.7(4)
O(1)-C(1)-C(10)	115.1(4)
C(2)-C(1)-C(10)	121.1(4)
C(3)-C(2)-C(1)	123.4(4)
O(2)-C(3)-C(2)	128.9(4)
O(2)-C(3)-C(16)	112.5(4)
C(2)-C(3)-C(16)	118.5(4)
C(11)-C(10)-C(15)	119.4(4)
C(11)-C(10)-C(1)	122.3(4)
C(15)-C(10)-C(1)	118.3(4)
C(12)-C(11)-C(10)	120.2(5)
C(11)-C(12)-C(13)	120.5(5)
C(12)-C(13)-C(14)	119.9(5)
C(15)-C(14)-C(13)	119.5(5)
C(14)-C(15)-C(10)	120.3(4)
F(2)-C(16)-F(3)	108.9(5)
F(2)-C(16)-F(1)	105.5(5)
F(3)-C(16)-F(1)	103.4(5)

163

F(2)-C(16)-C(3)	114.5(4)
F(3)-C(16)-C(3)	113.5(4)
F(1)-C(16)-C(3)	110.1(4)
O(3)-C(4)-C(5)	124.3(3)
O(3)-C(4)-C(17)	115.1(3)
C(5)-C(4)-C(17)	120.6(3)
C(6)-C(5)-C(4)	122.0(4)
O(4)-C(6)-C(5)	129.3(3)
O(4)-C(6)-C(23)	110.9(3)
C(5)-C(6)-C(23)	119.9(3)
C(18)-C(17)-C(22)	119.4(3)
C(18)-C(17)-C(4)	122.5(3)
C(22)-C(17)-C(4)	118.1(3)
C(17)-C(18)-C(19)	120.1(4)
C(20)-C(19)-C(18)	120.2(4)
C(19)-C(20)-C(21)	120.2(4)
C(20)-C(21)-C(22)	120.1(4)
C(21)-C(22)-C(17)	119.9(4)
F(5)-C(23)-F(6)	107.8(3)
F(5)-C(23)-F(4)	107.7(4)
F(6)-C(23)-F(4)	106.5(3)
F(5)-C(23)-C(6)	113.2(3)
F(6)-C(23)-C(6)	110.6(3)
F(4)-C(23)-C(6)	110.8(3)
O(5)-C(7)-C(8)	123.6(4)
O(5)-C(7)-C(24)	115.1(3)
C(8)-C(7)-C(24)	121.3(4)
C(9)-C(8)-C(7)	122.8(4)
O(6)-C(9)-C(8)	129.7(4)
O(6)-C(9)-C(30)	111.1(4)
C(8)-C(9)-C(30)	119.2(4)
C(25)-C(24)-C(29)	118.3(4)
C(25)-C(24)-C(7)	123.0(4)
C(29)-C(24)-C(7)	118.7(4)

C(26)-C(25)-C(24)	120.4(4)
C(27)-C(26)-C(25)	120.1(4)
C(28)-C(27)-C(26)	120.1(4)
C(27)-C(28)-C(29)	120.2(4)
C(28)-C(29)-C(24)	120.9(4)
F(9)-C(30)-F(7)	107.6(4)
F(9)-C(30)-F(8)	108.1(4)
F(7)-C(30)-F(8)	105.9(4)
F(9)-C(30)-C(9)	111.7(4)
F(7)-C(30)-C(9)	112.9(4)
F(8)-C(30)-C(9)	110.3(4)

Table D.16: Anisotropic displacement parameters (Å^2x 10^3) for Co(tfba)$_3$ {12}. The anisotropic displacement factor exponent takes the form: $-2^2[\ h^2\ a*^2U^{11} + ...\ + 2\ h\ k\ a*\ b*\ U^{12}\ ]$

	U^{11}	U^{22}	U^{33}	U^{23}	U^{13}	U^{12}
Co(1)	23(1)		27(1)	27(1)	-3(1)	2(1)
O(1)	30(1)		28(1)	34(2)	-4(1)	8(1)
O(2)	29(2)		37(2)	36(2)	-9(1)	10(1)
O(3)	24(1)		29(1)	22(1)	-3(1)	2(1)
O(4)	24(1)		32(2)	26(1)	-5(1)	-1(1)
O(5)	25(1)		28(1)	25(1)	1(1)	4(1)
O(6)	26(1)		33(2)	41(2)	-1(1)	3(1)
C(1)	31(2)		23(2)	30(2)	-1(2)	0(2)
C(2)	38(2)		35(2)	26(2)	-2(2)	6(2)
C(3)	32(2)		31(2)	29(2)	2(2)	7(2)
C(10)	33(2)		27(2)	33(2)	2(2)	-1(2)
C(11)	47(3)		38(2)	35(2)	-7(2)	0(2)
C(12)	59(3)		44(3)	47(3)	-12(2)	-3(2)
C(13)	59(3)		40(3)	56(3)	-11(2)	-8(3)
C(14)	41(3)		53(3)	54(3)	-3(2)	7(2)
C(15)	40(2)		31(2)	36(2)	-2(2)	7(2)
C(16)	46(3)		40(3)	42(3)	-2(2)	19(2)

F(1)	55(2)	144(4)	116(3)	52(3)	47(2)
F(2)	88(3)	204(5)	68(2)	-59(3)	49(2)
F(3)	92(3)	60(2)	170(4)	-15(2)	99(3)
C(4)	18(2)	30(2)	21(2)	1(2)	6(1)
C(5)	24(2)	27(2)	22(2)	-3(2)	1(1)
C(6)	19(2)	35(2)	20(2)	-4(2)	4(1)
C(17)	21(2)	35(2)	18(2)	-1(2)	3(1)
C(18)	27(2)	34(2)	27(2)	1(2)	3(2)
C(19)	41(2)	37(2)	35(2)	8(2)	6(2)
C(20)	32(2)	52(3)	26(2)	5(2)	1(2)
C(21)	31(2)	56(3)	30(2)	-9(2)	-4(2)
C(22)	31(2)	35(2)	31(2)	-3(2)	0(2)
C(23)	24(2)	37(2)	22(2)	-5(2)	-1(2)
F(4)	27(1)	79(2)	34(1)	-14(1)	2(1)
F(5)	61(2)	38(2)	41(2)	-16(1)	-14(1)
F(6)	50(2)	58(2)	19(1)	-4(1)	5(1)
C(7)	26(2)	23(2)	27(2)	-5(2)	0(2)
C(8)	32(2)	31(2)	37(2)	6(2)	5(2)
C(9)	31(2)	27(2)	36(2)	-4(2)	-1(2)
C(24)	29(2)	20(2)	31(2)	-1(2)	6(2)
C(25)	46(3)	38(2)	38(2)	11(2)	7(2)
C(26)	58(3)	49(3)	49(3)	12(2)	29(3)
C(27)	42(3)	43(3)	59(3)	1(2)	28(2)
C(28)	27(2)	41(2)	52(3)	-2(2)	8(2)
C(29)	31(2)	34(2)	34(2)	0(2)	4(2)
C(30)	36(2)	31(2)	63(3)	7(2)	4(2)
F(7)	66(2)	56(2)	78(2)	35(2)	18(2)
F(8)	59(2)	37(2)	91(2)	2(2)	21(2)
F(9)	36(2)	53(2)	120(3)	27(2)	-25(2)

Table D.17: Hydrogen coordinates (x 10^4) and isotropic displacement parameters ($Å^2$x 10^3) for $Co(dbm)_3$ {12}

	x	y	z	U(eq)
H(2)	7461	8173	522	41

H(11) 6205	7599	39	52
H(12) 4404	7102	-963	65
H(13) 2086	7143	-643	69
H(14) 1525	7709	608	62
H(15) 3357	8199	1667	44
H(5) 6398	10098	4258	31
H(18) 5420	10414	2164	36
H(19) 3571	10734	338	47
H(20) 1597	10341	-1054	46
H(21) 1466	9626	-655	51
H(22) 3334	9298	1126	41
H(8) 6676	8245	7476	42
H(25) 5119	8507	8403	50
H(26) 3020	8653	9060	59
H(27) 950	8955	7446	54
H(28) 980	9120	5190	50
H(29) 3096	9007	4554	41

Table D.18: Torsion angles [°] for Co(tfba)$_3$ {12}

O(5)-Co(1)-O(1)-C(1)	174.1(3)
O(3)-Co(1)-O(1)-C(1)	87.7(3)
O(2)-Co(1)-O(1)-C(1)	-2.3(3)
O(6)-Co(1)-O(1)-C(1)	-90.0(3)
O(4)-Co(1)-O(2)-C(3)	177.2(3)
O(3)-Co(1)-O(2)-C(3)	-87.1(3)
O(1)-Co(1)-O(2)-C(3)	-0.7(3)
O(6)-Co(1)-O(2)-C(3)	88.6(3)
O(5)-Co(1)-O(3)-C(4)	70.4(3)
O(4)-Co(1)-O(3)-C(4)	-18.0(3)
O(1)-Co(1)-O(3)-C(4)	157.6(3)
O(2)-Co(1)-O(3)-C(4)	-106.5(3)
O(5)-Co(1)-O(4)-C(6)	-68.6(3)
O(3)-Co(1)-O(4)-C(6)	17.4(3)

O(2)-Co(1)-O(4)-C(6)	107.6(3)
O(6)-Co(1)-O(4)-C(6)	-164.6(3)
O(4)-Co(1)-O(5)-C(7)	-87.7(3)
O(3)-Co(1)-O(5)-C(7)	176.5(3)
O(1)-Co(1)-O(5)-C(7)	89.9(3)
O(6)-Co(1)-O(5)-C(7)	0.7(3)
O(5)-Co(1)-O(6)-C(9)	-0.7(3)
O(4)-Co(1)-O(6)-C(9)	87.9(3)
O(1)-Co(1)-O(6)-C(9)	-87.6(3)
O(2)-Co(1)-O(6)-C(9)	176.5(3)
Co(1)-O(1)-C(1)-C(2)	3.4(5)
Co(1)-O(1)-C(1)-C(10)	-176.5(2)
O(1)-C(1)-C(2)-C(3)	-1.4(6)
C(10)-C(1)-C(2)-C(3)	178.5(4)
Co(1)-O(2)-C(3)-C(2)	2.7(6)
Co(1)-O(2)-C(3)-C(16)	-175.4(3)
C(1)-C(2)-C(3)-O(2)	-2.0(7)
C(1)-C(2)-C(3)-C(16)	176.0(4)
O(1)-C(1)-C(10)-C(11)	-156.7(4)
C(2)-C(1)-C(10)-C(11)	23.4(6)
O(1)-C(1)-C(10)-C(15)	22.9(5)
C(2)-C(1)-C(10)-C(15)	-157.1(4)
C(15)-C(10)-C(11)-C(12)	-3.9(7)
C(1)-C(10)-C(11)-C(12)	175.7(4)
C(10)-C(11)-C(12)-C(13)	1.5(8)
C(11)-C(12)-C(13)-C(14)	1.8(8)
C(12)-C(13)-C(14)-C(15)	-2.7(8)
C(13)-C(14)-C(15)-C(10)	0.3(7)
C(11)-C(10)-C(15)-C(14)	3.0(7)
C(1)-C(10)-C(15)-C(14)	-176.6(4)
O(2)-C(3)-C(16)-F(2)	-160.9(5)
C(2)-C(3)-C(16)-F(2)	20.7(6)
O(2)-C(3)-C(16)-F(3)	-35.0(6)
C(2)-C(3)-C(16)-F(3)	146.6(4)

O(2)-C(3)-C(16)-F(1)	80.4(5)
C(2)-C(3)-C(16)-F(1)	-98.0(5)
Co(1)-O(3)-C(4)-C(5)	10.6(5)
Co(1)-O(3)-C(4)-C(17)	-169.5(2)
O(3)-C(4)-C(5)-C(6)	2.6(6)
C(17)-C(4)-C(5)-C(6)	-177.3(4)
Co(1)-O(4)-C(6)-C(5)	-10.9(6)
Co(1)-O(4)-C(6)-C(23)	169.3(2)
C(4)-C(5)-C(6)-O(4)	-2.2(7)
C(4)-C(5)-C(6)-C(23)	177.7(4)
O(3)-C(4)-C(17)-C(18)	-152.2(4)
C(5)-C(4)-C(17)-C(18)	27.7(6)
O(3)-C(4)-C(17)-C(22)	27.4(5)
C(5)-C(4)-C(17)-C(22)	-152.7(4)
C(22)-C(17)-C(18)-C(19)	-2.0(6)
C(4)-C(17)-C(18)-C(19)	177.6(4)
C(17)-C(18)-C(19)-C(20)	1.6(7)
C(18)-C(19)-C(20)-C(21)	-0.3(7)
C(19)-C(20)-C(21)-C(22)	-0.6(7)
C(20)-C(21)-C(22)-C(17)	0.2(7)
C(18)-C(17)-C(22)-C(21)	1.1(6)
C(4)-C(17)-C(22)-C(21)	-178.5(4)
O(4)-C(6)-C(23)-F(5)	-175.1(3)
C(5)-C(6)-C(23)-F(5)	5.0(5)
O(4)-C(6)-C(23)-F(6)	-54.0(4)
C(5)-C(6)-C(23)-F(6)	126.1(4)
O(4)-C(6)-C(23)-F(4)	63.8(4)
C(5)-C(6)-C(23)-F(4)	-116.1(4)
Co(1)-O(5)-C(7)-C(8)	1.4(5)
Co(1)-O(5)-C(7)-C(24)	-176.8(2)
O(5)-C(7)-C(8)-C(9)	-3.9(6)
C(24)-C(7)-C(8)-C(9)	174.2(4)
Co(1)-O(6)-C(9)-C(8)	-1.4(6)
Co(1)-O(6)-C(9)-C(30)	177.9(3)

C(7)-C(8)-C(9)-O(6)	4.0(7)
C(7)-C(8)-C(9)-C(30)	-175.3(4)
O(5)-C(7)-C(24)-C(25)	-162.1(4)
C(8)-C(7)-C(24)-C(25)	19.7(6)
O(5)-C(7)-C(24)-C(29)	17.5(5)
C(8)-C(7)-C(24)-C(29)	-160.8(4)
C(29)-C(24)-C(25)-C(26)	-0.6(7)
C(7)-C(24)-C(25)-C(26)	178.9(4)
C(24)-C(25)-C(26)-C(27)	1.4(8)
C(25)-C(26)-C(27)-C(28)	-0.5(8)
C(26)-C(27)-C(28)-C(29)	-1.2(7)
C(27)-C(28)-C(29)-C(24)	1.9(7)
C(25)-C(24)-C(29)-C(28)	-1.1(6)
C(7)-C(24)-C(29)-C(28)	179.4(4)
O(6)-C(9)-C(30)-F(9)	63.9(5)
C(8)-C(9)-C(30)-F(9)	-116.7(5)
O(6)-C(9)-C(30)-F(7)	-174.6(4)
C(8)-C(9)-C(30)-F(7)	4.8(6)
O(6)-C(9)-C(30)-F(8)	-56.4(5)
C(8)-C(9)-C(30)-F(8)	123.1(5)

E. Computational

Optimized Cartesian coordinates (Å)

All the compounds were optimized with ADF, PW91/TZP

Table E.1: Optimized Cartesian coordinates of Cr(acac)$_3$ {1}, S = 3/2 with *D*3 symmetry.

	X	Y	Z
Cr	0.000000000	0.000000000	0.000000000
O	0.015492000	-1.602309000	-1.159443000
O	-1.395386000	-0.787738000	1.159443000
O	0.015492000	1.602309000	1.159443000
O	1.379894000	0.814570000	-1.159443000
O	1.379894000	-0.814570000	1.159443000
O	-1.395386000	0.787738000	-1.159443000
C	-0.710257000	-2.650674000	-1.021023000
C	-1.940423000	-1.940437000	1.021023000
C	-1.651938000	-2.861241000	0.000000000
C	-0.494821000	-3.714149000	-2.070461000
C	-2.969136000	-2.285602000	2.070461000
C	-0.710257000	2.650674000	1.021023000
C	-1.651938000	2.861241000	0.000000000
C	-0.494821000	3.714149000	2.070461000
C	2.650679000	0.710237000	-1.021023000
C	3.303877000	0.000000000	0.000000000
C	2.650679000	-0.710237000	1.021023000
C	3.463958000	1.428547000	-2.070461000
C	3.463958000	-1.428547000	2.070461000
C	-1.940423000	1.940437000	-1.021023000
C	-2.969136000	2.285602000	-2.070461000
H	-2.195882000	-3.803380000	0.000000000
H	-1.121595000	-4.595367000	-1.905202000
H	0.561597000	-4.011690000	-2.072653000

H	-0.713105000	-3.292103000	-3.059994000
H	-3.418908000	-3.269013000	1.905202000
H	-3.755024000	-1.519488000	2.072653000
H	-2.494493000	-2.263618000	3.059994000
H	-2.195882000	3.803380000	0.000000000
H	-1.121595000	4.595367000	1.905202000
H	0.561597000	4.011690000	2.072653000
H	-0.713105000	3.292103000	3.059994000
H	4.391765000	0.000000000	0.000000000
H	4.540502000	1.326354000	-1.905202000
H	3.193427000	2.492202000	-2.072653000
H	3.207598000	1.028485000	-3.059994000
H	4.540502000	-1.326354000	1.905202000
H	3.193427000	-2.492202000	2.072653000
H	3.207598000	-1.028485000	3.059994000
H	-3.418908000	3.269013000	-1.905202000
H	-3.755024000	1.519488000	-2.072653000
H	-2.494493000	2.263618000	-3.059994000

Table E.2: Optimized Cartesian coordinates of *fac*-Cr(ba)$_3$ {2}, S = 3/2 with *D*3 symmetry.

	X	**Y**	**Z**
Cr	0.033405000	0.015267000	-0.011088000
O	1.777577000	0.933389000	-0.115796000
C	2.784183000	0.625249000	-0.855598000
C	2.787943000	-0.431939000	-1.784044000
H	3.675249000	-0.586735000	-2.388555000
C	1.706778000	-1.293517000	-2.018523000
O	0.571759000	-1.253145000	-1.419119000
C	1.830934000	-2.380451000	-3.058401000
H	1.659352000	-3.354914000	-2.583377000
H	1.047006000	-2.247416000	-3.814977000
H	2.810053000	-2.381309000	-3.546350000
C	3.988429000	1.490652000	-0.685611000

C	3.864599000	2.677702000	0.055600000
C	4.960086000	3.516563000	0.242261000
C	6.203039000	3.181115000	-0.299868000
C	6.342063000	1.997980000	-1.029077000
C	5.245221000	1.160967000	-1.221876000
H	2.893280000	2.923258000	0.479356000
H	5.380154000	0.235615000	-1.777555000
H	4.845147000	4.435764000	0.815551000
H	7.310601000	1.723259000	-1.445127000
H	7.061390000	3.835468000	-0.150676000
O	-1.700450000	-0.910559000	0.106904000
C	-2.741287000	-0.672579000	-0.606609000
C	-2.859562000	0.336585000	-1.572929000
H	-3.802837000	0.394268000	-2.105477000
C	-1.844633000	1.252266000	-1.904993000
O	-0.671174000	1.253287000	-1.376438000
C	-3.910431000	-1.588778000	-0.338815000
H	-4.773036000	-1.360140000	-0.971497000
H	-3.599913000	-2.628019000	-0.506398000
H	-4.200429000	-1.504049000	0.716405000
C	-2.078429000	2.303398000	-2.938586000
C	-0.974709000	3.016024000	-3.434730000
C	-1.141582000	3.999532000	-4.406405000
C	-2.416256000	4.295761000	-4.894916000
C	-3.523928000	3.601992000	-4.400651000
C	-3.356958000	2.614697000	-3.432232000
H	0.012294000	2.778318000	-3.044005000
H	-4.234663000	2.099686000	-3.047515000
H	-0.273342000	4.537434000	-4.785259000
H	-4.522657000	3.834565000	-4.768211000
H	-2.547834000	5.065933000	-5.654295000
O	0.758692000	-1.214759000	1.344952000
C	0.741479000	-1.043744000	2.617979000
C	0.184717000	0.053437000	3.290649000

H	0.261092000	0.051633000	4.372536000
C	-0.429970000	1.151096000	2.661621000
O	-0.537518000	1.283049000	1.386047000
C	1.392320000	-2.151557000	3.409894000
H	1.337545000	-1.980603000	4.489022000
H	0.905909000	-3.104448000	3.165355000
H	2.444403000	-2.238728000	3.109118000
C	-1.001703000	2.270859000	3.466500000
C	-1.419605000	3.433703000	2.797767000
C	-1.963005000	4.504010000	3.503724000
C	-2.106640000	4.430376000	4.891390000
C	-1.702964000	3.276341000	5.566963000
C	-1.154804000	2.207091000	4.862062000
H	-1.308952000	3.475521000	1.716407000
H	-0.862057000	1.312751000	5.407546000
H	-2.278647000	5.399112000	2.969276000
H	-1.820253000	3.207057000	6.647705000
H	-2.535119000	5.265964000	5.444039000

Table E.3: Optimized Cartesian coordinates of *mer*-Cr(ba)$_3$ {2}, S = 3/2 with *D*3 symmetry.

	X	**Y**	**Z**
Cr	-0.036442000	0.022576000	-0.015365000
O	1.680769000	0.987820000	-0.016981000
O	-1.745812000	-0.954744000	0.001845000
O	-0.718095000	1.277141000	-1.377596000
O	0.599770000	-1.193449000	-1.428830000
O	-0.682701000	1.250150000	1.386486000
O	0.661221000	-1.227928000	1.342602000
C	-2.775250000	-0.748140000	-0.740928000
C	-1.862240000	1.219830000	-1.959977000
C	-2.867789000	0.279065000	-1.698923000
H	-3.769088000	0.344706000	-2.299279000
C	-0.539439000	1.132119000	2.659709000

C	0.664374000	-1.045449000	2.614441000
C	0.110065000	0.053025000	3.286315000
C	1.756026000	-1.176123000	-1.988247000
C	2.720464000	0.743994000	-0.734256000
C	2.795236000	-0.282202000	-1.693722000
H	3.706342000	-0.382749000	-2.273877000
C	1.340321000	-2.139017000	3.405405000
H	1.283954000	-1.969180000	4.484584000
H	0.876072000	-3.103093000	3.161882000
H	2.393843000	-2.201929000	3.103123000
C	1.957633000	-2.231855000	-3.048054000
H	1.825470000	-3.224138000	-2.597752000
H	1.184293000	-2.123379000	-3.819159000
H	2.946291000	-2.173067000	-3.512697000
H	0.214253000	0.069650000	4.365985000
C	-1.101526000	2.252575000	3.469501000
C	-1.465452000	3.439589000	2.812894000
C	-1.291059000	2.167731000	4.859109000
C	-1.987551000	4.515574000	3.525850000
C	-1.819598000	3.242247000	5.570975000
C	-2.165815000	4.422093000	4.908381000
H	-1.326992000	3.495194000	1.735208000
H	-1.046511000	1.250768000	5.391050000
H	-2.258634000	5.431572000	3.001818000
H	-1.967625000	3.156858000	6.646727000
H	-2.577444000	5.262205000	5.467013000
C	3.882014000	1.650747000	-0.498847000
C	3.680201000	2.821783000	0.250332000
C	5.171904000	1.375959000	-0.983049000
C	4.733049000	3.699467000	0.494403000
C	6.226475000	2.251452000	-0.732619000
C	6.010456000	3.418786000	0.003366000
H	2.682495000	3.024780000	0.633074000
H	5.365596000	0.463216000	-1.542433000

H	4.557819000	4.606430000	1.072249000
H	7.221980000	2.019102000	-1.108942000
H	6.835345000	4.103872000	0.196844000
C	-2.088327000	2.281728000	-3.008868000
H	-1.306461000	2.205216000	-3.775345000
H	-3.071106000	2.197914000	-3.481960000
H	-1.989911000	3.272831000	-2.547529000
C	-3.905081000	-1.701916000	-0.542932000
C	-5.202691000	-1.452894000	-1.019909000
C	-3.662333000	-2.895252000	0.156448000
C	-6.225029000	-2.375807000	-0.810958000
C	-4.682946000	-3.820521000	0.358202000
C	-5.968099000	-3.565406000	-0.125257000
H	-5.427311000	-0.522606000	-1.537409000
H	-2.657677000	-3.077688000	0.531610000
H	-7.228147000	-2.163362000	-1.178693000
H	-4.476324000	-4.745191000	0.896200000
H	-6.768278000	-4.287312000	0.035604000

Table E.4: Optimized Cartesian coordinates of Cr(dbm)$_3$ {3}, S = 3/2 with *D*3 symmetry.

	X	**Y**	**Z**
Cr	0.000000000	0.000000000	0.000000000
O	-1.379401000	0.797938000	1.148028000
O	1.380735000	-0.795627000	-1.148028000
O	-0.001334000	-1.593565000	1.148028000
O	-1.379401000	-0.797938000	-1.148028000
O	1.380735000	0.795627000	1.148028000
O	-0.001334000	1.593565000	-1.148028000
C	1.931174000	-1.954560000	-1.032994000
C	0.727112000	-2.649726000	1.032994000
C	1.654288000	-2.865311000	0.000000000
H	2.195122000	-3.802064000	0.000000000
C	1.931174000	1.954560000	1.032994000
C	0.727112000	2.649726000	-1.032994000

C	1.654288000	2.865311000	0.000000000
C	-2.658286000	-0.695166000	-1.032994000
C	-2.658286000	0.695166000	1.032994000
C	-3.308576000	0.000000000	0.000000000
H	-4.390245000	0.000000000	0.000000000
H	2.195122000	3.802064000	0.000000000
C	0.516022000	-3.681262000	2.090407000
C	-0.586074000	-3.544551000	2.951116000
C	1.376286000	-4.777895000	2.269696000
C	-0.828493000	-4.483037000	3.949775000
C	1.136303000	-5.713273000	3.273606000
C	0.030572000	-5.571960000	4.115228000
H	-1.244748000	-2.689471000	2.817028000
H	2.254514000	-4.898087000	1.638771000
H	-1.691838000	-4.364503000	4.603702000
H	1.817686000	-6.553163000	3.403540000
H	-0.157259000	-6.305539000	4.898610000
C	2.930055000	-2.287519000	-2.090407000
C	3.449636000	-3.580846000	-2.269696000
C	3.362708000	-1.264721000	-2.951116000
C	4.379688000	-3.840704000	-3.273606000
C	4.296671000	-1.524022000	-3.949775000
C	4.810173000	-2.812456000	-4.115228000
H	3.114611000	-4.401510000	-1.638771000
H	2.951524000	-0.266752000	-2.817028000
H	4.766363000	-4.850744000	-3.403540000
H	4.625690000	-0.717077000	-4.603702000
H	5.539386000	-3.016579000	-4.898610000
C	2.930055000	2.287519000	2.090407000
C	3.362708000	1.264721000	2.951116000
C	3.449636000	3.580846000	2.269696000
C	4.296671000	1.524022000	3.949775000
C	4.379688000	3.840704000	3.273606000
C	4.810173000	2.812456000	4.115228000

H	2.951524000	0.266752000	2.817028000
H	3.114611000	4.401510000	1.638771000
H	4.625690000	0.717077000	4.603702000
H	4.766363000	4.850744000	3.403540000
H	5.539386000	3.016579000	4.898610000
C	0.516022000	3.681262000	-2.090407000
C	1.376286000	4.777895000	-2.269696000
C	-0.586074000	3.544551000	-2.951116000
C	1.136303000	5.713273000	-3.273606000
C	-0.828493000	4.483037000	-3.949775000
C	0.030572000	5.571960000	-4.115228000
H	2.254514000	4.898087000	-1.638771000
H	-1.244748000	2.689471000	-2.817028000
H	1.817686000	6.553163000	-3.403540000
H	-1.691838000	4.364503000	-4.603702000
H	-0.157259000	6.305539000	-4.898610000
C	-3.446077000	1.393742000	2.090407000
C	-2.776634000	2.279830000	2.951116000
C	-4.825922000	1.197049000	2.269696000
C	-3.468177000	2.959015000	3.949775000
C	-5.515991000	1.872569000	3.273606000
C	-4.840744000	2.759504000	4.115228000
H	-1.706776000	2.422719000	2.817028000
H	-5.369125000	0.496577000	1.638771000
H	-2.933851000	3.647426000	4.603702000
H	-6.584049000	1.702419000	3.403540000
H	-5.382127000	3.288960000	4.898610000
C	-3.446077000	-1.393742000	-2.090407000
C	-4.825922000	-1.197049000	-2.269696000
C	-2.776634000	-2.279830000	-2.951116000
C	-5.515991000	-1.872569000	-3.273606000
C	-3.468177000	-2.959015000	-3.949775000
C	-4.840744000	-2.759504000	-4.115228000
H	-5.369125000	-0.496577000	-1.638771000

H	-1.706776000	-2.422719000	-2.817028000
H	-6.584049000	-1.702419000	-3.403540000
H	-2.933851000	-3.647426000	-4.603702000
H	-5.382127000	-3.288960000	-4.898610000

Table E.5: Optimized Cartesian coordinates of *fac*-Cr(tfba)$_3$ {4}, S = 3/2 with *D*3 symmetry.

	X	**Y**	**Z**
Cr	0.002763000	-0.014619000	-0.051060000
O	1.735224000	0.920870000	-0.126547000
O	-1.735680000	-0.934862000	0.043875000
O	-0.693046000	1.237391000	-1.402904000
O	0.567636000	-1.256259000	-1.471463000
O	-0.572793000	1.230569000	1.363691000
O	0.721593000	-1.264840000	1.290909000
C	-2.763280000	-0.622398000	-0.651425000
C	-1.859073000	1.275335000	-1.939913000
C	-2.902952000	0.383220000	-1.595640000
H	-3.870274000	0.490291000	-2.068635000
C	-0.484118000	1.095103000	2.637634000
C	0.660658000	-1.087721000	2.556349000
C	0.114290000	-0.026032000	3.261410000
C	1.729581000	-1.266983000	-2.006495000
C	2.760203000	0.653731000	-0.853314000
C	2.803037000	-0.419639000	-1.774461000
H	3.715004000	-0.609287000	-2.325377000
H	0.177465000	-0.061281000	4.341133000
C	-1.035195000	2.210875000	3.449151000
C	-1.438372000	3.386787000	2.792280000
C	-1.177341000	2.132865000	4.845949000
C	-1.957894000	4.457411000	3.513155000
C	-1.702617000	3.203761000	5.564121000
C	-2.091191000	4.369819000	4.901428000
H	-1.334523000	3.440263000	1.710896000
H	-0.895686000	1.229372000	5.381521000

H	-2.262990000	5.363478000	2.992209000
H	-1.813669000	3.126507000	6.644585000
H	-2.501029000	5.206836000	5.465502000
C	3.932924000	1.548089000	-0.674114000
C	3.923790000	2.468730000	0.388684000
C	5.046868000	1.515736000	-1.531836000
C	5.001157000	3.325026000	0.592352000
C	6.121358000	2.377585000	-1.328479000
C	6.103448000	3.282498000	-0.264999000
H	3.060019000	2.493568000	1.048937000
H	5.076009000	0.829053000	-2.374593000
H	4.983832000	4.028200000	1.424133000
H	6.975083000	2.344543000	-2.003595000
H	6.946675000	3.953713000	-0.105542000
C	-2.071355000	2.339632000	-2.954672000
C	-1.067227000	3.307010000	-3.136780000
C	-3.231755000	2.411576000	-3.746177000
C	-1.223794000	4.322014000	-4.075567000
C	-3.383330000	3.425344000	-4.688322000
C	-2.382334000	4.385148000	-4.854203000
H	-0.167886000	3.244039000	-2.528723000
H	-4.018733000	1.667974000	-3.644396000
H	-0.438954000	5.066035000	-4.203709000
H	-4.284311000	3.464445000	-5.298605000
H	-2.503746000	5.177815000	-5.591596000
C	-3.973982000	-1.524279000	-0.341188000
F	-5.074296000	-1.201536000	-1.082451000
F	-3.683424000	-2.823541000	-0.592739000
F	-4.324686000	-1.423217000	0.965577000
C	1.311970000	-2.244147000	3.340320000
F	1.228382000	-2.075822000	4.692832000
F	0.718165000	-3.424083000	3.041588000
F	2.628540000	-2.351135000	3.028547000
C	1.884592000	-2.396622000	-3.043984000

F	3.123795000	-2.418390000	-3.616900000
F	1.681843000	-3.607564000	-2.471747000
F	0.980056000	-2.254123000	-4.045377000

Table E.6: Optimized Cartesian coordinates of *mer*-Cr(tfba)$_3$ {4}, S = 3/2 with *D*3 symmetry.

	X	Y	Z
Cr	-0.110135000	0.048514000	0.011797000
O	1.544687000	1.113957000	-0.023153000
O	-1.762549000	-1.021125000	0.038599000
O	-0.873544000	1.243794000	-1.361223000
O	0.616672000	-1.170038000	-1.353545000
O	-0.817588000	1.267735000	1.394606000
O	0.629677000	-1.144318000	1.405748000
C	-2.838707000	-0.868432000	-0.643750000
C	-2.055993000	1.137135000	-1.844423000
C	-3.027285000	0.189545000	-1.568992000
H	-3.959476000	0.258280000	-2.113766000
C	-0.681939000	1.206049000	2.669910000
C	0.561637000	-0.924577000	2.664597000
C	-0.015170000	0.144894000	3.332019000
C	1.801672000	-1.104398000	-1.835613000
C	2.621220000	0.920999000	-0.696510000
C	2.791225000	-0.166518000	-1.588315000
H	3.725159000	-0.274924000	-2.123752000
H	0.064863000	0.159954000	4.411022000
C	-1.266803000	2.333409000	3.442621000
C	-1.763975000	3.446445000	2.741583000
C	-1.345258000	2.328282000	4.847304000
C	-2.315949000	4.525264000	3.426714000
C	-1.902986000	3.406151000	5.529580000
C	-2.388170000	4.508353000	4.822332000
H	-1.706119000	3.446641000	1.655310000
H	-0.984812000	1.476216000	5.418478000
H	-2.693119000	5.382963000	2.871761000

181

H	-1.963099000	3.383867000	6.616746000
H	-2.823566000	5.351415000	5.358242000
C	3.703122000	1.919952000	-0.496456000
C	3.434076000	3.058944000	0.284100000
C	4.986708000	1.767271000	-1.050634000
C	4.418263000	4.017855000	0.499333000
C	5.970775000	2.727511000	-0.831575000
C	5.689763000	3.855937000	-0.057420000
H	2.441068000	3.173912000	0.711772000
H	5.232089000	0.892965000	-1.648793000
H	4.195236000	4.896032000	1.103802000
H	6.960819000	2.594462000	-1.264542000
H	6.460436000	4.606838000	0.112514000
C	-3.898666000	-1.884711000	-0.424232000
C	-5.196332000	-1.750270000	-0.950962000
C	-3.592958000	-3.023264000	0.342552000
C	-6.159831000	-2.727331000	-0.716016000
C	-4.556833000	-4.000677000	0.570975000
C	-5.842748000	-3.855588000	0.043952000
H	-5.468131000	-0.875335000	-1.536518000
H	-2.588383000	-3.125903000	0.746458000
H	-7.161769000	-2.606751000	-1.125237000
H	-4.305542000	-4.880509000	1.160851000
H	-6.597029000	-4.621132000	0.224333000
C	1.213276000	-2.051911000	3.492759000
F	1.209207000	-1.790673000	4.833290000
F	0.545050000	-3.223297000	3.310188000
F	2.501121000	-2.252888000	3.122108000
C	2.097514000	-2.257890000	-2.814423000
F	3.357105000	-2.191623000	-3.339485000
F	1.984281000	-3.457736000	-2.188827000
F	1.223410000	-2.249720000	-3.852700000
C	-2.371595000	2.247954000	-2.865747000
F	-2.267002000	3.475488000	-2.286623000

| F | -1.505023000 | 2.211239000 | -3.908445000 |
| F | -3.633168000 | 2.151131000 | -3.379216000 |

Table E.7: Optimized Cartesian coordinates of *fac*-Cr(tfth)₃ {5}, S = 3/2 with *D*3 symmetry.

	X	**Y**	**Z**
Cr	-0.009275000	0.050421000	0.044607000
O	1.716258000	1.003234000	0.065659000
O	-1.748614000	-0.873363000	0.047448000
O	-0.646973000	1.347372000	-1.293812000
O	0.608989000	-1.142758000	-1.395507000
O	-0.635171000	1.256581000	1.476973000
O	0.669199000	-1.243316000	1.367159000
C	-2.745281000	-0.556630000	-0.691442000
C	-1.793617000	1.383138000	-1.874223000
C	-2.846846000	0.472107000	-1.614615000
H	-3.782797000	0.581917000	-2.153394000
C	-0.537491000	1.084480000	2.748565000
C	0.592643000	-1.099798000	2.636810000
C	0.049148000	-0.050814000	3.359836000
C	1.768247000	-1.093979000	-1.935964000
C	2.738750000	0.793963000	-0.684675000
C	2.813298000	-0.224063000	-1.667063000
H	3.727493000	-0.334375000	-2.241977000
H	0.078720000	-0.108580000	4.441334000
C	-1.072387000	2.155734000	3.577301000
C	-1.126538000	2.283681000	4.957782000
C	-1.729943000	3.486780000	5.376495000
C	-2.131543000	4.268600000	4.313876000
H	-0.744846000	1.532634000	5.642917000
H	-1.867907000	3.771242000	6.415839000
H	-2.621095000	5.235988000	4.348020000
C	-1.969526000	2.455856000	-2.848933000
C	-1.031319000	3.415965000	-3.188160000
C	-1.492173000	4.321632000	-4.166211000

C	-2.780840000	4.050396000	-4.572458000
H	-0.047558000	3.439288000	-2.728857000
H	-0.903605000	5.143843000	-4.564326000
H	-3.378426000	4.577887000	-5.308066000
C	-3.960284000	-1.476005000	-0.464341000
F	-5.017288000	-1.157415000	-1.265786000
F	-3.640037000	-2.769335000	-0.709195000
F	-4.388775000	-1.391879000	0.821355000
C	1.214683000	-2.284488000	3.400184000
F	1.122563000	-2.142995000	4.755580000
F	0.601384000	-3.446569000	3.071950000
F	2.531730000	-2.410723000	3.097495000
C	1.953722000	-2.167073000	-3.025961000
F	3.192097000	-2.126285000	-3.597572000
F	1.784184000	-3.409195000	-2.512411000
F	1.044472000	-2.002055000	-4.020096000
S	-3.437418000	2.687474000	-3.761824000
S	-1.779059000	3.543768000	2.799131000
C	3.865988000	1.698239000	-0.473110000
C	3.920556000	2.738554000	0.439694000
C	5.142957000	3.441878000	0.407757000
H	5.378825000	4.288060000	1.047363000
H	3.087425000	2.962263000	1.099318000
S	5.354930000	1.599811000	-1.376101000
C	6.018904000	2.937220000	-0.528558000
H	7.021052000	3.278829000	-0.763774000

Table E.8: Optimized Cartesian coordinates of *fac*-Cr(tfth)₃ {5}, S = 3/2 with *D*3 symmetry.

	X	**Y**	**Z**
Cr	0.028477000	0.026713000	-0.106707000
O	1.779971000	0.924264000	-0.144799000
O	-1.722442000	-0.873020000	-0.043166000
O	-0.607485000	1.265732000	-1.505720000
O	0.609524000	-1.269571000	-1.468844000

O	-0.587118000	1.329797000	1.238672000
O	0.664455000	-1.197494000	1.305509000
C	-2.783086000	-0.587817000	-0.711843000
C	-1.805457000	1.296328000	-1.959263000
C	-2.874527000	0.474614000	-1.647842000
H	-3.817067000	0.650260000	-2.152445000
C	-0.553632000	1.219651000	2.518062000
C	0.532639000	-0.991318000	2.562292000
C	-0.021396000	0.101763000	3.208715000
C	1.776371000	-1.302038000	-1.996993000
C	2.805529000	0.623920000	-0.862217000
C	2.852848000	-0.461167000	-1.772925000
H	3.766584000	-0.644170000	-2.325545000
H	-0.041520000	0.095428000	4.294014000
C	-1.113601000	2.346568000	3.259174000
C	-1.674000000	3.487904000	2.709904000
C	-2.137863000	4.400655000	3.680370000
C	-1.930041000	3.954563000	4.968057000
H	-1.733621000	3.632995000	1.635275000
H	-2.608617000	5.352326000	3.449290000
H	-2.185488000	4.447757000	5.899575000
C	3.969569000	1.481165000	-0.697213000
C	5.212688000	1.435657000	-1.311939000
C	6.079771000	2.458582000	-0.877937000
C	5.492901000	3.277339000	0.064204000
H	5.486530000	0.688955000	-2.050992000
H	7.095412000	2.592947000	-1.239986000
H	5.929820000	4.136015000	0.563144000
C	-3.939572000	-1.433074000	-0.458698000
C	-5.216350000	-1.396580000	-1.000758000
C	-6.061332000	-2.400176000	-0.486451000
C	-5.423315000	-3.195188000	0.443256000
H	-5.529182000	-0.670192000	-1.744773000
H	-7.096944000	-2.539153000	-0.784408000

H	-5.833956000	-4.036942000	0.990708000
C	-2.016215000	2.434789000	-2.973622000
F	-1.826413000	3.643451000	-2.377434000
F	-1.139731000	2.343278000	-4.001877000
F	-3.272567000	2.443486000	-3.506948000
C	1.928458000	-2.452588000	-3.008992000
F	3.168964000	-2.493156000	-3.577891000
F	1.719161000	-3.651275000	-2.410600000
F	1.026905000	-2.330906000	-4.015788000
C	1.080325000	-2.156134000	3.408453000
F	0.960084000	-1.935919000	4.749655000
F	0.415216000	-3.305865000	3.127225000
F	2.394615000	-2.366198000	3.149021000
S	-3.792982000	-2.727850000	0.696743000
S	-1.166550000	2.416577000	5.000410000
S	3.883384000	2.808015000	0.427225000

Table E.9: Optimized Cartesian coordinates of *fac*-Cr(tffu)$_3$ {6}, S = 3/2 with *D*3 symmetry.

	X	Y	Z
Cr	0.061614000	0.038920000	0.059089000
O	1.804646000	0.956479000	0.122765000
O	-1.696671000	-0.852081000	0.036516000
O	-0.509491000	1.333101000	-1.309591000
O	0.686265000	-1.173844000	-1.365507000
O	-0.585002000	1.274380000	1.453122000
O	0.680637000	-1.252638000	1.416221000
C	-2.682236000	-0.503496000	-0.703631000
C	-1.659465000	1.392928000	-1.884038000
C	-2.748563000	0.526112000	-1.627826000
H	-3.670263000	0.679326000	-2.177439000
C	-0.543367000	1.103123000	2.722762000
C	0.559703000	-1.095388000	2.681180000
C	0.002270000	-0.033141000	3.372449000
C	1.834590000	-1.108901000	-1.926882000

C	2.816846000	0.741802000	-0.642431000
C	2.883367000	-0.243340000	-1.655409000
H	3.796639000	-0.328612000	-2.233409000
H	-0.015223000	-0.077583000	4.455110000
C	-1.097699000	2.168911000	3.544443000
C	-1.232110000	2.343365000	4.907528000
C	-1.863537000	3.598945000	5.099587000
C	-2.074230000	4.110538000	3.846488000
H	-0.918246000	1.650574000	5.678476000
H	-2.132823000	4.066848000	6.039006000
H	-2.520989000	5.028457000	3.486011000
C	-1.799790000	2.454915000	-2.862526000
C	-0.917679000	3.421415000	-3.289860000
C	-1.600046000	4.192208000	-4.266789000
C	-2.852866000	3.649820000	-4.375131000
H	0.096308000	3.541735000	-2.929388000
H	-1.220023000	5.040300000	-4.824320000
H	-3.715975000	3.891702000	-4.982165000
C	-3.930355000	-1.375570000	-0.471359000
F	-4.957391000	-1.058336000	-1.310694000
F	-3.648629000	-2.688145000	-0.651595000
F	-4.387224000	-1.222738000	0.799922000
C	1.139809000	-2.277549000	3.478800000
F	0.994635000	-2.122886000	4.828774000
F	0.531503000	-3.438353000	3.137238000
F	2.467483000	-2.417426000	3.231494000
C	2.002780000	-2.153464000	-3.046463000
F	3.234490000	-2.104849000	-3.630431000
F	1.829747000	-3.408945000	-2.566875000
F	1.083768000	-1.955053000	-4.026755000
C	3.956491000	1.609920000	-0.406513000
C	4.149250000	2.633337000	0.493833000
C	5.460299000	3.130071000	0.271244000
H	5.960265000	3.936428000	0.794818000

H	3.419313000	2.968170000	1.220234000
C	5.984871000	2.381258000	-0.748312000
H	6.939804000	2.387275000	-1.257999000
O	-3.000419000	2.592309000	-3.531606000
O	5.090284000	1.450042000	-1.178780000
O	-1.617322000	3.261776000	2.890019000

Table E.10: Optimized Cartesian coordinates of *mer*-Cr(tffu)$_3$ {6}, S = 3/2 with *D*3 symmetry.

	X	Y	Z
Cr	-0.018675000	0.007918000	-0.161692000
O	1.705539000	0.953501000	-0.165571000
O	-1.752389000	-0.926981000	-0.123741000
O	-0.653861000	1.239451000	-1.570415000
O	0.615330000	-1.272141000	-1.518624000
O	-0.697551000	1.282090000	1.179060000
O	0.655258000	-1.200871000	1.247361000
C	-2.807237000	-0.635902000	-0.789067000
C	-1.848678000	1.258271000	-2.033189000
C	-2.910621000	0.427399000	-1.724826000
H	-3.855727000	0.592603000	-2.228690000
C	-0.626853000	1.170066000	2.458343000
C	0.562548000	-0.979078000	2.505041000
C	-0.019630000	0.097352000	3.154440000
C	1.803462000	-1.295130000	-1.998392000
C	2.754134000	0.655221000	-0.839810000
C	2.858553000	-0.439307000	-1.737087000
H	3.798864000	-0.611847000	-2.247406000
H	-0.014934000	0.122250000	4.238162000
C	-1.236678000	2.256704000	3.202381000
C	-1.882435000	3.396117000	2.779902000
C	-2.284396000	4.093660000	3.948946000
C	-1.859097000	3.338565000	5.009876000
H	-2.035851000	3.675634000	1.745216000
H	-2.819658000	5.034054000	4.006850000

H	-1.932078000	3.459365000	6.083154000
C	3.912653000	1.516098000	-0.662338000
C	5.181330000	1.521287000	-1.207939000
C	5.866420000	2.625958000	-0.640666000
C	4.976104000	3.223722000	0.212296000
H	5.572993000	0.816439000	-1.930761000
H	6.884276000	2.943002000	-0.833644000
H	5.037350000	4.087867000	0.861362000
C	-3.979457000	-1.463894000	-0.557394000
C	-5.256462000	-1.465452000	-1.083771000
C	-5.957328000	-2.524096000	-0.453416000
C	-5.067575000	-3.100477000	0.414974000
H	-5.642984000	-0.788514000	-1.835616000
H	-6.984818000	-2.826936000	-0.616790000
H	-5.138910000	-3.930303000	1.106112000
C	-2.064479000	2.390412000	-3.052304000
F	-1.897123000	3.604264000	-2.460075000
F	-1.177615000	2.307571000	-4.072732000
F	-3.316288000	2.380408000	-3.598071000
C	2.011966000	-2.451438000	-2.992480000
F	3.274946000	-2.478296000	-3.512307000
F	1.797740000	-3.648434000	-2.392326000
F	1.149429000	-2.353516000	-4.035814000
C	1.201361000	-2.098121000	3.348929000
F	1.119083000	-1.859867000	4.689675000
F	0.593497000	-3.288262000	3.112173000
F	2.516525000	-2.240163000	3.044434000
O	-3.864675000	-2.474307000	0.367735000
O	-1.218517000	2.215800000	4.582959000
O	3.787260000	2.568084000	0.214540000

Table E.11: Optimized Cartesian coordinates of *fac*-Cr(tfaa)₃ {7}, S = 3/2 with *D*3 symmetry.

	X	Y	Z
Cr	-7.775023000	-2.575508000	6.461430000
O	-8.188982000	-0.804122000	7.227995000
O	-7.321304000	-4.342744000	5.698720000
O	-8.895938000	-3.411006000	7.855097000
O	-9.346415000	-2.478504000	5.264744000
O	-6.220691000	-2.706201000	7.671279000
O	-6.676427000	-1.707115000	5.065073000
C	-7.745091000	-5.459913000	6.149054000
C	-9.123206000	-4.658417000	8.027878000
C	-8.588227000	-5.693514000	7.229468000
C	-10.036706000	-4.995431000	9.175736000
H	-11.026498000	-4.560523000	8.983717000
H	-10.138613000	-6.074020000	9.322422000
H	-9.652400000	-4.531073000	10.092374000
H	-8.848946000	-6.719418000	7.469035000
C	-5.022510000	-2.318127000	7.444819000
C	-5.431308000	-1.446826000	5.176465000
C	-4.587220000	-1.699966000	6.251735000
C	-10.164433000	-1.499238000	5.216179000
C	-9.161667000	-0.030942000	6.922073000
C	-10.148690000	-0.321265000	5.954303000
H	-10.930532000	0.410207000	5.776712000
C	-9.210780000	1.272925000	7.672508000
H	-10.100040000	1.859779000	7.427407000
H	-9.184755000	1.071278000	8.750542000
H	-8.313042000	1.857432000	7.431357000
H	-3.544466000	-1.410652000	6.169279000
C	-11.297742000	-1.727258000	4.195810000
F	-12.138654000	-0.658782000	4.095979000
F	-10.796895000	-1.969047000	2.961924000
F	-12.050198000	-2.800572000	4.556130000
C	-7.199954000	-6.662214000	5.352264000

F	-5.846333000	-6.726769000	5.459877000
F	-7.697953000	-7.853261000	5.790601000
F	-7.505320000	-6.550969000	4.038431000
C	-4.042200000	-2.564641000	8.560110000
H	-4.431736000	-2.126798000	9.487535000
H	-3.954458000	-3.646584000	8.725592000
H	-3.053660000	-2.151255000	8.342941000
C	-4.860067000	-0.749511000	3.925457000
F	-5.459712000	0.456366000	3.740408000
F	-3.518355000	-0.524719000	4.014955000
F	-5.076040000	-1.493228000	2.815482000

Table E.12: Optimized Cartesian coordinates of *mer*-Cr(tfaa)$_3$ {7}, S = 3/2 with *D*3 symmetry.

	X	Y	Z
Cr	-7.816681000	-2.572283000	6.498758000
O	-8.257021000	-0.798433000	7.245410000
O	-7.341820000	-4.336229000	5.746101000
O	-8.947107000	-3.411779000	7.880542000
O	-9.370740000	-2.493368000	5.276509000
O	-6.278107000	-2.676945000	7.735981000
O	-6.702943000	-1.718139000	5.111681000
C	-7.753534000	-5.456735000	6.201294000
C	-9.147262000	-4.661411000	8.069728000
C	-8.593595000	-5.694365000	7.281617000
C	-10.042380000	-5.003221000	9.229965000
H	-11.006897000	-4.495428000	9.103383000
H	-10.204107000	-6.080040000	9.326480000
H	-9.592333000	-4.616670000	10.153631000
H	-8.836837000	-6.722278000	7.530639000
C	-5.094163000	-2.284010000	7.459652000
C	-5.449911000	-1.467276000	5.162904000
C	-4.623927000	-1.716052000	6.282380000
C	-10.202607000	-1.526380000	5.218535000
C	-9.241334000	-0.043300000	6.935162000

C	-10.214671000	-0.349294000	5.957261000
H	-11.008061000	0.368260000	5.773887000
C	-4.857887000	-0.872188000	3.914015000
H	-3.813134000	-0.579140000	4.048260000
H	-4.925146000	-1.611579000	3.104729000
H	-5.453008000	-0.003900000	3.606053000
C	-9.325089000	1.253751000	7.694466000
H	-10.186347000	1.856563000	7.394169000
H	-9.383753000	1.037293000	8.768787000
H	-8.402385000	1.825858000	7.533015000
H	-3.573277000	-1.451353000	6.219612000
C	-4.116835000	-2.492832000	8.633529000
F	-4.517733000	-1.782313000	9.719701000
F	-4.065958000	-3.799495000	8.992208000
F	-2.845799000	-2.100331000	8.337971000
C	-11.313118000	-1.766342000	4.175893000
F	-12.192347000	-0.727513000	4.094153000
F	-10.783191000	-1.947839000	2.941380000
F	-12.028161000	-2.877784000	4.486991000
C	-7.205908000	-6.654027000	5.398973000
F	-5.849164000	-6.670941000	5.430460000
F	-7.639713000	-7.852991000	5.879886000
F	-7.587585000	-6.574864000	4.099785000

Table E.13: Optimized Cartesian coordinates of Cr(hfaa)$_3$ {8}, S = 3/2 with *D*3 symmetry.Cr(hfaa)3

	X	**Y**	**Z**
Cr	0.000000000	0.000000000	0.000000000
O	-1.396619000	0.790902000	-1.150088000
O	1.383251000	-0.814057000	1.150088000
O	1.383251000	0.814057000	-1.150088000
O	0.013368000	1.604959000	1.150088000
O	0.013368000	-1.604959000	-1.150088000

O	-1.396619000	-0.790902000	1.150088000
C	2.642106000	-0.703022000	0.995588000
C	2.642106000	0.703022000	-0.995588000
C	3.325135000	0.000000000	0.000000000
H	4.409203000	0.000000000	0.000000000
C	-0.712218000	-2.639642000	-0.995588000
C	-1.929888000	-1.936620000	0.995588000
C	-1.662568000	-2.879652000	0.000000000
C	-0.712218000	2.639642000	0.995588000
C	-1.929888000	1.936620000	-0.995588000
C	-1.662568000	2.879652000	0.000000000
H	-2.204602000	3.818482000	0.000000000
H	-2.204602000	-3.818482000	0.000000000
C	3.449277000	-1.462993000	2.071114000
F	4.790102000	-1.331227000	1.895857000
F	3.142988000	-0.998612000	3.304211000
F	3.153329000	-2.784023000	2.031721000
C	3.449277000	1.462993000	-2.071114000
F	3.142988000	0.998612000	-3.304211000
F	3.153329000	2.784023000	-2.031721000
F	4.790102000	1.331227000	-1.895857000
C	-0.457649000	3.718658000	2.071114000
F	-1.242174000	4.813963000	1.895857000
F	-0.706671000	3.221214000	3.304211000
F	0.834370000	4.122874000	2.031721000
C	-2.991628000	2.255665000	-2.071114000
F	-2.436317000	2.222602000	-3.304211000
F	-3.987699000	1.338851000	-2.031721000
F	-3.547928000	3.482736000	-1.895857000
C	-2.991628000	-2.255665000	2.071114000
F	-3.547928000	-3.482736000	1.895857000
F	-2.436317000	-2.222602000	3.304211000
F	-3.987699000	-1.338851000	2.031721000
C	-0.457649000	-3.718658000	-2.071114000

F	-0.706671000	-3.221214000	-3.304211000
F	0.834370000	-4.122874000	-2.031721000
F	-1.242174000	-4.813963000	-1.895857000

Table E.14: Optimized Cartesian coordinates of *mer*-Co(acac)$_3$ {9}, S = 0/2 with *D*3 symmetry.

	X	**Y**	**Z**
Co	0.000000000	0.000000000	0.000000000
O	-1.359205000	0.671646000	-1.156939000
O	1.261265000	-0.841283000	1.156939000
O	1.261265000	0.841283000	-1.156939000
O	0.097940000	1.512929000	1.156939000
O	0.097940000	-1.512929000	-1.156939000
O	-1.359205000	-0.671646000	1.156939000
C	2.527583000	-0.728608000	1.006044000
C	2.527583000	0.728608000	-1.006044000
C	3.180043000	0.000000000	0.000000000
C	3.343770000	1.466723000	-2.042009000
H	3.054808000	2.524958000	-2.048378000
H	4.417625000	1.382488000	-1.852351000
H	3.118033000	1.060846000	-3.036346000
C	3.343770000	-1.466723000	2.042009000
H	3.054808000	-2.524958000	2.048378000
H	4.417625000	-1.382488000	1.852351000
H	3.118033000	-1.060846000	3.036346000
H	4.267810000	0.000000000	0.000000000
C	-0.632798000	-2.553255000	-1.006044000
C	-1.894785000	-1.824647000	1.006044000
C	-1.590021000	-2.753998000	0.000000000
C	-0.632798000	2.553255000	1.006044000
C	-1.894785000	1.824647000	-1.006044000
C	-1.590021000	2.753998000	0.000000000
H	-2.133905000	3.696032000	0.000000000
C	-2.942105000	-2.162429000	2.042009000
H	-3.406082000	-3.134532000	1.852351000

H	-2.477736000	-2.169873000	3.036346000
H	-3.714081000	-1.383063000	2.048378000
C	-0.401666000	-3.629152000	-2.042009000
H	-0.640297000	-3.230719000	-3.036346000
H	0.659273000	-3.908020000	-2.048378000
H	-1.011543000	-4.517019000	-1.852351000
C	-0.401666000	3.629152000	2.042009000
H	-0.640297000	3.230719000	3.036346000
H	0.659273000	3.908020000	2.048378000
H	-1.011543000	4.517019000	1.852351000
C	-2.942105000	2.162429000	-2.042009000
H	-3.406082000	3.134532000	-1.852351000
H	-2.477736000	2.169873000	-3.036346000
H	-3.714081000	1.383063000	-2.048378000
H	-2.133905000	-3.696032000	0.000000000

Table E.15: Optimized Cartesian coordinates of *fac*-Co(ba)₃ {10}, S = 0/2 with *D*3 symmetry.

	X	**Y**	**Z**
Co	-0.010577000	-0.042560000	-0.022986000
O	1.612942000	0.922176000	0.187782000
O	-1.654876000	-1.004959000	-0.042964000
O	-0.444774000	1.178586000	-1.413157000
O	0.617876000	-1.268814000	-1.338272000
O	-0.794399000	1.201414000	1.182604000
O	0.595613000	-1.283153000	1.288233000
C	-2.655271000	-0.699447000	-0.788069000
C	-1.592033000	1.202869000	-1.984641000
C	-2.670371000	0.347382000	-1.724886000
C	-1.734318000	2.285586000	-3.029184000
H	-0.975757000	2.140323000	-3.808646000
H	-2.728014000	2.285754000	-3.486216000
H	-1.545060000	3.262602000	-2.567435000
H	-3.586516000	0.534193000	-2.274748000
C	-0.815690000	1.023076000	2.452133000

C	0.410319000	-1.137189000	2.550266000
C	-0.263233000	-0.058632000	3.149067000
C	1.798930000	-1.232185000	-1.842348000
C	2.662108000	0.678216000	-0.507501000
C	2.802159000	-0.318115000	-1.481168000
H	3.751410000	-0.362084000	-2.004151000
C	-1.523864000	2.118941000	3.214376000
H	-1.049322000	3.082347000	2.990193000
H	-2.565954000	2.181512000	2.876298000
H	-1.503269000	1.945797000	4.294137000
C	3.826451000	1.591749000	-0.202412000
H	4.694664000	1.371371000	-0.830013000
H	3.520601000	2.634207000	-0.354882000
H	4.105233000	1.483371000	0.853349000
H	-0.396412000	-0.069574000	4.225793000
C	-3.866334000	-1.550406000	-0.584914000
C	-4.931134000	-1.580359000	-1.500558000
C	-3.942921000	-2.355905000	0.563589000
C	-6.045493000	-2.383850000	-1.268088000
C	-5.059688000	-3.154771000	0.797020000
C	-6.116370000	-3.170945000	-0.116406000
H	-4.886340000	-0.989883000	-2.413167000
H	-3.113191000	-2.338693000	1.266664000
H	-6.859743000	-2.399585000	-1.991534000
H	-5.105982000	-3.767906000	1.696244000
H	-6.989613000	-3.796727000	0.065377000
C	0.956255000	-2.243749000	3.391397000
C	1.192180000	-2.095203000	4.767682000
C	1.257870000	-3.472807000	2.782776000
C	1.706760000	-3.151425000	5.517035000
C	1.765673000	-4.529525000	3.534662000
C	1.991297000	-4.373868000	4.904336000
H	0.998304000	-1.142262000	5.255959000
H	1.083428000	-3.580096000	1.714230000

H	1.892539000	-3.017411000	6.582086000
H	1.987958000	-5.479252000	3.049578000
H	2.391667000	-5.199492000	5.491802000
C	2.057012000	-2.255224000	-2.899689000
C	3.353449000	-2.593766000	-3.320195000
C	0.963689000	-2.908518000	-3.492516000
C	3.550395000	-3.548483000	-4.315843000
C	1.161795000	-3.858886000	-4.491338000
C	2.455234000	-4.181237000	-4.909078000
H	4.219526000	-2.128097000	-2.854298000
H	-0.038836000	-2.653759000	-3.155569000
H	4.563042000	-3.804267000	-4.625492000
H	0.302942000	-4.351485000	-4.945769000
H	2.610596000	-4.926013000	-5.689129000

Table E.16: Optimized Cartesian coordinates of *mer*-Co(ba)$_3$ {10}, S = 0/2 with *D*3 symmetry.

	X	**Y**	**Z**
Co	-0.028238000	-0.026794000	-0.086493000
O	1.623594000	0.910960000	0.039914000
O	-1.683908000	-0.960717000	-0.027841000
O	-0.495689000	1.180425000	-1.476870000
O	0.523055000	-1.288228000	-1.399992000
O	-0.741340000	1.253850000	1.128883000
O	0.607449000	-1.257538000	1.223242000
C	-2.696638000	-0.673715000	-0.763700000
C	-1.661674000	1.211109000	-2.009171000
C	-2.735131000	0.362567000	-1.711516000
C	-1.833383000	2.294910000	-3.048261000
H	-1.069406000	2.179383000	-3.826986000
H	-2.826682000	2.269728000	-3.505390000
H	-1.673936000	3.273956000	-2.579058000
H	-3.663584000	0.542402000	-2.242699000
C	-0.671206000	1.120840000	2.401651000
C	0.506595000	-1.068042000	2.488988000

C	-0.092049000	0.050620000	3.094849000
C	1.712538000	-1.324123000	-1.875532000
C	2.672105000	0.604808000	-0.635281000
C	2.764787000	-0.459691000	-1.548351000
H	3.722805000	-0.647063000	-2.022276000
C	-1.287354000	2.264060000	3.174569000
H	-0.822921000	3.207661000	2.862560000
H	-2.355482000	2.330842000	2.931572000
H	-1.169964000	2.138695000	4.254742000
C	1.939087000	-2.429507000	-2.881000000
H	1.691258000	-3.395065000	-2.423085000
H	1.259840000	-2.290697000	-3.731653000
H	2.971475000	-2.449982000	-3.241871000
H	-0.080785000	0.114104000	4.178063000
C	-3.895273000	-1.535983000	-0.536680000
C	-4.975167000	-1.576835000	-1.433825000
C	-3.940275000	-2.347505000	0.608451000
C	-6.074101000	-2.396717000	-1.185970000
C	-5.041255000	-3.162885000	0.857455000
C	-6.113657000	-3.189804000	-0.037114000
H	-4.953770000	-0.983402000	-2.345141000
H	-3.096422000	-2.324795000	1.294426000
H	-6.899872000	-2.421083000	-1.895922000
H	-5.062583000	-3.782493000	1.753255000
H	-6.974015000	-3.829668000	0.156564000
C	3.857051000	1.475195000	-0.375992000
C	3.898706000	2.236657000	0.803048000
C	4.925967000	1.572757000	-1.281243000
C	4.988887000	3.059106000	1.076668000
C	6.012542000	2.401982000	-1.009558000
C	6.050356000	3.144630000	0.172591000
H	3.064610000	2.165860000	1.497693000
H	4.899716000	1.019960000	-2.217959000
H	5.011665000	3.636872000	2.000067000

H	6.829263000	2.474166000	-1.726793000
H	6.901419000	3.790801000	0.385383000
C	1.105287000	-2.145921000	3.331178000
C	0.753283000	-2.329322000	4.678245000
C	2.046804000	-3.013706000	2.755173000
C	1.335778000	-3.346951000	5.431412000
C	2.633852000	-4.025156000	3.511281000
C	2.281892000	-4.195566000	4.852227000
H	0.001519000	-1.690952000	5.138234000
H	2.310506000	-2.873671000	1.709140000
H	1.045470000	-3.481898000	6.472622000
H	3.370292000	-4.684256000	3.053036000
H	2.739202000	-4.988882000	5.442802000

Table E.17: Optimized Cartesian coordinates of Co(dbm)$_3$ {11}, S = 0/2 with *D*3 symmetry.

Co	0.000000000	0.000000000	0.000000000
O	-0.089728000	1.508301000	-1.150665000
O	-0.089728000	-1.508301000	1.150665000
O	1.351091000	-0.676444000	-1.150665000
O	1.351091000	0.676444000	1.150665000
O	-1.261363000	-0.831857000	-1.150665000
O	-1.261363000	0.831857000	1.150665000
C	0.646708000	-2.553436000	1.017201000
C	1.887987000	-1.836784000	-1.017201000
C	1.591261000	-2.756146000	0.000000000
H	2.132279000	-3.693216000	0.000000000
C	-2.534695000	-0.716653000	-1.017201000
C	-2.534695000	0.716653000	1.017201000
C	-3.182523000	0.000000000	0.000000000
C	1.887987000	1.836784000	1.017201000
C	0.646708000	2.553436000	-1.017201000
C	1.591261000	2.756146000	0.000000000
H	2.132279000	3.693216000	0.000000000

H	-4.264558000	0.000000000	0.000000000
C	0.422494000	-3.606167000	2.052162000
C	1.355827000	-4.625672000	2.302341000
C	-0.756401000	-3.568882000	2.813968000
C	1.110782000	-5.587903000	3.279804000
C	-1.003296000	-4.535987000	3.785055000
C	-0.072404000	-5.549851000	4.021377000
H	2.294028000	-4.657333000	1.752029000
H	-1.471646000	-2.770805000	2.628304000
H	1.849074000	-6.366291000	3.468268000
H	-1.926553000	-4.497362000	4.361976000
H	-0.264346000	-6.304349000	4.783643000
C	-3.334279000	1.437193000	2.052162000
C	-4.683863000	1.138655000	2.302341000
C	-2.712542000	2.439503000	2.813968000
C	-5.394657000	1.831986000	3.279804000
C	-3.426632000	3.136873000	3.785055000
C	-4.770110000	2.837629000	4.021377000
H	-5.180383000	0.341980000	1.752029000
H	-1.663765000	2.659885000	2.628304000
H	-6.437907000	1.581801000	3.468268000
H	-2.931553000	3.917124000	4.361976000
H	-5.327554000	3.381105000	4.783643000
C	2.911785000	2.168974000	2.052162000
C	3.328036000	3.487016000	2.302341000
C	3.468943000	1.129379000	2.813968000
C	4.283875000	3.755917000	3.279804000
C	4.429928000	1.399114000	3.785055000
C	4.842514000	2.712222000	4.021377000
H	2.886355000	4.315353000	1.752029000
H	3.135411000	0.110920000	2.628304000
H	4.588833000	4.784491000	3.468268000
H	4.858106000	0.580237000	4.361976000
H	5.591899000	2.923245000	4.783643000

C	2.911785000	-2.168974000	-2.052162000
C	3.468943000	-1.129379000	-2.813968000
C	3.328036000	-3.487016000	-2.302341000
C	4.429928000	-1.399114000	-3.785055000
C	4.283875000	-3.755917000	-3.279804000
C	4.842514000	-2.712222000	-4.021377000
H	3.135411000	-0.110920000	-2.628304000
H	2.886355000	-4.315353000	-1.752029000
H	4.858106000	-0.580237000	-4.361976000
H	4.588833000	-4.784491000	-3.468268000
H	5.591899000	-2.923245000	-4.783643000
C	0.422494000	3.606167000	-2.052162000
C	-0.756401000	3.568882000	-2.813968000
C	1.355827000	4.625672000	-2.302341000
C	-1.003296000	4.535987000	-3.785055000
C	1.110782000	5.587903000	-3.279804000
C	-0.072404000	5.549851000	-4.021377000
H	-1.471646000	2.770805000	-2.628304000
H	2.294028000	4.657333000	-1.752029000
H	-1.926553000	4.497362000	-4.361976000
H	1.849074000	6.366291000	-3.468268000
H	-0.264346000	6.304349000	-4.783643000
C	-3.334279000	-1.437193000	-2.052162000
C	-2.712542000	-2.439503000	-2.813968000
C	-4.683863000	-1.138655000	-2.302341000
C	-3.426632000	-3.136873000	-3.785055000
C	-5.394657000	-1.831986000	-3.279804000
C	-4.770110000	-2.837629000	-4.021377000
H	-1.663765000	-2.659885000	-2.628304000
H	-5.180383000	-0.341980000	-1.752029000
H	-2.931553000	-3.917124000	-4.361976000
H	-6.437907000	-1.581801000	-3.468268000
H	-5.327554000	-3.381105000	-4.783643000

Table E.18: Optimized Cartesian coordinates of *fac*-Co(tfba)₃ {12}, S = 0/2 with *D*3 symmetry.

	X	Y	Z
Co	0.003819000	-0.016262000	0.324407000
O	1.496954000	0.201507000	-0.834832000
O	-1.511004000	-0.048178000	1.472929000
O	-0.547117000	-1.428689000	-0.822744000
O	0.792962000	-1.304082000	1.478297000
O	-0.944300000	1.161097000	-0.829533000
O	0.730553000	1.317688000	1.467800000
C	-2.470440000	-0.868775000	1.277466000
C	-1.642724000	-2.083551000	-0.699217000
C	-2.610139000	-1.842633000	0.301656000
H	-3.525446000	-2.420312000	0.297667000
C	-0.993773000	2.434936000	-0.690980000
C	0.470973000	2.555191000	1.287411000
C	-0.319476000	3.156445000	0.319999000
C	2.002973000	-1.680030000	1.317350000
C	2.624459000	-0.393124000	-0.689823000
C	2.918772000	-1.306921000	0.346337000
H	3.915204000	-1.724425000	0.411435000
H	-0.390109000	4.236611000	0.330572000
C	-3.597628000	-0.684274000	2.313232000
F	-4.630099000	-1.555183000	2.120758000
F	-3.133138000	-0.878552000	3.570745000
F	-4.110158000	0.569669000	2.248521000
C	1.185529000	3.444967000	2.324519000
F	0.882680000	4.766927000	2.173444000
F	0.841165000	3.091494000	3.584748000
F	2.532417000	3.324684000	2.211362000
C	2.433232000	-2.692494000	2.398214000
F	3.724735000	-3.104152000	2.241993000
F	2.326891000	-2.152921000	3.635559000
F	1.649546000	-3.798908000	2.358057000
C	-1.864159000	-3.141524000	-1.721154000

C	-1.085363000	-3.131210000	-2.891262000
C	-2.816678000	-4.159350000	-1.547363000
C	-1.267182000	-4.105339000	-3.868088000
C	-2.990799000	-5.137014000	-2.523883000
C	-2.220667000	-5.110977000	-3.688417000
H	-0.342355000	-2.346985000	-3.018497000
H	-3.409172000	-4.209077000	-0.636550000
H	-0.661903000	-4.082615000	-4.773462000
H	-3.726106000	-5.925794000	-2.372174000
H	-2.360104000	-5.875619000	-4.451784000
C	3.654475000	-0.051691000	-1.707627000
C	3.466835000	1.086214000	-2.511219000
C	4.803984000	-0.836691000	-1.899925000
C	4.411698000	1.436246000	-3.470922000
C	5.744170000	-0.487286000	-2.866350000
C	5.553470000	0.651707000	-3.651575000
H	2.574894000	1.690744000	-2.363780000
H	4.960418000	-1.737988000	-1.311509000
H	4.258917000	2.326239000	-4.079656000
H	6.627218000	-1.108348000	-3.008887000
H	6.292522000	0.926175000	-4.403629000
C	-1.811431000	3.150064000	-1.707061000
C	-2.161817000	2.481929000	-2.892152000
C	-2.258629000	4.467456000	-1.510879000
C	-2.926534000	3.122097000	-3.863106000
C	-3.031220000	5.102023000	-2.480551000
C	-3.363530000	4.433763000	-3.660929000
H	-1.821680000	1.458987000	-3.036544000
H	-2.029494000	4.994421000	-0.587324000
H	-3.185540000	2.596110000	-4.780902000
H	-3.380725000	6.119234000	-2.311007000
H	-3.966061000	4.932640000	-4.419127000

Table E.19: Optimized Cartesian coordinates of *mer*-Co(tfba)₃ {12}, S = 0/2 with *D*3 symmetry.

	X	Y	Z
Co	-0.017882000	0.005218000	-0.019376000
O	1.629127000	0.954987000	0.049873000
O	-1.660629000	-0.949271000	0.084201000
O	-0.568597000	1.264667000	-1.336024000
O	0.470433000	-1.198770000	-1.405478000
O	-0.671289000	1.231497000	1.274719000
O	0.690506000	-1.264556000	1.203913000
C	-2.649118000	-0.641160000	-0.665246000
C	-1.723455000	1.286163000	-1.891196000
C	-2.763242000	0.371876000	-1.602966000
H	-3.693256000	0.441716000	-2.151993000
C	-0.539577000	1.094776000	2.542295000
C	0.632012000	-1.069694000	2.466586000
C	0.084369000	-0.009469000	3.167919000
C	1.623443000	-1.246874000	-1.961077000
C	2.612948000	0.622816000	-0.697136000
C	2.697477000	-0.379395000	-1.648435000
H	3.648409000	-0.520633000	-2.146252000
H	0.176956000	-0.018276000	4.246596000
C	-3.843470000	-1.590750000	-0.447627000
F	-4.928205000	-1.249961000	-1.200623000
F	-3.507678000	-2.864753000	-0.779703000
F	-4.234583000	-1.591849000	0.848986000
C	1.291221000	-2.222181000	3.249619000
F	1.244537000	-2.030228000	4.598932000
F	0.669747000	-3.398657000	2.986812000
F	2.595518000	-2.357054000	2.905011000
C	3.839900000	1.522279000	-0.451137000
F	3.549480000	2.815871000	-0.754028000
F	4.225641000	1.479447000	0.845560000
F	4.914321000	1.162831000	-1.209920000
C	-1.920292000	2.359903000	-2.902163000

C	-0.799097000	3.068838000	-3.367488000
C	-3.190425000	2.697879000	-3.399197000
C	-0.944706000	4.078093000	-4.313792000
C	-3.333142000	3.712531000	-4.342695000
C	-2.211662000	4.402972000	-4.805660000
H	0.182563000	2.811467000	-2.976317000
H	-4.079186000	2.185634000	-3.037787000
H	-0.066593000	4.614839000	-4.670571000
H	-4.324308000	3.967585000	-4.714561000
H	-2.325119000	5.194248000	-5.545804000
C	1.788856000	-2.312858000	-2.983318000
C	2.833738000	-2.291696000	-3.922095000
C	0.862875000	-3.369478000	-3.016796000
C	2.951384000	-3.306226000	-4.869010000
C	0.988117000	-4.385274000	-3.959633000
C	2.031706000	-4.357223000	-4.888274000
H	3.547362000	-1.470604000	-3.934297000
H	0.054680000	-3.381571000	-2.289056000
H	3.760852000	-3.274195000	-5.596632000
H	0.269609000	-5.203640000	-3.970171000
H	2.127589000	-5.151981000	-5.627317000
C	-1.078522000	2.214611000	3.357053000
C	-1.319946000	3.451256000	2.734768000
C	-1.358010000	2.073846000	4.726182000
C	-1.813802000	4.524477000	3.469465000
C	-1.860930000	3.147939000	5.456419000
C	-2.085510000	4.377062000	4.832036000
H	-1.103860000	3.554387000	1.673853000
H	-1.208611000	1.117768000	5.222873000
H	-1.986774000	5.481173000	2.978802000
H	-2.082466000	3.023742000	6.515351000
H	-2.474075000	5.217372000	5.406116000

Table E.20: Optimized Cartesian coordinates of *fac*-Co(tfaa)₃ {13}, S = 0/2 with *D*3 symmetry.

	X	Y	Z
Co	-0.023472000	-0.031991000	-0.009603000
O	1.623262000	0.915394000	0.109343000
O	-1.678216000	-0.976521000	0.073086000
O	-0.527045000	1.210144000	-1.360878000
O	0.500333000	-1.247714000	-1.382071000
O	-0.719543000	1.207663000	1.255590000
O	0.660872000	-1.292922000	1.246708000
C	-2.662374000	-0.653472000	-0.670711000
C	-1.674657000	1.221577000	-1.922917000
C	-2.744207000	0.351934000	-1.625811000
C	-1.839660000	2.267803000	-2.995792000
H	-1.204898000	2.003636000	-3.852024000
H	-2.877091000	2.345739000	-3.331696000
H	-1.495293000	3.237846000	-2.619137000
H	-3.674189000	0.471593000	-2.172088000
C	-0.659682000	1.040681000	2.521100000
C	0.546416000	-1.104785000	2.502781000
C	-0.055728000	-0.050922000	3.178339000
C	1.669928000	-1.209810000	-1.888707000
C	2.651239000	0.643365000	-0.599488000
C	2.729310000	-0.365416000	-1.581543000
H	3.662892000	-0.490152000	-2.120655000
C	-1.316434000	2.129149000	3.331539000
H	-0.979384000	3.108588000	2.973002000
H	-2.402954000	2.079842000	3.180148000
H	-1.100351000	2.028450000	4.398431000
C	3.859488000	1.498053000	-0.310912000
H	4.651620000	1.344289000	-1.048234000
H	3.566527000	2.554069000	-0.291600000
H	4.244723000	1.245513000	0.685918000
H	-0.064405000	-0.069740000	4.263288000
C	-3.899892000	-1.534563000	-0.405200000

F	-4.931436000	-1.252916000	-1.250421000
F	-3.603671000	-2.846692000	-0.546150000
F	-4.354178000	-1.344448000	0.862000000
C	1.205337000	-2.235809000	3.318051000
F	1.015622000	-2.089720000	4.659750000
F	0.710476000	-3.444014000	2.965157000
F	2.547314000	-2.256306000	3.100877000
C	1.852659000	-2.265713000	-2.997578000
F	3.122497000	-2.287659000	-3.492298000
F	1.571786000	-3.506995000	-2.539553000
F	1.018686000	-2.008210000	-4.039870000

Table E.21: Optimized Cartesian coordinates of *fac*-Co(tfaa)$_3$ {13}, S = 0/2 with *D*3 symmetry.

Co	-0.026786000	-0.010268000	-0.042593000
O	1.629115000	0.927452000	0.046648000
O	-1.685333000	-0.942453000	0.067935000
O	-0.544207000	1.228659000	-1.391690000
O	0.469743000	-1.240292000	-1.409842000
O	-0.688390000	1.242230000	1.230865000
O	0.662749000	-1.276369000	1.204129000
C	-2.683489000	-0.607588000	-0.651813000
C	-1.706002000	1.260850000	-1.920924000
C	-2.777979000	0.400834000	-1.602223000
C	-1.895265000	2.336442000	-2.960455000
H	-1.098788000	2.264087000	-3.710659000
H	-2.870668000	2.264198000	-3.448704000
H	-1.801512000	3.319223000	-2.480626000
H	-3.720328000	0.533737000	-2.123739000
C	-0.573092000	1.095697000	2.494979000
C	0.584269000	-1.076517000	2.461816000
C	0.029362000	-0.001890000	3.143628000
C	1.633773000	-1.288086000	-1.932065000
C	2.620928000	0.589296000	-0.682211000

C	2.709176000	-0.427313000	-1.622836000
H	3.649981000	-0.568314000	-2.145111000
C	-1.137658000	2.228530000	3.313422000
H	-0.560145000	3.139234000	3.108073000
H	-2.172748000	2.420744000	3.006933000
H	-1.103459000	2.013538000	4.384563000
C	1.829932000	-2.388857000	-2.942803000
H	1.920447000	-3.344326000	-2.408569000
H	0.950533000	-2.458112000	-3.592172000
H	2.730847000	-2.233326000	-3.542831000
H	0.058729000	-0.007940000	4.228346000
C	-3.919139000	-1.485067000	-0.366655000
F	-4.984428000	-1.156962000	-1.151336000
F	-3.644166000	-2.794104000	-0.582148000
F	-4.312977000	-1.350907000	0.925485000
C	1.213516000	-2.231614000	3.266627000
F	1.135086000	-2.033954000	4.612069000
F	0.591684000	-3.404569000	2.991279000
F	2.525973000	-2.375645000	2.953672000
C	3.848666000	1.487861000	-0.432895000
F	3.569949000	2.778183000	-0.752176000
F	4.215723000	1.455788000	0.871335000
F	4.930163000	1.111921000	-1.171121000